## REVIEW ARTICLE

Check for updates

# Aryl ether-free polymer electrolytes for electrochemical and energy devices†

Eun Joo Park, [a] Patric Jannasch, [b] Kenji Miyatake, [cd] Chulsung Bae, [e] Kevin Noonan, [f] Cy Fujimoto, [g] Steven Holdcroft, [h] John R. Varcoe, [i] Dirk Henkensmeier, [jkl] Michael D. Guiver *[m] and Yu Seung Kim *[a]

Anion exchange polymers (AEPs) play a crucial role in green hydrogen production through anion exchange membrane water electrolysis. The chemical stability of AEPs is paramount for stable system operation in electrolysers and other electrochemical devices. Given the instability of aryl ether-containing AEPs under high pH conditions, recent research has focused on quaternized aryl ether-free variants. The primary goal of this review is to provide a greater depth of knowledge on the synthesis of aryl ether-free AEPs targeted for electrochemical devices. Synthetic pathways that yield polyaromatic AEPs include acid-catalysed polyhydroxyalkylation, metal-promoted coupling reactions, ionene synthesis *via* nucleophilic substitution, alkylation of polybenzimidazole, and Diels−Alder polymerization. Polyolefinic AEPs are prepared through addition polymerization, ring-opening metathesis, radiation grafting reactions, and anionic polymerization. Discussions cover structure−property−performance relationships of AEPs in fuel cells, redox flow batteries, and water and $CO_2$ electrolysers, along with the current status of scale-up synthesis and commercialization.

## 1. Introduction

Anion exchange polymers (AEPs) are anion-conductive polymers with cationic functionality appended to the chain such as quaternary ammonium or metal cation complexes. The concentration of cations in an AEP is expressed by its ion exchange capacity (IEC), measured as milliequivalents per gram of the polymer (mequiv. $g^{-1}$ of dry AEP). Generally, an increase in IEC results in higher anion conductivity and water uptake of an AEP, but a decrease in its mechanical strength in film form.

[a] *Los Alamos National Laboratory, Los Alamos, NM 87545, USA.*
  *E-mail: yskim@lanl.gov*
[b] *Lund University, SE-221 00 Lund, Sweden*
[c] *University of Yamanashi, Kofu 400-8510, Japan*
[d] *Waseda University, Tokyo 169-8555, Japan*
[e] *Rensselaer Polytechnic Institute, Troy, NY 12180, USA*
[f] *Carnegie Mellon University, Pittsburgh, PA 15213, USA*
[g] *Sandia National Laboratories, Albuquerque, NM 87123, USA*
[h] *Simon Fraser University, Burnaby, BC V5A 1S6, Canada*
[i] *University of Surrey, Guildford GU2 7XH, UK*
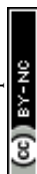[j] *Korea Institute of Science and Technology (KIST), Seoul 02792, South Korea*
[k] *KIST School, University of Science and Technology (UST), Seoul 02792, South Korea*
[l] *KU-KIST School, Korea University, Seoul 02841, South Korea*
[m] *State Key Laboratory of Engines, Tianjin University, Tianjin 300072, China.*
  *E-mail: michael.guiver@outlook.com*
† Electronic supplementary information (ESI) available. See DOI: **https://doi.org/10.1039/d3cs00186e**

For over 60 years, AEPs have been widely used for electrodialysis (ED) and reverse electrodialysis (RED), in the form of anion exchange resin, an anion exchange membrane (AEM), and as one component of a bipolar membrane (BPM) (Fig. 1a and b).[1,2] In ED and RED applications, AEPs selectively separate monovalent and multivalent ions from wastewater. Since 2006, AEPs have been also used for membrane capacitive deionization (MCDI) for water purification or valuable metal ion recovery.[3,4] In MCDI, a cation exchange membrane (CEM) is attached to the cathode, and an AEM is attached to the anode (Fig. 1c). The role of ion exchange membranes is to prevent co-ions from being flushed out of electrodes during the ion removal process. Thus, MCDI improves device efficiency compared to conventional CDI.

In 2004, the U.S. Department of Energy (DOE) increased federal funding for hydrogen and fuel cell research, development, and demonstration through the hydrogen fuel initiative. This increased funding allowed the hydrogen program to expand and address a broad range of barriers facing the widespread use of hydrogen and fuel cell technologies in transportation. One of the focused R&D areas was developing AEM fuel cells (AEMFCs) that have the potential to operate with platinum group metal-free (PGM-free) catalysts.[5] In AEMFC applications, AEPs are used both as a hydroxide-conducting medium in the form of a membrane and as an anion exchange ionomer (AEI) at the electrodes (Fig. 1d).

**5704** | *Chem. Soc. Rev.*, 2024, **53**, 5704–5780

This journal is © The Royal Society of Chemistry 2024

As interest in fuel cell vehicles shifted from light-duty to heavy-duty vehicles, such as class 8 long-haul trucks and other heavy-duty transportation applications, including trains, ships, and aviation in the late 2010s, heat rejection in fuel cell vehicles based on low-temperature proton-exchange membrane fuel cells (LT-PEMFCs) became a challenging issue. For LT-PEMFCs, operating fuel cells at a higher cell voltage at rated power with a fuel cell/battery hybrid strategy can mitigate the negative impact of the heat dissipation issue. Alternatively, polybenzimidazole (PBI) or AEPs can be used as a proton exchange membrane (PEM) after phosphoric acid (PA) doping.[6,7] Since PA-doped polymers can conduct protons without water, the operating temperature of fuel cells can exceed 100 °C (Fig. 1e), effectively resolving the heat dissipation issue. Compared to PBI-based fuel cells, AEP-based ion-pair fuel cells have shown higher stability under dynamic operating conditions due to stronger ion-pair interactions between cationic functional groups of AEPs and PA.[8,9]

In 2021, the U.S. DOE announced the energy earthshots initiative, aiming to accelerate breakthroughs in more abundant, affordable, and reliable clean energy solutions within this decade. The first energy earthshot, "Hydrogen Shot," seeks to reduce the cost of clean hydrogen by 80% to $1 per 1 kilogram in one decade ("1 1 1"). To achieve this goal, AEM water electrolysers (AEMWEs) have been drawing substantial interest. AEMWEs use PGM-free catalysts and less expensive metal interconnects while enabling differential pressure operation and operating at higher current densities than conventional liquid alkaline electrolysers.[10] AEPs play critical roles in the performance and durability of AEMWEs. Unlike in AEMFCs, a low-concentration of liquid electrolyte is often added in AEMWEs to reduce cell resistance, prevent ionomer adsorption,

**Eun Joo Park**

*Eun Joo Park is a Research Scientist at Los Alamos National Laboratory. She obtained her BS in chemistry from University of Toronto in 2010, MA in Science Education from Teachers College, Columbia University in 2012. She received her PhD in chemistry in 2016 from Rensselaer Polytechnic Institute, where she focused on synthesis of functional polymers via post-polymerization modification under supervision of Prof. Chulsung Bae. Her research interests are design, synthesis and characterization of ionic polymers used in electrochemical devices.*

**Patric Jannasch**

*Patric Jannasch received his PhD degree in Chemical Engineering from Lund University, Sweden, in 1996. He was appointed full professor of Polymer Technology at the same university in 2010, and was a guest professor at the University of Tartu (Estonia) during 2017–2022. His current research focuses on molecular design, synthesis, and function of polymer electrolytes and ion-exchange membranes for fuel cells, water electrolysers, and flow batteries, as well as on new bio-based monomers, polymers and plastics from renewable resources. He presently serves as editor of Solid State Ionics.*

**Kenji Miyatake**

*Prof. Kenji Miyatake received his PhD degree in polymer chemistry from Waseda University, Japan in 1996. He was a postdoc (JSPS overseas research fellow) at McGill University, Canada, from 1999 to 2001. In 2001, he was appointed an associate professor in Clean Energy Research Center at the University of Yamanashi, where he currently serves as a professor. He also holds a professor position at Waseda University. He is a Fellow of the Royal Society of Chemistry. He serves as an associate editor of Fuel Cells (Wiley). His research interest involves new functional polymers for energy device applications.*

**Steven Holdcroft**

*Steven Holdcroft is a Professor and Canada Research Chair, and former President of the Canadian Society for Chemistry. He researches materials for electrochemical energy conversion & storage. He is the author of 300 peer-reviewed articles and inventor of 20+ patents. He has received the Macromolecular Science and Engineering Division Award of the Chemical Institute of Canada (CIC), and the CSC RioTinto Alcan Award for Electrochemistry. In 2021, he was elected to the fellowship of the Royal Society of Canada and in 2024 awarded the CIC Montreal Medal for his contributions to the Canadian chemical community.*

and increase local pH, thereby improving hydrogen and oxygen evolution reactions (HER and OER, respectively, Fig. 1f).[11]

The second energy earthshot, "Long Duration Storage Shot," aims to reduce the cost of energy storage systems by 90% within a decade. Electrical energy storage is recognized as an underpinning technology for maintaining power network stability and reliability from energy generation and load balance maintenance. Redox flow batteries (RFBs) store energy in two soluble redox couples contained in external liquid electrolyte tanks. During the charging phase, one electrolyte is oxidized at the anode, while another is reduced at the cathode, converting electrical energy into chemical energy of the electrolyte. AEMs can be used as separators in RFBs, offering high coulombic efficiency (CE) by providing superior barrier properties against cations. During the charging and discharging of the RFBs, both anions and protons are transported through the AEM *via* diffusion and the Grotthuss mechanism (Fig. 1g).[12]

The third energy earthshot, "Carbon Negative Shot," aims to develop energy-efficient carbon capture from dilute sources, transferring it to durable storage or converting it into products. Using AEPs for both direct air capture (DAC) of $CO_2$ and its electrochemical reduction is highly promising. In the $CO_2$ capture device, $CO_2$ dissolved in water as (bi)carbonate is regenerated using electrochemical cells with several configurations (Fig. 1h).[13,14] $CO_2$ electrolysers that convert $CO_2$ into carbon monoxide and other value-added chemical products can utilize a membrane electrode assembly (MEA) containing AEPs for highly efficient electrochemical $CO_2$ reduction.[15] AEPs are typically used for AEMs, AEIs in the catalyst layers, and as a component of BPMs. In AEP-based $CO_2$ electrolysers, the cationic functional groups of AEPs facilitate anion transport from the cathode to the anode, enabling the $CO_2$ reduction reaction ($CO_2RR$) to occur in a basic environment. This environment suppresses the competing HER by decreasing the concentration of protons at the catalyst surface (Fig. 1i).

AEPs are critical materials not only for the emerging technologies mentioned above but also for other applications, including reverse osmosis (RO), sensors, photo-electrolysis, and metal ion batteries. Fig. 2 shows the number of publications about AEPs over the last 25 years. The total number of publications on AEPs has increased fivefold from 2000 to 2023, with over 1500 AEP papers published each year since 2021. The largest portion of AEP-related papers in 2023 is in the field of fuel cells (584 papers), followed by water electrolysis (343 papers). Compared to the number of publications five years ago, the relative proportions in ED, RED, MCDI, fuel cell, and RFB have remained similar. However, the proportions in water electrolysis and $CO_2$ capture/electrolysis have increased approximately fourfold, reflecting the current trend of research. Another notable research trend from Fig. 2 is that modern AEP research has become more device-specific rather than focusing on general material development. In 2000, only 23% of papers were device-specific, but by 2023, 88% of the papers on AEPs were related to specific device applications. This indicates that the design of AEPs is evolving to meet the specific requirements of the electrochemical devices.

## 2. Chemical stability of AEPs

The electrochemical applications using AEP materials require essential properties tailored to specific applications, such as ion conductivity, permselectivity, chemical stability, thermal stability, mechanical properties, and gas permeability (high gas permeability for ionomers, low for membranes). The most critical property for electrochemical applications is the chemical stability of AEPs under the operating conditions of the devices. Fig. 3 shows the typical pH and potential ranges of various electrochemical devices utilizing AEPs. While AEMs for gas separation applications do not face a chemical stability

*John Varcoe is a Professor of Materials Chemistry at the University of Surrey and Director of Research for the School of Chemistry and Chemical Engineering. He is also a Fellow of the Royal Society of Chemistry. He was awarded his BSc and PhD chemistry degrees at the University of Exeter. For the past 25 years, his research has focused on ion-exchange membranes, with specialisms in radiation grafted materials, anion-exchange membranes, and Raman microscopy. His group's membranes and ionomers have been tested in many types of electrochemical devices including fuel cells, hydrogen and carbon dioxide electrolysers, and electrodialysis systems.*

**John R. Varcoe**

*Dirk Henkensmeier received a PhD in chemistry at Hamburg University and worked at LG Chem, Sartorius and Paul Scherrer Institute, before joining Korea Institute of Science and Technology (KIST) in 2009, where he is a principal researcher. Concurrently he is a full professor at University of Science and Technology and teaches at Korea University. His research focus is on polymers and membranes for energy conversion and storage, especially for fuel cells, water electrolysis and flow batteries. He is a co-organizer of the EMEA workshop series and a section board member of MDPI's Membranes.*
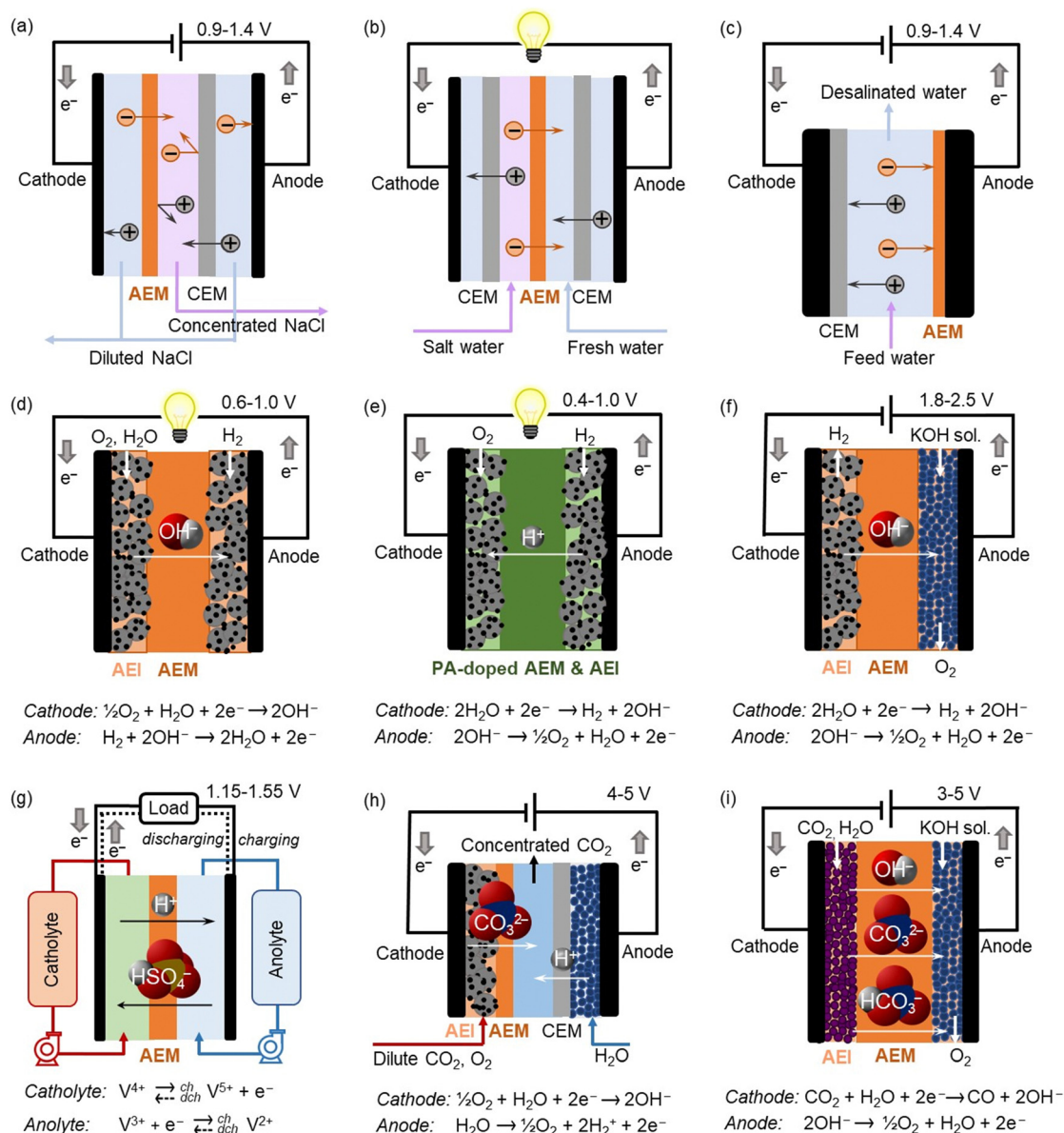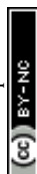
**Dirk Henkensmeier**

5706 | *Chem. Soc. Rev.*, 2024, **53**, 5704–5780

This journal is © The Royal Society of Chemistry 2024

**Fig. 1** Schematic diagrams, cell reactions and operating cell voltages of electrochemical devices using AEPs: (a) ED, (b) RED, (c) MCDI, (d) AEMFC, (e) ion-pair HT-PEMFC, (f) AEMWE, (g) vanadium RFB, (h) electrochemical $CO_2$ capture, and (i) $CO_2$ electrolyser.

issue, the AEPs for RO, ED, RED, and MCDI applications require chemical stability under medium to high pH conditions (pH 4–13), especially in the presence of multivalent metal cations. AEPs for AEMFC, AEMWE, and $CO_2$ capture/electrolyser applications need chemical stability under higher pH conditions (pH > 13). Conversely, AEPs for HT-PEMFC applications require chemical stability under low pH conditions (pH 1–3) and elevated temperatures (100–200 °C). AEPs for aqueous RFB applications need chemical stability under lower pH conditions (pH < 1), particularly in the presence of multivalent metal cations with high oxidation states and potentials. In addition to alkaline stability, AEPs for AEMWE and $CO_2$ electrolyser applications require high electrochemical oxidative stability at >1.8 V. It is important to note that although Fig. 3 depicts typical pH and potential ranges of electrochemical devices, AEPs may encounter even harsher environments under specific cell configurations and operations. For example, a few recent studies reported the operating voltage of BPM-based MCDIs, EDs, or AEMWEs exceeding >2 V.[16–18] Furthermore, the cleaning of ED cells with acid and base solutions may result in membrane degradation due to the extreme pH conditions.[19]

## 2.1. AEP synthesis before 2012

Before 2012, AEPs were primarily prepared for ED separation processes using one of two synthetic routes. The first route involves chemical modification of perfluoroacid precursors through multiple steps, forming anion-conducting counterparts of Nafion™. In 1986, Matsui *et al.* prepared quaternized
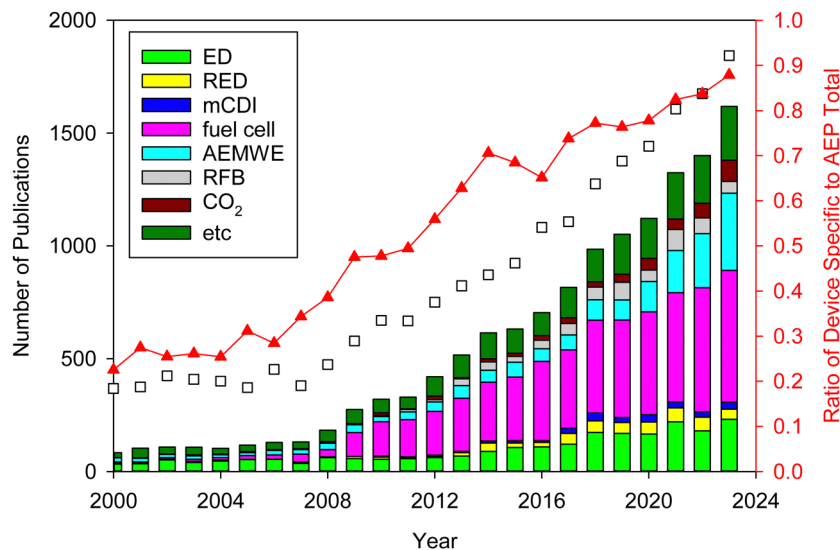
This journal is © The Royal Society of Chemistry 2024

*Chem. Soc. Rev.*, 2024, **53**, 5704–5780 | **5707**

Fig. 2 Number of publications on AEPs for various applications over the last 25 years. The related articles were identified using the keywords "anion exchange membrane" and corresponding applications from Web of Science™, Thomson Reuters (coloured bar). The total number of publications on AEPs (black square) represents those found with the keyword "anion exchange membrane". The "etc." category includes supercapacitor, metal ion batteries, gas separation, actuators, sensors, photo-electrolysis, microbial/enzymatic fuel cells, metal ion recovery, and RO.
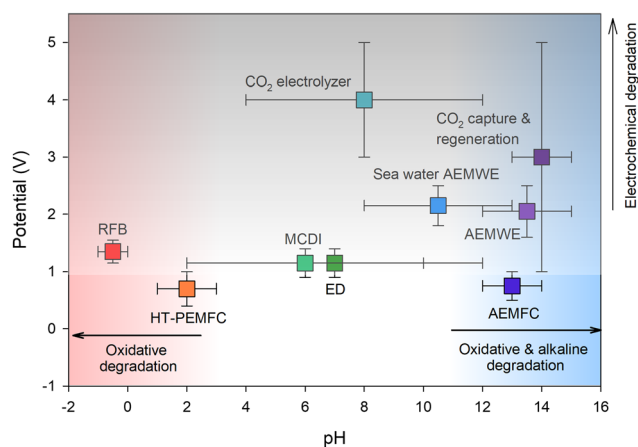


Fig. 3 Typical pH and potential ranges of various electrochemical devices using AEPs.

perfluorinated AEMs by modifying the sulfonic acid functional groups of Nafion™.[20] The multiple steps include (i) conversion of a carboxylic ester to an amide, (ii) reduction of the carbonyl group to methylene, and (iii) quaternization using methyl iodide (Scheme 1a). Other perfluorinated AEPs were also prepared from the carboxylic ester precursor (Scheme 1b)[15] and sulfonamide precursor (Scheme 1c)[21,22] of Nafion™, incorporating various ammonium structures, including guanidinium and hexylammonium. Perfluorinated AEMs can also be prepared in a single step via amination of the sulfonyl fluoride precursor under anhydrous conditions (Scheme 1d and e).[23,24] However, attempting to prepare AEMs via amination of sulfonyl fluoride under aqueous conditions is unsuccessful, as it leads to hydrolysis of sulfonyl fluoride into sulfonic acid paired with an ammonium counterion.[25,26]

The quaternized perfluorinated AEPs exhibited excellent chemical stability under chlorine and acidic conditions, making them suitable for ED and RED applications. For example, quaternized perfluorinated AEMs with difluoroethane linkages remained chemically stable in chlorine-saturated water at 60 °C for 1000 hours without structural change.[20] These membranes also demonstrated stability in 6 N hydrochloric and nitric acids at 60 °C. However, the mechanical properties of these quaternized AEMs deteriorated under basic conditions. Additionally, the difluoroethylene linkage in the AEMs is susceptible to hydroxide attack.[27,28] Although amide and sulfonamide linkages in other perfluorinated AEMs showed improved chemical stability under basic conditions, slow hydrolysis may occur under AEMFC operating conditions,[29] limiting their use in alkaline devices over extended time.

The second route involves post-polymerization modification of a hydrocarbon polymer with a desired cationic group. Quaternized polystyrenes are typically prepared by chloromethylation of polystyrene or copolymerization of styrene and vinylbenzyl chloride, followed by amination to form benzylammonium cation (Scheme 2a). A commercial polystyrene AEP (Selemion®, AGC) is prepared using this method. In 1985, Zschochke and Qullmalz synthesized a quaternized poly(aryl ether sulfone) via chloromethylation and subsequent quaternization of benzyl chloride (Scheme 2b).[30] Due to the high toxicity and carcinogenic nature of the common chloromethylation agent, chloromethyl methyl ether, and its tendency to undergo crosslinking via methylene bridges,[31] bromination of methylbenzene-containing poly(aryl ether sulfone)s or poly(p-phenylene oxide) (PPO) has been adopted for obtaining quaternized polymers (Scheme 2c).[32–34] However, it was shown that the free-radical bromination pathway leads to radical-induced side reactions that produce polymers of lower

5708 | Chem. Soc. Rev., 2024, 53, 5704–5780

This journal is © The Royal Society of Chemistry 2024
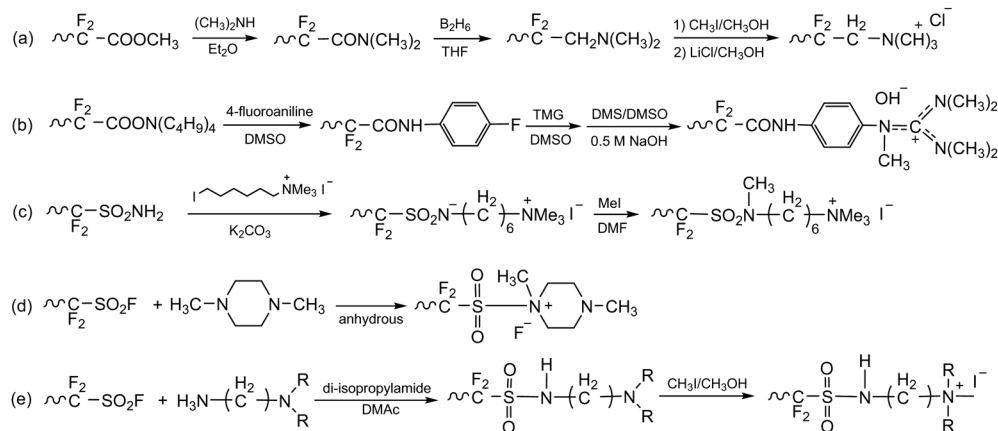
**Scheme 1** AEPs from chemical modification of perfluorinated polymer precursors: (a) quaternized perfluorinated AEM,[20] (b) guanidinium perfluorinated AEP,[21] (c) sulfonamide-linked alkyl ammonium perfluorinated AEM from sulfonamide precursor,[22] (d) methylpiperazinium perfluorinated AEM,[23] and (e) sulfonamide-linked alkyl ammonium perfluorinated AEM from sulfonylfluoride precursor.[24]
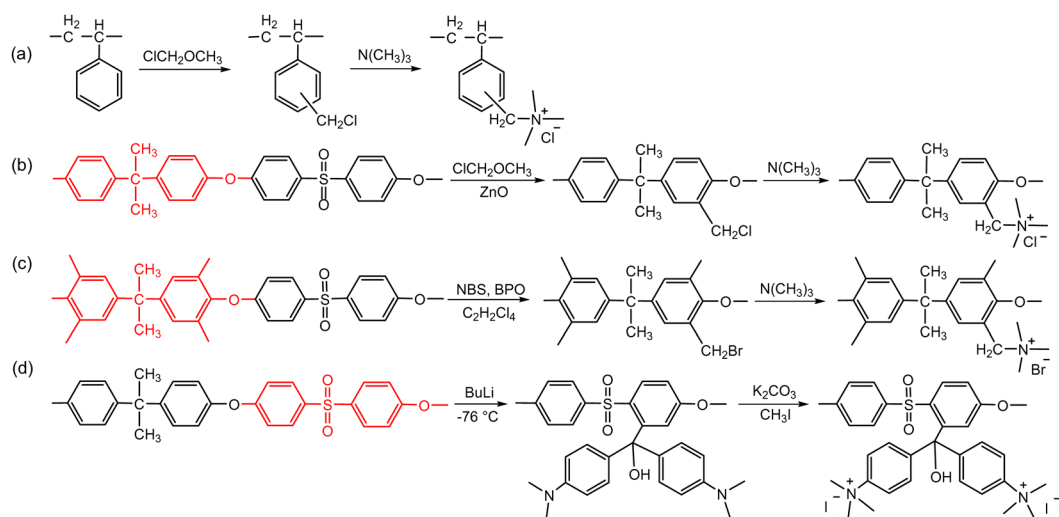


**Scheme 2** AEPs from polymer functionalization: (a) quaternized polystyrene, (b) quaternized poly(aryl ether sulfone) *via* chloromethylation,[30] (c) quaternized poly(aryl ether sulfone) *via* bromination of benzyl groups,[32] and (d) quaternized poly(aryl ether sulfone) *via* lithiation.[46]

molecular weight.[35,36] Despite this, due to the commercial availability and versatile applicability of ether-containing aromatic polymers, functionalization using chloromethylation and bromination was the most popular synthetic pathways over the last decade, before the emergence of diverse aryl ether-free poly(arylene) AEPs.[37–45] Another method includes lithiation chemistry to prepare quaternized poly(aryl ether sulfone) (Scheme 2d).[46] The bis(dimethylamine)-containing side chain was functionalized onto the lithiated polymer, followed by methylation to introduce quaternary ammonium groups and produce AEMs.
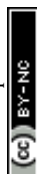
The AEPs prepared from post-polymerization modification showing reasonably high stability under low to medium pH conditions are commercially available as water purification membranes. However, chemical stability tests of these poly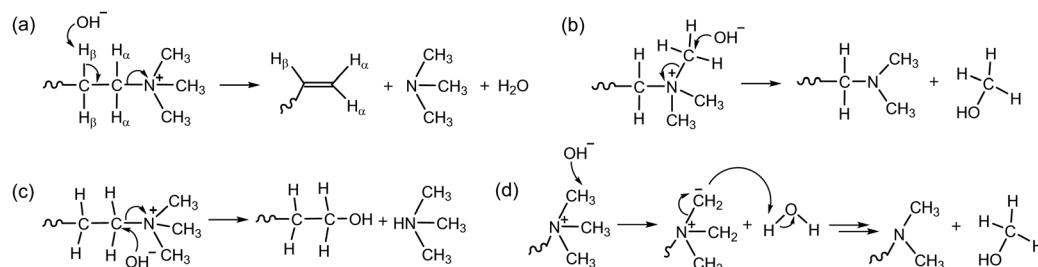mers under alkaline conditions often reveal significantly reduced IEC values or mechanical failure of the membranes, indicating the need for improved chemical structure.

## 2.2. Alkaline stability of cationic groups

The generally lower alkaline stability of AEPs, compared to non-functionalized polymers, suggests that the chemical degradation of the cation headgroups predominates over that of the polymer backbone. Therefore, it has been assumed that the alkaline stability of AEPs is determined by the stability of the positively charged groups.[47,48]

A hydroxide ion, acting as a strong nucleophilic base, can cause degradation through several different chemical mechanisms and pathways. The chemical degradation mechanism of quaternary ammonium groups under high pH conditions was well established before 2012. The attack of a hydroxide ion at the β-H-atom of the alkyl ammonium leads to a Hofmann

This journal is © The Royal Society of Chemistry 2024

*Chem. Soc. Rev.*, 2024, **53**, 5704–5780 | **5709**

**Scheme 3** Degradation mechanisms of quaternary ammonium initiated by a hydroxide ion: (a) E2 (Hofmann) elimination, (b) nucleophilic methyl substitution, (c) $S_N2$ reaction, and (d) ylide intermediate formation.

elimination reaction, resulting in the formation of a tertiary amine from the neighbouring carbon, along with the formation of an alkene, a tertiary amine, and water (Scheme 3a). Another common degradation mechanism involves a nucleophilic substitution reaction at the α-C-atom of the quaternary ammonium. This reaction either yields methanol and a tertiary amine-functionalized polymer from methyl substitution (Scheme 3b) or a tertiary amine and an alcohol-functionalized polymer from the $S_N2$ reaction (Scheme 3c). The degradation mechanism *via* the ylide pathway begins with a hydroxide ion abstracting a proton from a methyl group of ammoniums to produce a water molecule and a ylide intermediate. This intermediate then undergoes rearrangement to produce either an amine or an alcohol as a by-product (Scheme 3d).[49]

The chemical degradation of various heterocyclic ammonium groups has also been reported. Methyl imidazolium undergoes ring-opening degradation triggered by the nucleophilic attack of a hydroxide ion on the imidazolium ring at the C2 position (the carbon adjacent to both nitrogen atoms), leading to the degradation of the cyclic cations (Scheme 4a).[50,51] Methyl pyridinium degrades through a nucleophilic ring-opening reaction, which results in the replacement of the hydrogen by a hydroxide ion, followed by ring closure and dehydrogenation of the hydroxy group (Scheme 4b).[52,53] The degradation of aliphatic-heterocyclic ammonium, such as dimethyl pyrrolidinium or piperidinium, can occur through three pathways: exocyclic demethylation (Scheme 4c), ring-opening elimination (Scheme 4d), and ring-opening substitution (Scheme 4e).[54–56] The ring-opening reactions are predominant, but the degradation rate is influenced by ring size and the geometry of the transition state.

Research on the chemical stability of cationic functional groups has been further expanded to include quaternary ammonium with different substituents and more stable cationic structures (Fig. 4).[57–60] The study of benzyltrimethyl ammonium (BTMA) has been extensively conducted because it is the simplest, synthetically accessible quaternary ammonium cation and thus the most commonly used in the early stages of AEP development.[61–64] Phenyltrimethyl ammonium is much less stable than BTMA; for example, while 90% of BTMA solids remained in 5 M NaOH at 80 °C after 29 days, only 30% of phenyltrimethyl ammonium remained under the same conditions.[65] Benzyl-tethered ammonium cations, such as benzyl pyridinium, benzyl pyrrolidinium, benzyltrimethyl guanidinium, benzylmethyl diazabicyclo[2.2.2] octane (DABCO), and benzyl 1,2-dimethylimidazolium, are less stable and prone to substitution. Alkyltrimethyl ammonium, phenyl-substituted imidazolium, and some heterocyclic cationic groups with high activation energy toward hydroxide attack, including piperidinium, quinuclidinium, and 6-azoniaspiro[5.5]undecane, have been reported to be more stable than BTMA under high pH conditions.[48,58,66–71] Extensive discussions of headgroup stability have been reviewed recently.[72]

## 2.3. Alkaline stability of backbones

Polyvinylidene fluoride (PVDF)-based proton exchange materials are among the most promising alternatives to perfluorinated sulfonic acid polymers (PFSAs) due to their high hydrophobicity, inertness to electrocatalytic activity, and high chemical and mechanical stability.[73,74] However, under high pH conditions, the PVDF backbone composed of difluoroethane, rapidly degrades through dehydrofluorination
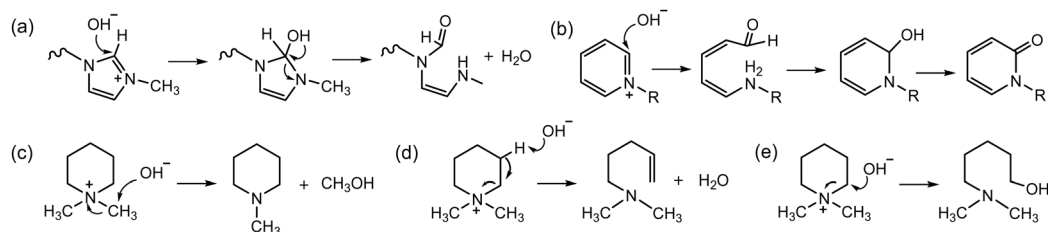


**Scheme 4** Degradation mechanisms of heterocyclic cations: (a) ring opening of imidazolium, (b) nucleophilic ring opening of pyridinium, (c) nucleophilic (methyl) substitution of dimethyl piperidinium (DMP), (d) ring-opening E2 elimination of DMP, and (e) ring-opening nucleophilic substitution of DMP.
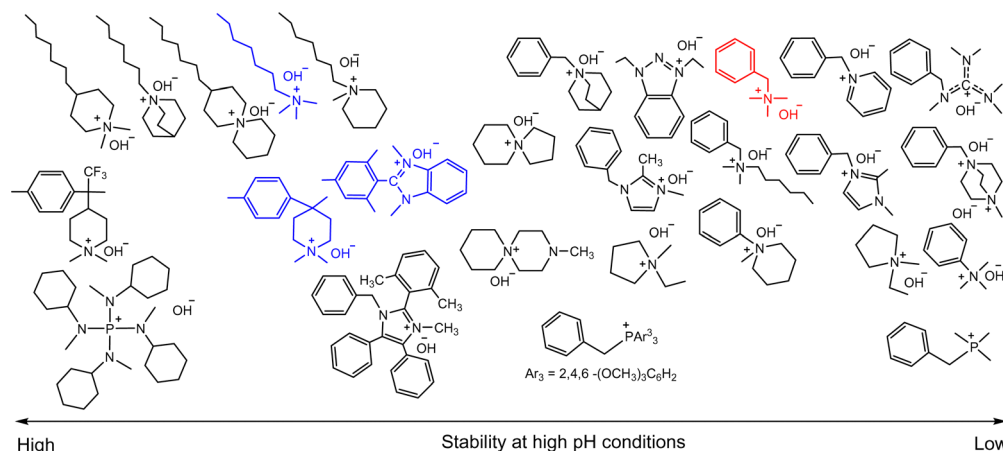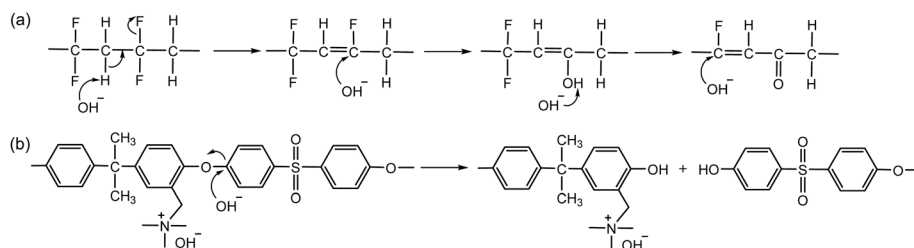
**5710** | *Chem. Soc. Rev.*, 2024, **53**, 5704–5780

This journal is © The Royal Society of Chemistry 2024

**Fig. 4** Chemical stability comparison of quaternary ammoniums under high pH conditions. Red: BTMA (control), Blue: popular cationic groups in modern AEPs.



**Scheme 5** Degradation mechanisms of polymer backbone under high pH conditions: (a) dehydrofluorination and subsequent oxidation reactions of PVDF and (b) aryl ether cleavage of benzyl ammonium functionalized poly(aryl ether sulfone).

(1,2-HF elimination) and subsequent oxidation reactions (Scheme 5a).[75,76]

Polystyrene and poly(aryl ether sulfone)s were among the first choices during the early AEP development period, as their sulfonated derivatives are chemically stable under high pH conditions (40% NaOH at 70–80 °C for 300 hours).[77] However, several studies showed notably better alkaline stability of quaternized polystyrenes compared to quaternized poly(aryl ether sulfone) under high pH conditions.[78–80] Only a few studies reported more than 100 hours of AEMFC durability using a quaternized poly(aryl ether sulfone) AEM, whereas several studies reported more than 200 hours of AEMFC

durability using quaternized polystyrene or other polyolefinic AEMs during the early AEP development period.[81–84] In 2012 and 2013, Fujimoto et al.[85] and Ramani et al.[86] independently reported that the backbone of quaternized poly(aryl ether sulfone)s cleaves at the aryl ether linkage under high pH conditions (Scheme 5b).

Follow-up studies investigated the effect of substituent groups on the barrier energy of the aryl ether cleavage reaction. The energy barrier for trimethylammonium-functionalized phenyl ether (85.8 kJ mol$^{-1}$) was found to be lower than that for nucleophilic benzyl substitution (90.8 kJ mol$^{-1}$) (Fig. 5a).[87] The energy barrier was substantially lower in the presence of



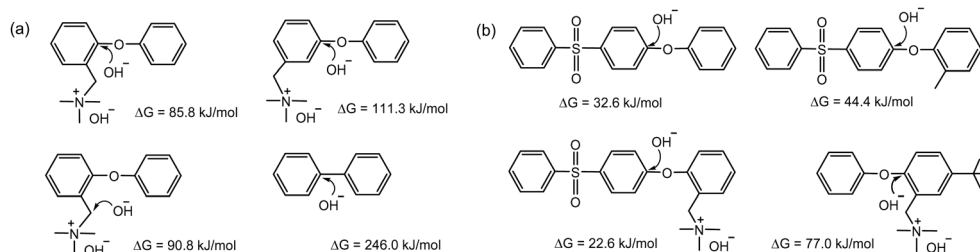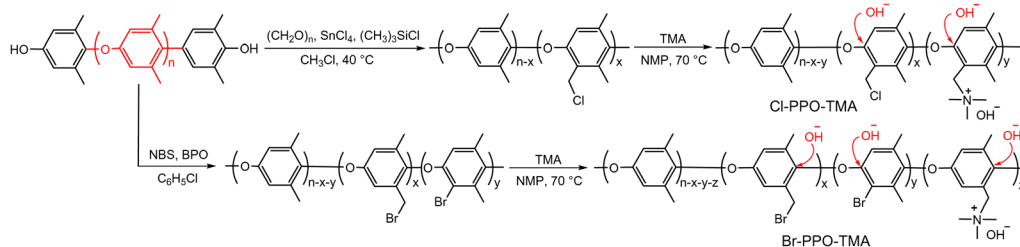**Fig. 5** The energy barriers of aromatic fragments and hydroxide ions: (a) comparison between aryl backbone and quaternary ammonium. Geometry optimization by ωB97XD functional with a 6-311++G(2d,2p) basis set. (b) Effect of sulfone group substituent. Geometry optimization by M06-2X functional with a 6-31+G(d) basis set.

This journal is © The Royal Society of Chemistry 2024

Chem. Soc. Rev., 2024, **53**, 5704–5780 | **5711**

**Scheme 6** Synthetic pathways for quaternized PPOs *via* chloromethylation and bromination. Denoted are the reaction sites of aryl ether cleavage.

electron-withdrawing sulfone groups (32.6 kJ mol$^{-1}$), but higher with an electron-donating methyl group (77.0 kJ mol$^{-1}$) (Fig. 5b).[88] These calculations are in good agreement with experimental data from MEA testing, where an MEA fabricated with a quaternized AEM containing two methyl groups on an adjacent aryl ring of ether showed much higher durability than an MEA using a quaternized poly(aryl ether sulfone) AEM.[89] This indicates that the polymer backbone of electron-rich quaternized PPOs has better alkaline stability than that of electron-deficient aryl sulfone-containing polymers under high pH conditions.

Although several model compound studies on dimethyl phenylene oxide indicated no trace of the aryl ether cleavage reaction occurring, backbone degradation of quaternized PPOs was observed under high pH conditions.[90,91] Ramani *et al.*[35,92] and Becerra-Arciniegas *et al.*[93] observed that quaternized PPO showed different backbone degradation depending on their synthetic process; the quaternized PPO prepared by bromination (Br-PPO-TMA) showed more substantial backbone degradation than the quaternized PPO prepared by chloroalkylation (Cl-PPO-TMA). This disparity was explained by the structural differences between Br-PPO-TMA and Cl-PPO-TMA that may influence the different rates of backbone degradation: (i) Cl-PPO-TMA has an extra methyl group in its backbone, increasing electron density, and (ii) the presence of unreacted bromine directly substituted on the benzene ring in Br-PPO-TMA accelerates the backbone degradation (Scheme 6).

Without cationic or electron-withdrawing groups in close proximity, the polymer backbone remains chemically stable in alkaline conditions. Several unfunctionalized aryl ether-free polymers, including both polyaromatic and vinyl polymers, did not show any sign of degradation at a high base concentration (10 equiv. of NaOCH$_3$ in THF/methanol).[88] The result suggests that aryl ether-free polymers are chemically stable to serve as a backbone for AEP materials.

### 2.4. Chemical stability at low pH

The chemical stability of AEPs under low pH conditions is known to be higher than that under high pH conditions, as there is no strong nucleophile in the acidic system. Several papers reported reasonably high chemical stability of quaternized polystyrene[94] and poly(aryl ether sulfone).[95–103] AEMs under vanadium RFB operating conditions need to be highly acidic to solvate multivalent vanadium ions with high oxidation
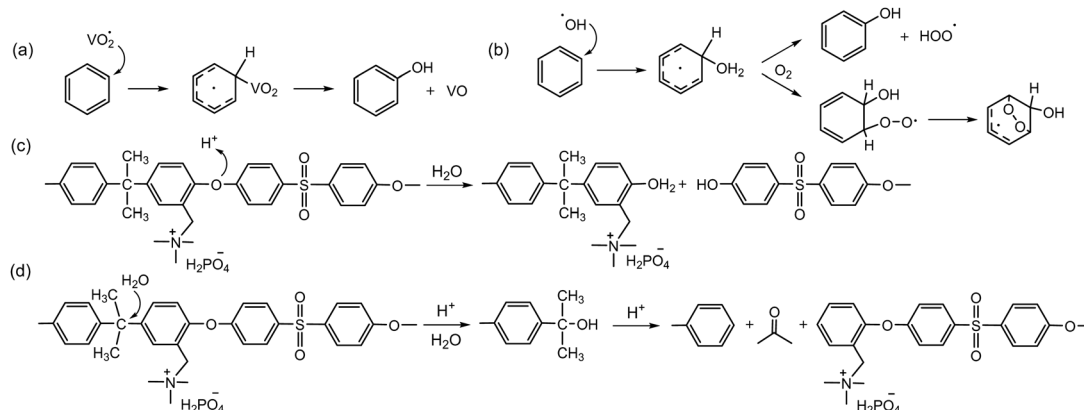
states. The chemical degradation of AEPs detected in RFBs appears to be associated more with oxidative degradation than with acid-assisted degradation. Notable aryl ether cleavage reactions were observed for quaternized poly(aryl ether sulfone)s or poly(aryl ether ketone)s under the oxidative conditions of VO$_2^+$ in concentrated H$_2$SO$_4$ solution (Scheme 7a).[104–106] The rate of backbone degradation of quaternized poly(aryl ether sulfone)s by VO$_2^+$ is similar to that of sulfonated poly(aryl ether sulfone)s,[106] which contrasts starkly with the rate of backbone degradation of quaternized poly(aryl ether sulfone)s by hydroxide ions being much greater than that of sulfonated poly(aryl ether sulfone)s. The similar oxidative degradation rates between sulfonated and quaternized polyaromatics suggest that oxidative polymer degradation occurs in the aryl ether sulfone fragment rather than in the ionic groups. The oxidative degradation of polyaromatics primarily occurs at the electron-rich aryl groups because strong oxidizers such as hydroxyl and vanadium oxide radicals are highly electrophilic (Scheme 7a and b).[107]

In HT-PEMFCs, the polymer backbone degradation of quaternized poly(aryl ether sulfone)s may occur in a protonic environment at a high temperature, around 160 °C. To date, only a limited number of studies have reported on chemical degradation under HT-PEMFC operating conditions. A different degradation mechanism of PA-doped poly(aryl ether sulfone) has been proposed: the aryl ether cleavage reaction *via* protonation of the ether oxygen followed by nucleophilic attack of water (Scheme 7c), as well as the scission of C–C bond at the isopropylidene carbon *via* a retro-Friedel–Crafts alkylation process (Scheme 7d).[108]

### 2.5. Electrochemical oxidative stability

Radical generation during the operation of electrochemical devices in aqueous conditions has been commonly observed, especially active oxygen species, *e.g.*, hydroxyl radical (HO•), reportedly formed with hydrogen peroxide by permeating O$_2$ reacting with Pt/H$_2$ to form H$_2$O$_2$ under alkaline conditions and at relatively low electrode potentials, *ca.* <1 V.[109] Hydroxyl radicals can be further produced by hydroxide ion transfer. Wierzbicki *et al.* observed both HO• and HOO• on the cathode and H• on the anode under AEMFC operating conditions.[110] The oxidative degradation of quaternized polystyrene and other polyaromatics by reactive oxygen radicals is well documented. Superoxide anion radicals can be formed from carbanions followed by subsequent reduction (Scheme 8a).[111,112] Reactive

5712 | *Chem. Soc. Rev.*, 2024, **53**, 5704–5780

This journal is © The Royal Society of Chemistry 2024

**Scheme 7** Degradation mechanisms of polymer backbone under low pH conditions: (a) and (b) suggested oxidative degradation of poly(aryl ether sulfone) by $VO_2^+$ in $H_2SO_4$, (c) aryl ether cleavage of quaternized poly(aryl ether sulfone) in 85% PA at 160 °C, and (d) C−C bond scission *via* retro-Friedel–Crafts alkylation in 85% PA at 160 °C.
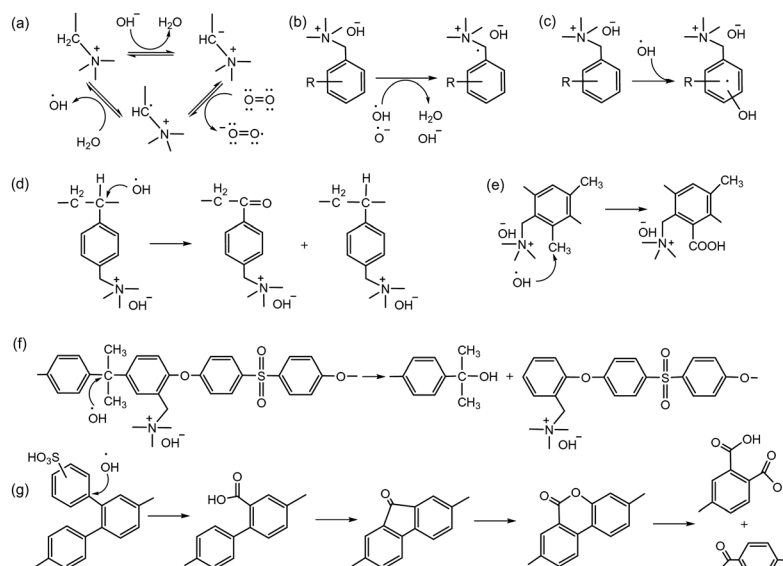
**Scheme 8** Degradation mechanisms by oxidative radicals: (a) reactive oxygen generation under high pH conditions, (b) electrochemical degradation of benzyltrimethyl ammonium by hydrogen abstraction, and (c) electrochemical degradation of benzyltrimethyl ammonium by radical addition. Different mechanism of radical-induced degradation of (d) the backbone of quaternized polystyrene, (e) quaternized PPO, (f) diphenyl isopropylidene unit of quaternized poly(aryl ether sulfone), and (g) sulfonated polyphenylene.

oxygen radicals can abstract hydrogen from vulnerable positions (Scheme 8b) or add to aromatic compounds, forming hydroxycyclohexadienyl radicals (Scheme 8c).[113] These oxidative radical species attack the vulnerable ternary carbon connected to the benzyltrimethyl ammonium hydroxide, resulting in chain scission (Scheme 8d).[114,115] The rate of chain scission increases with exposure to higher oxygen concentrations. Similar oxidation reactions can occur with the dimethyl phenyl group in quaternized PPO (Scheme 8e) and with the diphenyl isopropylidene unit, which has a higher electron concentration in quaternized poly(aryl ether sulfone)s (Scheme 8f). Holdcroft *et al.* showed that backbone chain scission of sulfonated polyphenylene and formation of benzoic acid can occur through hydroxyl radical-induced oxidative degradation

(Scheme 8g),[116] with the degradation mainly occurring in non-sulfonated phenyl rings rather than in electron-withdrawing sulfonic acid-containing phenyl rings. Unlike highly nucleophilic hydroxide ions, radicals generated in an electrochemical environment, such as HO• and H•, are electrophilic and tend to attack electron-rich sites of the substrate.[117] Consequently, AEPs with high electron density, such as those containing methoxy or piperidino groups, have lower resistance to radical-induced oxidation.[113] On the other hand, AEPs with electron-withdrawing groups possess a high electrophilic character and remain stable against oxygen radical attack.

Another critical oxidation process of AEPs is the catalytic oxidation of phenyl groups. The catalytic oxidation of benzene by transition metals and carbon-based catalysts under oxidative
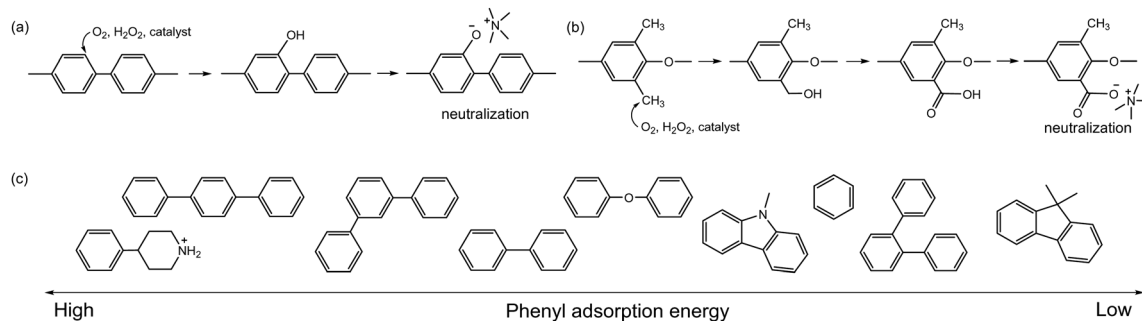
This journal is © The Royal Society of Chemistry 2024

*Chem. Soc. Rev.*, 2024, **53**, 5704–5780 | 5713

**Fig. 6** Electrochemical oxidation: (a) phenyl oxidation to form phenol, (b) methylphenyl oxidation to form carboxylic acid, (c) phenyl adsorption energy of polyaromatic fragments on Pt(111) surface. The adsorption energy was calculated by density functional theory (DFT) using optPBE-vdW.

conditions is well documented.[118–121] The electrochemical oxidation of phenyl groups to form phenol has been observed in quaternized poly(biphenyl) AEPs in AEMFC and AEMWE after prolonged operation at high cell voltages (0.9 V for AEMFC and 2.1 V for AEMWE) (Fig. 6a).[122,123] Electrochemical oxidation of methylphenyl by noble metal catalysts has also been reported[124–126] and may occur under the operating conditions of the device with applied voltages.[127] The electrochemical oxidation of methylphenyl groups to form benzoate was observed with quaternized PPO AEPs in AEMWE, which substantially increased the degradation rate at the anode of the AEMWE (Fig. 6b).[93,128] With electrochemical oxidation potentials, other AEP fragments can also degrade under device operating conditions (Fig. 7). For example, the electrochemical oxidation of cyclic alkanes and cyclic olefins, such as norbornene, occurs at approximately 1.0 V, resulting in the production of cycloaliphatic ketones and aliphatic (di)carboxylic acids.[129] The electrochemical oxidation of heterocycles occurs at around 1.5 V or higher, depending on the chemical environments.[130–132]

The detection of electrochemical oxidation products is challenging since the oxidation occurs at the catalyst and ionomer interface. However, the impact of electrochemical oxidation on device performance can be significant because the oxidative products can lower the local pH near the catalyst's active site. The device operating potential and the adsorption energy of the phenyls and other AEP fragments onto the catalyst surface are the two most important factors for catalytic oxidation. Consequently, AEPs in the electrodes that are exposed to high potentials, such as those in the anode of AEMWEs and CO$_2$ electrolysers, are much more vulnerable to the catalytic oxidation of AEPs. Matanovic et al. investigated the adsorption

energy of the phenyl groups derived from AEP fragments (Fig. 6c) and found that more durable device performance was achieved with ionomers having lower phenyl adsorption energy.[133,134] The adsorption behaviours of ionomers are also significantly influenced by the type of catalysts and their surface and electronic structures. Matanovic et al. noted that Pt alloyed catalysts exhibit less aromatic adsorption characteristics, attributed to electron transfer between phenyl and metal surfaces induced by alloying.[135] The same research group observed that the adsorption energy of benzyltrimethyl groups on the surface of the La$_{0.85}$Sr$_{0.15}$CoO$_3$ perovskite catalyst was substantially lower than on Pt or IrO$_2$ catalysts.[122]

### 2.6. Demand for aryl ether-free AEPs

The literature survey in the previous sections suggests that the degradation pathways of AEPs are dependent upon the operating conditions of electrochemical devices. The two most critical factors are the pH environment and the electrode potential required for electrochemical reactions. In general, aryl ether-free polymers exhibit considerably higher oxidative stability than aryl ether-containing polymers.[136,137] For AEMFC, AEMWE, and electrochemical CO$_2$ conversion/capture devices, the alkaline stability of AEPs is most critical, and most aryl ether-containing AEPs lack chemical stability for durable operation in these applications. High electrochemical oxidative stability is required for AEMWE and CO$_2$ electrolyser/capture devices. Given that the nature of degradation by hydroxide ions (alkaline, nucleophilic) and hydroxyl radicals (oxidative, electrophilic) are different, AEPs with balanced chemical stability specific to an electrochemical device can enable long-term operation. AEIs in the catalyst layers require higher electrochemical oxidative stability compared to AEMs.[138] However, some
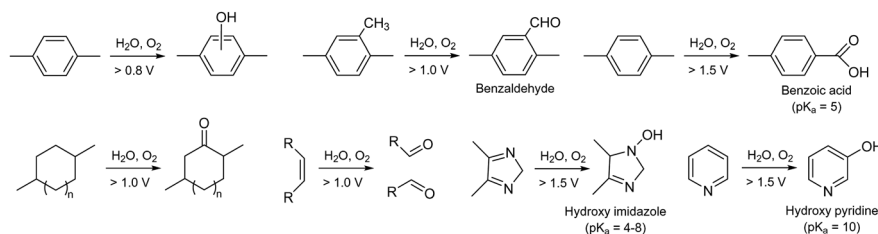


**Fig. 7** Electrochemical oxidation process and oxidation potentials of various ionomer fragments.

5714 | Chem. Soc. Rev., 2024, **53**, 5704–5780

This journal is © The Royal Society of Chemistry 2024

studies indicate that supplying a liquid alkaline solution to the electrode can mitigate the electrochemical oxidation of ionomers by reducing ionomer fragment adsorption.[122,139,140] Therefore, if an electrochemical device can incorporate a supplemental liquid alkaline solution, the requirements for electrochemical stability may be less stringent.

The chemical stability studies on AEPs indicate that aryl ether-free AEPs are excellent candidates for various electrochemical devices. Alternative material candidates may include ion-solvating polymers with basic functional groups, such as benzimidazole. Reasonably high performance and durability of ion-solvating membranes have been demonstrated in RFB,[141–144] HT-PEMFC,[145–147] and electrolyser[148–151] applications. However, these polymers can only be used in electrochemical devices supplying liquid electrolytes, which have additional stability issues associated with highly concentrated liquid electrolytes. Therefore, aryl ether-free AEPs remain a strong contender for use in modern electrochemical devices. In the following sections, we will discuss various synthetic pathways that have been implemented to prepare cation-functionalized aryl ether-free AEPs, demonstrating outstanding material properties, chemical stability, and successful performance in electrochemical devices.

# 3. Chemistry of polyaromatics

Polyaromatics are a class of polymers whose main chains are composed of phenylene units. They are best known for their excellent thermal and mechanical properties, making them suitable for various applications. The most promising design of polyaromatics for high chemical stability and longevity in alkaline conditions involves backbones that are devoid of labile aryl ether linkages, predominantly consisting of C–C bonds.[152] In this section, we will focus on the notable chemistry of polymerization used to prepare quaternized aryl ether-free polyaromatics. This includes the reaction mechanism, the representative AEPs from each method, and their general properties for electrochemical devices.

## 3.1. Acid-catalysed polyhydroxyalkylation

For the synthesis of AEPs, it is desirable to have a polymerization method that leads to high molecular weight growth, allows for various monomer choices, and is tolerant of any functional groups present. Acid-catalysed polyhydroxyalkylation offers many advantages in these factors with respect to other reactions and has been widely adopted for the synthesis of aryl ether-free polyaromatic-based AEPs in recent years.

When strong Brønsted or Lewis acids interact with electrophiles and undergo superelectrophilic activation, they can form highly reactive electron-deficient compounds known as superelectrophiles.[153] The early demonstrations of superelectrophiles for Friedel–Crafts alkylation used selective carbonyl compounds, including benzaldehyde, and electron-rich aromatics.[154] The enhancement of the reactivity of carbonyl electrophiles heavily depends on the acidity of the system;
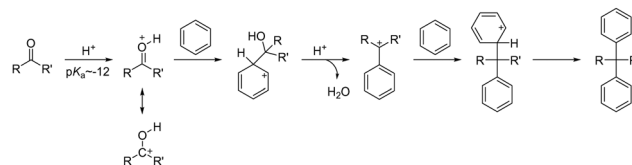


Scheme 9  General reaction mechanism of acid-catalysed Friedel–Crafts hydroxyalkylation.

while 100% sulfuric acid ($pK_a = -12$) is not sufficiently strong to activate most carbonyl compounds, superacids such as trifluoromethanesulfonic acid (TFSA, $pK_a = -14$) or even stronger acids are required. During the reaction, a carbonyl compound is protonated by high acidity proton donating species, forming extremely electron deficient carboxonium/hydroxycarbenium intermediates that react with nucleophilic aromatics via hydroxyalkylation (Scheme 9).[155]

The reactivity of electrophiles can be further increased by the presence of electron-withdrawing substituents, such as trifluoromethyl or nitro groups, in close proximity to the carbonyl group. An electronegatively substituted carbonyl compound was used to form a linear, high molecular weight, yet still soluble polymer using an aromatic hydrocarbon in a superacid environment via polyhydroxyalkylation.[156] Several carbonyl-containing compounds and aromatic compounds were screened for their reactivity in a superacid medium to form high molecular weight polymers (number-averaged molecular weight, $M_n$, $> 50$ kg mol$^{-1}$).[155,157–159] According to the proposed mechanism, based on theoretical and experimental studies,[155,159] the substituents of carbonyl compounds (R and R′ in Scheme 9) influence the rate-determining step of polymerization, which can be either the aromatic electrophilic substitution or the subsequent dehydration reaction. Strong electron-withdrawing groups on both substituents can increase the electrophilicity of the carbonyl carbon, allowing for a fast reaction with an aromatic compound, but they may also increase the activation energy required for the formation of carbocation from dehydration, thus slowing down the rate of polymerization. Therefore, a number of ketone monomers containing a trifluoromethyl group along with an electron-donating methyl or phenyl group (e.g., trifluoroacetone and trifluoroacetophenone) have been used for the formation of ultrahigh molecular weight polymers ($M_n > 10^6$ g mol$^{-1}$).[158]

In the case of aromatic monomers, H–Ar–H, the nucleophilicity of the aromatic compound is another factor that determines the polymerization rate.[160] Highly nucleophilic aromatic compounds lead to the continuous growth of polymer chains via this step-growth polymerization by reacting with carbonyl electrophiles. Symmetrical and electron-rich phenyl compounds, such as biphenyl, p-terphenyl, and diphenyl ether, are typically used to enable the formation of high molecular weight polymers. Depending on the reactivity of the monomers, the stoichiometric ratio between carbonyl and aromatic monomers can be adjusted to increase the polymerization rate, but a large excess of one monomer over the other may result in low molecular weight polymers or cross-linking.[160] Anhydrous
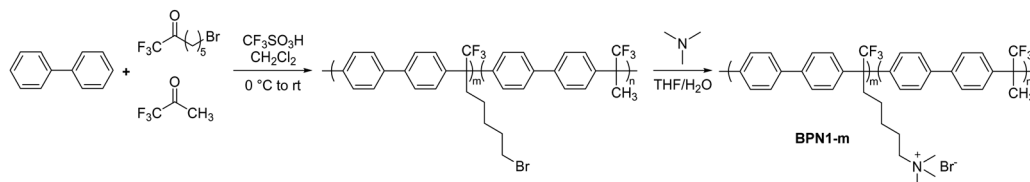
**Scheme 10** Representative reaction schematic of acid-catalysed polyhydroxyalkylation to synthesize biphenyl-based AEP BPN1-m.

dichloromethane is mainly used as a polymerization solvent due to its inertness towards strong acids and its solvating power for most of the monomers utilized.

The first report using the acid-catalysed polyhydroxyalkylation chemistry to produce AEPs was in 2015 by Bae *et al.* They employed biphenyl and a ketone monomer containing a bromoalkyl precursor for subsequent quaternization using trimethylamine (BPN1-m, Scheme 10).[161] Alkylhalide is tolerant in a superacid environment; although the reactivity of a bromoalkyl-containing ketone monomer is lower than that of trifluoroacetone, the polymerization proceeds efficaciously, growing to high molecular weight polymers at room temperature in 12 hours ($M_n$ > 70 kg mol$^{-1}$ and weight-averaged molecular weight, $M_w$, >100 kg mol$^{-1}$). Copolymers bearing a repeat unit of biphenyl and non-functional trifluoroacetone have been prepared to adjust the IEC of the polymers (1.5–2.6 mequiv. g$^{-1}$). Despite being composed of rigid aromatic rings, the polyaromatic-based AEPs from the superacid-catalyzed polyhydroxyalkylation, such as BPN1-m, are readily soluble in common organic solvents due to the insertion of a kinked $C_{sp^3}$ in every repeating unit. The quaternized polymers have high solubility in polar aprotic organic solvents for easy processability, and high tensile strength (up to 35 MPa at 50 °C, 50% relative humidity (RH)). The hydroxide conductivity at 80 °C of BPN1-100 (IEC = 2.6 mequiv. g$^{-1}$) was 122 mS cm$^{-1}$, with a water uptake of 145%.[161] The AEPs did not show any change in IEC values or hydroxide conductivity after immersion in 1 M NaOH at 80 °C for 30 days, demonstrating high chemical stability in an alkaline environment and opening up the possibility of using this chemistry for the synthesis of alkaline stable AEPs.

Since then, various combinations of monomer choices for both aromatic and carbonyl monomers have been utilized to form AEPs in recent years, as summarized in Fig. 8.[66,71,162–175] Most polymerization reactions have been done in one-pot mode to obtain precursor polymers, either containing bromoalkyl or tertiary amine groups, followed by quaternization using a tertiary amine or alkylation using an alkyl bromide to form their corresponding AEPs. The high tolerance of the acid catalyst allows the inclusion of cation- and secondary amine-containing monomers, which can be used as AEPs once polymerized[71,169,172,174] or simply quaternized *via* a post-grafting reaction using alkyl ammoniums.[176] For the superacid catalysts, TFSA alone or in combination with trifluoroacetic acid (TFA) has been used for polymerization, where TFA can serve as a solvent medium, covering a wide range of acidity to increase the reactivity of monomers.[177] The ratio of the ketone
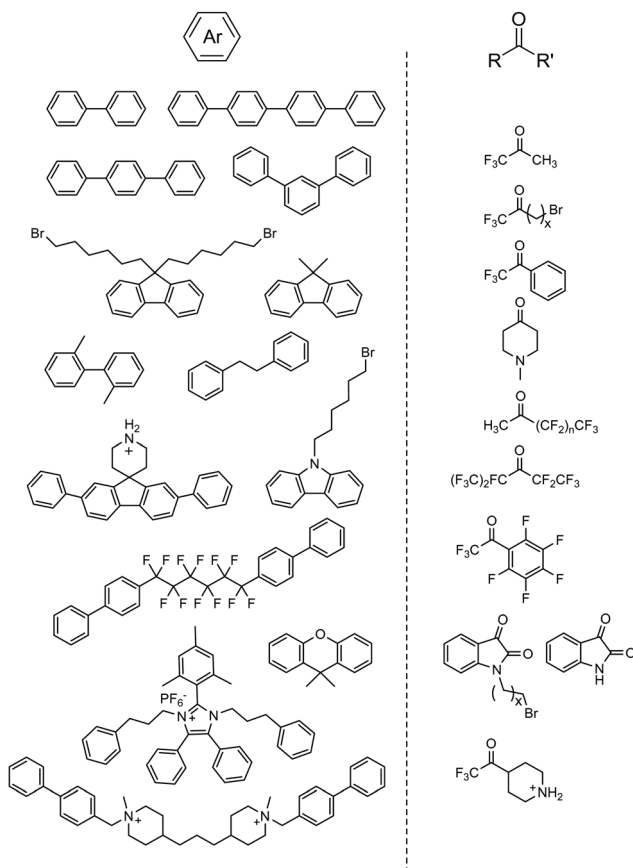


**Fig. 8** Representative aromatic hydrocarbon and carbonyl-containing monomers used for acid-catalysed polymerization.

monomer varies depending on the reaction conditions and electrophilic reactivity, but it is nearly stoichiometric with respect to aromatic monomers (approximately 1.0–1.2 equivalents of the carbonyl monomer for superelectrophilic activation; up to 1.5 equivalents for less reactive monomers[173]). To promote molecular weight growth of polymers for membrane applications, non-functional high-reactivity monomers (*e.g.*, *p*-terphenyl, 2,2,2-trifluoroacetophenone) have been incorporated as repeat units of copolymers. Poly(terphenyl piperidinium) with 85% ionic repeat units exhibits a much higher molecular weight (intrinsic viscosity 4.71 dl g$^{-1}$, $M_w$ = 70.5 kg mol$^{-1}$)[166] compared to the terphenyl piperidinium homopolymer (0.39 dl g$^{-1}$) (Fig. 9a).[66]

The effect of the polymer backbone arrangement and morphology on membrane properties was investigated using two

5716 | *Chem. Soc. Rev.*, 2024, **53**, 5704–5780

This journal is © The Royal Society of Chemistry 2024

Fig. 9 Selected examples of polyaromatic-based AEPs synthesized by acid-catalysed polyhydroxyalkylation: (a) poly(terphenyl piperidinium) copolymer, (b) poly(terphenyl alkylene)s, (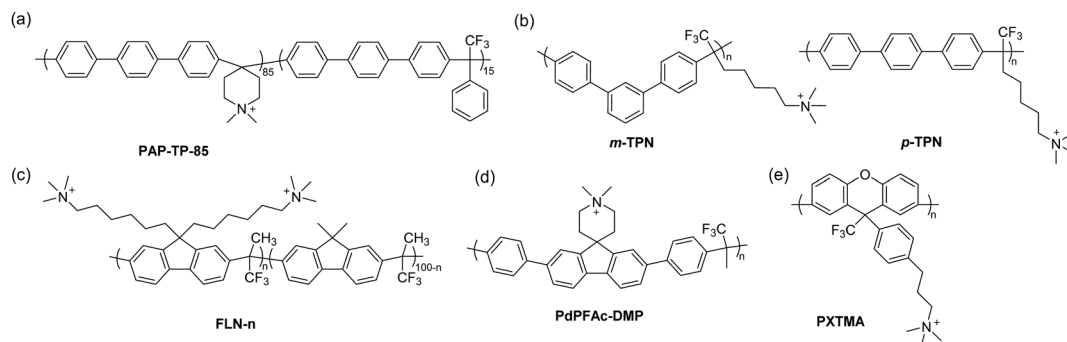c) bis-quaternary ammonium functionalized fluorene-based AEPs, (d) *N*-alicyclic cation-containing polyfluorene, and (e) polyxanthene-based AEPs.

different terphenyl monomers, *p*-terphenyl and *m*-terphenyl, to synthesize their respective AEMs (Fig. 9b).[163] *m*-TPN, consisting of *meta*-terphenyl in the backbone, exhibited higher molecular weight, better solubility, water uptake, hydroxide conductivity, and fuel cell performance in AEMFC than *para*-terphenyl containing *p*-TPN. This improvement is ascribed to the favourable morphology and polymer chain packing for ion transport, as confirmed by wide-angle X-ray scattering, likely from the kinked structure of *m*-terphenyl.[163] The alkaline stability of *m*-TPN (IEC = 2.2 mequiv. g$^{-1}$) was found to be higher than that of BPN1-100. It showed no signs of degradation in the $^1$H NMR spectrum and titrated IEC in 1 M NaOH at 95 °C for 60 days, while a slight decrease was observed in BPN1-100 under the same condition, likely due to the higher IEC (2.6 mequiv. g$^{-1}$).[178]

9,9-Bis(6-bromohexyl)fluorene has been a popular choice for the aromatic component in AEPs because it allows the inclusion of two quaternary ammonium groups per repeat unit, increasing the resulting IEC of the polymer up to 3.5 mequiv. g$^{-1}$ when polymerized with trifluoroacetone (Fig. 9c).[164] The ionic repeat unit was optimized to be 55% by incorporating non-functionalized 9,9-dimethylfluorene as a co-monomer, adjusting the IEC to 2.5 mequiv. g$^{-1}$, which showed a high hydroxide conductivity of 127 mS cm$^{-1}$ at 80 °C. Fluorene-based AEPs also have the advantage of being effective electrode AEIs, as their fused ring structure has minimal adsorption energy to the surface of electrocatalysts compared to other phenyl-containing monomers, such as biphenyl.[134] This offers benefits of high oxidative stability of AEIs, especially for electrochemical devices operated at high voltage conditions.[122,123] The wide range of IECs of fluorene-based ionomers can aid in controlling water management in electrodes or operate at low RH conditions by using an asymmetric electrode approach.[179] Recently, fluoroalkyl-containing fluorene ionomers were reported to effectively control electrode hydrophobicity for appropriate water management in AEMFCs.[173] The downsides of employing fluorene in the AEP structure would be that the monomer synthesis to include the bis(bromohexyl) group requires tedious purification steps,[164] and AEMs using only fluorene as an aromatic monomer tend to result in brittle

membranes, likely due to the bulky structure of fluorene interfering with chain entanglement.

Because of the high regioselectivity of the polymerization, using aromatic monomers containing unsubstituted terminal phenyl groups is highly effective. An *ortho*-methyl substituted biphenyl, designed to increase the fractional free volume of the polymer chains for efficient hydrogen diffusion on the anode electrode, did not form sufficiently high molecular weight polymers, unlike its unsubstituted biphenyl counterpart.[165] Several studies reported the polymerization of aromatic monomers having electron-deficient groups, such as unsubstituted phenyl rings at both terminal positions. With this approach, even aromatic monomers that are challenging to polymerize, *i.e.*, those containing electron-deficient substituents or ionic moieties that affect electron density, can be used in acid-catalysed polymerization. Miyatake and co-workers reported perfluorohexylene-containing AEMs by synthesizing a fluorinated monomer bearing terminal biphenyl groups.[175] The AEM exhibited a well-defined phase-separated morphology due to the incorporation of the hydrophobic perfluorohexylene group in the backbone and showed high hydroxide conductivity (115 mS cm$^{-1}$ at 80 °C, IEC = 2.0 mequiv. g$^{-1}$). The membrane properties remained unchanged after immersion in 8 M KOH at 80 °C for 1000 hours, confirming that the phenylene-based backbone with a perfluoroalkyl moiety is highly alkali stable. Jannasch *et al.* prepared an *N*-alicyclic cation-containing fluorene monomer with terminal phenyl groups, which directly produced AEMs incorporating a piperidinium cation (Fig. 9d).[174] PdPFAc-DMP with an IEC of 1.9 mequiv. g$^{-1}$ showed a hydroxide conductivity of 84 mS cm$^{-1}$ at 80 °C with a water uptake of 57%. Indications of cation degradation were observed in the $^1$H NMR spectra after immersion in 1 M NaOH at 80 °C for 30 days, occurring in the piperidinium ring attached to the fluorene backbone. Zhang and co-workers demonstrated the direct polymerization of an imidazolium-containing monomer fully substituted with phenyl groups, sequentially polymerized with additional biphenyl and trifluoro-acetone to form ionene segmented block copolymers (more about ionenes in Sections 3.3 and 3.4).[172] The AEM exhibited a hydroxide conductivity of 57 mS cm$^{-1}$ at 80 °C with an IEC of

This journal is © The Royal Society of Chemistry 2024

*Chem. Soc. Rev.*, 2024, **53**, 5704–5780 | 5717

1.2 mequiv. g$^{-1}$. Similarly, Wang *et al.* synthesized a bis-piperidinium monomer with terminal biphenyl groups, polymerizing it with a superacid to form poly(bis-alkylimidazolium) ionenes (IEC = 2.3 mequiv. g$^{-1}$, $\sigma_{80°C}$ = 45 mS cm$^{-1}$).[180] The approach of using terminal phenyl groups expands the library of aromatic monomers available for polymerization, but the downside of this approach might be that aromatic monomers need to be prepared *via* metal-catalysed coupling reactions[165,175] or *via* multistep synthesis.[172,174]

Superacid catalysts are also effective for the synthesis of another type of polyaromatic, polyxanthene, where its backbone is composed of a pyran ring fused with two phenyl rings.[181] This tricyclic aromatic structure in the polymer backbone may exhibit intrinsic microporosity, favouring both ion and gas transport.[182] 4,4'-Biphenol and bromopropyl trifluoroacetophenone were polymerized *via* polyhydroxyalkylation followed by cyclodehydration to form xanthene, which was then converted into AEMs with a tertiary amine (Fig. 9e).[182] Although the polymer contains C–O–C bonds as part of the main chain, no sign of backbone degradation was detected after immersion in 1 M NaOH at 80 °C for 720 hours, likely due to the absence of electron-withdrawing groups near the aryl ether bonds. The TMA-containing AEM, PXTMA, showed the highest IEC of 2.3 mequiv. g$^{-1}$ and hydroxide conductivity of 129 mS cm$^{-1}$ at 80 °C among the reported polyxanthene AEMs. Another polyxanthene-based AEP, synthesized using 9,9-dimethylxanthene and isatin with TFSA, was subsequently functionalized using bromobutyl trimethylammonium bromide.[183] The hydroxide conductivity at 80 °C of this AEM with an IEC of 2.1 mequiv. g$^{-1}$ was found to be 205 mS cm$^{-1}$, ascribed to the twisted, intrinsically microporous arrangement of the xanthene backbone for efficient ion transport, as confirmed by microstructure characterization using atomic force microscopy (AFM) and small-angle X-ray scattering (SAXS).

To enhance the mechanical properties of polymers for membrane applications, various branching and crosslinking strategies have been employed for acid-catalysed AEPs. A branched AEM was reported using 2.5% of 1,3,5-triphenylbenzene as a branching node with *p*-terphenyl and *N*-methyl piperidine for polymerization. The resulting cast thin films (20 μm) exhibited improved membrane properties compared to previously reported terphenyl piperidinium-based AEMs.[184] Other strategies include using the thiol–ene click reaction with a hexane-tethered piperidine polymer and a dithiol compound[185] and *in situ* crosslinking of 9-vinylcarbazole during polymerization with *N*-methyl piperidine.[186]

Acid-catalysed polyhydroxyalkylation can be done in a one-pot, metal-free condition at low to room temperature to produce highly conductive and alkaline-stable AEPs. The acid catalyst is tolerant to various monomers with functionality including haloalkyl, amine, and even quaternary ammonium, but the strong acidity and hygroscopic nature of TFSA may restrict the choice of reactors, especially for larger-scale reactions. It is also important to note that successful superelectro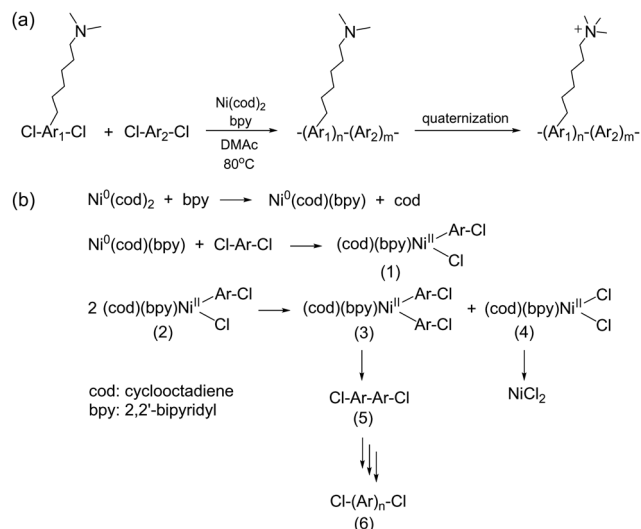philic activation for high molecular growth of polymers can primarily be achieved by trimethylfluoro-containing carbonyl compounds, with only a few exceptions, which limits the choice for synthesizing non-fluorinated AEPs. Nevertheless, this polymerization method has led to the development of several commercially available products, such as PiperION by Versogen and TM1 by Orion Polymer, demonstrating its practical utility for various applications.

## 3.2. Metal-promoted coupling reaction

Metal-promoted C–C coupling reactions have been used to prepare phenylene-based polymers carrying quaternary ammonium precursors, such as halides or tertiary amino groups. Classical Ullmann-type condensation reactions, which have been used to prepare polyaromatics utilizing copper catalysts,[187] require high reaction temperatures. However, the yield and selectivity are often insufficient for polymer synthesis, even with the most reactive aryl iodide. Among various metal promoters/catalysts for coupling reactions, Ni(0) is the most promising in terms of the reactivity and selectivity for intermolecular C–C coupling reactions or reductive dehalogenative polycondensation, and thus, has been utilized for the formation of high-molecular-weight polyaromatics. Typically, Ni(0) is used as complexes with organic ligands such as cyclooctadiene (cod) and triphenylphosphine (PPh$_3$) because of their stability in inert conditions, easy handling, high reactivity, and good solubility in organic solvents, although they are expensive and require high purity. Ni(cod)$_2$ is one of the most extensively used polymerization promoters as it can be used with aromatic chlorides, which are usually less reactive than bromides and iodides but are more versatile and widely available. In addition to functionalized polyphenylene-based ionomers, quaternized polyaromatics containing heterocyclic groups (*e.g.*, poly(arylimidazoliums)) have also been prepared *via* Ni(0)-mediated coupling reaction (refer to Scheme 16 in Section 3.4).

A general synthetic scheme of polyaromatics used in AEPs, utilizing Ni(0)-promoted coupling reactions, is shown in Scheme 11a.[188–203] Typically, pre-aminated, tertiary amino group-containing aromatic monomers and hydrophobic aromatic monomers are copolymerized. The polymerization reaction usually proceeds rapidly and quantitatively within 3–8 hours at 80 °C in polar aprotic solvents such as DMSO and DMAc. During the reaction, Ni(cod)$_2$ undergoes ligand exchange with 2,2'-bipyridine (bpy), which then oxidatively reacts with aryl chlorides to form adducts (1) (Scheme 11b).[204,205] The complexes form bisaryl complexes (2) and dichloro complexes (3) through a disproportionation reaction. The former yields the corresponding biaryl as the dimer (4), while the latter provides NiCl$_2$. The successive reaction from (1) to (5) provides precursor polymers (6), which are then quaternized to produce the final AEP products. As the polymerization reaction is based on oxidative addition, and Ni(0) is recovered as Ni(II) or NiCl$_2$, a stoichiometric amount of Ni(cod)$_2$ is required as a promoter, as it does not provide high molecular weight polymers with catalytic amounts. In fact, an excess of Ni(cod)$_2$, often 1.5 to 2 times

(a)



(b)

$$Ni^0(cod)_2 + bpy \longrightarrow Ni^0(cod)(bpy) + cod$$

$$Ni^0(cod)(bpy) + Cl\text{-}Ar\text{-}Cl \longrightarrow (cod)(bpy)Ni^{II}\begin{matrix}Ar\text{-}Cl\\Cl\end{matrix}$$
(1)

$$2\ (cod)(bpy)Ni^{II}\begin{matrix}Ar\text{-}Cl\\Cl\end{matrix} \longrightarrow (cod)(bpy)Ni^{II}\begin{matrix}Ar\text{-}Cl\\Ar\text{-}Cl\end{matrix} + (cod)(bpy)Ni^{II}\begin{matrix}Cl\\Cl\end{matrix}$$
(2)　　　　　　　　　　　　　(3)　　　　　　　　(4)

cod: cyclooctadiene
bpy: 2,2'-bipyridyl

Cl-Ar-Ar-Cl　　　NiCl$_2$
(5)

Cl-(Ar)$_n$-Cl
(6)

**Scheme 11** (a) Synthesis of polyaromatic-based AEPs *via* a Ni(0)-promoted coupling reaction and (b) polymerization mechanism of poly-aromatics promoted by Ni(cod)$_2$.

the equimolar amount, is typically utilized for efficient polymerization due to its susceptibility to water and oxygen in the environment.

The IEC of the resulting AEPs can be tailored for different applications by adjusting the molar ratio of repeating units. These units are composed of hydrophilic components containing pendent quaternary ammonium groups and hydrophobic aromatic units. AEPs are commonly prepared from tertiary aminated monomers (*e.g.*, containing dimethylaminoalkyl or alicyclic aminoalkyl groups) as precursors for the quaternized ammonium groups. These groups do not interfere with the Ni(0)-promoted aryl halide insertion reactions and remain intact during the polycondensation reactions. The tertiary amino groups are readily quaternized by a typical Menshutkin reaction with alkyl halides. For the methylating reagent, although methyl iodide is most commonly used, dimethyl sulfate is sometimes preferable despite its carcinogenic properties, since trace amounts of iodide ions could remain in the AEPs even after subsequent ion exchange reactions, which may deteriorate some of the favourable properties of the resulting AEMs.

Another approach for producing polyaromatic-based quaternized AEPs involves chloromethylate precursor copolymers that contain electron-rich phenylene rings, followed by a reaction with tertiary amines to introduce quaternary ammonium groups. This method is versatile and has been widely practiced with many polyaromatics, as aromatic groups (without electron-withdrawing groups) are reactive in electrophilic Friedel–Crafts reactions using chloromethyl methyl ether. However, as mentioned in Section 2, the toxic nature and technical problems of using chloromethyl methyl ether make this approach less attractive compared to using tertiary aminated monomers. Alternatively, *in situ* generation of chloromethyl groups using paraformaldehyde, trimethylchlorosilane and

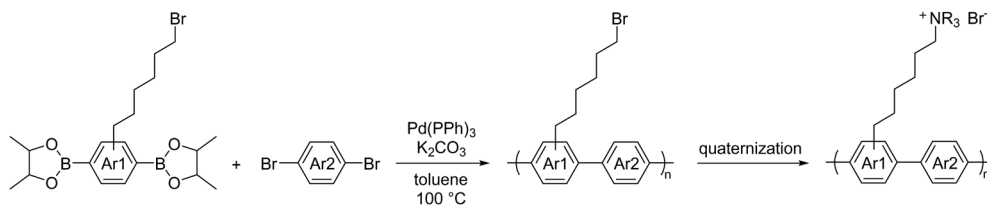Lewis acid catalyst, such as tin chloride, has been also used for AEP synthesis.[206]

The molecular weight of the polyaromatic-based precursor copolymers, as measured by gel permeation chromatography (GPC), typically falls within the range of several tens of thousands for $M_n$ and several hundreds of thousands for $M_w$. These copolymers often have a somewhat higher molecular weight distribution, or polydispersity index (PDI), which is likely due to the relatively rapid polymerization reaction promoted by Ni(0). Typical PDIs are around 4 but can be higher than 10, depending on the reactivity of the monomer and the polymerization conditions. The coupling reaction can produce polymers with sufficiently high molecular weights to afford thin flexible membranes by solution casting. Since the Ni(0)-promoted aryl C–C coupling reaction is very fast and many aryl chloride monomers are highly reactive, the resulting copolymers are randomized rather than sequenced, even when there are considerable differences in the reactivity of the comonomers. Terpolymers composed of two different hydrophobic components, introduced to include additional functionality, have also been investigated.[201,203] Furthermore, some semi-block copolymer AEPs have employed pre-synthesized telechelic (chlorine-terminated) hydrophobic oligomers, which were then copolymerized with hydrophilic monomers.[207] In most cases, traces of metal catalysts can be easily removed by appropriate workup with mineral acids (*e.g.*, hydrochloric or nitric acid) after the polymerization reaction to the level that does not affect the properties of the resulting membranes and the performance/durability of the devices.

A remaining challenge of using the Ni(0)-promoted coupling reaction for the synthesis of polyaromatic-based AEPs is enabling the polymerization reaction with catalytic, or less than stoichiometric, amounts of costly Ni(cod)$_2$. One report reveals that the amount of Ni(cod)$_2$ could be reduced to half of the conventional amount by using excess bpy ligands.[205] Another approach involves using ZnX$_2$, where X = Cl or Br, as a catalyst in the presence of reducing agents (*e.g.*, Zn powder) and ligands (such as bpy or PPh$_3$). In this method, the *in situ* reduction of Ni(II) to Ni(0) and ligand exchange reactions produce reactive Ni(0) species (Scheme 12). Iodide-containing additives, like NaI or Et$_4$NI, also facilitate the reduction of Ni(II).[205] The
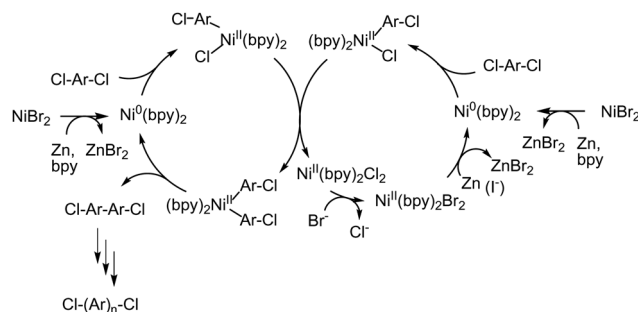


**Scheme 12** Possible polymerization mechanism for the synthesis of polyphenylenes from dichloroaromatics catalysed by Ni(II) in the presence of Zn as a reducing agent.

This journal is © The Royal Society of Chemistry 2024

*Chem. Soc. Rev.*, 2024, **53**, 5704–5780 | 5719

**Scheme 13** Synthesis of polyaromatic-based AEPs *via* Suzuki coupling reaction using Pd(0) catalyst.

polymerization is effective for non-ionic monomers, yielding corresponding high molecular weight polyaromatics, but it is less successful with functionalized monomers, such as those that are brominated or tertiary aminated. Employing appropriate protecting groups may prevent side reactions and increase the reactivity of these functional monomers, although the accompanying protecting and deprotecting reactions are cumbersome.

A few other metal-promoted polymerization reactions have been developed for AEPs. The most successful and promising one is based on Suzuki coupling using Pd(0) catalyst.[162,208,209] The polymerization reaction requires dibrominated and diboronic acid (or in many cases, as pinacol boronate, Bpin) aromatic compounds as reactive monomers. It proceeds quantitatively with a catalytic amount (*ca.* 2 mol% of the total monomers) of $Pd(PPh_3)_4$ under basic conditions. A typical polycondensation reaction shown in Scheme 13 is carried out in toluene at 100 °C for 1.5 to 5 days to provide the pendent brominated precursors ($M_w$ = *ca.* 30 to 80 kg mol$^{-1}$, PDI = *ca.* 2–3). These precursors are then quaternized with tertiary amines, such as trimethylamine and methylpiperidine to obtain desired AEPs with targeted IECs.

Fig. 10 lists some recent polyaromatic-based AEPs that have been synthesized *via* metal-promoted polycondensation reactions, most commonly using Ni(cod)$_2$. Fluorenyl groups are often employed as hydrophobic components and/or scaffolds

for pendent ammonium groups since the halogenated fluorenyl monomers are readily available and highly reactive in both Ni(0)- and Pd(0)-promoted polymerization reactions. The hydrophobic groups are often partially fluorinated to augment the differences in hydrophobicity between the units. This approach helps to develop a phase-separated morphology, creating efficient ion transport pathways.[188,197]

Most polyaromatic-based AEMs exhibit high anion conductivity in water within the temperature range of 20–80 °C. Fig. 11 plots water uptake and hydroxide ion conductivity (both measured at 30 °C in water) as a function of the IEC obtained by titration for recent polyaromatic-based AEMs. These membrane samples feature various main chain and side chain structures, ionic groups, and copolymer/terpolymer compositions. The water uptake demonstrates a roughly linear relationship with the IEC, where two distinct trend lines are observed (Fig. 11a). The trend line with higher slope corresponds to AEMs containing perfluoroalkyl groups (*i.e.*, QPAF-1,[188] QPAF-4,[192] and BAF-QAF[197]) as hydrophobic component, while the lower slope line is of those containing alkyl and fluorenyl hydrophobic groups (*i.e.*, PFB+,[162] PFF+,[162] PFBFF+,[162] PFPE,[208] and PFPB[209]). An interesting and counterintuitive finding is that AEPs with more hydrophobic perfluorinated main chains tend to show higher water uptake. The hydroxide ion conductivity of the membranes does not show a strong correlation with the IEC (Fig. 11b). In fact, the highest conductivity (89 mS cm$^{-1}$) is
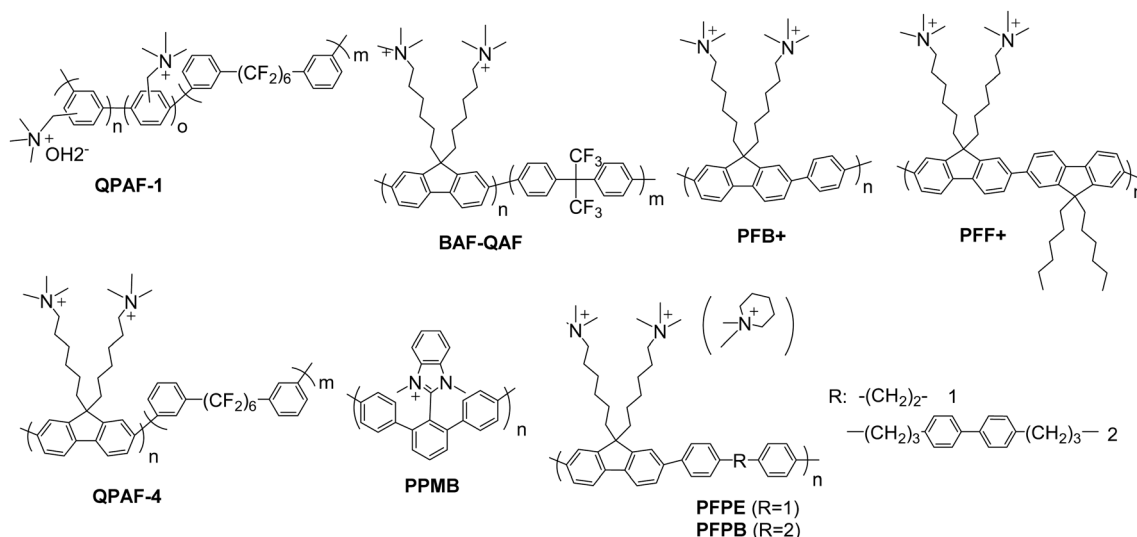


**Fig. 10** Selected examples of polyaromatic-based AEPs synthesized *via* metal promoted polycondensation (PFBFF+ of which structure is not shown is a copolymer of PFB+ and PFF+).
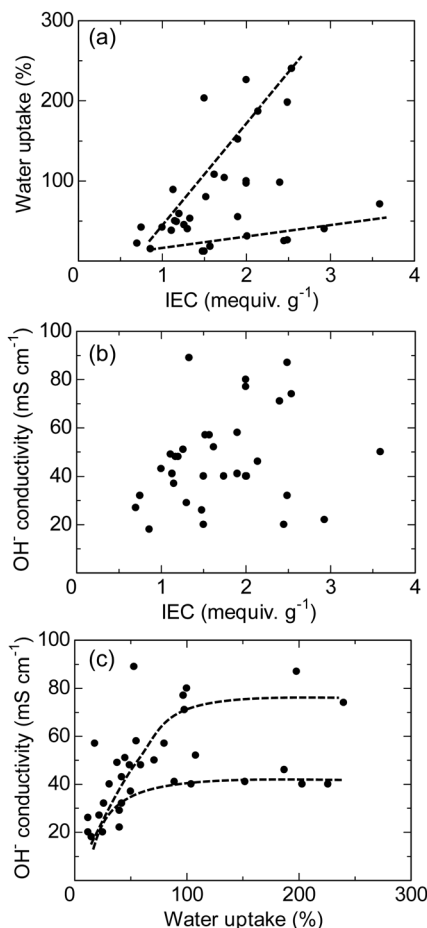
5720 | *Chem. Soc. Rev.*, 2024, **53**, 5704–5780

This journal is © The Royal Society of Chemistry 2024

**Fig. 11** (a) Water uptake, (b) hydroxide conductivity as a function of the IEC, and (c) hydroxide ion conductivity as a function of water uptake for Ni-catalysed polyaromatic-based AEMs (the data were measured at 30 °C).[162,188,192,193,197,208,209]

exhibited by the QPAF-1 membrane, which has a relatively low IEC of 1.33 mequiv. g$^{-1}$.[193] The conductivity appears to be more closely related to the water uptake (Fig. 11c), where two different trend curves are obtained, similar to the water uptake/IEC relationship. Both curves exhibit similar conductivity plateaus when the water uptake exceeds approximately 100%, likely due to a dilution effect.

Polyaromatic-based AEMs exhibit Arrhenius-type temperature dependence for hydroxide ion conductivity in water, at least up to 80 °C, reaching conductivity values higher than 160 mS cm$^{-1}$. The activation energy, estimated from the slopes of the lines, is approximately 10–12 kJ mol$^{-1}$. Since the membranes absorb large amounts of water, and the absorbed water molecules are predominantly located in the vicinity of the ammonium groups or within the hydrophilic channels, it is reasonable to assume that the hydroxide ions migrate *via* the Grotthuss mechanism, including the H-bonding between water molecules/hydroxide ions.

The alkaline stability of AEPs synthesized by metal-promoted polycondensation reactions has been evaluated in hot (60–90 °C) and concentrated (1–10 M) alkaline solutions

(NaOH or KOH aqueous solution). A negligible decrease in conductivity was observed over one month or even longer under most conditions. However, in more concentrated solutions (*e.g.*, >8 M KOH), the conductivity gradually decreases by up to 20%[201] depending on the ammonium structure. Post-structural analyses, including $^1$H NMR spectra and mechanical properties, suggest that the aryl ether-free polyphenylene backbones prepared by metal-promoted coupling reactions remain stable in alkaline solutions even when the ammonium groups degrade to some extent. Despite the disadvantages, such as the requirement for dichloro-containing monomers, a stoichiometric amount of the Ni catalyst, or the use of an expensive Pd catalyst, metal-promoted polycondensation has been employed as a tool to demonstrate various structures of AEPs with high backbone chemical stability.

### 3.3. Ionenes by nucleophilic substitution

**3.3.1. Ammonium ionenes.** Ionenes are polymers containing quaternary nitrogen atoms integral to their backbone structure. Ionenes must not be confused with ionomers, which denote polymers containing both ionic and non-ionic units along the backbone. However, in the context of the present review, ionomers usually refer to AEPs employed in electrode layers. A wide variety of different ionenes can be prepared through repetitive Menshutkin reactions, for example, between a dihalide and a nucleophilic tertiary diamine. This process leads to the quaternization of the amine and chain growth at each step. The first ionenes were reported in 1933 by Marvel *et al.*, who polymerized dimethylamino-*n*-alkyl halides to form corresponding polymeric products (Fig. 12a).[210] Subsequently, Rembaum and co-workers conducted polymerizations of tertiary diamines and dihalides, preparing and studying a range of different aliphatic ionenes (Fig. 12b).[211] During the same period, Salamone and Snider demonstrated the synthesis of ionenes using a rigid, cyclic tertiary diamine, specifically DABCO (Fig. 12c).[212] These early studies revealed that the choice of solvent is important for the polymerization rate in ionene synthesis, and that alkyl bromides are more reactive than alkyl chlorides. Achieving high molecular weights requires strict stoichiometric conditions, necessitating the use of pure monomers. Moreover, conditions must be carefully tailored to minimize potential side reactions, such as ring formation and the elimination of HBr.[213,214]

Following the pioneering work of Marvel and Rembaum, a large number of different aliphatic ionenes have been synthesized and studied, although most of these ionenes have not been utilized for membrane applications.[213–217] Due to their high chain flexibility and high ionic content, aliphatic ionenes are typically water-soluble and act as polyelectrolytes in solution.[213] Hence, in order to be employed as AEMs these ionenes need to be efficiently immobilized by, for example, blending[218–223] or through covalent coupling with hydrophobic polymers to form segmented block[224] or graft[225] copolymers. Besides ammonium ionenes, phosphonium-based ionenes have been prepared through nucleophilic substitution polymerizations of tertiary diphosphines and dibromoalkanes.[226]

This journal is © The Royal Society of Chemistry 2024

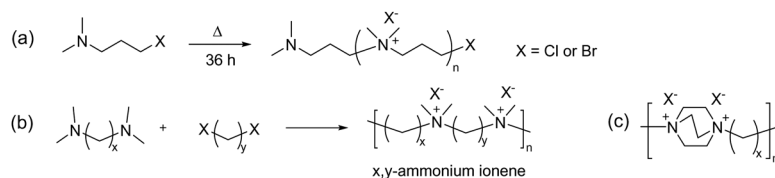*Chem. Soc. Rev.*, 2024, **53**, 5704–5780 | **5721**

Fig. 12 Early examples of ionenes: (a) the first ionene reported in 1933, (b) ionenes using different aliphatic chain lengths of dihalide and diamine monomers, and (c) ionene structure derived from DABCO.

However, these polymerizations are complicated because of the sensitivity of the diphosphites to air and water.[214] To date, no membrane properties of this type of ionenes have been reported.

**3.3.2. Spirocyclic ionenes.** Aliphatic and benzylic ammonium cations in linear ionenes are prone to degrade under alkaline conditions, resulting in both ionic loss and polymer backbone cleavage.[213,214] In this context, Marino and Kreuer have demonstrated that certain cycloaliphatic ammonium cations with low ring strain, particularly N-spirocyclic quaternary ammonium cations, display very high alkaline stability. It is attributed to the restrictions on the bond angles imposed by the ring configuration, which raises the activation energy of the transition state in the ionic degradation reactions.[57] As a result, N-spirocyclic ionenes ("spiro-ionenes") have become attractive for application as AEMs.[48,227]

Early work by Müllen et al. demonstrated the synthesis of a spiro-ionene employing benzobis(tetrahydropyrrole), a tricyclic secondary diamine, and 1,2,4,5-tetrabromomethylbenzene in a repetitive Menshutkin-type cyclo-quaternization reaction.[228] Because this reaction involves a secondary amine, it is necessary to employ a non-nucleophilic base to deprotonate the secondary amine to form the nucleophile. From the solubility properties, it was inferred that the ionomer had a rod-like shape and exhibited polyelectrolyte effects. Aiming to prepare AEM materials with high alkali stability, Jannasch and co-workers developed a cyclo-quaternization polymerization involving 1,2,4,5-tetrabromomethylbenzene and two different

secondary bis-piperidines using N,N-diisopropylethylamine (DIPEA) as the base to produce spiro-ionene 1 and 2, respectively (Fig. 13a).[218] Despite the potential side reactions, the cyclization reaction was very efficient, yielding high molecular weight polymer products ($M_n$ = up to 80 kg mol$^{-1}$) with IECs of 4.0–4.6 mequiv. g$^{-1}$ in quantitative yields after merely 1–2 hours. The spiro-ionenes were film-forming and thermally stable up to 300 °C, with no degradation detected by $^1$H NMR analysis after storage in 1 M KOD/D$_2$O at 80 °C. However, signs of degradation through ring-opening elimination and ring-opening substitution (Scheme 4d and e, respectively) emerged when the temperature was raised to 120 °C, with spiro-ionene 2 (10% total ionic loss after 336 hours) being more stable than spiro-ionene 1. The authors hypothesized that the flexible trimethylene bridge of the former ionene greatly facilitates ring relaxation compared to the latter.[218] Water-stable AEMs were obtained by blending spiro-ionene 2 with PBI to form ammonium-benzimidazolate complexes for ionic crosslinking under basic conditions (Fig. 13b). A transparent AEM blend containing 70 wt% spiro-ionene 2 gave a hydroxide conductivity of 120 mS cm$^{-1}$ at 90 °C.[218]

Li and co-workers prepared a family of ionenes based on biphenyl (PBP-ASN), naphthalene, and bi-naphthalene, respectively (Fig. 13c), and benchmarked the properties against spiro-ionene 2.[219] These spiro-ionenes combine 5-/6- and 6-/6-membered rings, respectively, in their spirocyclic arrangement, which are expected to influence the stability of the materials. Model compound testing and DFT calculations indicated that
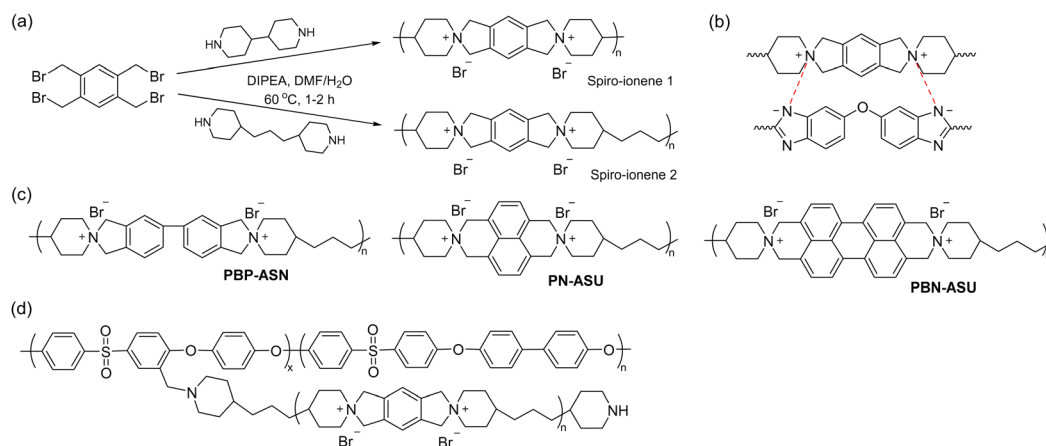


Fig. 13 Chemical structures of spirocyclic ionenes used for AEP: (a) spiro-ionenes from bis-piperidines, (b) ionic crosslinking of spiro-ionenes with PBI to form water-stable AEMs, (c) ionenes based on biphenyl, naphthalene and bi-naphthalene, respectively, and (d) the grafting approach of oligomeric ionene to polysulfone for AEM formation.

**5722** | Chem. Soc. Rev., 2024, **53**, 5704–5780

This journal is © The Royal Society of Chemistry 2024

the 5-/6-membered rings, originating from the tetrabenzylbrominated phenyl and biphenyl monomers, were more stable than the corresponding 6-/6-membered rings of the naphthalene-based monomers, probably due to the strongly electron-withdrawing effect of the naphthalene rings.[219] Additionally, the naphthalene-based monomers produced ionenes with lower molar masses than those derived from phenyl and biphenyl monomers. Ionically crosslinked blends based on spiro-ionene 2 and PBP-ASN, each containing 20% of a naphthalene-based PBI, were prepared and reached a hydroxide conductivity just above 50 mS cm$^{-1}$ at 80 °C. After 1000 hours in 5 M NaOH at 80 °C, the blend containing spiro-ionene 2 retained more than 60% of its original conductivity, whereas the blend with PBP-ASN only maintained 40% of its original value, suggesting that spiro-ionene 2 is the more stable ionene.

Jana et al. prepared ionically crosslinked AEM blends of spiro-ionene 2 and a pyridine-containing PBI.[220] An AEM (IEC = 2.39 mequiv. g$^{-1}$) containing 70% of the ionene reached a hydroxide conductivity of 129 mS cm$^{-1}$ at 90 °C and retained 80% of the conductivity after 500 hours in 2 M KOH at 60 °C. Fu and co-workers employed molecular dynamics (MD) and DFT calculations to study the effect of the degree of deprotonation and backbone flexibility of the PBI component in blends of spiro-ionene 2 and PBI as AEMs. The results showed that electrostatic interactions between the ammonium cations and the deprotonated imidazole play a central role in restricting the water uptake of the AEMs. The electrostatic interactions were found to be enhanced by protonation but weakened by the chain flexibility of the PBI.[229] In subsequent work, the same group used MD simulations to study the mechanism of hydroxide conductivity in blend AEMs composed of spiro-ionene 2 and a naphthalene-based PBI.[230]

Besides blending, water-soluble spiro-ionenes can also be immobilized by grafting onto hydrophobic polymers. Following this strategy, Liu et al. tethered oligomeric spiro-ionene 2 to PES (Fig. 13d).[225] First, an oligomeric spiro-ionene 2 terminated with secondary piperidine rings was prepared.[218] Next, a benzylbrominated PES was prepared by first conducting a K$_2$CO$_3$ catalysed polycondensation of bis(4-fluorophenyl)sulfone, 4,4'-dihydroxybiphenyl, and methylhydroquinone, followed by a radical-mediated benzylbromination using benzoylperoxide and N-bromosuccinimide. The grafting reaction was subsequently performed in a DMSO solution at 90 °C using DIPEA as the catalyst. AEMs prepared from the graft copolymers retained 84% of the hydroxide conductivity and 86% of their IEC after immersion in 2 M NaOH at 80 °C for 864 hours. NMR analysis revealed that nucleophilic substitution was the dominant degradation mechanism. AFM and TEM analysis showed a distinct microphase-separated morphology. The AEM with IEC = 1.75 mequiv. g$^{-1}$ exhibited a hydroxide conductivity of 96 mS cm$^{-1}$ at 80 °C, a water uptake of 33%, and a dimensional swelling ratio of 8%.[225]

**3.3.3. (Benz)imidazolium ionenes.** Imidazole and benzimidazole are 1,3-diazoles and can be considered as cyclic aromatic diamines.[231] Ionenes based on (benz)imidazolium cations have mainly been prepared in polymerizations where the heterocycles are directly formed in a cyclocondensation reaction, and this work is reviewed in Section 3.4. In the present section, a few examples of ionenes prepared by nucleophilic substitution reactions involving pre-made (benz)imidazoliums are discussed.[221–223,232] Yang et al. prepared two imidazolium ionenes by polymerizing a butyl-bridged bis-imidazole with either 1,4-dibromobutane or 1,4-dibromomethylbenzene, resulting in low-to-medium molecular weight polymers (Fig. 14a).[222] AEMs cast from blends of these ionenes with PBI exhibited IECs ranging from 0.71 to 2.29 mequiv. g$^{-1}$, water uptake of 24–68%, and achieved conductivities of up to 74 mS cm$^{-1}$ at 80 °C when immersed in 1 M KOH. The AEMs derived from 1,4-dibromobutane generally showed higher conductivity. After immersion in 1 M KOH at 80 °C for 100 hours, the blend AEMs retained 62–76% of their hydroxide conductivity. Following NMR analysis, it was concluded that the degradation of the AEMs occurred through hydrolysis of the imidazolium cations.

Holdcroft et al.,[233] and later Coates and co-workers,[234] have shown that imidazolium and benzimidazolium cations can be efficiently sterically protected from hydroxide attack by appropriate substitution, especially by incorporating bulky groups at the C2 position. Using butyl-bridged bis-(2-phenylbenzimidazole) and bis-(2,4,5-triphenylimidazole), Yang et al. carried out nucleophilic substitution polymerizations with 1,4-dibromomethylbenzene to prepare phenyl-substituted benzimidazolium and imidazolium ionenes, respectively (Fig. 14b).[221] These ionenes were then blended with PBI to produce water-stable and mechanically strong AEMs with IECs in the range of 1.0–1.5 mequiv. g$^{-1}$, water uptake of 39–57%, and area dimensional swelling of 14–17% at 80 °C. A triphenylimidazolium-based AEM with an IEC of 1.5 mequiv. g$^{-1}$ achieved a hydroxide conductivity of 52 mS cm$^{-1}$ at 80 °C. Alkali-stability testing in 1 M KOH at 80 °C showed that the imidazolium-containing AEMs retained conductivity better than the benzimidazolium-based AEMs.
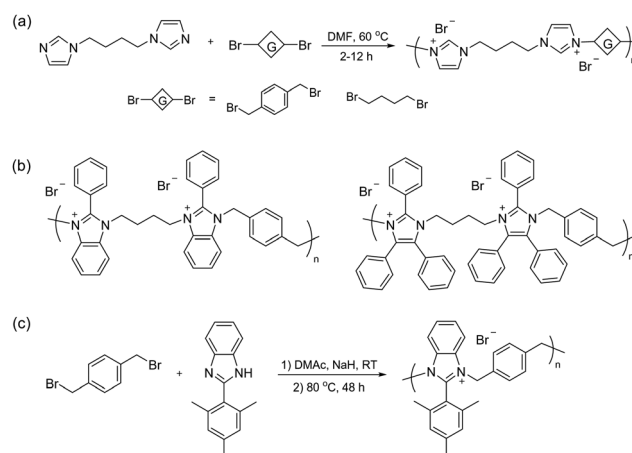


Fig. 14 Chemical structures of imidazolium and benzimidazolium-based ionenes: (a) nucleophilic substitution polymerization to prepare imidazolium ionenes, (b) sterically-protected phenyl-substituted benzimidazolium and imidazolium ionenes, and (c) sterically-protected benzimidazolium ionene.

This journal is © The Royal Society of Chemistry 2024

Chem. Soc. Rev., 2024, 53, 5704–5780 | 5723

However, all the AEMs suffered from a significant conductivity loss during the first 200 hours. $^1$H NMR analysis revealed that the benzimidazolium ionene had degraded (as will be discussed later in Section 3.4.1), while the corresponding imidazolium ionene was much more stable.

Henkensmeier and co-workers synthesized a sterically-protected benzimidazolium ionene by polymerizing 2-(2,4,6-trimethylphenyl)benzimidazole and 1,4-dibromomethylbenzene by first deprotonating the benzimidazole using NaH, and then adding the dibromo monomer (Fig. 14c).[223] The former monomer was obtained by reacting 2,4,6-trimethylbenzoic acid and 1,2-diaminobenzene in polyphosphoric acid at 200 °C.[233] However, the resulting ionene was not film-forming, likely due to its moderate molecular weight ($M_w$ = 40 kg mol$^{-1}$) and the highly rigid backbone structure. Self-supporting blend AEMs were instead obtained after co-casting with PBI, which reduced the IEC from 2.67 mequiv. g$^{-1}$ for the neat ionene, to 1.33–1.78 mequiv. g$^{-1}$ for the blend AEMs. The water uptake and conductivity of the blend AEMs ranged from 32–49% and 0.35–0.64 mS cm$^{-1}$ at 60 °C, respectively, in the Cl$^-$ form. The AEMs were subsequently evaluated in vanadium RFB, and hence the hydroxide conductivity and alkali stability of these materials were not evaluated.

Ionenes synthesized by nucleophilic substitution have emerged as an important class of AEPs. Depending on the structure of quaternary ammonium, an ionene can exhibit enhanced alkaline stability, as shown for the spiro-ionene structures. However, the location of the anion exchange groups in the backbone and the high-water uptake make these materials less ideal for membrane applications as free-standing films. Consequently, various blending strategies, inducing ionic crosslinking, have been developed to improve membrane stability and evaluate ionene-based AEPs in electrochemical devices.

### 3.4. Polybenzimidazoliums and polyimidazoliums

**3.4.1. Early development of polybenzimidazoliums.** PBIs are a class of high-performance polymers first reported in the 1950s.[235] The noteworthy *m*-PBI, (poly(2,2'-(*m*-phenylene)-5,5'-bibenzimidazole)), was reported by Vogel and Marvel in 1961.[236] *m*-PBI forms tough membranes and fibres, possessing outstanding chemical resistance and thermal stability,[237] making it attractive for aerospace materials, fire-resistant fabrics, and high-temperature PEMs.[238] The original synthetic route to PBI involved a two-step melt condensation of 3,3'-diaminobenzidine with diphenyl isophthalate, which entailed melting, cooling, grinding, and reheating mixtures of monomers to high temperatures. Catalysts allow for less expensive isophthalic acid monomers to be used.[239] A third route involves a solution polycondensation of monomers in polyphosphoric acid.[240] However, PBIs exhibit poor solubility in organic solvents due to strong H-bonding, which limits their processability. Consequently, significant research has been directed toward functionalizing the nitrogen to reduce H-bonding. Using a strong base, *m*-PBI may be deprotonated to its anionic, soluble form, whereby the addition of an alkyl halide functionalizes the anionic nitrogen, as shown in Scheme 14a.[241] This strategy has been used to attach various *N*-functional groups.[242] Nonetheless, this method generally employs an excess of alkylating agent, resulting in polymers with more than 50% degree of *N*-substitution, *i.e.*, more than two of the four nitrogen sites are functionalized. In 1993, Hu *et al.* reported the use of excess alkylating agent to prepare 100% methylated *m*-PBI (polydimethylbenzimidazole, denoted PDMBI, Scheme 14b), enhancing its solubility.[243] This was the first attempt to fully *N*-alkylate PBI into a polybenzimidazolium. Nearly two decades passed before the realization that alkylated polybenzimidazoliums were recognized as useful polymers in the design of AEMs. In 2011, the research groups of both Henkensmeier[244] and Holdcroft[245] independently published studies on the synthesis and anionic conductivity of PDMBI, reporting that the hydroxide ion form was elusive because the C2-position of the benzimidazole undergoes facile nucleophilic attack by hydroxide, as shown in Scheme 14c.

**3.4.2. C2-Protected polybenzimidazolium ionenes.** Faced with the rapid degradation of polybenzimidazoliums in alkaline media, it was demonstrated that substituting the phenylene group in the backbone with a mesitylene group significantly improves their stability in the base. This improvement results from the increased orthogonality of the mesitylene group with respect to the benzimidazolium ring and the steric hindrance created around the C2-carbon by the flanking methyl
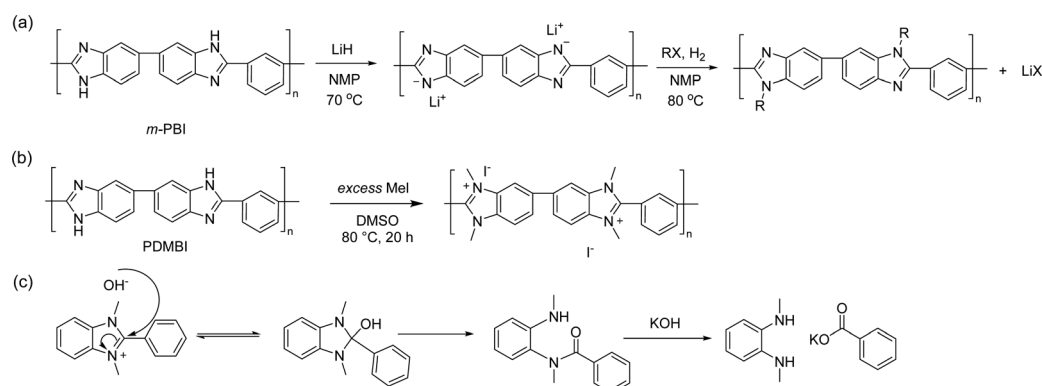


**Scheme 14** (a) Deprotonation and alkylation of *m*-PBI, (b) alkylation to PDMBI, and (c) the degradation route of dimethylbenzimidazolium hydroxide.
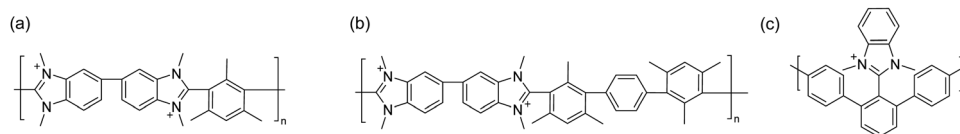
Fig. 15 Structures of C2-phenyl-substituted benzimidazolium polymers: (a) mesitylene–polydimethylbenzimidazolium (Mes–PDMBI); (b) hexamethyl-*p*-terphenylene–polydimethylbenzimidazolium (HMT–PDMBI); and (c) polyphenylene benzimidazolium (PPMB).
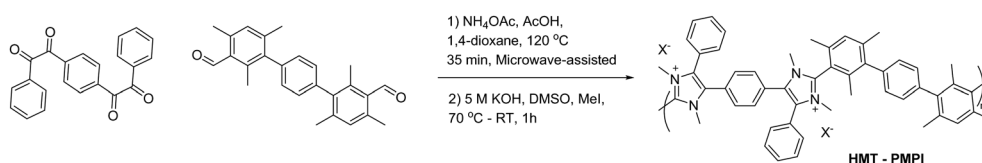
groups.[233] C2-Phenyl-substituted benzimidazolium, Mes-PDMBI (Fig. 15a), exhibited no observable degradation in 6 M KOH at 20 °C or 2 M KOH at 60 °C for 10 days, yet possessed a high IEC of 4.5 mequiv. g$^{-1}$, conferring water solubility, which facilitated *in situ* NMR spectroscopic studies of its stability while dissolved in caustic solutions. Its high IEC, however, rendered the polymer impractical as a standalone membrane in aqueous electrochemical devices. Therefore, Mes-PMDBI was blended with water-insoluble PBI to prepare water-insoluble membranes, yielding AEMs with bicarbonate conductivity of 10 mS cm$^{-1}$. Noting that blending with a polymer limits processability, the short mesitylene unit in the main chain was replaced with hexamethyl-*p*-terphenylene (HMT) to increase the hydrophobicity of the polymer while maintaining steric C2-protection of the benzimidazolium.[246,247] HMT-PDMBI (Fig. 15b) features a tunable IEC from 1.1 to 2.7 mequiv. g$^{-1}$ (controlled by the degree of methylation) and showed no signs of degradation in 2 M KOH at 60 °C for extended periods and only minor signs of chemical degradation when subjected to 6 M NaOH for several days. Its hydroxide ion conductivity was reported to be 100 mS cm$^{-1}$.[248] Dynamic computational simulations revealed that water molecules are imbibed to form a tortuous but contiguous, narrow pathway for ion conduction, even at modest levels of hydration,[249] which explained the high ion conductivity in the lack of ion-containing side chains and the absence of long-range morphological structures, as typically observed in ion-conducting polymers. Scaled-up synthesis of HMT-PDMBI has been reported in kilogram quantities in high yield. Membranes cast from HMT-PDMBI solutions are reported to be mechanically strong, with tensile strength and Young's modulus of 33 MPa and 225 MPa, respectively, surpassing those of a Nafion™ benchmark. The hydroxide anion form exhibits high *ex situ* chemical and mechanical stability, which remained unchanged after exposure to 1 M NaOH at 80 °C or 6 M NaOH at 25 °C for 7 days, showing only 6% degradation when exposed to 2 M NaOH at 80 °C for 7 days.

Given that the methyl groups attached to the C2 position of mesitylene (Fig. 15b) are paramount to stabilizing PBI, it was speculated that bulkier groups could provide even greater protection against hydroxide attack. Consequently, the methyl groups were replaced with phenyl groups to instil even greater steric hindrance around the C2-positon (Fig. 15c).[247,250] These *m*-terphenyl-protected benzimidazolium AEMs, poly(4,4″-[2′-(1,3-dimethyl-1*H*-benzimidazolium-2-yl)-*m*-terphenylene]) (PPMB), are reported to exhibit an exceptional half-lifetime stability of more than 3000 hours in 3 M NaOH at 80 °C. This enhanced stability is believed to be due to the suppression of ring-opening by hydroxide ion attack at the C2 position.

**3.4.3. Polyimidazolium ionenes.** DFT studies have revealed that the dimethyl-imidazolium cation is more stable against C2-hydroxide attack than its dimethyl-benzimidazolium counterpart,[251] which was experimentally verified in small molecule model compound studies.[234] Hexamethyl terphenylene polyimidazolium ionene analogues of these small molecules, HMT-PPI, have been prepared through microwave-assisted polycondensation of a dialdehyde and bisbenzil. The subsequent deprotonation of the imidazole N–H and alkylation produced the C2-protected poly(arylene-imidazolium) with high molecular weight (Scheme 15). The resulting material yielded tough pliable, transparent films with exceptionally high tensile strength. These films demonstrated an order of magnitude improvement in stability over their benzimidazolium analogues under highly caustic conditions.[252] In their hydroxide form, they exhibited an IEC of 2.6 mequiv. g$^{-1}$ and a carbonate/bicarbonate conductivity of 14 mS cm$^{-1}$ at 25 °C. Analysis by $^1$H NMR spectroscopy indicated no signs of degradation in 10 M KOH at 100 °C over 7 days.

**3.4.4. Poly(bisimidazolium) ionenes.** The suppression of degradation in C2-protected imidazolium from ring-opening revealed that the next mode of degradation was dealkylation. The dealkylation degradation pathway was subsequently minimized by incorporating bulkier alkyl side chains attached to the N1/N3 positions of the imidazole.[234,253] Longer alkyl chain derivatives (with more than four carbons) are reported to be significantly more stable (with half-life exceeding 10 000 hours) than their methyl derivatives, but to the detriment of reduced IEC and dilution of the charge carriers. A reduction in charge carrier concentration can be compensated by introducing bis-imidazolium cations into the polymer, which can achieve



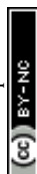Scheme 15 Synthesis of hexamethylterphenylene polyimidazolium (HMT–PMPI).

This journal is © The Royal Society of Chemistry 2024

Chem. Soc. Rev., 2024, **53**, 5704–5780 | 5725
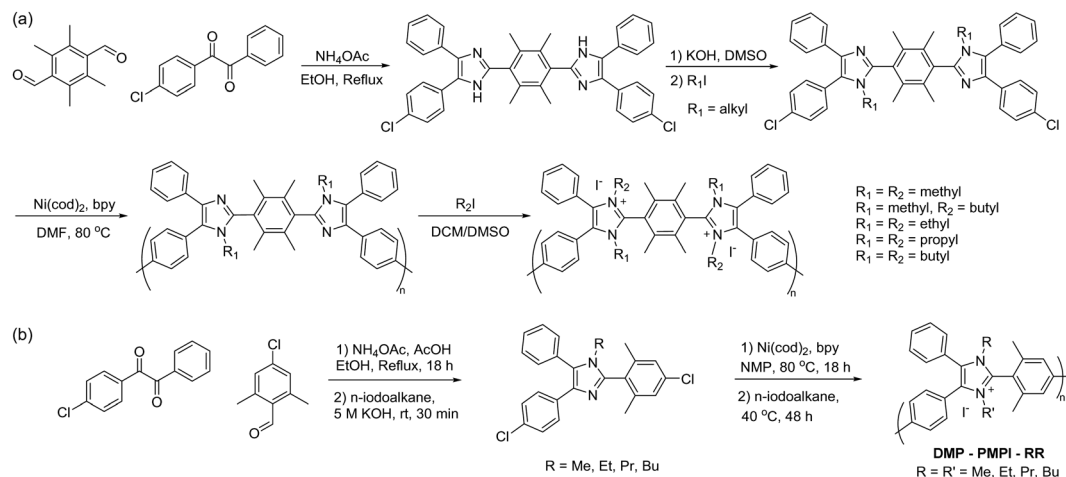
**Scheme 16** (a) Synthesis of C2-protected poly(bisarylimidazolium) AEPs (PAIM). (b) Synthesis of aryl imidazole monomers and the poly(arylimidazolium) (DMP-PMPI-RR) having *N,N'*-dialkyl functionality.

theoretical IECs as high as 3.0 mequiv. $g^{-1}$ (*i.e.*, when fully methylated).[253] Such sterically-protected poly(arylimidazolium) AEPs were prepared by Yamamoto-coupling polymerization (the Ni-mediated coupling reaction discussed in Section 3.2) of dichloro-imidazole monomers as shown in Scheme 16a. This synthetic route is substantially different from the previously reported poly(arylimidazolium) AEPs, which were based on bis-diketone/dialdehyde/ammonium polycondensation. The biaryl-coupling polymerization route typically results in low molecular weight polymers because of the limited solubility of highly rigid aromatic backbones. However, the adopted synthetic strategy allows for the preparation of an intermediary polymer in its semi-alkylated form, which exhibited much higher solubility and resulted in high molecular weight poly(arylimidazole)s ($M_w$ = 140 kg mol$^{-1}$). *N*-Alkylation of the polymers was achieved by reacting them with various alkylating reagents to produce different poly(arylimidazolium) AEPs. These sterically-protected poly(bis-arylimidazolium) polymers demonstrated high stability in caustic solutions; for example, a butylated derivative is reported to exhibit a half-life exceeding 8000 hours in 10 M KOH at 80 °C.[253]

Having established a viable route for designing robust poly(imidazolium) AEPs through C2-protection of the imidazolium, it became paramount to be able to tune these polymers for specific properties. The water content, or more specifically, the number of water molecules per ion, affects every physico-chemical property of an AEM.[215,254] To achieve higher ionic conductivity, a high ionic content of AEMs is considered necessary. However, increasing the IEC enhances the hydrophilicity and water content, which in turn induces significant changes in AEM properties due to osmotic pressure, such as deleterious volumetric and morphological transformations. Furthermore, reduced solvation of hydroxide ions under low hydration conditions decreases the shielding of their negative charge, promoting mechanisms of nucleophilic attack. Consequently, water content is a critical parameter in considering the electrochemical applications of AEMs,[255,256] and a deeper

understanding of the structure–property relationships is required to fully comprehend the influence of the molecular structure of polyimidazolium ionenes on water content and the effect of water. Due to the rapidly rising interest in this class of polymers, attention to the complex interplay between ionic content and conductivity/hydration relationships is still in the earlier stages of investigation.

A pioneering case study, published in 2020, presented a cross-correlation of ionic conductivity and water uptake in poly(arylimidazolium) ionenes. These polymers were prepared by Yamamoto coupling of penta-substituted imidazolium monomers having steric protection at the imidazolium C2-position (Scheme 16b).[257] The monomers having one *N*-alkyl function were synthesized in several steps. *N*-Alkylation occurs at either of the two nitrogen sites, resulting in the monomer being obtained as a mixture of the two structural isomers. Consequently, polymerizations yield polymers with mixed repeat unit configurations forming either of three possible configurations. The ionic conductivities of these poly(imidazolium) membranes vary significantly with IEC, and this trend holds regardless of repeat unit structure and coupling configuration. Polymerization and quaternization are reported to be near-quantitative in yield, but the conversion of the second *N*-alkylation decreases with increasing alkyl chain length, consistent with the general trend of decreasing reactivity with increasing alkyl chain length of *n*-haloalkanes in quaternization reactions. This leads to a decreasing degree of quaternization and decreasing ionic content with increasing alkyl chain length. AEMs in their hydroxide counterion forms convert to their mixed carbonate form upon exposure to air containing $CO_2$. Therefore, the cross-correlation of water uptake and ionic conductivity was presented using the chloride form, which remained stable in the air. The observed trends of $\sigma_{(Cl)} \sim$ IEC for these polymers are in agreement with those of comparable poly(arylimidazolium)s. AEMs with higher IEC exhibit a lower range of ion conductivity ($\sigma$) and hydration number ($\lambda$) within certain limits of temperature and humidity.

**5726** | *Chem. Soc. Rev.*, 2024, **53**, 5704–5780

This journal is © The Royal Society of Chemistry 2024

Decreasing the IEC correlates with an increase in the effective activation energy of ion transport at a constant $\lambda$, leading to the conclusion that AEMs with lower IEC are more dependent on environmental conditions, such as RH and temperature.

**3.4.5. AB polyimidazolium ionenes.** Vogel and Marvel originally synthesized PBI polymers through polycondensation of two bifunctional monomers: bis-tetraamines and bis-carboxylic acids.[236,258] Additionally, AB polymerization of bifunctional 3,4-diaminobenzoic acid to form poly(2,5(6)-benzimidazole) was reported, where the inherent viscosities ($\eta_{inh}$) of the polymers were correlated with their chemical structure. As mentioned earlier, the most processable of these polymers, the AA + BB poly(2,2'-[m-phenylene]-5,5'-bibenzimidazole) (m-PBI) was commercialized in 1983.[259,260] Sol–gel processing developed by Benicewicz et al.[261] significantly enhanced the membrane-forming properties of this polymer.[146] Inspired by Debus–Radziszewski condensation in AA + BB macromolecular syntheses of polyimidazoles pioneered by Marestin and Mercier,[262–264] Overton and Holdcroft recently reported the first AB-type poly(arylimidazole) (AB-PAIM) synthesis (Scheme 17),[265] introducing C2-protection at the imidazolium repeat units. AB polycondensation facilitates the introduction of end-group chemistry onto these polymers, offering a synthetic opportunity for further optimisation and stabilization of their physicochemical properties.[266] End-group chemistry was used, for example, to control the number-average degree of polymerization ($\bar{X}_n$) of AB-PAI polymers, as $\bar{X}_n$ is often crucial for the effective processing of polymers. Advantageously, it was found that steric encumberment of the imidazole C2 introduced in the AB-type monomer did not inhibit polycondensation. Partially quaternized, primary chain AB-PAI polyelectrolytes, such as ionenes, have zwitterionic imidazolate-imidazolium character, owing to the conjugate base of imidazole ($pK_a \approx 7$). Therefore, AB-PAI polymers and their derivatives could be useful in complex and heterogeneous ion transport applications.

## 3.5. Diels–Alder polymerization

Diels–Alder polymerization was first employed to develop ion-conducting polymers for fuel cell applications by Sandia National Laboratories in 2001. Polyphenylene composed of para- or meta-linkages of phenylene units can be synthesized by [4+2] Diels–Alder cycloaddition of a bis-diene (such as bistetracyclone, BTC) and a bis-dienophile (1,4-diethynyl-benzene, DEB), reported by Frietag,[267] Ried,[268] and Stille et al.[269–272] The mechanism of this reaction is shown in Scheme 18; depending on the diene and dienophile used, either para- or meta-linkages are generated. For instance, a para-linkage is formed when $R_2$ of the diene is on the opposite side of $R_3$ of the approaching dienophile. The [4+2] cycloaddition forms a carbonyl-bridged intermediate that subsequently extrudes carbon monoxide, driven by the formation of a more energetically stable aromatic centre. The resultant polymer contains pendent phenyl rings and a mixture of backbone para/meta-linkages that inhibit molecular weight limiting $\pi$–$\pi$ interactions,[273] leading to good solubility in organic solvents[270] and favourable mechanical, film-forming properties.[274,275] Proton conducting membranes have been developed by sulfonating the Diels–Alder poly(phenylene)(DAPP) backbone, controlling the ratio of chlorosulfonic acid to the polymer repeat units.[276]

In the early 2000s, no alkaline-stable AEMs had been reported; the primary degradation mode was believed to be hydroxide nucleophilic attack of the cationic ammonium group, either by Hofmann elimination or direct displacement, as discussed in Section 2.3.[277–279] Hibbs et al. developed the first example of an AEM with the DAPP backbone by polymerizing a methylated bis(tetracyclone) (tetramethylbis(cyclopentadienone), TMBTC) with DEB (Scheme 19).[280] The pendent methyl groups were brominated via radical bromination, and then the bromo functional groups were nucleophilically replaced by trimethylammonium via the Menshutkin reaction using trimethylamine, forming benzyltrimethyl ammonium-substituted DAPP (TMA-MDAPP). This conversion was carried out heterogeneously by immersing cast films of bromomethylated DAPP in concentrated aqueous trimethylamine at room temperature for 48 hours. However, the values of theoretical IEC, calculated by $^1$H NMR of bromomethyl groups, and the experimental IEC via titration were disproportionate, with the titrated values being 25–45% lower than theoretical ones. The lower-than-expected titrated IEC was attributed to incomplete nucleophilic substitution due to the slow heterogeneous reaction between the bromomethyl groups and
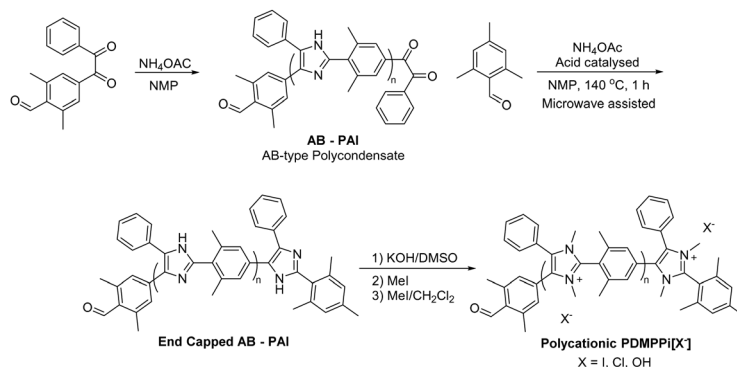


**Scheme 17** First instance of AB polymerization to synthesize poly(aryleneimidazolium) (AB-PAI), demonstrating molecular weight control and end group functionalization.

This journal is © The Royal Society of Chemistry 2024

Chem. Soc. Rev., 2024, **53**, 5704–5780 | **5727**
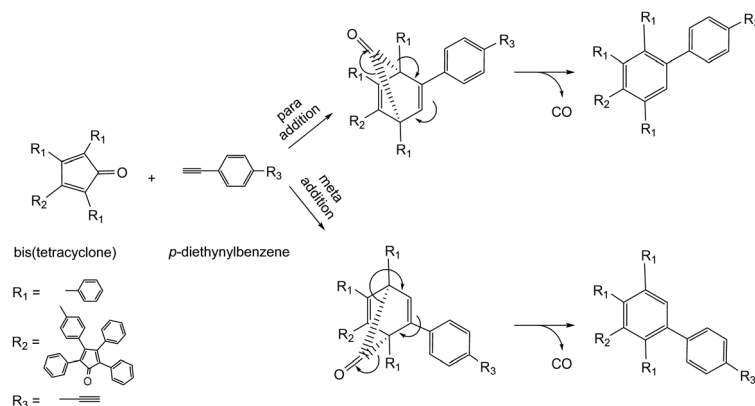
Scheme 18 Two possible regioisomers of the [4+2] Diels−Alder polycondensation of bis(tetracyclone) and *p*-diethynylbenzene.
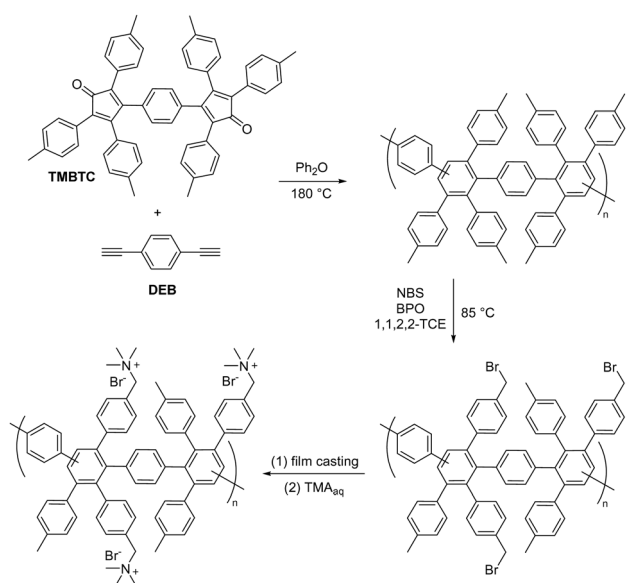


Scheme 19 Synthesis scheme of DAPP AEM functionalized with BTMA groups.
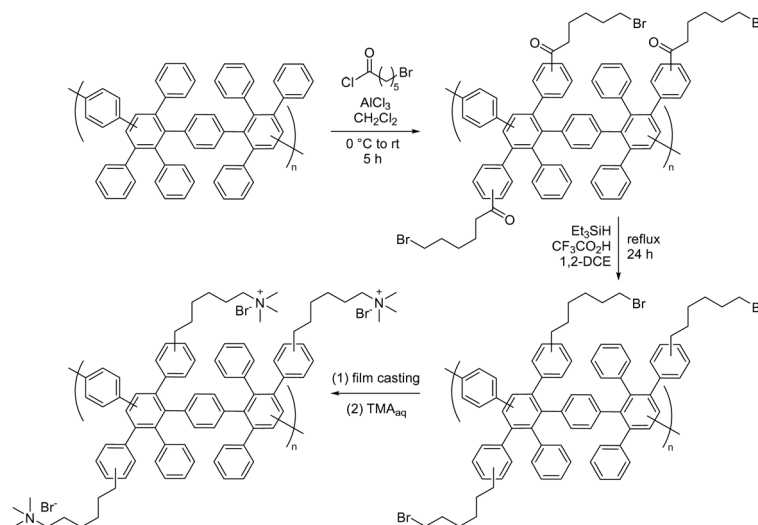
trimethylamine, with the remaining bromomethyl groups converting to hydroxymethyl groups over time and exposure to humid environments. The highest IEC reported for TMA-MDAPP was 1.57 mequiv. g$^{-1}$ (films with a higher targeted IEC dissolved in the trimethylamine bath), exhibiting a water uptake of 120% and hydroxide conductivity of 50 mS cm$^{-1}$ at room temperature, comparable to the highest values reported for AEMs at that time. Hibbs compared the durability of PES-based AEM and TMA-MDAPP in 4 M NaOH at 60 °C for 30 days, reporting that the IEC and mechanical properties of TMA-MDAPP did not change over the course, whereas the PES AEM became extremely brittle.

The BTMA group is unstable above 60 °C under alkaline conditions, leading to efforts to improve the stability of organic cations by examining resonance stabilized guanidinium[281] and imidazolium[282] or sterically bulky phosphonium cation.[283] However, a novel approach was demonstrated in the mid-1990s by Tomoi, where increasing the separation between the aromatic backbone and ammonium group by methylene spacers (more than 3 carbons) led to improved alkaline stability.[284] Building on this, Hibbs sought to combine the alkaline-stable DAPP backbone with this long-chain spacer approach to further optimize alkaline stability.[285] The first step began with the Friedel–Crafts acylation of DAPP with bromohexanoyl chloride, to form DAPP with attached 6-bromo-1-phenylhexan-1-one. Since the attached ketone could react with hydroxide either by enolate formation (due to the acidic α-proton of ketones) or by direct nucleophilic attack of the ketone to form a geminal diol, it was reduced to a methylene group. The resultant bromohexyl functionalized DAPP was cast as films and immersed in aqueous trimethylamine to form trimethylammonium hexyl DAPP (TMAH-DAPP, Scheme 20). As observed with TMA-MDAPP, the measured IEC of TMAH-DAPP was slightly lower than theoretical values, likely due to the incomplete heterogeneous conversion of the hexylbromo groups. The stability of TMAH-DAPP was monitored by immersing the films in 4 M KOH at 90 °C for two weeks. Periodically, the film was removed from the bath, and chloride ions were exchanged to measure chloride conductivity and then re-immersed in the alkali solution. After one week, the chloride conductivity of TMAH-DAPP reduced by 5%, but did not change during the second week, suggesting that the change in conductivity was due to the reorganization of the hydrophilic/hydrophobic domains, rather than to cation group degradation. This conclusion was further supported since the IEC of TMAH-DAPP remained unchanged throughout the experiment.[286]

The functionalization of DAPP has focused on inducing the formation of hydrophilic ionic channels through the aggregation of neighbouring ionic functional groups attached to the pendent aryl rings. A novel approach in ionomeric DAPP materials involves controlling the position of the ionic groups on the DAPP backbone. This is achieved by attaching a strong electron-withdrawing moiety, such as pentafluorobenzoyl, to the backbone to inhibit electrophilic aromatic substitution reaction (*i.e.*, sulfonation) on the pendent aryl rings.[137] Incorporating fluorine into the backbone serves as an internal reference, helping to determine the degree of functionalization with pentafluorobenzoyl groups using $^{19}$F NMR spectroscopy.

5728 | *Chem. Soc. Rev.*, 2024, **53**, 5704–5780

This journal is © The Royal Society of Chemistry 2024

**Scheme 20** Synthesis of TMAH–DAPP AEMs.

The polymer was functionalized to attach up to six pentafluorobenzoyl groups, followed by sulfonation on the backbone to induce ionic aggregation.

Compared to other quaternized polyaromatic polymers, quaternized DAPPs exhibit higher gas permeability is desirable for ionomeric binders, but it is less advantageous for AEM applications, as increased gas crossover can lead to higher overpotential in the device. Additionally, the bulky structure of these polymers hinders chain entanglement, resulting in poor mechanical properties at a given molecular weight. However, quaternized DAPPs also offer distinctive advantages, including all-phenylene and non-ionic backbones, good processibility, chemical robustness, and a wide range of IECs.

# 4. Chemistry of vinyl polymers

Vinyl polymers have a long history as commodity polymers, displaying excellent chemical stability stemming from their fully saturated backbone. This section explores various synthetic strategies for preparing polyolefin-based AEPs.

## 4.1. Addition polymerization

Addition polymers, broadly speaking, encompass polymers obtained through a chain-growth mechanism, forming a structure where the repeat unit contains the same atoms as the monomer. The range of vinyl monomers that can be polymerized via vinyl-addition polymerization is exclusively limited. Many cyclic olefins necessitate highly reactive catalysts, often accompanied by co-catalysts and activators for polymerization. Moreover, these catalysts often have poor functional group tolerance.[287] Only a select number of cyclic olefins, such as norbornene and cyclopentene, have been identified as monomers capable of forming functional polymers. In the context of AEP synthesis, addition polymerization has primarily been reported for the synthesis of quaternized polynorbornene.

Norbornene, a reactive bicyclic olefin with high ring strain, has the capability to polymerize through three independent pathways, resulting in different norbornene-based polymers: ring-opening metathesis polymerization (ROMP), isomerization polymerization, and addition polymerization.[288–290] ROMP, the most well-known method for polymerizing norbornene, will be discussed in detail in Section 4.2. Isomerization polymerization of norbornene can be catalysed by radical, cationic, and anionic initiators,[291] but it has been scantily studied due to the low molecular weight and poorly defined structures of the resulting polymers. Vinyl-addition or addition polymerization of norbornene (Scheme 21), first reported in the 1960s,[292] produces polymer backbones with a bicyclic structure by only opening
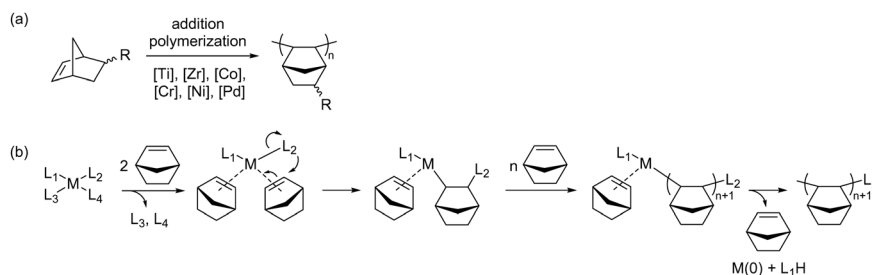


**Scheme 21** (a) Vinyl-addition polymerization of functional norbornene using transition metal catalysts and (b) suggested mechanism of norbornene polymerization using a metal catalyst.

This journal is © The Royal Society of Chemistry 2024

Chem. Soc. Rev., 2024, **53**, 5704–5780 | **5729**

the double bond of the vinyl group, which is distinct from polyolefins generated from ROMP. Although the polymerization reactivity is lower than that of ROMP,[293] addition polymerization can grow norbornene into high molecular weight polymers, featuring rigid and fully saturated backbones. Catalysed by late transition metal catalysts including Ti, Zr, Co, Cr, Ni, and Pd,[294] the polymers composed of polyolefin backbones are known for their chemical inertness, good mechanical strength, and high thermal stability, including an extremely high $T_g$ (norbornene homopolymer is $> 300$ °C).

The known disadvantages of polynorbornenes are their high melting points, poor solubility in organic solvents, and poor adhesion. To increase thermal processability, norbornene is often copolymerized with other alkene monomers, e.g., ethene or propene. Its adhesion properties can be enhanced by polar group substitution, such as with triethoxysilane,[295] making it suitable for use in discs, films, fibres, binders, packaging, and optical applications.[296]

Scheme 21b illustrates the suggested mechanism for the addition polymerization of norbornene.[297,298] The norbornene monomers initially coordinate with the metal catalyst, replacing weakly coordinating labile ligands ($L_3$, $L_4$), forming a complex. Subsequently, norbornene insertion occurs for chain initiation. Chain propagation then proceeds to increase the molecular weight of the polymer, and the polymerization terminates via the reductive elimination of the catalyst. Catalysts based on nickel and palladium exhibit the highest reactivity towards addition polymerization and the highest tolerance to substituted norbornene monomers, making them the most employed catalysts.[289,290]

The post-polymerization modification of substituted alkyl halides with tertiary amines via the Menshutkin reaction is currently the most applied method to introduce anion exchange groups to the polynorbornene prepared by addition polymerization. Alkyl halide (either Cl or Br)-substituted norbornenes can be synthesized by Diels–Alder cycloaddition reactions of cyclopentadiene and terminal 1-haloalkenes as a mixture of endo (major) and exo (minor) isomers in a ratio of endo:exo = 85:15 (Scheme 22).[299] A variety of catalysts (e.g., bis(β-ketonaphthylamino) Ni/B(C$_6$F$_5$)$_3$,[300] (η$^3$-allyl)Pd(PPh$_3$)Cl/Li[FABA],[301] Pd(t-Bu$_3$P)MeCl,[302] and trans-[Ni(C$_6$F$_5$)$_2$(SbPh$_3$)$_2$]$^{303}$) have been successfully used to polymerize alkyl halide-substituted norbornene, producing copolymers in combination with other norbornene monomers, which were converted into anion exchange groups. Very recently, a direct coordination–insertion polymerization of cationic norbornene monomers has been reported, using the Pd(t-Bu$_3$P)MeCl catalyst.[304]

Addition polymerization was initially employed in the synthesis of AEPs in 2015 when He and co-workers reported quaternary ammonium-containing addition-type norbornene

copolymers for direct methanol fuel cells (Fig. 16a).[300] For norbornene monomers, alkyl- and bromoalkyl-substituted 5-norbornene-2-methanol was used for copolymerization with a Ni catalyst. The polymers underwent functionalization via chloromethylation using chloromethyl methyl ether and were quaternized using tertiary amines of varying chain lengths. The resulting AEM demonstrated an IEC of 1.8 mequiv. g$^{-1}$ and low dimensional swelling of 0.9–3.3%, but the anion conductivity at 80 °C was only 4.1 mS cm$^{-1}$.

Kohl et al. synthesized tetrablock copolymers of polynorbornene through the sequential addition of butylnorbornene and bromopropylnorbornene utilizing a palladium catalyst with an activator (Fig. 16b).[301] The bromopropyl-containing tetrablock copolymer was cast as a film and quaternized by immersion in an aqueous trimethylamine solution. The $M_n$ of the polymers was from 38 to 115 kg mol$^{-1}$, as determined by GPC. The molecular weight growth of each block was also monitored to confirm the sequential growth of block copolymers. The AEMs showed phase-separated morphology confirmed by SAXS and TEM, attributed to the hydrophobic–hydrophilic block structure. The AEMs with the IEC value of 1.9 mequiv. g$^{-1}$ and the highest molecular weight ($M_n$ = 115 kg mol$^{-1}$) showed the highest hydroxide conductivity of 122.7 mS cm$^{-1}$ at 80 °C, higher than that of the AEM with higher IEC (2.6 mequiv. g$^{-1}$, $\sigma_{80 °C}$ = 80 mS cm$^{-1}$, $M_n$ = 45 kg mol$^{-1}$), likely due to the higher molecular weight causing lower water uptake and better chain entanglement for higher hydroxide mobility.[301] The polynorbornene AEMs exhibited high alkaline stability, showing minimal sign of a change of ionic conductivity (less than 1%) observed over 1400 hours after immersion in 1 M NaOH at 80 °C, demonstrating the high potential of this polyolefinic AEMs for alkaline electrochemical devices.
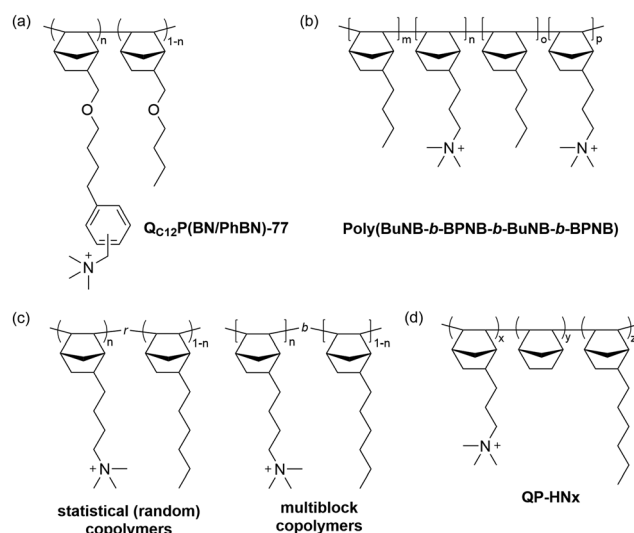


Fig. 16 Selected examples of polynorbornene AEPs using addition polymerization: (a) quaternary ammonium-functionalized polynorbornene reported in 2015, (b) tetrablock copolymers of polynorbornene, (c) statistical copolymers synthesized by one-pot addition polymerization and multiblock copolymers made via sequential addition, and (d) solvent-processable random copolymers of polynorbornene.
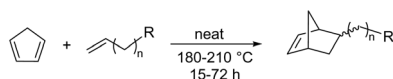


Scheme 22 Substituted norbornene monomer synthesis.

5730 | Chem. Soc. Rev., 2024, 53, 5704–5780

This journal is © The Royal Society of Chemistry 2024

As demonstrated, based on how monomers are introduced to the polymerization reaction, either one-pot or sequentially, addition-polymerized polynorbornene can form either random (statistical) or multiblock copolymers (Fig. 16c). In addition to the tetrablock copolymers, in a follow-up study Kohl *et al.* prepared AEMs based on homopolymer and random copolymers of polynorbornene with similar IECs (3.5–4.5 mequiv. g$^{-1}$) and compared their hydroxide conductivity, water uptake, dimensional swelling, and membrane morphology from polymer nanostructures. While only the block copolymer exhibited well-defined microphase-segregated morphology, its hydroxide conductivity (201 mS cm$^{-1}$ at 80 °C) was comparable to that of the random copolymer (194 mS cm$^{-1}$ at 80 °C), as well as other membrane properties (WU 119% *vs.* 114%, dimensional swelling 32% *vs.* 31% at room temperature, respectively). Usually, higher IEC membranes have increased concentration of unbound water, enabling more favourable proton conduction while lower IEC membranes only contain primarily bound water. However, this study indicates that AEMs with very high IECs and an excess volume of unbound water lead to flooding of the ionic channels, and the phase-separated morphology does not play a significant role in improving membrane properties. All AEMs showed less than 1.4% loss of ion conductivity after immersion in 1 M NaOH at 80 °C for 1000 hours.

Noonan and co-workers conducted a similar study, systematically comparing a statistical copolymer and a series of multiblock copolymers of addition-polymerized polynorbornene to investigate the impact of polymer composition on hydroxide transport in AEM.[302] Two monomers, hexyl-substituted norbornene, and bromobutyl-substituted norbornene were copolymerized *via* addition polymerization using a palladium catalyst to form two different polynorbornene architectures. Four block copolymers were prepared, from diblock to pentablock, with the targeted molecular weight ($M_n$ = 80–130 kg mol$^{-1}$) and the IEC value (1.7 mequiv. g$^{-1}$). All block copolymers showed higher hydroxide conductivity and water uptake than those of random copolymers owing to their phase-separated microstructure and more interconnected networks for facile ion transport. The tetrablock copolymer showed the highest conductivity of 105 mS cm$^{-1}$ at 80 °C and a water uptake of 85%, while the random copolymer showed 60 mS cm$^{-1}$ at 80 °C with a water uptake of 30%. The block copolymer and microstructure might have shown a more accentuated impact on conductivity and water uptake in this study[302] because the IEC values of the AEMs were lower than those of the other study[305] (1.7 *vs.* 3.5 mequiv. g$^{-1}$). The location of the ionic block also affects the water uptake; it was found to be more effective in controlling water uptake if the ionic block is located in the middle block of multiblock copolymers.

Saito and co-workers investigated a series of random copolymers of norbornene for AEMs (Fig. 16d).[303] The composition of different chain lengths of bromoalkyl and alkyl-containing norbornene monomers, along with unsubstituted norbornene used in polymerization was tailored to control the AEM properties. The molecular weight of the synthesized terpolymers was remarkably high ($M_n$ > 160 kg mol$^{-1}$) owing to the highly

reactive Ni-based catalyst[306] to ensure high mechanical stability of the membranes. The AEM was made with trimethylammonium propyl group and unsubstituted norbornene with an IEC of 2.0 mequiv. g$^{-1}$, showed a hydroxide conductivity of 109 mS cm$^{-1}$ and a water uptake of 71% at 80 °C. The membranes showed no significant difference in their hydroxide conductivity and mechanical properties (tensile strength, elongation at break) after immersion in 1 M NaOH at 80 °C for 1000 hours.

Functionalized polynorbornenes often exhibit poor solubility in organic solvents due to the saturated olefinic backbone structure; therefore, quaternization of polynorbornene is mostly done under heterogeneous conditions by immersing the precast film in an aqueous amine solution to prepare AEMs. The resulting quaternized polymers are typically insoluble in any organic solvents, limiting their use as AEIs for electrodes to only particulate dispersions.[307] In a follow-up study, Saito *et al.* further tuned the ratio of the terpolymer with a hexyl-substituted monomer and prepared quaternized polynorbornene, which was solvent-processable in an alcohol-based dispersing agent. The polynorbornene ionomer used for AEMFC and AEMWE demonstrated outstanding performance compared to those cells using state-of-the-art phenyl-containing AEIs, which can be ascribed to the phenyl-free backbone structure of polynorbornene.

Various crosslinking strategies have been employed for the addition of polynorbornene to avoid excessive water uptake and membrane swelling and increase the mechanical properties of polyolefin-based AEPs. Crosslinking of AEMs with high IEC (>3.5 mequiv. g$^{-1}$) is necessary because excessive membrane water uptake limits their physical stability. The tetrablock copolymer (Fig. 16b) reacted with *N,N,N′,N′*-tetramethyl-1,6-hexanediamine to form both quaternary ammonium functional groups and crosslinks (Fig. 17a).[308] Different mole ratios of the crosslinking agent (4–50 mol%) were investigated, and the AEM with an IEC of 3.5 mequiv. g$^{-1}$ and a low degree of crosslinking of 5% showed good control of water uptake with the highest hydroxide conductivity of 198 mS cm$^{-1}$ at 80 °C, which is higher than non-crosslinked block copolymers. By incorporating polytetrafluoroethylene (PTFE) reinforcement, the membrane demonstrated one of the highest performance in AEMFCs (3.4 W cm$^{-2}$ at 80 °C, 500 hours continuous operation).[309]

Crosslinking also helped to improve the adhesion properties of quaternized polynorbornene when used as catalyst AEIs. Polynorbornene was crosslinked by a triamine crosslinker to react with an epoxy binder to induce adhesion between the ionomer and catalyst particles (Fig. 17b).[310] The study reported that the approach of crosslinking quaternary ammonium AEIs helped to improve the durability of AEMWE operation by improving catalyst adhesion on the electrode. You *et al.* demonstrated the synthesis of crosslinked AEMs through copolymerization of vinyl-substituted norbornene, which reacts with dithiol reagents by UV-initiated thiol–ene click reaction (Fig. 17c).[311] After quaternization, a crosslinked AEM was obtained, and the strategy helped to solve the trade-off between high IEC/hydroxide conductivity and membrane dimensional stability. Other crosslinking strategies include
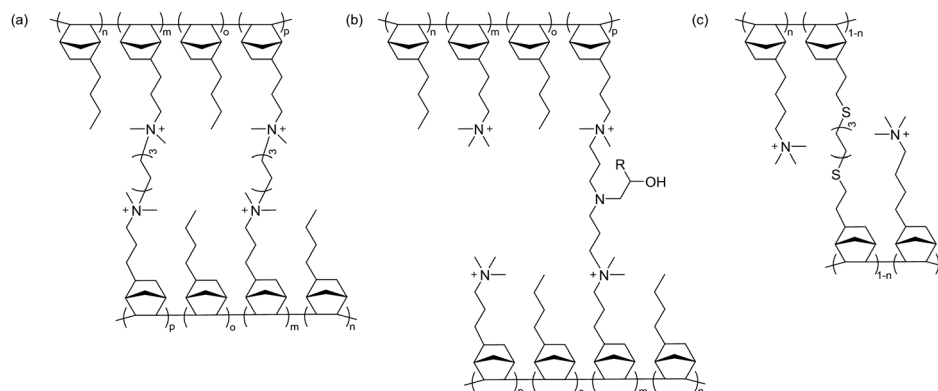
This journal is © The Royal Society of Chemistry 2024

*Chem. Soc. Rev.*, 2024, **53**, 5704–5780 | 5731

**Fig. 17** Selected examples of crosslinked addition polynorbornene AEPs: (a) diamine-crosslinked tetrablock copolymers of polynorbornene, (b) triamine-crosslinked polynorbornene ionomers with an epoxy group for enhanced adhesion, and (c) dithiol-crosslinked polynorbornene.

using bis(quaternary ammonium siloxane) linkage,[312] bis(siloxane imidazole) linkage,[313] and bisimidazole cationic crosslinker.[314]

Norbornene-based polyolefins are promising materials for AEPs, and their synthesis has been explored intensively in recent years. With appropriate catalysts, selected norbornene monomers with haloalkyl groups can be readily polymerized in either random or block fashion. The synthesized cyclic olefinic polymers have a fully saturated backbone, which is ideal for achieving high alkaline stability and very low adsorption energy on catalyst surface in electrochemical device applications,[179] although its radical oxidative stability is still questionable.[140] In addition, end groups present in these and many other polyolefin systems have not been examined in detail. These groups will likely impact the alkaline and oxidative stability of the system, especially for low molecular weight AEPs, and should be identified where possible. Some challenges and needs that have been addressed[290] to make further progress in addition polymerization chemistry for polynorbornene, which can also be applied for AEP applications include: (a) development of more tolerant and air-stable catalysts with enhanced activity, (b) simplified synthesis of more reactive *exo*-norbornene monomers than *endo*-isomers, and (c) improvement of both catalysts and functionalized monomers for better-controlled microstructures, compositions, and molecular weight of resulting polymers.

## 4.2. Ring-opening metathesis polymerization

Post-polymerization modification of pendent alkyl halides or tertiary amines *via* the Menshutkin reaction or methylation, respectively, is by far the most common strategy to obtain quaternary ammonium groups to prepare AEPs. However, monomers can also be prefunctionalized with cationic groups and polymerized directly. Copolymerization of a cationic monomer with a neutral monomer/crosslinker serves as a straightforward approach to balance conductivity, mechanical strength, and water uptake. Direct polymerization of cationic monomers is particularly valuable if the cationic moiety is difficult to synthesize, or when synthetic methods to append the cation

to the polymer backbone may not be highly efficient.[215] One benefit of this approach is that a cationic monomer can be carefully prepared and purified for incorporation into an AEP. The polymerization chemistry and cationic functional group must be compatible, where enchainment of the monomer can be accomplished in the presence of the functionality. Olefin metathesis has emerged as a valuable tool for this process.[215]

Olefin metathesis refers to the redistribution or exchange of C=C bonds and is a critically important reaction in the construction of polymers, macrocycles, and a wide range of complex organic substrates.[315] The widely accepted mechanism by which olefin metathesis occurs was described by Chauvin and Hérrison in 1971 (Scheme 23a).[316] This involves a [2+2] cycloaddition where a metal–carbene reacts with an alkene to form a metallocyclobutane intermediate, followed by cycloelimination to form either the original alkene or a new olefin. Metathesis of strained cyclic olefins leads to polymeric materials as shown in Scheme 23b, driven by the release of ring-strain, which is termed ROMP.[317] Alternatively, dienes can be combined with the loss of a small molecule (typically ethylene) for the preparation of polyolefins (acyclic diene metathesis polymerization, ADMET).[318] The kinetic profile for these reactions is different, as ROMP proceeds *via* a chain-growth mechanism, and ADMET proceeds *via* a step-growth process. To date, AEMs have been primarily synthesized using ROMP.

Heteroatom-free polyolefin backbones can be obtained using olefin metathesis, and a wide range of catalysts can be used to effect ROMP or ADMET, though molybdenum and ruthenium catalysts are the most popular.[315] Ruthenium catalysts are most common in AEP synthesis,[215] as they are less
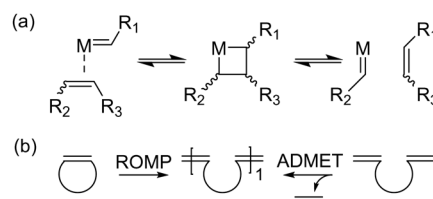


**Scheme 23** (a) General olefin metathesis mechanism and (b) polymerization chemistries possible using olefin metathesis.

**5732** | *Chem. Soc. Rev.*, 2024, **53**, 5704–5780

This journal is © The Royal Society of Chemistry 2024

oxophilic than molybdenum catalysts, signifying that polymerizations can be carried out in the presence of a wide range of functional groups such as alcohols, esters, amides, and ketones, to name a few.[315] Commercially available Ru-complexes known as Grubbs catalysts (1st, 2nd, and 3rd generation) are typically used in the preparation of AEMs (abbreviated as Ru cat in Scheme 24).[319–321] Living polymerization of highly strained cycloolefins is possible with fast-initiating catalysts,[321,322] and a few examples of block copolymer AEMs have been reported.[323,324]

The typical monomers used in AEP synthesis are norbornenes, cyclooctenes, and dicyclopentadiene (Scheme 24). Some of the first polymers to be synthesized *via* olefin metathesis were ring-opened polynorbornenes and polyalkenamers.[325,326] Ring-opened polynorbornenes were commercialized in the 1970s under the trade name Norsorex, and polyoctenamers, prepared from ROMP of *cis*-cyclooctene, are commercial products sold under the trade name Vestenamer.[315] Polydicyclopentadiene, derived from polymerization of *endo*-dicyclopentadiene, is a thermoset polymer, which has also found use in a range of applications.[315] The resultant polyolefins all have alkenes present in the repeat unit of the polymer backbone, and the relative concentrations of *cis* and *trans* content in the polymer backbone can be influenced by the choice of polymerization catalyst. Generally, Ru catalysts lead to mixtures of *cis/trans* content in the polymer backbone. Stereospecific polymerizations of norbornene, *endo*-dicyclopentadiene, and tetracyclododecene are possible,[327–332] but Ru catalysts are typically non-stereospecific.[333,334] The alkene units present in the polymer backbone are susceptible to oxidation, so hydrogenation and crosslinking can be used to prepare stable saturated hydrocarbons. Hydrogenation of ring-opened polynorbornenes has been accomplished using tosyl hydrazide (>95%) at 120 °C,[333] and with 5 wt% reduced Pd on CaCO$_3$ at 100 °C with 400–600 psi of H$_2$. Hydrogenation of polyalkenamers can also be accomplished with tosyl hydrazide at high temperatures (often with tri-*n*-propylamine),[322,335] or with iridium catalysts and high pressures of H$_2$.[336] Hydrogenation of ring-opened polynorbornenes and polyoctenamers can also result in semicrystalline polymers,[322,333,334,337] which is an important consideration in the design of AEMs.

Functional norbornene monomers are prepared from Diels–Alder cycloaddition reactions and functional cyclooctene monomers are typically prepared from 1,5-cyclooctadiene. Multistep synthetic pathways are often needed to obtain cationic monomers, which can be used directly in polymerization. Copolymerization of the cationic monomer with a neutral comonomer is common, as shown in Scheme 24a and b, affording linear polymers that can be soluble in organic solvents. Sometimes, the combination of hydrophilic headgroups and hydrophobic polyolefins can make solution processing difficult, particularly after hydrogenation. Crosslinking is also commonly employed with ROMP as this can help control swelling and water uptake in these materials. This can be accomplished by copolymerization of a cationic monomer with dicyclopentadiene (Scheme 24a) or by synthesizing a difunctional cationic monomer, as shown in Scheme 24c.

Historically, the first reports of ROMP-based AEMs appeared in 2009–2010.[336,338,339] Coates developed a straightforward approach to a norbornene monomer bearing a trimethylammonium group.[338] The β-position was blocked with a methyl group to prevent Hofmann degradation in the polymer.[338] The resultant monomer was copolymerized with dicyclopentadiene to yield a crosslinked polymer film, xPNB-NMe$_3$ (Fig. 18a). Upon conversion to the hydroxide form, this material did not swell appreciably in MeOH, and had a $\sigma_{22°C}$ = 18 mS cm$^{-1}$, which, at the time, was one of the highest hydroxide conductivities for an AEM.[338] Since then, the Coates group has primarily reported on cyclooctene-based ROMP polymers (Fig. 18a),[336,339–341] where the resultant cationic polyoctenamers were converted into polyethylene-based AEMs using an Ir-catalysed hydrogenation. The ratio of cationic monomer was optimized with cyclooctene comonomer, and the final optimized PE-NMe$_3$ and recently synthesized PE-pip have higher water uptake and significantly higher hydroxide conductivities than the original crosslinked xPNB-NMe$_3$ (PE-NMe$_3$ $\sigma_{22°C}$ = 48 mS cm$^{-1}$ and WU = 132%, PE-pip $\sigma_{22°C}$ = 41 mS cm$^{-1}$ and WU = 87%).[336,340]

Beyer and co-workers reported a hydrogenated polynorbornene derivative where ether linkages were used to tether the ammonium cation to the polymer backbone (hPN-NMe$_3$ in Fig. 18a).[342] The goal was to partially mimic some of the structural features of Nafion™ (semicrystalline backbone, ether
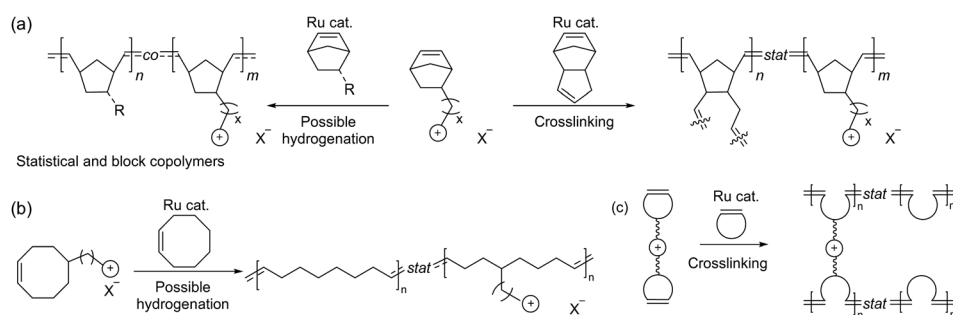


**Scheme 24** Synthetic approaches to ROMP-based AEMs: (a) general scheme for polymerization of norbornene monomers, (b) general scheme for polymerization of cyclooctene monomers, and (c) crosslinking approach with difunctional monomers.
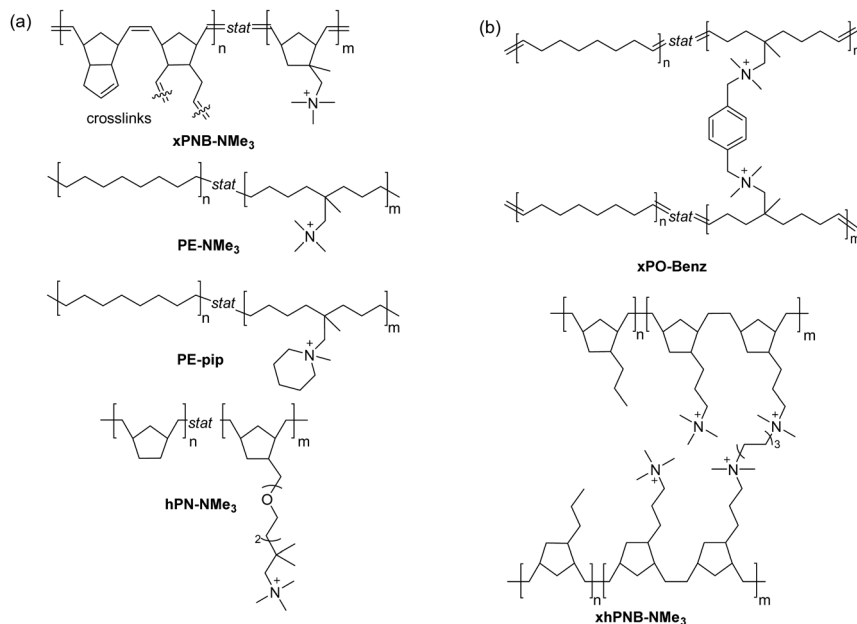
Fig. 18 Selected examples of ammonium-based AEMs prepared using ROMP: (a) linear polymers and polymers crosslinked using dicyclopentadiene and (b) crosslinked films *via* ammonium linkages.

linkages to the side chain) to see if the performance characteristics could be replicated. Exceptional conductivities for these materials were noted (optimized structure $\sigma_{80°C}$ = 177 mS cm$^{-1}$ with WU$_{80°C}$ = 82%), but the mechanical properties of the film were a concern for long-term fuel cell operation.[342]

Multiple reports on crosslinked AEMs derived from both norbornenes and cyclooctenes have appeared.[323,339,343,344] Coates reported on a crosslinked polyalkenamer comprised of dicyclooctene tethered with two benzyl ammonium groups (Fig. 18b).[339] Copolymerization with cyclooctene (1.5 equiv.) afforded the highly conductive xPO-Benz, which exhibited a $\sigma_{22°C}$ = 68.7 mS cm$^{-1}$, outperforming PE-NMe$_3$.[336,339] The high conductivity was attributed to the high IEC, which was made possible by crosslinking. Kohl *et al.* also recently reported on a crosslinked polynorbornene material xhPNB-NMe$_3$, which had high ionic conductivity (Fig. 18b).[323] In that work, block copolymers of 5-bromopropylnorbornene and 5-propylnorbornene were synthesized and hydrogenated using tosyl hydrazide. Then, *N,N,N′,N′*-tetramethyl-1,6-hexanediamine was used to crosslink the material *via* a reaction with two bromoalkyl groups, and the remaining pendents were replaced with trimethylammonium groups.[323] The crosslink density was key in these materials, and the authors noted that with 20 mol% crosslinker, the highest hydroxide conductivity of 99 mS cm$^{-1}$ at 25 °C and 195 mS cm$^{-1}$ at 80 °C (WU = 115%) was obtained.[323] No detectable degradation in conductivity was noted in 1 M NaOH at 80 °C over 792 hours. Finally, although the conductivity for this optimized material was high, the AEMFC open-cell voltage was still somewhat low (0.70 V), which was most likely due to the high gas crossover from the high water uptake.[323] The peak power density (PPD) was 126 mW cm$^{-2}$ for the optimized membrane, demonstrating how conductivity and mechanical properties must be optimized

for specific applications.[323] Beyond these reports, pyrrolidinium-based crosslinked ROMP membranes have also been described.[343,344]

Coates and co-workers reported on an imidazolium-fused cyclooctene monomer in 2018, which was combined with the Grubbs second-generation metathesis catalyst to produce cyclic oligomers (cPO-imid in Fig. 19).[345] The formation of macrocycles was attributed to the moderate ring strain of the fused imidazolium monomer (−7.5 kcal mol$^{-1}$), which slows propagation and thus renders secondary metathesis competitive, and to the planar imidazolium creating "U-turns" in the propagating chain.[345] To synthesize an AEM, a crosslinked imidazolium polymer was prepared using a bifunctional imidazolium crosslinker. Upon hydrogenation, this imidazolium-based AEM had good alkaline stability and hydroxide conductivity ($\sigma_{22°C}$ = 37 mS cm$^{-1}$, WU = 94%).[345] In a follow-up study, imidazolium-functionalized *trans*-cyclooctene monomers were synthesized.[346] These have increased ring-strain relative to the previous derivatives, and both statistical and block copolymer PE-imidazolium could be synthesized (Fig. 19).[346] Much higher conductivities were noted for the statistical copolymers, partially attributed to the more disordered block copolymer microphase segregation, which may impede ion mobility.[346] A crosslinked variant of the statistical copolymer was highly conductive ($\sigma_{22°C}$ = 49 mS cm$^{-1}$, WU = 115%).[346] Interestingly, the authors noted that the crosslinked films showed no degradation after 30 days in 1 M KOH at 80 °C, while the non-crosslinked films became brittle after 7 days under identical conditions.[346] Several other reports on imidazolium-based ROMP AEMs have appeared.[347,348]

The exceptional stability of tetraaminophosphonium has led to its exploration as cationic moieties in AEMs. The bulky P(N(Cy)Me)$_4$[Cl] was reported to be highly stable as a phase-
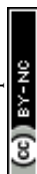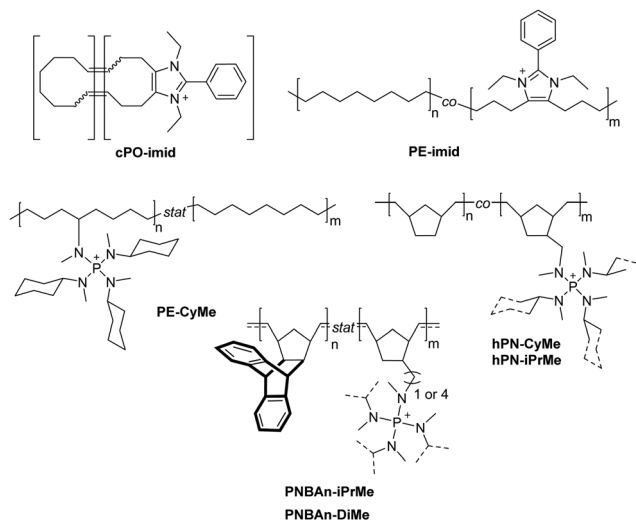
Fig. 19 Selected examples of imidazolium- and phosphonium-based AEMs prepared using ROMP.

transfer catalyst under alkaline conditions ($t_{1/2}$ = 67 hours at 100 °C in $C_6H_5Cl$/50 wt% NaOH).[349] This cation was appended to a cyclooctene monomer and polymerized. After hydrogenation, the PE-CyMe copolymer was obtained (Fig. 19).[64] The hydroxide conductivity for PE-CyMe was $\sigma_{22°C}$ = 22 mS cm$^{-1}$ with moderate WU (52%).[64] PE-CyMe was exceptionally stable to alkaline media, with hydroxide conductivity retained even after 20 weeks in 15 M KOH at 22 °C.[64] The fairly complicated synthesis of PE-CyMe led to some more recent improvements in monomer synthesis. Noonan and co-workers reported a simple synthesis of tetraminophosphonium norbornenes in 2020.[324] Both block and statistical copolymers with norbornene as a comonomer were synthesized (hPN-CyMe and hPN-iPrMe in Fig. 19), but the diblock copolymers were brittle.[324] Statistical copolymers were much more effective AEMs, and hPN-CyMe (Fig. 19) had a hydroxide conductivity of 19 mS cm$^{-1}$ at 25 °C with a water uptake of 82%.[324] The hPN-iPrMe had higher hydroxide conductivity (27 mS cm$^{-1}$) at 25 °C and slightly lower water uptake (~75%).[324] This was partially attributed to the increased IEC because of the more compact cation, but also to the increased crystallinity of the polymer as hPN-CyMe was completely amorphous, but hPN-iPrMe had some crystalline domains as evidenced by AFM studies and differential scanning calorimetry measurements. Going beyond 20 mol% of the cationic monomer was challenging for these materials without excessive swelling.[64,324]

Noonan and co-workers followed up on the hPN copolymers and demonstrated that copolymerization of a rigid norbornene anthracene cycloadduct with tetraaminophosphonium norbornenes was an effective approach to decrease segmental mobility in polynorbornene-based AEMs.[350] The PNBAn-iPrMe swelled less (WU = 49%) at 25 °C and had higher hydroxide conductivity (30 mS cm$^{-1}$) than the counterpart without anthracene (hPN-iPrMe).[350] The authors also noted that the unsaturated PNBAn derivatives (with double bonds) had higher conductivities than the saturated ones, providing further support that decreasing

segmental mobility is beneficial in these phosphonium copolymers.[350] Stability studies in 10 M KOH also revealed the need for the bulky isopropyl groups around the P center for improved hydroxide stability.[350] Though mechanical embrittlement of all the PNBAn copolymers was noted over time, the study demonstrated how modification of the ring-opened polynorbornene backbone can be used to enhance AEM performance.[350]

Various cobaltocenium AEMs have been synthesized via ROMP.[351–354] These metallocene-based cations consist of a Co(III) metal centre sandwiched between two cyclopentadienyl ligands. These have been investigated as an alternative to the commonly used ammonium headgroups in AEMs. Two reports have appeared that highlight how to tailor the cyclopentadienyl ligands with substituents to impart good alkaline stability to cobaltoceniums.[353,355] Yan and Coughlin demonstrated that the permethylated cyclopentadienyl ligand ($C_5Me_5$ or Cp*) can be used to make an ultra-stable $Cp^*_2Co^+$ cation[355] when compared to the $C_5H_5$ (Cp) parent derivative $Cp_2Co^+$. They conducted a stability test at 140 °C in 1 M NaOD/$D_2O$ and demonstrated that only 8.5% of $Cp^*_2Co^+$ had degraded after 1000 hours, whereas the parent $Cp_2Co^+$ degraded completely in 1 week. Under the same conditions, the well-known benzyltrimethyl ammonium had degraded by 18% in 24 hours.

Tang and co-workers also systematically explored the impact of alkylation on cyclopentadienyl ligands for cobaltocenium alkaline stability.[353] They found, as expected based on Yan and Coughlin's work, that increasing methylation offers marked improvements in alkaline stability.[349,353] They also noted that either 1 or 2 t-butyl groups on the cyclopentadienyl ring can lead to alkaline-stable cations. The authors carried out stability tests in 5 M KOH/$CD_3OH$, which is similar to reports from Coates and co-workers who have developed a protocol to examine cation headgroup stability and compare different families of cations.[59,356] In Tang's work, the studies were also carried out under air rather than $N_2$, which also impacts cobaltocenium stability.[353] The authors found that the octamethyl cobaltocenium only degraded by ~11% and ~19% after 553 and 1025 hours, in 5 M KOH/$CD_3OH$ at 80 °C. They also discovered that the tetra-tert-butyl cobaltocenium (1,3-orientation of substituents on the Cp ring) only degraded ~8% after 1025 hours. Under the same conditions, the benzyltrimethyl ammonium was almost completely degraded in just over 700 hours.

In early work, Tang and co-workers synthesized PE-$Cp_2Co$ using ROMP, and that material had hydroxide conductivities ranging from ~20–90 mS cm$^{-1}$ from 22–90 °C and water uptake ranging from 35–160% between 20 and 80 °C (Fig. 20).[351] These AEMs could be crosslinked to mitigate dimensional swelling in water.[352] As noted above, the parent $Cp_2Co^+$ has limited stability in alkaline media, and so the authors followed up on that work with ROMP polymers bearing more stable octamethyl cobaltocenium as a headgroup.[353] The synthesized PE polymer exhibited good hydroxide conductivity (33–87 mS cm$^{-1}$ from 22–80 °C). This polymer retained 91% of its conductivity after immersion in 3 M KOH at 60 °C for

This journal is © The Royal Society of Chemistry 2024

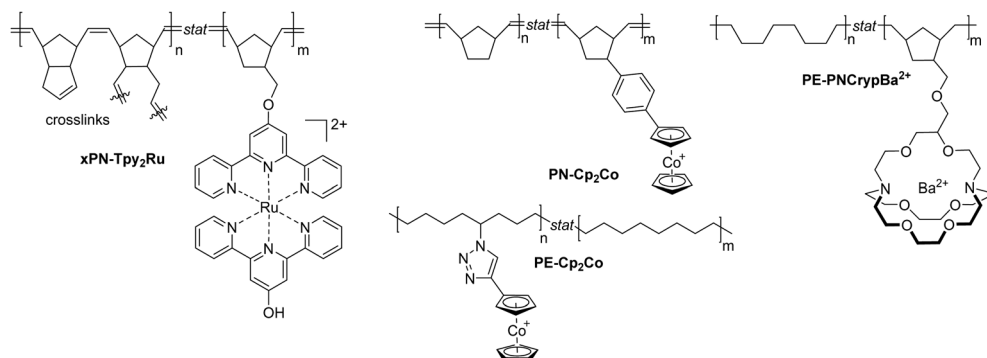Chem. Soc. Rev., 2024, 53, 5704–5780 | 5735

**Fig. 20** Selected examples of metal-based AEMs prepared using ROMP.

30 days and was evaluated in an AEMFC. A PPD of 350 mW cm$^{-2}$ was noted with an OCV of almost 1.0 V. Another ROMP-based AEM, PN-Cp$_2$Co (Fig. 20), had a high chloride conductivity of 50 mS cm$^{-1}$ at 90 °C and only 13.2% water uptake (95% RH) for an IEC of 1.5 mequiv. g$^{-1}$.[354] The cobaltocenium monomer was prepared in a unique manner, from lithium halogen exchange on an *exo*-4-bromophenyl substituted norbornene. Although the hydroxide conductivity of the polymer was not reported, this study highlighted the potential of polynorbornene polymers for metal-based AEMs.

The first example of a transition metal cation implemented in AEMs was a bis(terpyridine)Ru(II) functionalized polynorbornene made in 2012 by Hickner and Tew.[357] These cations were directly polymerized *via* ROMP with dicyclopentadiene as a crosslinking comonomer (xPN-Tpy$_2$Ru in Fig. 20). The optimized AEM had a 1:5 ratio of cationic monomer to hydrophobic/crosslinking monomer, resulting in relatively high water uptake (126%) and hydroxide conductivity of 28.6 mS cm$^{-1}$ at 30 °C (IEC of 1.4 mequiv. g$^{-1}$).[357] The membrane was stable in 1 M NaOH at room temperature for 6 months.[357] A follow-up study by Hickner and Tew on the copolymerization of this monomer included 1,5-cyclooctadiene and dicyclopentadiene as comonomers in polymerization.[358]

A 2017 study by Kwasny and Tew explored how altering the site of crosslinking in the polymer backbone impacted water uptake.[359] Membranes were prepared from heteroleptic and homoleptic Ru complexes, where polymerizable norbornene units were either on one or both terpyridine ligands.[359] Crosslinker to non-crosslinker and ionic to non-ionic monomer were held constant, and a substantially lower water uptake of 30–35% was obtained by utilizing a homoleptic ruthenium cation in comparison to the heteroleptic derivative (water uptake of ~230%).[359] The homoleptic complex also resulted in a decrease in Cl$^{-}$ conductivity.[359] The authors also examined Ni- and Co-terpyridine complexes for AEMs as part of that work.[359] Tew *et al.* also synthesized bis(terpyridine)Ni(II) AEMs through RAFT polymerization and crosslinking *via* thiol–ene click reaction to create phase-separated morphology.[360] To our knowledge, the alkaline stability of these different terpyridine-based metal complexes has not been compared to ammonium headgroups.

You and co-workers recently reported on a cryptand-based AEM prepared using ROMP (Fig. 20).[361] The authors noted that the cryptand is key to having a high binding constant for metal cations in water and developed a synthetic method to append this structure to a norbornene monomer and copolymerize it with cyclooctene to afford PE-PNCryp.[361] Then, the choice of metal salt for binding was examined, and the only one that resulted in minimal leaching was Ba$^{2+}$. This was attributed to the high binding constant of Ba$^{2+}$ with the cryptand compared to Na$^+$ and K$^+$.[362] The optimized PE-PNCrypBa$^{2+}$ had a hydroxide conductivity of 23 mS cm$^{-1}$ at 40 °C. A series of PECryp Ba$^{2+}$ copolymers prepared by a different method was even more conductive than the PE-PNCrypBa$^{2+}$ copolymer. The corresponding physical studies suggested that the ionic clustering network in the PECryp above the $T_g$ is more robust. The PECrypBa$^{2+}$ copolymers retained 70% of their chloride conductivity after immersion in 15 M KOH at 40 °C and 60 °C for 1600 hours. These are unprecedentedly harsh alkaline conditions and highlight the potential of this framework for future exploration. The authors noted that this membrane performed well in AEMWE with 0.1 M KOH, similar to the commercially available PiperION.

ROMP is a useful tool to make polyalkenamers, which can subsequently be hydrogenated to form heteroatom-free polymer backbones. A wide range of functionalities is tolerated in ROMP, and strained cycloalkenes bearing cationic groups can be directly polymerized, which is advantageous for the creation of new materials. The synthesis of AEPs decorated with main group and metal-based cations is a particularly important outcome of using ROMP chemistry. The stability of metal cations in AEPs under device operating conditions is a critical subject of research for the practical use of these polymers, as this will dictate their potential success in devices.

A direct benefit of the ROMP approach is the double bond present along the polymer backbone, which can be used to bring about crosslinking and facilitate the preparation of polymers with high IECs. However, the Ru catalysts used for ROMP are somewhat expensive, and a two-step process is needed to achieve a fully saturated hydrocarbon backbone (*e.g.*, polymerization and hydrogenation), which adds an additional step to the overall process.

**5736** | *Chem. Soc. Rev.*, 2024, **53**, 5704–5780

This journal is © The Royal Society of Chemistry 2024

## 4.3. Radiation grafting method

Radiation-grafting is a useful method for the chemical modification of pre-formed, inert polymer substrates such as films,[363] powders,[364] and fibres[365] to form useful functional materials. Radiation-grafted (RG) polymers are being investigated for use in a wide variety of applications across many fields (e.g., clean energy, environmental remediation, healthcare) including electrolyte membranes for low- and high-temperature polymer electrolyte fuel cells and membrane-based water electrolysers,[366–370] $CO_2$ electrolysis to high-value chemicals;[371] $CO_2$ adsorbents;[365] ion exchange membranes and separators for ED/RED,[372–374] RFBs,[367,375,376] actuators,[377] Li-ion batteries,[378] and supercapacitors;[367] biofouling-resistant membranes for microfiltration;[379] materials for the recovery, extraction, and separation of inorganics including heavy metals ions;[380,381] chromatography materials for protein purification;[382] biomaterials for tissue engineering and engineered skin;[383] and UV absorbers.[384]

Scheme 25 summarizes the key stages behind the most commonly encountered pre-irradiation grafting (PIG) method:[367,369,370] (1) irradiation of inert polymer substrates to "activate" them (functionalize with radicals or peroxide groups, both of which can initiate copolymerisation); (2) monomer grafting onto the substrates (after an $N_2$ purge to remove all traces of $O_2$); and (3) an optional post-graft functionalization process.

The radiation is commonly a high dose-rate electron-($e^-$)-beam ($\beta$ radiation), a low dose-rate $\gamma$-ray, or an ultraviolet (UV) source. Radiation grafting of polymer substrates using lower energy UV electromagnetic radiation typically leads to a bias towards surface grafting, unless the films are thin enough to allow for reasonable levels of grafting into the bulk.[374] The use of high energy and high dose-rate radiation (e.g., $e^-$-beams) leads to bulk grafting where there is a high concentration of short-length (low molecular weight) grafted chains, while the use of high energy lower dose-rate radiation (e.g., $\gamma$-rays) also leads to bulk grafting, but where there is a lower concentration of longer-length grafted chains;[114,385] the latter scenario is less desirable if chemical degradation is a concern (e.g., oxidative cleavage of entire grafted chains, vide infra) as there is a greater loss of functionality per cleaved chain.

With large polymer substrates, low dose-rate point sources such as $\gamma$-rays are also subject to inverse square law limitations (radiation intensity is inversely proportional to the square of the distance from the source), therefore requiring the periodic

suspension of the irradiation process so that they can be moved around to ensure equal absorbed doses on all parts of the sample. With high energy (1–10 MeV) commercial e-beam facilities, more commonly known for sterilizing plastics and medical equipment,[386] as well as for fabricating heat-shrink polymers,[387] the e-beam source is often wider than the samples being irradiated.

Homogeneous irradiation is more easily controlled by passing the substrates at a controlled speed through the e-beam, with higher doses being enabled by multiple passes; this also helps with minimising sample heating (due to the high energy radiation), where the radicals/peroxide groups would be decomposed as they form. It has recently been found that irradiation of polymer films whilst being kept cool ($< -10\ °C$) led to a higher degree of grafting (DoG (%) = % mass of grafted chains normalized to the mass of substrate used) and membranes with better properties;[388,389] the radicals formed during radiation are preserved more during the lower temperature irradiation.

With fluorinated (e.g., PTFE, FEP) or partially fluorinated (e.g., ethylene-tetrafluoroethylene ETFE) substrates, low total absorbed radiation doses need to be used (typically $< 50$ kGy) as high energy radiation can cleave the backbone C–C bonds, leading to mechanically weak functionalized membranes. Non-fluorinated substrates (e.g., polyethylene) can tolerate higher total absorbed doses ($> 100$ kGy), but such high total doses can lead to radiation crosslinking (this can be desirable and undesirable depending on the required final membrane properties).[388,390]

If the irradiation step is conducted with the substrate exposed to air (rather than vacuum or inert atmospheres), then it is known as the peroxidation-PIG method.[367,369,370] This typically requires a higher total radiation dose for a target DoG, compared to when irradiation of polymer substrates was conducted in inert atmospheres.[389,391] Therefore, this can place a limit on practical grafting levels when functionalising polymer substrates containing C–F bonds (see discussion vide supra on upper limits of radiation doses that can be used).[392] Peroxidation-PIG also leads to the formation of peroxide groups on the chains of irradiated polymer substrates, which can lead to the formation of ether (C–O–C) links between the polymer chains on the substrate and the grafted polymer chains (not shown in Scheme 25 to aid clarity).[370] A major practical advantage of using the peroxidation-PIG method is that an onsite radiation source is not needed. The offsite irradiated and peroxidated polymer substrates can be transported back to a
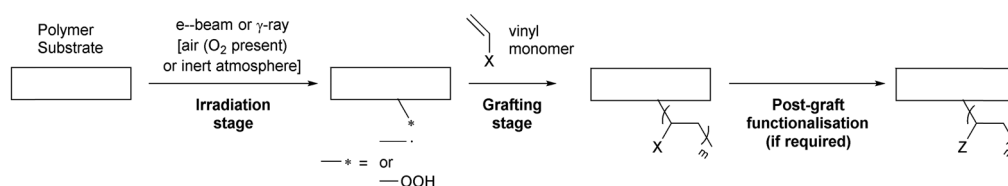


**Scheme 25** The key stages behind the pre-irradiation PIG. It is known as the peroxidation-PIG method if the polymer substrate is irradiated in air (which can result in an ether links between the substrate and grafted chains [not shown]). If the polymer substrate is submerged in the grafting mixture containing the monomer before irradiation treatment, this is the MIG.

laboratory in dry ice and stored in low-temperature freezers ($< -40$ °C) for 6–12 months (storage time achievable depends on the polymer substrate used).[393] Such peroxidation-PIG grafting processes often use commercial e-beam facilities, as large volumes of substrate can be treated in a single beaming session.

If inert atmosphere PIG is used, then fewer main chain bond scissions occur (*cf.* peroxidation-PIG), especially as lower radiation doses can be used, while more radiation crosslinking can also occur (*cf.* same radiation dose peroxidation-PIG);[389] grafting times can also be quicker. This can lead to RG-AEMs (Scheme 26) with enhanced mechanochemical stabilities. When the polymer substrates are grafted immediately after irradiation, the radicals on the polymer chains of the substrate can directly co-graft without the formation of ether links. However, if the inert atmosphere-irradiated polymer substrates are cold stored in the air, peroxide groups will eventually form (as with the peroxidation-PIG).[389] An alternative to PIG is the mutual-(simultaneous)-grafting method (MIG), where the polymer substrate is submerged in the grafting mixture to combine the irradiation and grafting stages into a single step.[367,369,370] However, this requires a radiation facility on site and typically uses a low dose-rate γ-ray source (with radiation security issues to attend to); commercial e-beam facilities are often reluctant to irradiate containers containing toxic and flammable monomers. A major downside to MIG is that there can be a high level of homopolymerisation occurring; this is where the monomer polymerizes without the chains being covalently grafted onto the substrate. This can lead to a large amount of effort to remove the grafted substrates from the homopolymer (it has been known for the substrate to be encased in a block of homopolymer), as well as leading to materials with lower degrees of grafting. Despite this, MIG can be useful for small-scale trials of new RG-material chemistries, and it tends to lead to reduced levels of radiation crosslinking.[391]

With the radiation-grafting of dense substrates, such as ETFE films, the grafting front mechanism can operate.[385,394] This is where the monomer initially co-polymerizes onto the surface of the film (after low grafting durations), after which the monomer can penetrate further and further into the core of the film (after longer grafting durations), until homogeneous grafting levels are achieved throughout the bulk of the newly formed membrane. If such a mechanism is operating, then this can place an upper limit to the thickness of the films (or diameters of powders/fibres) that can be homogeneously grafted through

the bulk; a good rule of thumb range is 100–200 μm maximum film thicknesses, depending on the substrate and grafting conditions. With less dense films, such as low-density polyethylene (LDPE), where the monomer can diffuse more quickly into the core of the film, then the grafting does not always follow such a front mechanism.[392] Note that for RG-AEMs, PVDF is not a suitable substrate as it is unstable in alkali conditions (see Section 2.3).[395] There is also some interest in making RG-AEMs from non-fluorinated non-polyethylene substrates such as cellulose acetate, and Nylon-6,6 nanofibrous sheets.[396,397]

The crystallinity of the substrate can also influence the final properties of RG-PEMs and RG-AEMs, as their final nano-morphologies can be complex.[398–402] The radicals formed on irradiation tend to be more stable in the crystalline domains, but they can migrate to the interphase and amorphous domains,[388,389] where they will react with any oxygen species, and grafting will predominantly propagate into the amorphous domains.[403] For example, Sproll *et al.* reported that ETFE with a smaller number of larger crystallites produced an RG-PEM with better conductivity performance in a fuel cell;[404] this is partly due to better connected amorphous domains.

The most common monomer used to fabricate RG-AEMs is vinylbenzyl chloride (Scheme 26).[114,371–373,388,389,391,392,394,395,405–410] On amination/quaternization, cationic groups are introduced, resulting in an anion-conducting material, and the most commonly encountered amine is trimethylamine (TMA), which yields benzyltrimethylammonium headgroups. This class of RG-AEM has ease of handling, high hydroxide conductivities, and rapid water diffusion dynamics.[411–413] Disadvantages include high levels of swelling in water without additional crosslinking,[373] especially laterally (area swelling as opposed to thickness swelling), which will be a particular problem for their use in devices such as AEMFC that can experience humidity cycles. Without mitigations, this will also mean that pre-swelling of the RG-AEM may be needed if they are to be used in large-area AEMWE cells.[414]

A diversity of quaternization agents for VBC-based RG-substrates has been investigated including aliphatic heterocyclic types like *N*-methylpiperidine (MPIP) and quinuclidine (QUN), 2-butyl-1,1,3,3-tetramethyl-butylguanidine (TMBG), as well as aromatic types such as 1,2-dimethylimidazole (DMI) and pyridine (PYR) (Scheme 27).[115,415–417] Alternative quaternization agents include 1,2,4,5-tetramethylimidazole (TMI, the cation found in Sustainion® AEMs), *N*-methylpyrrolidine
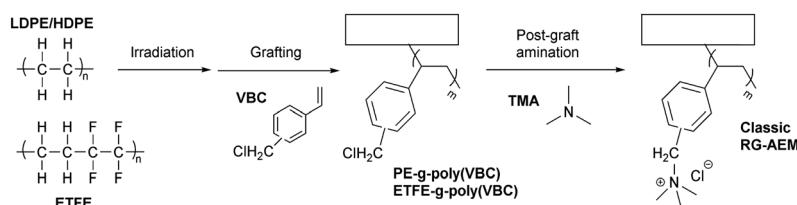


**Scheme 26** The PIG of vinylbenzyl chloride (VBC) onto ETFE and polyethylene (PE, either low- or high-density) film substrates with subsequent post-grafting amination with trimethylamine to form a classical benzyltrimethylammonium radiation-grafted anion-exchange membrane (TMA-RG-AEM).

5738 | *Chem. Soc. Rev.*, 2024, **53**, 5704–5780

This journal is © The Royal Society of Chemistry 2024
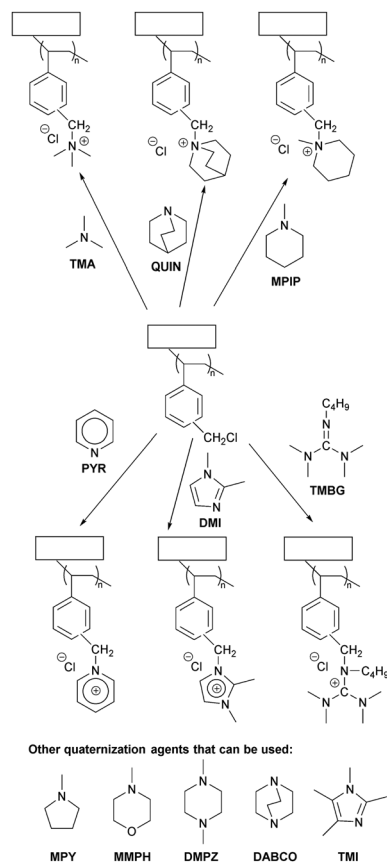
**Scheme 27** Different N-containing reagents that can be used for post-graft quaternization of VBC-based RG-substrates.

(MPY), *N*-methylmorpholine (MMPH), 1,4-dimethylpiperazine (DMPZ), and DABCO, the latter two have the potential to form crosslinks as they contain two tertiary amine groups.[115,415,418,419] RG-AEMs made with isoindolinium headgroups have also been fabricated,[420] as have those with more complex imidazolium and pyridinium groups.[407] As well as affecting the conductivity and alkali stability of the RG-AEMs (*vide infra*), the choice of cations can affect their water uptakes: *e.g.*, the water uptakes of TMA types are generally less than MPIP analogues.[372,415] Crosslinking can be used to reduce the excessive levels of swelling on hydration, but this can have a negative impact on other properties such as conductivity.[373,421]

Despite the possibility of hydroxide-derived nucleophilic substitution and elimination degradation pathways ($S_N2$, E2, and Hofmann eliminations), VBC-grafted TMA- and MPIP-RG-AEMs are generally stable in hydroxide forms at 60 °C (at medium to high RH) and at higher temperatures when well hydrated.[422,423] An LDPE-TMA-RG-AEM has even been shown to maintain a hydroxide conductivity of *ca.* 300 mS cm$^{-1}$ over several hours at 110 °C when hydrated under pressurized conditions.[424] An ETFE-TMA-RG-AEM made using 3-VBC (*meta* isomer, synthesised in-house due to commercial unavailability) appeared to be more alkali stable compared to a benchmark made with commercially available 4-VBC (*para* isomer), but the 3-VBC monomer did not graft very well, leading to a low IEC

RG-AEM.[425] Similarly, the grafting of a monomer containing a butyl-spacer between the vinylbenzene group and the chloride leaving group led to a more alkali stable ETFE-MPY-RG-AEM (*cf.* a VBC-grafted MPY-benchmark), but again this had a low IEC due to poor monomer grafting characteristics.[426]

Benzyl-DMI and -PYR cations have poorer stabilities in alkali and will not be suitable for application in AEMWEs.[427,428] A benzyltriethylammonium (TEA) RG-AEM was also less stable in alkali than the TMA benchmark, especially at lower hydration levels, due to elimination reactions on the ethyl groups.[429] Obviously, the RG-AEM contains benzene-rings and thus has the potential to be oxidized when in contact with OER anodes of AEMWEs (as mentioned in Section 2.5, leading to the formation of weakly acidic phenolic groups resulting in chemical instabilities and poor *in situ* performances).[430]

With RG-PEMs made from styrene, the reactive C–H bonds in the grafted hydrocarbon chains that are in the alpha position to the benzene rings are highly susceptible to radical attack, which leads to the cleavage of entire grafted chains; this is one of the reasons RG-PEMs made *via* co-grafting of α-methylstyrene (AMS) and methylacrylonitrile (MAN) are a preferred formulation (MAN is needed to boost the grafting of AMS and also to lower gas crossover reactions, while AMS contains α-C–CH$_3$ groups and not labile α-C–H groups).[370,431] Due to the historic low stability of AEMs to alkali, with degradations over 10 s to 100 s of hours, radical/oxidative degradation (ROD) pathways have been generally neglected. However, with the recent development of alkali-stable AEMs, a debate has raged on the significance of RODs.[110] A recent study has also proven that significant concentrations of radicals can be observed in AEMFCs.[432] Espiritu *et al.* have reported that grafted poly(vinylbenzyltrimethylammonium hydroxide) cations degrade more (loss of IEC) in $O_2$ purged $D_2O$ than they do in $N_2$ purged $D_2O$;[115] degradations included the loss of complete benzyltrimethylammonium groups (not just the loss of trimethylamine). A LDPE-TMA-RG-AEM also showed a higher degradation of conductivity in $O_2$ gas compared to $N_2$ gas.[433]

Espiritu *et al.* conducted a detailed degradation study on LDPE- and HDPE-based TMA-RG-AEMs (MIG with low dose-rate γ-ray) and an ETFE-TMA-RG-AEM (peroxidation-PIG with an e$^-$-beam), where the hydroxide forms were submerged in (CO$_2$-free) air-saturated deionised water.[114] This study, which also involved $^{17}$O solid-state NMR, confirms that loss of entire grafted chains can occur *via* ROD, where higher dose-rates lead to a lower rate of IEC loss (due to there being more grafted chains of shorter length). These ROD reactions were the main contributor to IEC loss at lower pHs, over E2 and $S_N2$ attack on the headgroups. An LDPE-DABCO-RG-AEM was also evaluated, which was observed to have slightly less stability.

Other classes of RG-AEM have been reported that do not involve the radiation-grafting of VBC monomer. Several papers from the Takasaki Advanced Radiation Research Institute have documented work on RG-AEMs made using vinylimidazole monomers (vinyl group attached to one of the N-atoms in the imidazole ring), followed by a methyl iodide quaternization reaction to yield the imidazolium headgroups.[399–401,434] As

This journal is © The Royal Society of Chemistry 2024

*Chem. Soc. Rev.*, 2024, **53**, 5704–5780 | 5739

1-vinylimidazole and 1-methyl-2-vinylimidazole graft poorly on their own, a co-monomer boosting strategy was employed; this involves adding a co-monomer that easily grafts, such as styrene or MAN, to the grafting mixture to enhance the grafting levels of the poorer grafting primary monomer.[370,434,435] There are concerns with the alkali stability of such pendent imidazolium groups, as they can undergo OH⁻-derived ring-opening reactions, especially if there is a C–H group in the C2 position.[427]

Further alternative RG-AEM chemistries involve imidazolium head groups where they are not linked to the grafted chains *via* an imidazolium N atom.[435] An anilinium-type RG-AEM has also been fabricated using *N,N*-dimethylaminostyrene, with subsequent methylation with methyl iodide, to yield trimethylammonium groups that are directly bound to benzene rings on the grafted chains (and not connected to the benzene rings *via* methylene CH$_2$ groups);[436] however, the resulting RG-AEMs had very poor alkali stability. Finally, RG-AEMs made using the grafting of vinylpyridines, with subsequent methylation, have also been produced.[377] Given that such unprotected pyridinium groups have low stability in alkali, these were being prepared for use in ionic polymer–metal composite actuators.

Despite only a small number of evaluations of RG-AEMs in AEMWEs (see Section 6.2), they have been studied much more for use in AEMFCs with precious-metal-free electrodes.[437–441] They show a lot of promise as the complex nano-morphologies of RG-AEMs provide a good range of mechanical properties and gas permeability, along with high conductivities and facile water transport behaviours, leading to high performances in devices.[393] The RG method also allows for the introduction of multiple different functional group chemistries in controlled ratios,[373,431,434,442] which yields the ability to fabricate highly functional, tailored polymer materials. However, RG-AEMs can suffer from excess swelling, especially at high IECs, and due to the underlying radical polymerization mechanism, not all monomers are amenable for grafting (most reports have focused on monomers with styrene groups or carbonyl-containing groups such as with acrylates and arylamides, where the latter may not be useful for application in high pH

environments). The RG method also requires access to high-energy radiation facilities and may only be amenable to batch processes on scale-up, rather than use with continuous processes such as roll-to-roll. For improvements and tailoring of RG-AEMs for specific use in AEMWEs, the following adaptations should be researched: (1) covalent and ionic cross-linking to reduce swelling in water to yield more dimensional stability;[373,443,444] (2) incorporation of co-monomers to improve stability towards ROD including introducing antioxidants[442,445] or MAN (the latter to reduce gas crossover);[446] (3) incorporation of co-monomers such as styrene to modify nanomorphologies to alter conduction and water transport properties as well as to tailor mechanical properties;[447] (4) incorporation of aliphatic sidechains (non-aromatic) on the grafted component.

### 4.4. Anionic polymerization

Styrene-diene block copolymers are an important class of thermoplastic elastomers. Using two industrially important chemicals as raw materials, the sequential living anionic polymerization of styrene and 1,3-butadiene (or other dienes such as isoprene) is known to construct a diverse range of diblock and triblock copolymers.[448–451] The covalent bond connection between incompatible polystyrene and polydiene generates a wide array of microdomain morphology, as shown in Scheme 28. Polystyrene chains function as a hard block, providing mechanical strength and physically crosslinked domains, while polydiene chains serve as a soft matrix, providing elasticity to the material at ambient temperature. Among block copolymers, poly(styrene-*b*-butadiene-*b*-styrene) and its hydrogenated form poly(styrene-*b*-(ethylene-*co*-butylene)-*b*-styrene) (SEBS) (SBS of Scheme 28 and SEBS of Scheme 29, respectively) are commercially available and have been extensively studied for polymer microstructure-mechanical property relationship investigation for decades.[449,450]

In SEBS, the midblock poly(ethylene-*co*-butylene) is composed of inert saturated C–C and C–H bonds. Thus, a selective functionalization of aromatic rings of polystyrene chain with ionic group could create ionic block copolymers using the commercial polymer as a starting material platform. For example, sulfonation of the polystyrene block of SEBS
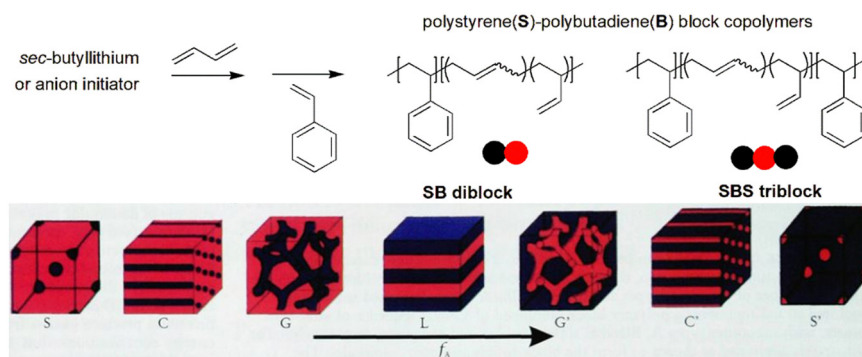


**Scheme 28** Synthesis of styrene-diene block copolymers and microdomain morphology based on the composition of each polymer; spherical (S), cylindrical (C), gyroid (G), and lamella (L), and volume fraction of A polymer ($f_A$) in AB diblock copolymers. Reproduced from ref. 448, with the permission of the American Institute of Physics, copyright 1999.

**5740** | *Chem. Soc. Rev.*, 2024, **53**, 5704–5780

This journal is © The Royal Society of Chemistry 2024
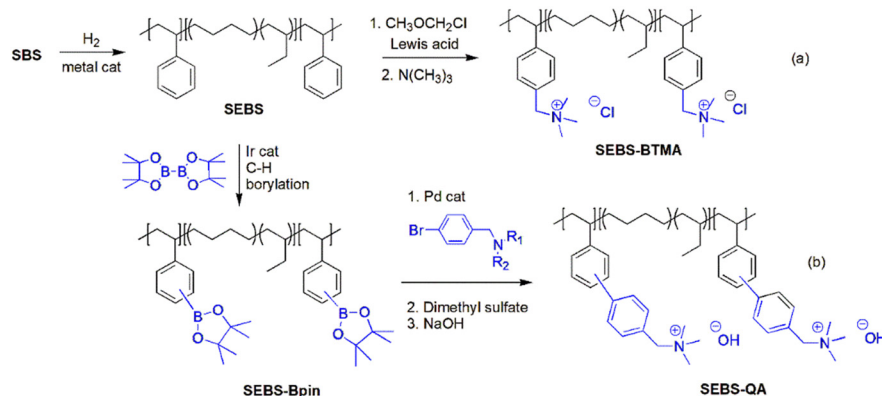
**Scheme 29** Synthesis of SEBS AEMs by (a) chloromethylation and (b) transition metal-catalysed C–H borylation–Suzuki coupling approaches.

transforms the commercial elastomeric material into an elastic proton exchange membrane in one step.[452,453] In general, the chemical functionalization of SEBS to prepare AEM involves the chloromethylation route shown in Scheme 29a. The reaction of SEBS with chloromethyl methyl ether in the presence of a Lewis acid catalyst incorporates a –CH$_2$Cl group into the benzylic position of the polystyrene end block. Subsequent substitution of the benzyl chloride in the polymer with trimethylamine gives a BTMA-functionalized SEBS (SEBS-BTMA). As stated in Section 2.1, although commonly practiced in laboratories, chloromethylation in polymer substrates frequently results in low efficiency and side reactions, including extensive cross-linking.[454–456] To overcome the limitations of chloromethylation, Bae and co-workers reported a transition metal-catalysed C–H borylation route for the synthesis of quaternary ammonium-functionalized SEBS AEMs (Scheme 29b).[457] Once the Bpin group is incorporated into the aromatic ring of polystyrene by replacing a C–H bond with a C–B bond, the Bpin group is replaced by functionalized aromatics through a Pd-catalysed Suzuki-coupling reaction. Although this synthetic approach allows the incorporation of a wide array of quaternary ammoniums at the terminal benzylic position, the requirement for expensive transition metal catalysts (Ir and Pd) would limit the scalability of the process.

Among the commonly practiced organic reactions for polymers, the most frequently used catalysis is an acid-catalysed reaction, employing either Brønsted or Lewis acid. Therefore, for the chemical modification of polymers to be practical and scalable, acid-catalysed functionalization would be highly desirable. Furthermore, among quaternary ammonium structures in AEMs, the insertion of a long alkyl chain spacer between the polymer chain and quaternary ammonium structure is known to enhance alkaline stability and the mobility of ionic groups compared to BTMA functionality.[57,58,458] Accordingly, the incorporation of a long spacer-tethered quaternary ammonium group to SEBS has been studied by utilizing Friedel–Crafts reactions. The Friedel–Crafts acylation of SEBS yields a ketone-functionalized polymer (SEBS-acylC5-Br of Scheme 30b), which can be subsequently reduced to –CH$_2$– by reaction with triethylsilane. After being cast into a film, immersion of SEBS-
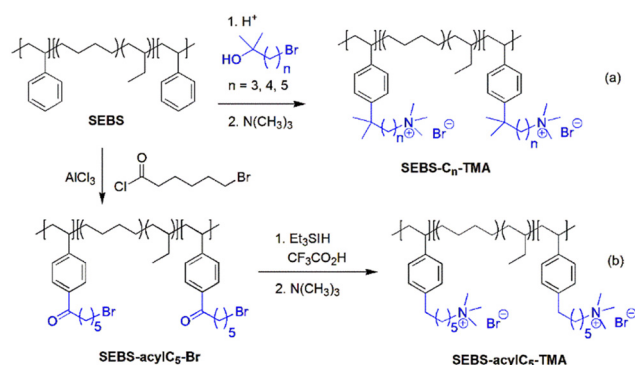


**Scheme 30** Synthesis of SEBS AEMs by (a) Friedel–Crafts alkylation and (b) Friedel–Crafts acylation-reduction approaches.

acylC5-Br into a solution of trimethylamine forms SEBS-acylC5-TMA as an AEM.[459] Although each reaction in this method is well-established in organic chemistry, the Friedel–Crafts acylation with an acid chloride that has terminal alkyl bromide moiety needs caution because both acid chloride and alkyl bromide can undergo Friedel–Crafts acylation and alkylation, respectively, in the presence of strong Lewis acid catalyst. If both reactions occur on polystyrene chains, crosslinking of polymer chains would occur, causing reduced solubility and gelation. The Friedel–Crafts alkylation with a brominated tertiary alcohol substrate eliminates that possible side reaction because Brønsted acid would react only with tertiary alcohol functionality, forming a tertiary carbocation, without affecting the terminal –CH$_2$Br group (Scheme 30a).[460] Compared to the Friedel–Crafts acylation method, the alkylation approach also has the advantage of a shorter reaction scheme by eliminating the reduction step of the acyl group in SEBS.

Other methods of synthesizing styrene-diene block copolymer AEMs through anionic polymerization include radical-induced bromination of poly(4-methylstyrene) using NBS and AIBN (Scheme 31a). Once diblock copolymer PB-b-P4MS was prepared by living anionic polymerization, followed by hydrogenation using p-toluenesulfonyl hydrazide. Subsequent radical bromination at the benzylic position generates a –CH$_2$Br moiety

This journal is © The Royal Society of Chemistry 2024

*Chem. Soc. Rev.*, 2024, **53**, 5704–5780 | **5741**

at the side chain of the polystyrene block. Amination of the block copolymer film in a solution of trimethylamine converts the benzyl bromide to benzyltrimethylammonium bromide in the polymer (PE-b-PS(BTMA) of Scheme 31a).[461] Kraton Performance Polymers Inc. (Houston, TX) specializes in the synthesis of poly(4-tert-butylstyrene)-b-poly(2-methylbutylene)-b-poly(4-methylstyrene)-b-poly(2-methylbutylene)-b-poly(4-tert-butylstyrene) (tbS-MB-4mS-MB-tbS of Scheme 31b). The midblock sulfonated version of the symmetric pentablock copolymer is commercially available with the trade name Nexar® and has attracted significant attention as a functional material for water transport and separation applications. The tertiary butyl group at the end block of the polystyrene chain increases $T_g$ and enhances mechanical strength, while the low $T_g$ poly(2-methylbutylene) block provides flexibility. The midblock poly(4-methylstyrene) was functionalized with benzyltrimethylammonium bromide using a similar protocol of radical-induced bromination and investigated as an AEM (Scheme 31b).[462]

Most styrene-diene triblock copolymer AEMs have polystyrene chains as an end block because rigid polystyrene functions as a hard block component in ABA triblock copolymer systems. An interesting approach to using semicrystalline polyethylene as a hard block component has been reported.[463] In this system, a sequence of anionic polymerization of butadiene and styrene in cyclohexane solvent generates a triblock copolymer poly(butadiene)-b-polystyrene-b-poly(butadiene). Although minor formation of poly(1,2-butadiene) is unavoidable, the polybutadiene end block consists primarily 1,4-configuration unit (over 90% based on $^1$H NMR spectroscopic analysis). This high percentage of 1,4-configuration in polybutadiene allows the conversion of the soft polymer chain at the end of the triblock copolymer to a rigid polyethylene block upon hydrogenation (ESE of Scheme 31c). The bromoalkyl functionalization using Friedel–Crafts alkylation chemistry[460] and subsequent amination results in triblock copolymer AEMs where midblock polystyrene is functionalized with a quaternary ammonium group. (ESE-C5-TMA). This midblock

functionalized AEM is equivalent to complemental SEBS AEM where the end block polystyrene is functionalized with an ionic group (SEBS-C$_n$-TMA of Scheme 30a).

Living anionic polymerization affords polymers with well-defined block composition and narrow molecular weight distribution but requires strict reaction conditions of an inert atmosphere and purification of reagents and solvents. Due to the strong nucleophilicity of anionic catalyst (e.g., sec-BuLi), the polymerization is not tolerant to common precursor groups typically used for AEPs, such as halides and amine, limiting the choice of polymers for AEP synthesis. Thus, the synthesis of AEP block copolymers from anionic polymerization first requires the installation of a precursor functional group by post-functionalization of the aromatic rings of the styrene block, such as chloromethylation or Friedel–Crafts reactions, which needs to be subsequently converted to alkaline stable quaternary ammonium groups.

# 5. Commercialization and milestones

## 5.1. Scale-up synthesis and markets

**5.1.1. Markets for AEM.** In 1998–2000, membranes and module sales amounted to 4400 million US$ with a growth rate of >8%. Notably, the application segments "electrochemical industry" and "miscellaneous" contributed only with 3% and 8%, respectively. Process-wise, the segments "electrodialysis" and "electrolysis" accounted for 110 and 70 million US$, respectively.[464] While Nafion™ membranes are essential for polymer electrolyte fuel cells, their main application is chlorine production. In 2003, chlor-alkali electrolysers with an active membrane area of 645 000 m$^2$ were in service, and a service life of longer than 3 years indicates a replacement business of up to 215 000 m$^2$ year$^{-1}$.[465] Based on a price of 850 US$ per m$^2$ for the 300 μm-thick Nafion 954 membranes used in this application, this represents a potential business of 180 million US$ per year.

For AEM, the situation is similar. While AEMs are an essential component for AEMWE, their main markets are
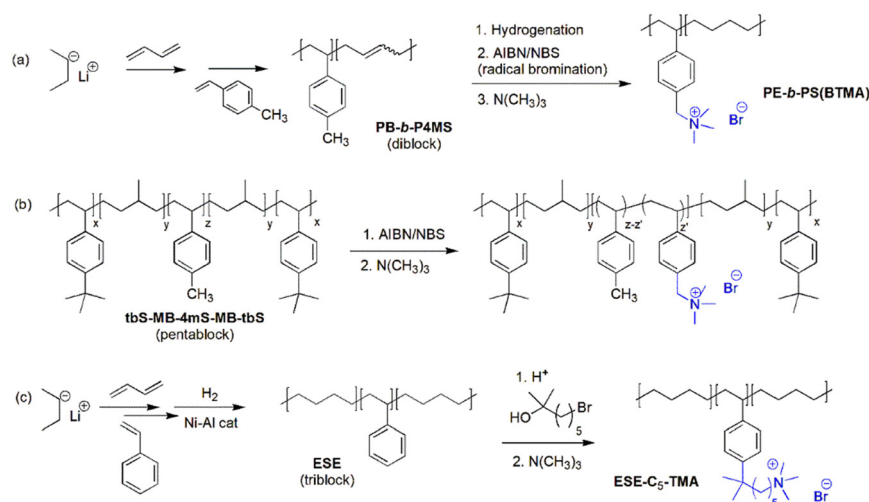


**Scheme 31** Additional synthetic methods of styrene–diene block copolymer AEMs.

5742 | Chem. Soc. Rev., 2024, 53, 5704–5780

This journal is © The Royal Society of Chemistry 2024

currently in the field of water treatment, such as seawater desalination, tap water softening, or ED, which are already established markets. Although the requirements for conductivity, thermal and alkaline stability are quite different, it would be attractive for membrane producers to use the same membrane platform to serve the well-established water treatment/purification markets and the just-starting AEMWE market. In this light, it is not surprising that Fumatech, which strongly supports the energy community by providing a variety of ion exchange membranes, is part of BWT Holding (Best Water Technology), a company with over 5000 employees.

The European Union aims to install 40 GW of new electrolysis capacities by 2030. Using a very rough estimation, if the average electrolysis performance is 2 A cm$^{-2}$ at 2 V (i.e., 4 W cm$^{-2}$), the required active membrane area would be $1\,000\,000$ m$^2$, translating to a production volume of $125\,000$ m$^2$ year$^{-1}$ (2023–2030). A cell design published by Loh et al. for a 100 cm$^2$ cell indicates that the total area required for the cell is up to 30–76% larger than the active area.[466] As an estimate, $200\,000$ m$^2$ year$^{-1}$ may be needed to satisfy the European membrane demand for water electrolysis – if all installed systems would be AEMWE.

**5.1.2. Commercial aryl ether-free membranes.** Older AEMs often contain ethers in the backbone with limited chemical stability,[467] and some AEMs are not readily commercially available and only accessible through bilateral agreements, like Tokuyama's A201[467] or Evonik's Duraion.[468] In contrast to some older AEMs, the newer generations often show higher conductivity. Brand names are Sustainion® from Dioxide Materials, AEMION and AEMION + ® from Ionomr, TM1 from Orion Polymer, Hollex from TailorMem, and PiperION from Versogen (Table 1). The chemical structures of these membranes are shown in Fig. 21. Table 1 also lists some key membrane

properties, though not from a direct comparison using the same measuring condition. Furthermore, the more important property governing the electrolyser performance is area-specific resistance (i.e., thickness/conductivity). While low thickness will result in low resistance, it will also result in higher hydrogen crossover and lower mechanical stability (not as tensile strength in MPa, but as absolute stress at break in Newton). Reinforcements decrease the overall IEC and conductivity, and increase the resistance, but also increase the mechanical strength. If the reinforcement and the ion-conducting matrix have a stable interface, reinforcements will reduce the hydrogen crossover, but different responses to humidity and temperature can result in different swelling behaviour, and thus voids along the support, which increases the gas crossover.[469,470]

**5.1.3. Upscaling chemical reactions.** The first challenge towards commercialization is the scale-up of polymer synthesis. One potential hurdle is the availability and cost of the monomers, which may be limited. Another challenge is the process engineering. Although a reaction works well in the lab, it will be necessary to adjust the reaction parameters when moving to the pilot scale to compensate for changes in heat and mass transfer. For example, Song et al. reported the synthesis of a polymer by reacting m-terphenyl, p-terphenyl, and 1-methylpiperidine-4-one in a ratio of 1:1:2 in a Friedel–Crafts polymerization, followed by functionalization with vinylbenzylchloride as a crosslinking point and permethylation. Moving to the kg-scale (Fig. 22a) required several changes.[478] While the monomer concentration remained unchanged during polymerization, the polymer concentration was increased to 50% for the functionalization step, possibly to reduce the amount of the solvent and to gain more robust polymer fibres in the precipitation step. Another concern is the dissipation of heat in large

**Table 1** Companies which offer aryl ether-free AEMs; IEC (mequiv$_{OH}$ g$^{-1}$), hydroxide conductivity ($\sigma$, mS cm$^{-1}$)

| Company | Country | Trade name | Comment | Key properties |
|---|---|---|---|---|
| Dioxide materials | USA | Sustainion® | Imidazolium-functionalized polystyrene, various grades available[471] | Sustainion® X37-50<br>Non-reinforced<br>Thickness: 50 μm<br>IEC: 1.1;[472] $\sigma_{25°C}$: 72 (1 M KOH)[472] |
| Ionomr | Canada | AEMION/AEMION + ® | Poly(bis-arylimidazolium)-based, various grades available[253,473] | AF3-HWK9-75-X<br>Reinforced (woven Polyether ether ketone)<br>Thickness: 75 μm<br>IEC: 1.9–2.7;[474] $\sigma$: >39[474] |
| Orion polymer | USA | TM1 | TMA-based polyphenylene membrane, various grades available[163] | TM1<br>Non-reinforced<br>IEC: 2.1; $\sigma_{80°C}$: 130 (water)[163] |
| TailorMem | Czechia | Hollex | Non-reinforced PSEBS-DABCO | Hollex ADL 911 NR<br>Non-reinforced<br>IEC: 0.76–0.94;[475,476] $\sigma_{30°C}$: >30,[476] 75 (water)[475] |
| Versogen | USA | PiperION | Piperidinium-functionalized polymer, various grades available[166] | PI-20<br>Non-reinforced<br>Thickness: 20 μm<br>IEC: 2.35 (PAP membrane which appears to be PI-20)[477]<br>$\sigma$: 71 (30 °C),[469] 58 (25 °C, PAP membrane which appears to be PI-20)[477]<br>PI-15<br>Reinforced with ePTFE<br>Thickness: 15 μm<br>$\sigma_{30°C}$: 77[469] |

This journal is © The Royal Society of Chemistry 2024
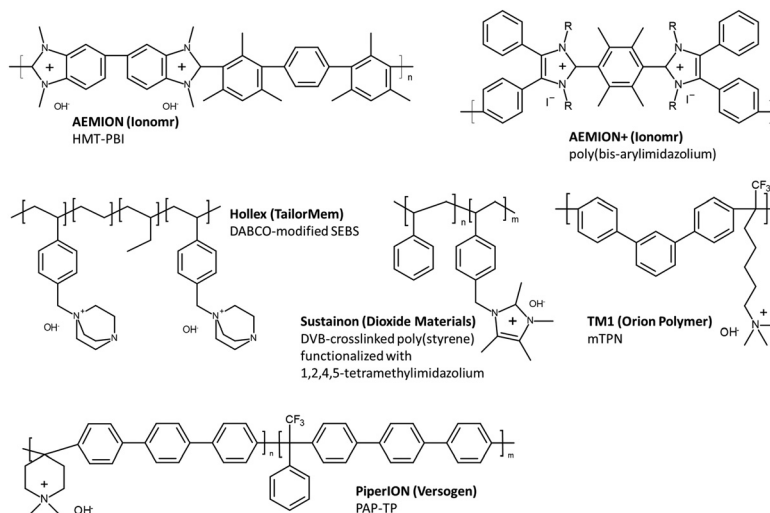
Chem. Soc. Rev., 2024, 53, 5704–5780 | 5743

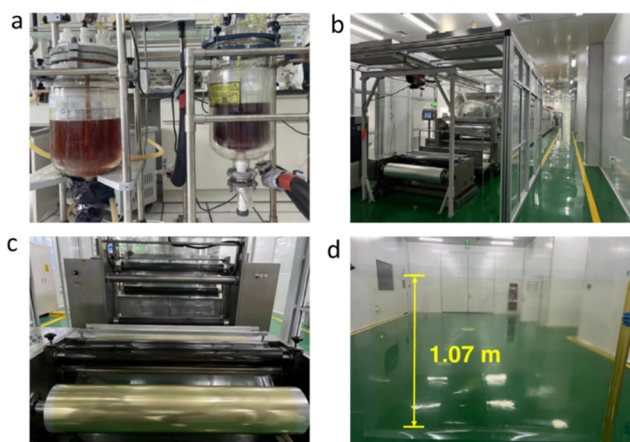**Fig. 21** Chemical structures of commercial aryl ether-free AEMs.



**Fig. 22** (a) Upscale production of a polymer made by polymerizing *m*-terphenyl, *para*-terphenyl and 1-methylpiperidine-4-one in a ratio of 1:1:2, followed by functionalization with vinylbenzylchloride as cross-linking point and permethylation; (b)–(d) pilot-scale membrane production of the membrane. Reproduced with permission.[478]

reactors. While small flasks can be efficiently stirred with magnetic stirrers and heat transfer to the wall of the flask is efficient, cooling large reactors can be challenging. Especially when the viscosity of the polymerization mixture increases, the temperature distribution becomes uneven. The choice of optimal stirrer designs and additional cooling circuits becomes necessary. The endpoint of polymerisation is often defined by reaching a certain viscosity. Qualitatively, Song *et al.* stopped the lab reaction after 9 hours when the magnetic stir bar stopped stirring. In the kg scale, the stirring paddle stopped moving after 24 hours.

For radical polymerisations, especially with polymerizing undiluted monomers, auto-acceleration by the Trommsdorff–Norrish Effect, or simply the gel effect, poses a safety threat and increases the polymer molecular weight.[479] When the viscosity

increases, which may also happen locally, the mobility of the reactive chain ends decreases, and termination reactions slow down. At the same time, because the mobility of small monomers is still high, chains continue to grow, resulting in an overall accelerated reaction rate and a temperature increase. If this heat cannot be dissipated, the reactor may experience a thermal runaway situation.

**5.1.4. Upscaling membrane fabrication.** Although a few membranes may be produced in batch processes, by casting on a tray, most membranes will eventually be produced in a roll-to-roll process to reduce production costs and improve membrane homogeneity. As an example, Song *et al.* dissolved 1.5 kg of their AEM polymer in DMSO to get a 25 wt% solution and cast at a speed of 0.3 m min$^{-1}$.[478]

Based on information from IRENA, Chatenet *et al.* reported that the active areas of AEMWE and AWE are in the range of $<300$ cm$^2$ and 1–3 m$^2$, respectively, and will increase to 1000 cm$^2$ and 3 m$^2$, respectively.[480] Traditionally, many electrolysers are produced in a circular cell design, in contrast to fuel cells, which usually have square cell designs. While circular designs appear to have advantages in cell sealing and pressure distribution, square designs will lead to less material losses when cutting membrane sheets from a roll. If electrolyser companies request circular membranes of 1000 cm$^2$ area, it will be necessary to provide sheets of $>36$ cm width and length, which may necessitate investments into casting equipment for some membrane companies. On the other hand, the standard roll widths for Nafion 212 membranes are 61 cm and the half roll width of 30.5 cm is made by splitting a roll. Song *et al.* showed the production of a 107 cm broad AEM (Fig. 22d),[478] and ETFE films are available in 150 cm roll width.[481]

In roll-to-roll casting, membranes are typically prepared by pouring a polymer solution onto a moving support film, for example, a PET film. The thickness of the wet solution is then controlled by passing a blade, and the solvents are evaporated by passing through a drying unit. Finally, some

**5744** | *Chem. Soc. Rev.*, 2024, **53**, 5704–5780

This journal is © The Royal Society of Chemistry 2024

online inspections may control the thickness or absence of pinholes. At the end of the production line, the membrane is rolled up, and sometimes an additional cover sheet is added to fully protect the membrane.[482]

Blade- or knife-coating (Fig. 23a) may lead to slight wave-like variations in the thickness. An alternative to blade or knife coating is the application of the polymer solution to the support by slot-die coating (Fig. 23b).[483] In this method, the polymer solution is pumped into a long reservoir that spans the entire membrane width and has a slit opening on the bottom, through which the polymer solution falls onto the support film. Control parameters include the polymer flow rate, the gap width, and the distance between the slit and the support. A potential issue with this method is that the polymer solution is fed into the slot-die in the middle of the tool, which can result in different flow velocities and thus shear rates close to the solution inlet and at the ends of the tool.[484] This can result in a different degree of orientation for the polymer chains in the middle and at the edges of the roll, especially when membranes are melt-processed. For example, Brack and Scherer reported different shrinking behaviour, when membrane stripes sampled at different width positions of an ETFE roll (which presumably was prepared by slot-die-coating of an ETFE melt) were heated.[481]

A special case is RG membranes, which do not require casting solutions. While all steps ((i) irradiation, (ii) grafting by immersion in a solution containing the monomers, (iii) final functionalization by reaction with an amine) can be easily done by moving the membrane from one roll to another through a radiation source or reaction bath, the kinetic control of the grafting step could be a potential challenge for mass production and will necessitate online control, *e.g.* online IR measurements to ensure the degree of grafting. In addition, any change in monomer concentration and solution viscosity, and possible formation of homopolymers, also need to be monitored during the process.

Industry prefers to cast membranes continuously for hours or even days before changing to another membrane type. One reason is that the first several meters of membrane leaving the casting machine are often not within the specifications. It takes time for the heat profile in the drying unit to become uniform, and the gap width of the casting knife may need adjustment. At the end of the casting process, some polymer may be lost in the pumps and tubes, resulting in significant losses for small batches. Therefore, to produce continuously, large solution

volumes need to be prepared and used for hours or days, and the shelf-life of the solutions needs consideration. One potential problem is agglomeration and sedimentation, not only of additives like inorganic nanoparticles,[485] but also of the polymer itself. For example, while PBI is fully soluble in DMAc, obtained solutions may gel suddenly. To suppress this gelation, which occurs due to an increasing number of chain-chain interactions, LiCl is added to the solutions to shield the hydrogen bond acceptor groups.[486]

The inclusion of porous supports increases the complexity of the casting process. To some extent, the application of porous supports is easier on a large scale, because the porous membrane will be under constant tension between the two roles, thus resisting wrinkling and allowing for easy pressing into the casted wet film. However, this requires high precision of the porous material. If one side of the porous film is slightly thicker than the other, the thicker side will be stretched when the film is wound up on a roll. When such support is embedded into the straight, freshly cast AEM, the curvature of the porous film will result in wrinkles.

**5.1.5. Environmental concerns.** While the small amount of solvents evaporated during membrane fabrication at the lab scale is typically released in a hood and then blown into the atmosphere, large amounts of solvents evaporated during industrial membrane production should be recovered in a condenser. Sensors and nitrogen flushing should be employed to prevent reaching explosion limits of air/solvent mixtures. Furthermore, some chemicals and solvents used in AEM fabrication are toxic.

One example is methyl iodide, which is commonly used for the quaternization of tertiary amine groups like polymer-bound dimethylamine, DABCO, or MPIP. Methyl iodide has a very high vapour pressure ($\sim$23 times higher than that of water at 20 °C) and is toxic when inhaled, and is suspected of causing cancer.

Another example is polar aprotic solvents, which are commonly used to cast ion-conducting polymers. DMAc, DMF, and NMP have been identified by the European Chemicals Agency as Substances of Very High Concern.[487] One factor to be considered is whether a substance is classified as carcinogenic, mutagenic, or toxic for reproduction, category 1A or 1B. One of the hazard statements for NMP is H360: May Damage Fertility or the Unborn Child. In addition to H360, the hazard statements for DMF and DMAc also include H351: Suspected of Causing Cancer. In December 2022, US EPA published a new risk determination for NMP and announced plans to propose a rule to regulate NMP.[488]

Ideally, casting solutions should be changed into water- or alcohol-based systems. Water-based systems could reduce capital expenditures, because water can be evaporated in open casting systems without the need to condense the evaporated solvents from the exhaust or take precautions like using an inert atmosphere to avoid explosive solvent vapour mixtures with air. However, the challenge is more complex than simply preparing solutions and obtaining a membrane from them, as there can be a strong correlation between membrane properties and casting solvents for ion exchange membranes. It has been
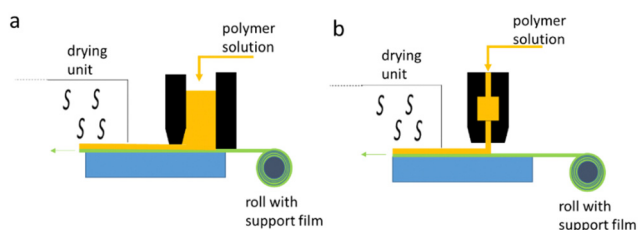


Fig. 23 Continuous roll-to-roll membrane production using (a) knife-coating and (b) slot-die coating.

This journal is © The Royal Society of Chemistry 2024

*Chem. Soc. Rev.*, 2024, **53**, 5704–5780 | **5745**

shown for Nafion™ that the choice of solvents has a strong effect on the membrane's mechanical strength, which depends on the degree of crystallization and entanglement.[489,490]

## 5.2. Property measurement

The properties of AEPs, especially anion conductivity and water uptake, are heavily impacted by counter anions. Even other traits, such as dimensional stability, mechanical properties, and gas permeability, can all be influenced by counter ions because they change the polarity of the polymers. Understanding the balance between hydroxide, carbonate, and bicarbonate ions is critically important, especially for devices like electrochemical $CO_2$ capture and electrolysers. When it comes to devices designed to separate anionic species, membrane properties with different counter ions are typically reported. Furthermore, even for electrochemical devices relying on hydroxide conduction, polymer properties with other counter ions are often reported because quaternized polymers with a hydroxide counter ion are less processable and more sensitive to carbonation.

Because the properties of AEPs are highly influenced by carbonate equilibrium,[491] standardized protocols become critical. Back in the early days before 2015, most of the property measurements for AEP materials were adopted by modifying PEM measurement protocols.[492] However, AEP-specific property measurement techniques have been developed to compare the material properties with different chemistry. In this section, we briefly review measurements of five key properties.

### 5.2.1. Anion conductivity. 
The ion conductivity of an AEP is typically measured by the AC impedance technique where a small AC signal in the frequency range of 0.1–10 000 kHz is applied to perturb the system to obtain the impedance data. The most common cell geometries for AEM conductivity are two-probe in-plane window cells[493] and four-probe in-plane or through-plane geometries.[494,495] In two-probe cell geometry, the current-generating electrodes serve as the voltage-measuring probes, while the four-probe in-plane geometry is connected separately. These two- and four-probe cells provide accurate halogenated and carbonated anionic conductivity,[496–498] but accurate measurement of hydroxide conductivity of the AEMs in the trace of carbonate and bicarbonate ions is challenging due to the fast reaction rate of hydroxide ions with atmospheric $CO_2$, replacing hydroxide ions with less mobile carbonate and bicarbonate ions.[499] The hydroxide conductivity was measured in deionized water purging and blanketing with an inert gas such as nitrogen or argon,[163] but even a short exposure to ambient air may cause carbonation. Ziv and Dekel proposed a method that measures hydroxide conductivity more accurately with an *ex situ* test set-up that forces the release of (bi)carbonate ions by applying an external electric current through the membrane.[500] While the method was initially developed to analyse the conductivity of AEMs for AEMFC with humidified gas streams to transport the released (bi)carbonates away, membranes for AEMWE can be conveniently measured in water without the need for expensive equipment.[469]

The hydroxide conductivity of AEMs can also be measured with an MEA single cell. In this method, the ohmic resistance of MEAs is normally obtained by current interrupt[501] or high-frequency resistance methods.[502,503] The hydroxide conductivity is obtained by subtracting the non-membrane resistance from the measured ohmic resistance.[504] Some high-performance AEIs are too brittle to cast into free-standing films.[165,173] The anionic conductivity of the AEIs can be estimated by the solution (or dispersion) conductivity[505] or sheet resistance of the electrode.[506] The conductivity of AEIs from the solution and electrode does not reflect the true anionic conductivity; the solution conductivity depends on the dielectric constant of the solvent, and sheet resistance is a function of the tortuosity of the ionomer. Nevertheless, these methods provide useful conductivity-related information for comparison with the standard material that has the known conductivity value. The anion conductivity of some AEI materials that do not form free-standing films can still be measured by preparing a thin film coating on a substrate.[507–509]

### 5.2.2. Gas permeability. 
The physical crossover of reactant gases (fuel cells) or gas products (water electrolysers) through ion exchange membranes has been an important concern, and several methods to measure gas crossover, such as the gas permeation rate (mol $cm^{-2}$ $s^{-1}$) have been reported.[510] A pressure permeation cell uses a conventional diffusion cell with controlled humidified gas flow coupled with a detector such as gas chromatography or mass spectrometry.[511] It is a suitable method for evaluating membranes under differential pressure operation conditions in AEMWE. Chronoamperometry analysis can be used for measuring the gas permeability of ionomer thin film using a microelectrode. Hydrogen and oxygen permeability are calculated from the diffusion coefficient and solubility of gases in the membrane.[510] Since the ionomer needs to be cast as a thin layer on the microdisk electrode, this method is favoured for AEPs prepared as the ionomer solution and is useful for the permeation rate measurement of AEI.[512] Gas permeability can be also measured *in situ* using an MEA. With the standard fuel cell MEA set up, the limiting current of the electrochemical reaction caused by the hydrogen that crosses over the AEM is measured to calculate hydrogen permeability.[513]

The gas permeability is strongly affected by the hydration level of membranes. Increasing the membrane hydration level increases permeability; therefore, AEMs used in water electrolysers need to be fully hydrated for the measurement. Oxygen crossover is of less concern for hydrocarbon-based AEMs because of its low permeability compared to hydrogen.[514,515]

### 5.2.3. Ion exchange capacity (IEC). 
The IEC value is used to quantify the amount of the anion exchangeable groups in an AEP and is typically measured by titration using counter anions. Among several methods that have been reported, acid–base back titration and Mohr titration have been the most commonly used techniques for measuring IEC for AEPs.[516] Acid–base back-titration uses phenolphthalein as a colorimetric indicator to detect the endpoint of titration using the base titrant and the acid analyte-containing hydroxide anions

5746 | *Chem. Soc. Rev.*, 2024, **53**, 5704–5780

This journal is © The Royal Society of Chemistry 2024
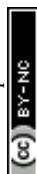
from AEPs. Mohr titration uses halide counterions exchanged from AEPs as the analyte, the silver nitrate titrant, and potassium chromate as an indicator. The red precipitate of silver chromate formed indicates the endpoint. Volhard titration, another back-titration method, was also used for the determination of IEC.[517] This method uses iron(III) nitrate as an indicator, silver nitrate solution containing halide ions from AEPs as the analyte, and potassium thiocyanate as a titrant. A control sample of silver nitrate is titrated with potassium thiocyanate for IEC calculation. These colorimetric titration methods are easily practiced, but several reports have mentioned the large range of errors of titrated IEC values due to the multiple experimental factors causing errors, including incomplete ion exchange during the analyte preparation, incomplete drying of AEP, and missing the endpoint of the indicator due to the different colour perception of humans.[457,518] Potentiometric titration using an automated titrator with the silver selective electrode has been proposed for IEC measurement.[516] Although the scope of the instrument to be used is narrow, the method does not use colorimetric indicators, which can help to reduce a common error from the conventional titration methods. Other methods include the detection of nitrate ions by UV/VIS,[519] the detection of chloride ions with an ion-selective electrode,[520] and ion exchange chromatography.[521]

The polymer structure analysis using NMR spectroscopy is also an effective method to calculate IEC. The peak integration of a $^1$H NMR spectrum is typically used for IEC calculation.[522] The sample of interest needs to be fully dissolved in a deuterated solvent (e.g., DMSO-$d_6$, MeOD) for the solution NMR analysis. The method cannot be used for AEPs with limited solubility, such as crosslinked/reinforced polymers, block copolymers, and grafted copolymers. AEPs prepared by heterogeneous quaternization (cast as a film and then quaternized by immersion in aqueous amine solution) also show limited solubility; the degree of functionalization of precursor groups in these polymers is often analysed using NMR before quaternization using a less polar solvent, e.g., CDCl$_3$, and compared with the titrated IEC value after quaternization to confirm quantitative conversion into cation.[285] Solid-state NMR techniques have not been used much for measuring IEC due to their insufficient resolution for integration.[523]

**5.2.4. Alkaline stability.** The standard procedure to evaluate the alkaline stability of AEMs is to immerse the AEM sample in 1 M KOH (or NaOH) at 60 or 80 °C for a 4-week period.[524] The degree of degradation is evaluated by changes in IEC, ionic conductivity, chemical structure (NMR, FTIR), and mechanical properties. The alkaline solution saturated with oxygen is reported to show higher degradation rates of AEMs, compared to those immersed in nitrogen degassed alkaline solution.[111] Kreuer and Jannasch developed a thermogravimetric method for quantifying the IEC loss of AEMs at controlled temperature and hydration levels.[525] This method measures the hydration number under controlled temperature and RH conditions while continuously recording the sample weight. Compared to the tests in aqueous solutions of KOH, no additional cations, anions, and water are present in the membrane. Coates et al.

developed a protocol for the quantitative assessment of cation stability.[356] In this protocol, they suggested a procedure involving $^1$H NMR to evaluate model cation stability in a 1 M KOH/CD$_3$OH solution (or higher base concentrations) in a sealed NMR tube at 80 °C. $^1$H NMR analysis is employed to quantitatively follow the course of reactions in situ. Diesendruck and co-workers developed an ex situ stability protocol using a dry potassium hydroxide solution. The dry solution is prepared with potassium metal, which was added to 18-crown-6 then dissolving it in dry DMSO-$d_6$ to form the stock solution.[526] Then quaternized polymers (0.035 mmol of cationic group) are dissolved in the solution to monitor the rate of cation decomposition using $^1$H NMR. For experiments with a hydration number greater than 0, the required concentration of water is added. This method may estimate the alkaline stability of quaternized polymers under reduced RH conditions, e.g., AEMFC cathode.

**5.2.5. Adsorption properties.** The adsorption properties in AEPs have only recently gained attention within the AEP research community. Two crucial components in AEPs have been identified as significant. Firstly, the presence of positively charged cationic groups drives their adsorption,[139,527,528] occurring at electrodes with a negative charge, namely the anode. This is in contrast to proton exchange ionomers, where anionic adsorption, such as sulphate or phosphate, takes place on the positively charged electrode, i.e., the cathode. The second critical component is the polar fragments of ionomers,[135,529–531] involving polar interactions, including the van der Waals interaction of the phenyl group. This type of adsorption occurs with a broader range of electrode potentials.

The evaluation of ionomer adsorption on catalyst surfaces can be conducted through either direct or indirect methods. Direct measurements offer precise information about the adsorbed species but are often challenging due to the intricate behaviour of these species and the difficulty in separating them from bulk ionomers. On the other hand, indirect measurements, while sensitive, provide information specific to the measuring conditions during electrochemical responses.

Cationic species, commonly adsorbed at the anode of fuel cells and electrolysers, can be directly measured using techniques like infrared reflection absorption spectroscopy[139] and neutron reflectometry.[532] Alternatively, cyclic voltammetry can be employed as an indirect method to gauge the reduction in electrochemical surface area (ECSA) caused by adsorbed cationic group species. However, it is important to note that the ECSA reduction might not precisely correlate quantitatively with the adsorption area of cationic groups, as the adsorption sites for hydrogen and cationic groups may not be identical. Additionally, the ECSA is typically measured at relatively low potentials, and the adsorption of cationic groups at high potentials, such as the anode of electrolyser, may exhibit different behaviours.

For ionomer fragment adsorption, the electrochemical oxidized products of ionomers are examined by $^1$H NMR.[122,123,533] This involves MEA testing at high potentials, followed by dissolving the ionomer in the NMR solvent to observe the structural changes induced by electrochemical oxidation. While

This journal is © The Royal Society of Chemistry 2024

Chem. Soc. Rev., 2024, **53**, 5704–5780 | **5747**

this method offers detailed insights into the ionomer's structural alterations, it may pose challenges when dealing with insoluble ionomers. In such cases, X-ray photoelectron spectroscopy can be employed to detect oxidation products.[127,140,534] Electrochemical analysis, a sensitive technique for measuring electro-oxidative current density, involves studying cyclic voltammograms of the electrodes. These voltammograms can reveal the delayed potential of catalyst oxide formation and the electrochemical oxidative current density at high potentials,[135] typically exceeding 1.2 V, which differs from normal cyclic voltammograms used in catalyst studies.

### 5.3. Milestones

The property milestones of AEMs were first set by the US DOE the Hydrogen and Fuel Cell Technologies Office (HFTO) for AEMFCs in 2013,[535] focusing on the alkaline stability of AEMs. The target performance is retaining $\geq 99\%$ of the original IEC after 1000 hours in an alkaline solution at a temperature higher than 80 °C. In 2016, the US DOE ARPA-E Integration and Optimization of Novel Ion-Conducting Solids (IONICS) program set the AEM milestones in the 11 categories (Table 2). In 2019, the US DOE HFTO Alkaline Membrane Fuel Cell Workshop suggested a few modifications to the IONICS technical target based on the participants' opinions.[536]

In 2016, the participants in the Alkaline Membrane Fuel Cell Workshop sponsored by US DOE HFTO suggested the AEM property milestone should be connected with PGM loading.[537] Based on the suggestion, US DOE HFTO published the milestones for AEMFC[538] and AEMWE (Table 3).[539] The 2026 target performance of AEMWE is $\sim 60\%$ compared to that of the PEMWE.

## 6. Device performance

### 6.1. Anion exchange membrane fuel cells

AEMFC performance is typically measured by polarization curves. Because AEMFC is not yet a mature technology, most AEMFC performance has been measured under $H_2/O_2$ conditions to decouple $CO_2$-related complications and cell degradation. Most papers reported the PPD as a metric of the performance and voltage degradation rate at a constant current as a metric of cell durability. The properties of materials constituting the MEAs and their operating conditions affect the fuel cell performance as a result,[5,540,541] and thus it is difficult to assess AEM and AEI independently from the PPD measured with different MEAs under different operating conditions. However, since AEMs and AEIs play a critical role in fuel cell performance and durability, it is useful to survey these components that show high performance in AEMFCs. In this section, we analyse the data that report more than 0.5 W cm$^{-2}$ PPD to provide information regarding the implementation of aryl ether-free AEMs and AEIs for high-performance AEMFCs.

Before 2015, the PPDs of most AEMWEs were less than 0.3 W cm$^{-2}$. The first high-performance AEMFC was reported by Zhuang and co-workers using poly(aryl ether sulfone) membrane and ionomers, which achieved a PPD of 1 W cm$^{-2}$ at 80 °C.[542] Since then, about 10 articles reported more than 0.5 W cm$^{-2}$ PPD using aryl ether-containing polyaromatic membranes (Table S1, ESI†). The first aryl ether-free polyaromatic AEM that showed more than 0.5 W cm$^{-2}$ in AEMFCs is a perfluoroalkylene with a pendent ammonium group, reported by Miyatake and co-workers in 2017.[192] Subsequently, several research groups reported MEAs that exhibited more than

**Table 2** Technical metrics of AEM set by US DOE

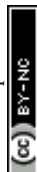| Number | Metric | ARPA-E (2016) | HFTO (2019) |
|---|---|---|---|
| 1 | Membrane chemical stability (at $\geq 80$ °C immersed in a pH $\geq 14$ solution) | $\geq 1000$ hours with $\leq 2\%$ loss in IEC, ionic ASR, spectroscopic measures of membrane state, and mechanical properties | $\geq 1000$ hours with $\leq 5\%$ loss in IEC and conductivity: should include spectroscopic characterization. |
| 2 | Component area over which property values are achieved to within $\geq 90\%$ uniformity | $\geq 100$ cm$^2$ | Delete this target or decrease priority |
| 3 | Ionic ASR (hydroxide form, 80 °C, liquid equilibrated) | $\leq 0.04$ $\Omega$ cm$^2$ | Add a target at 40 °C: 0.04 $\Omega$ cm$^2$ |
| 4 | Ionic ASR (80 °C, $\leq 50\%$ RH, under air exposure, *i.e.*, in presence of 400 ppm $CO_2$) | $\leq 0.08$ $\Omega$ cm$^2$ | Change to a measurement at 80% RH under $CO_2$-free air exposure. |
| 5 | Mechanical durability during humidity cycling | $\geq 20\,000$ RH cycles | Delete this target. |
| 6 | Electronic ASR | $\geq 1000$ $\Omega$ cm$^2$ | No change proposed |
| 7 | Humidity stability factor | $> 5$ | No change proposed |
| 8 | Swelling in liquid water at 25 °C | $< 50\%$ | To be measured as linear swell in $X$–$Y$ plane in water, membrane in OH$^-$ form. |
| 9 | Pressure differential (bar) | $\geq 1$ | Delete for fuel cell and flow battery applications; electrolyser industry input on burst test or other relevant test and metrics needed. |
| 10 | $H_2$ crossover and $O_2$ crossover | $\leq 25$ nmol cm$^{-2}$ s$^{-1}$ | Change to $< 5$ mA cm$^{-2}$ for $H_2$ crossover, eliminate $O_2$ crossover target. |
| 11 | Cost for membrane that can be practically integrated in a device | $\leq 20$ \$ m$^{-2}$ | No change proposed |
| 12 | $H_2O$ transport | n/a | New target proposed for water transport: $> 4$ mmol cm$^{-2}$ s$^{-1}$. |
| 13 | Ionic permeability | n/a | New target proposed for flow batteries to limit permeability of other ions: $< 7 \times 10^{-8}$ cm$^2$ s$^{-1}$. |

**5748** | *Chem. Soc. Rev.*, 2024, **53**, 5704–5780

This journal is © The Royal Society of Chemistry 2024

**Table 3**   U.S. DOE MEA milestones

| Year | Milestone |
|---|---|
| **AEMFC** | |
| 2021 | *Initial performance*: 100 mW cm$^{-2}$ at 0.8 V with $\leq 0.2$ mg$_{PGM}$ cm$^{-2}$, H$_2$/air, $T \geq 80$ °C, $P \leq 250$ kPa |
| 2022 | *Initial performance*: 0.65 V at 1000 mA cm$^{-2}$ on H$_2$/O$_2$; durability: $\leq 10\%$ voltage degradation over 1000 hours; $T \geq 80$ °C, $P \leq 150$ kPa; total PGM loading: $\leq 0.2$ mg cm$^{-2}$ |
| 2024 | *Membrane*: H$_2$ crossover $\leq 15$ mA cm$^{-2}$ during 1000 hours OCV hold at 70% RH and $\geq 80$ °C, H$_2$/N$_2$ |
| 2025 | *Initial performance*: 1000 mW cm$^{-2}$ at 0.65 V; H$_2$/air (CO$_2$-free) with total PGM loading $\leq 0.125$ mg cm$^{-2}$, H$_2$/air, $T \geq 80$ °C, $P \leq 250$ kPa |
| 2030 | *Initial performance*: $\geq 600$ mW cm$^{-2}$ under H$_2$/air (maximum pressure of 1.5 atm) in PGM-free MEA |
| Ultimate | *Initial performance*: $\geq 1000$ mW cm$^{-2}$ at rated power; PGM-free; H$_2$/air; $T \geq 80$ °C, $P \leq 250$ kPa |
| **AEMWE** | |
| 2026 | $\geq 2.0$ A cm$^{-2}$ at 1.8 V with a degradation rate of $<4$ mV kh$^{-1}$ (tested at least 25 cm$^2$) in both water and supporting electrolyte feed ($\sim 0.5$ M) |
| **PEMWE** | |
| 2026 | $\geq 3.0$ A cm$^{-2}$ at 1.8 V with a degradation rate of 2.3 mV kh$^{-1}$ over at least 1000 hours (tested at least 25 cm$^2$) |

0.5 W cm$^{-2}$ with aryl ether-free polyaromatic AEM and polyfluorene (FLN) AEI combinations (Table S2, ESI†). A lightly-branched AEM with enhanced stability exhibited AEMFC performance of approximately 2 W cm$^2$ PPD operating at 100 °C, and 195 hours of durability with 140 mV h$^{-1}$ voltage decay rate, and showed balanced water management.[543] Scott and co-workers reported a PPD of 0.61 W cm$^{-2}$ using radiation-grafted aryl ether-free polyolefinic AEM in 2015.[433] Approximately 15 articles report more than 0.5 W cm$^{-2}$ PPD using various aryl ether-free polyolefinic AEMs as of August 2023 (Table S3, ESI†).

At least ten articles reported more than 0.5 W cm$^{-2}$ PPD for PGM-free catalysed AEMFCs under H$_2$/CO$_2$-free air conditions (Table S4, ESI†). The AEMFCs that showed high performance mostly used either radiation-grafted or acid-catalysed phenyl piperidinium, probably because of the commercial availability of the latter. However, one should note that those AEMs have high IEC (2.1–2.9 mequiv. g$^{-1}$), low thickness (15–25 µm) and relatively high operating temperature ($\sim 80$ °C).

Fig. 24a shows the number of publications of high-performance AEMWEs as a function of types of AEMs. The number of publications reporting aryl ether-containing polyaromatic AEMs in high-performance AEMFCs ranges from 1 to 4 each year. The number of publications for aryl ether-free polyaromatic (aryl ether-free PAr) AEMs substantially increased in recent years, suggesting that tailoring aryl ether-free PAr
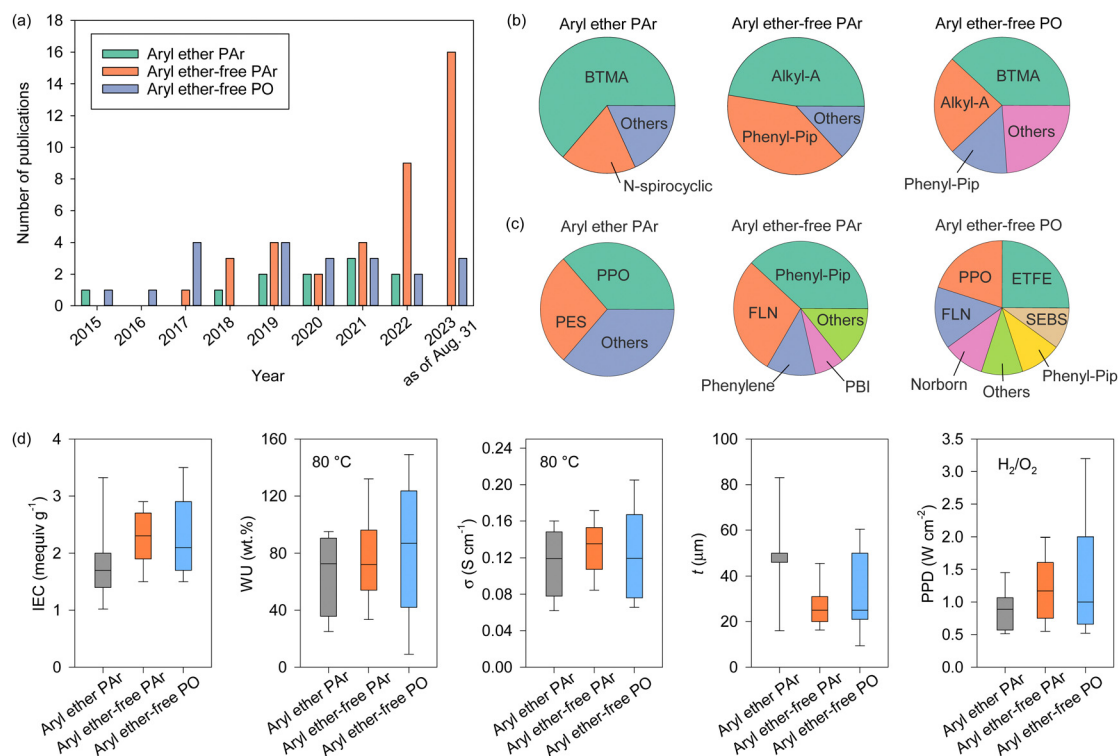


**Fig. 24** Summary of AEMFC performance using aryl ether-free polymers. (a) The number of publications that reported the PPD of more than 0.5 W cm$^{-2}$. (b) The cationic functional group of the AEMs used for high-performance AEMFCs, (c) the AEI in MEAs used for high-performance AEMFCs, (d) the average IEC, WU, $\sigma$, $t$, and PPD of the AEMs used for high-performance AEMFCs. The WU and $\sigma$ are data at 80 °C.

This journal is © The Royal Society of Chemistry 2024

*Chem. Soc. Rev.*, 2024, **53**, 5704–5780 | **5749**

structure using different chemistries has now become well-established. Also, note that 80% of the AEMs in the aryl ether-free PAr publications used the acid-catalysed polyhydroxyalkylation route.

Fig. 24b shows the cationic functional groups of the AEMs in the high-performance AEMFCs. For aryl ether-PAs, most studies used BTMA, likely because quaternization with trimethylamine in the chloromethylated or methylbrominated phenyl is well-established. For aryl ether-free PArs, alkaline-stable cationic functional groups such as alkyl ammonium (alkyl-A)[168,230,544–554] or phenyl-piperidinium (phenyl-PiP)[184,478,551,555–561] are prevalent as cationic functional groups. Other alkaline-stable cationic functional groups such as benzimidazolium[562] and alkyl piperidinium[563–565] have been frequently used as well. For aryl ether-free polyolefins (aryl ether-free POs), BTMA, alkyl-A, and phenyl-Pip are the most widespread functional groups. BTMA is commonly used for radiation-grafted polymers and other polyolefinic AEMs. Overall, the most prevalent cationic functional group is alkyl-A (appearing in 23 publications), followed by phenyl-PiP (appearing in 17 publications) and BTMA (appearing in 15 publications).

Fig. 24c illustrates the type of AEIs in the catalyst layers used for high-performance AEMFCs.[566] For most of the aryl ether PAr studies, the same materials used for the AEM are employed as the ionomeric binders and quaternized PPO and poly(aryl ether sulfone) being the two most usual choices of aryl ether-containing AEI. The ionomeric binder that exhibited the highest performance in AEMFCs when paired with an aryl ether PAr-based AEM was a radiation-grafted ETFE powder.[567] For aryl ether-free PArs, polyaromatics with the phenyl-Pip functional group were widely utilized. It is worth noting that phenyl-PiP is the most prevalent cationic group (appearing in 19 publications) compared to alkyl piperidinium, despite its lower alkaline stability (see Fig. 3). This is probably due to the higher fuel cell performance of phenyl-PiP, as competitive adsorption of piperidinium reduces phenyl adsorption on electrocatalysts.[530] FLN ranks as the second most popular ionomer (appearing in 14 publications), possibly because its weaker interaction with electrocatalysts enhances AEMFC performance. Kim and co-workers demonstrated that the AEMFC performance using FLN ionomers is significantly higher than that using poly(phenylene) ionomers due to less phenyl adsorbing characteristics of fluorene.[164] The superiority of the polyfluorene backbone to poly(phenylene) ionomers was also discussed by Lee and colleagues, who prepared poly(fluorenyl aryl piperidinium) AEMs by combining phenyl-PiP and FLN, resulting in high fuel cell performance.[170] Similar FLN ionomers showed the highest $H_2/O_2$ AEMFC performance for polyaromatic-based MEAs (2.6 W cm$^{-2}$), although the cell was evaluated under very high flow rate and back pressures.[556] For aryl ether-free PArs, various AEIs, including quaternized PPO, ETFE, FLN, polynorbornene, and phenyl-Pip were utilized. The wider range of ionomeric binders used for aryl ether-free PO-based MEAs is likely due to the low solubility of quaternized polyolefins. Note that ETFE and most norbornene-based AEIs reported are used as particulate dispersion. Using a particulate ionomer, Kohl
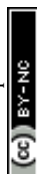
and co-workers demonstrated the highest performance (PPD = 3.5 W cm$^{-2}$).[307]

Fig. 24d illustrates the properties of AEMs used in high-performance AEMFCs. The average IEC of the aryl ether PAr AEMs was 1.7 mequiv. g$^{-1}$, notably lower than those of the aryl ether-free PArs and POs (2.3 and 2.0 mequiv. g$^{-1}$, respectively). The higher IEC for the aryl ether-free systems reflects the trend of using more conductive AEMs to enhance AEMFC performance.[568] Due to their higher IEC, these aryl ether-free systems also exhibited higher water uptake (WU) and hydroxide conductivity ($\sigma$). The average thickness of the aryl ether PAr AEMs was 48 μm, thicker than the aryl ether-free PAr AEMs (25 μm) and aryl ether-free PO AEMs (24 μm). Owing to their higher conductivity and lower thickness, the aryl ether-free system demonstrated higher PPD compared to the aryl ether PArs-based AEMFCs. The average PPDs of the aryl ether-free PAr and aryl ether-free PO-based AEMFCs were comparable, at 1.24 and 1.31 W cm$^{-2}$, respectively. The relatively high variation of PPD for the aryl ether-free PO-based AEMFCs can be attributed to the substantially high performance of MEAs using particulate AEIs.

In assessing the durability of AEMFCs, we note the following key points: (i) MEAs using more alkaline-stable cationic groups, such as alkyl-A, demonstrated greater durability than those using less alkaline-stable cationic groups like BTMA;[435,569] (ii) MEAs using AEMs with lower IEC and WU are more durable than those with higher IEC and WU;[567,570] (iii) MEAs using aryl ether-free AEMs exhibited greater durability compared to those with aryl ether-containing AEMs;[85,571,572] (iv) While high current density operation poses more challenges in water management, comparable AEMFC durability can still be achieved with appropriate humidity control.[547,573]

Table S5 (ESI†) presents the durability of AEMFC using aryl ether PAr AEMs from 2012 to 2023. Only three cases with a PPD greater than 0.5 W cm$^{-2}$ demonstrated durability exceeding 100 hour.[567,569] The most durable MEA used an N-spirocyclic-functionalized PES AEM, showing only 7% voltage loss after 550 hours of operation at 61 °C.[567] The second most durable MEA used an imidazolium-functionalized AEM, exhibiting 70% voltage loss after 960 hours at 60 °C.[569] Both cells used low IEC (∼1.4 mequiv. g$^{-1}$) to maintain cell durability. In contrast to the lower durability of aryl ether PAr-based MEAs, those based on aryl ether-free AEMs showed high durability (Table S6, ESI†). The longest durability reported in AEMFC used an alkyl-A-functionalized polynorbornene AEM (10 μm-thick) with polynorbornene AEI, operating for up to 3600 hours at 75 °C.[574] A ferrocenium-functionalized polyethylene AEM also demonstrated remarkable durability, with only a 4% voltage loss after 500 hours of operation at 120 °C.[575]

In analysing the durability of AEMFCs, we focused on MEAs with a PPD greater than 0.5 W cm$^{-2}$, as detailed in Tables S5 and S6 (ESI†) (Fig. 25). We identified five MEAs with aryl ether PAr AEMs, eleven MEAs with aryl ether-free PAr AEMs, and six MEAs with aryl ether-free PO AEMs. The average IEC of the aryl ether PAr AEMs was substantially lower (1.5 mequiv. g$^{-1}$) compared to the aryl ether-free AEMs (2.5 mequiv. g$^{-1}$).

5750 | Chem. Soc. Rev., 2024, 53, 5704–5780

This journal is © The Royal Society of Chemistry 2024

Interestingly, the aryl ether PAr AEMs used in durability evaluations were thinner than the AEMs used for those performance evaluations. For instance, the average thickness of aryl ether PArs for durability tests was 20 μm, compared to 24 μm for performance tests. This enhanced durability with thinner AEMs is likely attributed to improved water management facilitated by higher water back-diffusion.[567,576] Operating at slightly higher temperatures and thinner AEMs, the PPD of aryl ether-free PO AEM-based MEAs was higher (2.0 W cm$^{-2}$) than that of others (1.0 W cm$^{-2}$ for aryl ether PAr MEA and 1.5 W cm$^{-2}$ for aryl ether-free PAr MEAs). MEAs using aryl ether-free PAr and PO AEMs were tested for longer operation times. The average duration for aryl ether PAr, aryl ether-free PAr, and aryl ether-free PO MEAs was 100, 400, and 610 hours, respectively, suggesting superior durability with aryl ether-free AEMs.

In our analysis of AEIs, we selected the MEAs that achieved a PPD of greater than 0.5 W cm$^{-2}$ and operated for a duration of $\geq$120 hours. We observed that the voltage degradation rate strongly depends on the type of cationic group and the method of AEI preparation (whether dissolved/dispersed in solution or ground to powder and used as particulate). Interestingly, only four types of AEIs demonstrated both high performance and durability, BTMA, phenyl-Pip, alkyl-A, and particulate ionomers, as compared in Fig. 25b. The cationic functional groups in the particulate ionomers were either BTMA or alkyl-A. Particulate ionomers exhibit distinctive characteristics, including high gas transport properties, and therefore can be categorized separately from ionomers prepared as dispersions. The AEMs for the BTMA AEI cells were slightly thinner (20 μm) compared to those for the phenyl-PIP (25 μm) and alkyl-A

(30 μm) AEI cells. Despite having thinner AEMs, the BTMA AEI cells were lower (1.1 W cm$^{-2}$) than the cells using phenyl-Pip (1.6 W cm$^{-2}$) and alkyl-A (1.5 W cm$^{-2}$) AEIs at similar operating temperatures. The MEA using particulate ionomers utilized thinner AEMs and showed higher PPDs. The most notable finding from this analysis is the voltage degradation rate; the BTMA cells exhibited more than two times higher voltage degradation rate (1.1 mV h$^{-1}$) than those of phenyl-Pip (0.47 mV h$^{-1}$) and alkyl-A (0.26 mV h$^{-1}$) cells. The particulate AEI cells showed the lowest voltage degradation rate (019 mV h$^{-1}$), suggesting that water and gas transport in the electrodes significantly influence AEMFC durability.

## 6.2. Water electrolysers

AEMs used for AEMFCs can be adapted for use in AEMWEs. We surveyed the AEMs used in high-performance AEMWEs over the last three years, focusing on those with high performance (Tables S7 and S8, ESI†). It is interesting to note that the AEMWE performance has been reported under both water and liquid electrolyte-feed conditions. This is because the performance of AEMWE greatly improves with liquid electrolyte-feed conditions. The main cause of this is the subject of ongoing work, but it is still under debate. The possible reasons include increasing catalyst-electrolyte contact area,[577,578] lowering cell resistance,[11] enhanced basicity,[579,580] and mitigating ionomer adsorption[140] by liquid electrolytes.

Fig. 26a displays the types of AEMs used in high-performance AEMWEs. Compared to the number of publications on AEMs for AEMFCs, there have been fewer numbers on AEMs for AEMWEs, reflecting the more recent focused interest
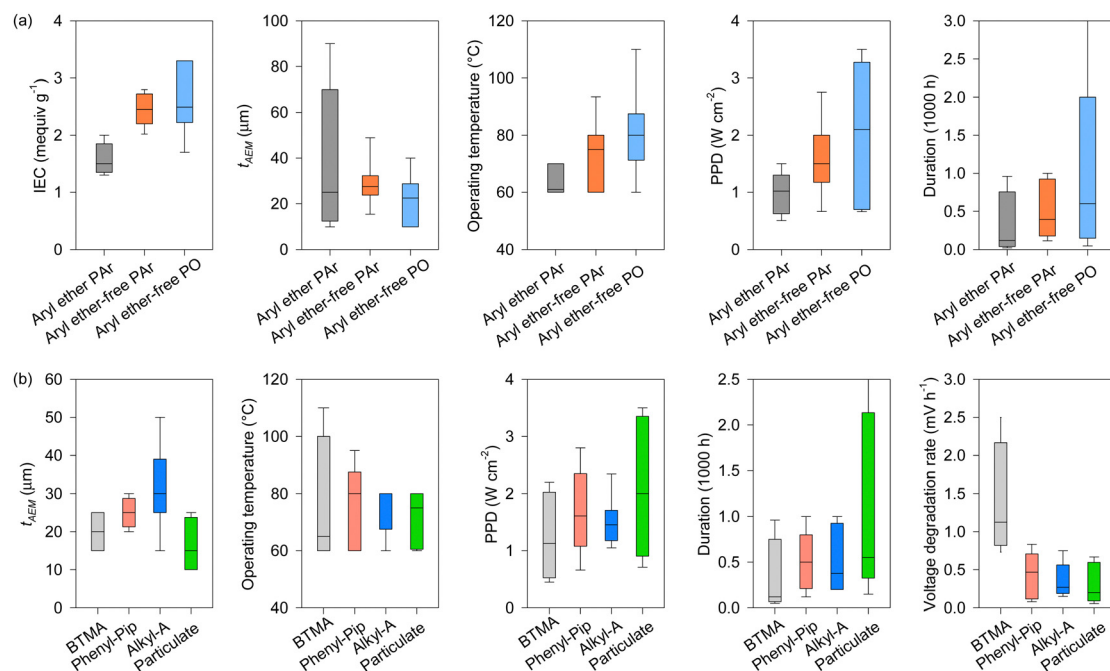
**Fig. 25** Summary of AEMFC durability using aryl ether-free AEPs. (a) Analysis in terms of AEMs. AEMs were selected from Tables S5 and S6 (ESI†) with the criterion of PPD higher than 0.5 W cm$^{-2}$. (b) Analysis in terms of the cationic functional groups and the form of AEIs. AEIs were selected from Tables S5 and S6 (ESI†) with the criteria of PPD higher than 0.5 W cm$^{-2}$ and duration is 120 hours.

This journal is © The Royal Society of Chemistry 2024

*Chem. Soc. Rev.*, 2024, **53**, 5704–5780 | **5751**

**Fig. 26** Summary of AEMWE performance using different types of AEMs and AEIs. (a) The number of publications of high AEMWE performance over the last three years (the current density of pure water and 1 M KOH-fed PGM-catalysed AEMWEs at 1.8 V: > 0.4 A cm$^{-2}$). (b) The properties of AEMs used in high performance AEMWEs. (c) The number of publications of AEIs as a function of the type of AEI binders in MEAs used for the pure water-fed AEMWEs, and the number of publications of AEIs as a function of the type of AEIs in MEAs used for the 0.1 M KOH-fed AEMWEs.
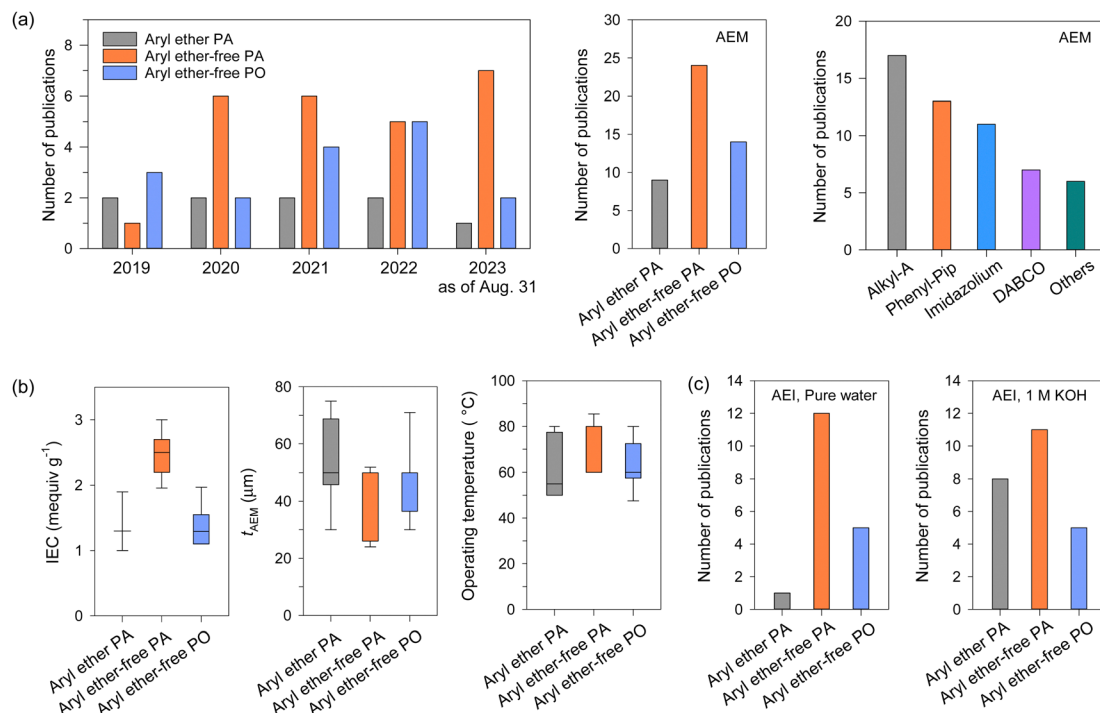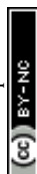
in AEMWEs. Aryl ether-free PAr AEMs outnumbered aryl ether PAr and aryl ether-free PO AEMs, although the difference in publication numbers was not significant. alkyl-A and phenyl-PiP are the two most commonly used cationic functional groups in AEMs for AEMWE applications, similar to their use in AEMFCs. However, imidazolium and DABCO are also widely used. The relatively high number of articles on imidazolium and DABCO can be attributed to the frequent use of commercially available AEMs such as X37-50 (Sustainion®) and Fumion (AGC Inc.) in high-performance AEMWEs.

The property requirements of AEMs used for AEMWEs slightly differ from those in AEMFCs, as shown in Fig. 26b. For AEMWEs, the average IEC of aryl ether-free PO AEMs is lower (1.3 mequiv. g$^{-1}$) compared to their use in AEMFCs (2.5 mequiv. g$^{-1}$). This discrepancy is because commercial AEMs with relatively low IECs have shown high performance in the presence of a liquid electrolyte. The AEM thickness for AEMWEs is about 20 μm thicker than that for AEMFCs, suggesting that more resistant AEMs are needed for AEMWEs. This requirement is due to the higher mechanical demands under AEMWE operating conditions, the need to prevent gas crossover, and a less strict requirement for low membrane resistance when liquid electrolyte is present. The operating temperatures of AEMWEs reported in research papers are similar to those of AEMFCs (50–90 °C). However, it is important to note that the operating temperature of AEMWEs in a commercial unit tends to be at the lower end of this range for longer-term operations.

Fig. 26c compares the AEI used in AEMWEs under pure water and 1 M KOH feed conditions. Under both conditions, aryl ether-free PAr AEIs were more frequently used than other types of AEIs. Interestingly, aryl ether PAr AEIs were often used for 1 M KOH-feed conditions, which could be due to several reasons. First, adverse phenyl adsorption on the catalyst may be mitigated under the liquid alkaline solution feed conditions.[140] Secondly, the degradation of AEI is less of a concern with liquid electrolyte feed. Third, commercially available aryl ether PAr AEIs are more accessible for catalyst developers. Unlike AEMFCs, no significant correlation between the reported AEMWE performance and the types of AEIs used.

Before 2015, several papers reported the performance and durability of AEMWEs under relatively mild conditions. The performance reported during this period was poor, yet those studies provided insights into performance-limiting factors. In 2012, Wang and co-workers reported on the 1 M KOH-fed AEMWE performance of a commercial A201 AEM (Tokuyama Corporation), which operated for over 500 hours at 50 °C and a constant density of 0.2 A cm$^{-2}$.[581] This work suggested that AEMWE operations exceeding 500 hours are possible with alkaline unstable aryl ether-containing ionomer (aminated Radel®) under KOH-fed conditions. A UV-grafted LDPE-DABCO-RG-AEM was tested in a 1 wt% K$_2$CO$_3$-fed AEMWE, yielding less than 0.05 A cm$^{-2}$ at 1.75 V.[582] However, the AEMWE cell demonstrated durability for 500 hours at 45 °C and outlet pressure of 20 bar. Since 2013, the team led by Scott and Mamlouk at Newcastle University also tested AEMWEs

**5752** | *Chem. Soc. Rev.*, 2024, **53**, 5704–5780

This journal is © The Royal Society of Chemistry 2024

containing RG-AEMs.[583–586] These studies generally involved RG-AEMs alongside non-RG-ionomers (such as SEBS or PPO-based ionomers). The best performance reported in 2021 was 0.13 A cm$^{-2}$ at 1.75 V with an LDPE-TMA-RG-AEM (IEC = 2.3 mequiv. g$^{-1}$) and a SEBS-based ionomer (IEC = 1.9 mequiv. g$^{-1}$); other conditions included a Pt/C cathode, NiCo$_2$O$_4$-based cathode, 0.1 M supporting electrolyte, and testing at 40 °C. Around 0.8 A cm$^{-2}$ was achieved by 2.0 V. In 2014, Kim *et al.* reported more than 2000 hours of long-term performance of pure water-fed AEMWEs at 50 °C and 0.2 A cm$^{-2}$ using aryl ether-free DAPP AEM.[87] Although the performance of the AEMWE was modest (0.2 A cm$^{-2}$ at 2.2 V), this work was the first to demonstrate long-term performance with 100 psi differential pressure. In the same year, Comotti *et al.* reported the outstanding PGM-free catalysed AEMWE durability (1000 hours, voltage degradation rate: ∼0.15 mV h$^{-1}$) under 1 wt% K$_2$CO$_3$ feed conditions.[87] This paper highlighted the potential for long-term operation using PGM-free Ni/(CeO$_2$-La$_2$O$_3$)/C HER and CuCoO$_x$ anode catalysts. After 2015, more publications reported aryl ether-free AEPs to enhance the durability of AEMWEs.[515]

We compiled the data from recent papers on AEMWE MEAs that showed high durability (≥100 hours with a low voltage degradation rate), presented in Table S9 (ESI†) and Fig. 27. The performance and durability of AEMWEs are strongly influenced by liquid electrolytes and PGM-free catalysts (Fig. 27a). A 1 M KOH feed solution significantly enhanced cell performance with an average current density at 1.8 V for the 1 M KOH-fed

AEMWEs was 1.2 A cm$^{-2}$, considerably higher than that for the pure water-fed AEMWEs (0.75 A cm$^{-2}$). PGM-free catalysed AEMWEs achieved a comparable current density (0.72 A cm$^{-2}$) under 1 M KOH-fed conditions. However, durability test durations showed more variation between pure water and 1 M KOH-fed AEMWEs. The average duration for pure-water-fed AEMWEs was only 180 hours, whereas 1 M KOH-fed AEMWEs exhibited a much longer average duration of approximately 1000 hours. Li and co-workers conducted comparative durability tests of AEMFC and AEMWE using the same AEM and AEI for each cell, demonstrating that AEMWE under 1 M KOH feed conditions has significantly better durability than that of AEMFC.[587] Holdcroft and co-workers investigated the pure water-fed AEMWEs using polybenzimidazolium-based AEM and AEIs. They found that a crosslinked derivative of the hexamethyl-*p*-terphenyl (HMT-PMBI) membrane, with four times lower volumetric swelling, did not enhance voltage stability with pure water feed, suggesting that excessive swelling of HMT-PMBI membrane is not the primary cause of performance loss. However, the hydrophobic and lower water uptake properties of the benzylated version of the non-crosslinked polybenzimidazolium AEI reduced dimensional swelling, leading to a four-fold increase in the lifetime of the AEMWE system operating with pure water. This indicates that the development of AEIs and catalyst layer is crucial for maximizing AEMWE lifetimes.[184] This result suggests that the dimensional stability of the state-of-the-art aryl ether-free AEMs is not the primary factor limiting the durability of AEMWEs. Several AEMWEs
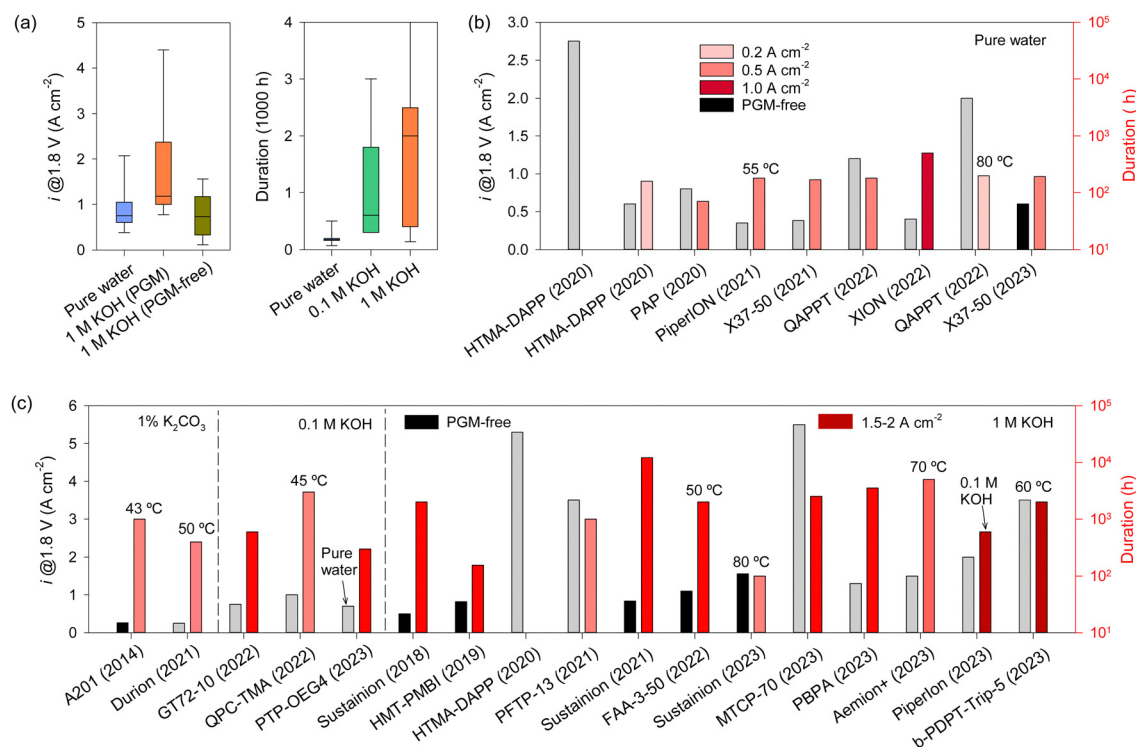


**Fig. 27** Summary of AEMWE durability using aryl ether-free polymers: (a) the AEMWE performance as a function of liquid electrolytes, (b) the performance and durability of the pure water-fed AEMWEs,[430,588,591–593,595–597] and (c) the performance and durability of the liquid electrolyte-fed AEMWEs.[310,471,473,478,587,594,597–606]

with 1 wt% $K_2CO_3$ or 0.1 M KOH feeding conditions showed stable operation for over 300 hours, while AEMWEs with 1 M KOH feed demonstrated more than 1000 hours of stable operation. These results indicate that a major limiting factor for AEMWEs with low-concentration KOH feed is not necessarily the alkaline stability of the AEM, but rather issues related to the AEI. Several potential reasons for this include the accumulation of carbonated species in electrodes from water-feed AEMWEs, making it challenging to remove all the carbonated species from pure water and thereby increasing cell resistance of pure water-fed AEMFCs.[430] Another possibility is phenyl adsorption and subsequent electrochemical oxidation of AEIs.[122] Liquid electrolytes aid in the desorption of phenyl groups from the electrocatalysts.[140] A third possibility is catalyst reconstruction with the pure water-fed AEMWEs due to the relatively low local pH environment.[588] Although supplying highly concentrated KOH-supporting electrolytes (>1 M KOH) raises concerns about AEM and AEI degradation, lifetimes exceeding 1000 hours have been demonstrated. Nonetheless, more alkaline-stabile AEM and AEI need to be developed and tested. In this context, alkaline-stable non-quaternized ion-solvating membranes have been proposed as an alternative approach.[150,589,590] Current durability tests generally lack post-mortem analysis of AEM/AEI components, which is necessary to understand the degradation mechanisms of AEPs under the AEMWE's operating conditions.

Since 2020, there have been notable improvements in pure water-fed AEMWEs. In 2020, Kim and co-workers reported high performance of AEMWEs using a high IEC polystyrene ionomer.[430] The high IEC (3.3 mequiv. $g^{-1}$) increases the local pH in the electrodes, thereby improving cell performance. The Ni–Fe anode catalysed AEMWE reached a current density of 2.7 A $cm^{-2}$ at 1.8 V. However, the durability of the cell was compromised due to excessive water uptake by the AEI, leading to the loss of catalyst particles from the electrodes. In 2021, Boettcher et al. reported a durability of 180 hours using a commercially available aryl ether-free PiperION ionomer.[591] Despite a high voltage degradation rate of 0.67 mV $h^{-1}$, the cell operated at a reasonably high current density of 0.5 A $cm^{-2}$. The same year, a similar durability (170 hours with a voltage loss rate of 0.7 mV $h^{-1}$) at the constant current density of 0.5 A $cm^{-2}$ was reported with a commercial ionomer (Sustainion®).[592] In 2022, Mustain and co-workers achieved stable performance in a polynorbornene-based cell at 1 A $cm^{-2}$ for 500 hours (voltage degradation rate: 93.5 μV $h^{-1}$). They hypothesized that performance loss in polynorbornene-based AEM and AEI for pure water-fed AEMWEs might be due to the incomplete removal of salt or other impurities when exposed to KOH solution.[593] Zhuang et al. reported a stable AEMWE performance at a relatively low current density (0.2 A $cm^{-2}$) at low cell voltage (0.55 V) using a phosphate buffer solution. They suggested that the electrocatalysts might be reconstructed at neutral pH, requiring periodical replenishing of the cell with KOH and buffer solution to maintain stable performance at a relatively high operating temperature of 80 °C. The AEMWE showed high performance (2 A $cm^{-2}$ at 1.8 V) with

pure water-fed conditions.[588] More recently in 2023, Kwon and co-workers reported stable, pure water-fed, PGM-free catalysed AEMWEs using a commercial AEM (Sustainion®). The high performance (current density at 1.8 V = 0.6 A $cm^{-2}$) and low current density loss with PGM-free catalysts are encouraging. The performance and durability of pure water-fed AEMWEs are summarized in Fig. 27b. Notably, all the high-performing pure water-fed AEMWEs used aryl ether-free AEMs and AEIs, indicating that aryl ether-containing polymer electrolytes may not be practical for pure water-fed AEMWEs due to their apparent instability.

The durability of AEMWEs under 1 wt% $K_2CO_3$ or 0.1 M KOH feed conditions have been reported as much superior, mainly because the electrodes are unaffected by $CO_2$ contamination (Fig. 27c). In 2021, Ayers et al. reported 400 hours of stable operation with near-zero voltage degradation in an AEMWE using a commercial AEM (Durion®, Xergy) at 0.75 A $cm^{-2}$ under 1 wt% $K_2CO_3$ feed conditions.[594] This work utilized a 30 μm-thick polyphenylene-based composite membrane in a 28 $cm^2$ cell and demonstrated durability under differential pressures (60–100 psig). The following year, Kohl and co-workers demonstrated 600 hours of durability under 0.1 M NaOH feed condition. They used a 30 μm-thick polynorbornene composite AEM and Ni–Fe anode catalysts for the MEA and demonstrated improved performance after the durability test at the current density of 1 A $cm^{-2}$. In the same year, Choi and co-workers reported 3000 hours of durability for a PGM-free anode-catalysed AEMWE operating at 0.5 A $cm^{-2}$ under 0.1 M KOH conditions, with a voltage degradation rate of only 11.3 μV $h^{-1}$. These reports attest that 1 wt% $K_2CO_3$ or dilute alkali metal solution feed is sufficient for the long-duration operation of AEMWEs.

Using higher concentration KOH further improves AEMWE performance (Fig. 27c). The first demonstration of high durability in 1 M KOH-fed PGM-free catalysed AEMWEs was reported by Masel and co-workers in 2018. They successfully operated AEMWEs using a commercially available AEM (Sustainion®) at a high current density (1 A $cm^{-2}$) and 60 °C for 2000 hours, with a voltage degradation rate of only 5 μV $h^{-1}$.[471] In 2019, Holdcroft et al. reported stable performance for 150 hours in 1 M KOH-fed AEMWEs. The Ni alloy-based, PGM-free electrodes showed high performance and durability at a high current density (1 A $cm^{-2}$).[600] In 2021, Meroueh et al. used the same membrane and extended the duration to 12 000 hours with a voltage degradation rate of 1 μV $h^{-1}$.[602] Arico and co-workers reported high durability of 2000 hours using another commercially available membrane (FAA-3-50, Fumasep®) during start-stop cycles. Despite some recoverable performance loss during the test, a very small unrecoverable loss was observed at the end of the durability test.[603] In 2023, Wang and co-workers reported high-performance PGM-free AEMWEs using a commercial AEM (Sustainion®). The current density of the cell reached 1.56 A $cm^{-2}$ at 80 °C with stable performance at 0.5 A $cm^{-2}$ for 100 hours.[607] In 2023, two notable results were published using non-commercial AEMs. Xu and co-workers reported high-performance AEMWEs

5754 | Chem. Soc. Rev., 2024, 53, 5704–5780

This journal is © The Royal Society of Chemistry 2024

(5.3 A cm$^{-2}$ at 1.8 V) with stable performance for 3000 hours. They used phenyl-piperidinium AEM having relatively high IEC (2.5 mequiv. g$^{-1}$) with crosslinking to reduce the water uptake of the AEM.[478] Zhang and co-workers used a poly(biphenyl alkylene) membrane to demonstrate 3500 hours of stability at 1 A cm$^{-2}$ where the AEMWE cell showed a very low voltage degradation rate (6.5 μV h$^{-1}$).[604] Also in 2023, Holdcroft et al. reported approximately 5000 hours of operation of an MEA using a polyimidazolium-based commercial AEM (Aemion+$^{®}$), Nafion$^{™}$ binder, and PGM-based catalysts at a current density of 0.6 A cm$^{-2}$ and with a low H$_2$ crossover less than 0.4%.[473] The voltage degradation rate over the long-term test was 13 μV h$^{-1}$. This study suggests that future research should focus on developing active and stable materials for catalysts, catalyst layers, and the integration of catalyst layers into MEAs, particularly as the anode components are highly susceptible to oxidative conditions. Also, more recent results by Peng et al.[605] and Lee et al.[606] demonstrated a relatively low degradation rate (5–50 μV h$^{-1}$) of 1 M KOH-fed AEMWEs employing aryl ether-free AEMs at 1.5 and 2 A cm$^{-2}$, achieving a practical level of hydrogen generation.

Although the MEAs using currently available AEMs and AEIs have shown promising performance and durability, there are several technical challenges related to polymer electrolytes that must be addressed to enable the practical adoption of this technology for hydrogen production. Firstly, the demonstration of the long-term performance of liquid electrolyte-fed AEMWEs at temperatures above 60 °C is rare. While some ex situ tests claim that certain aryl ether-free AEMs and AEIs are stable for over 1000 hours at 80 °C or higher, proving this durability at elevated operating temperatures in practical settings is a task that may be achievable in the coming years. Secondly, stable long-term performance (exceeding 1000 hours) of pure water-fed AEMWEs needs to be demonstrated. This challenge is more daunting, as the performance degradation mechanism in pure water-fed AEMWEs is not well understood. Nonetheless, demonstrating high durability in pure water-fed systems is critical for commercialization. Thirdly, the capability of AEMWEs to operate under differential pressure conditions should be established. While current demonstrations focus on performance and durability, the ability to operate effectively under varying pressure conditions, ranging from 5 to 100 bar, is essential for practical application. This requires careful consideration of mechanical properties and AEM thickness. Lastly, achieving higher current densities, ideally up to 2 A cm$^{-2}$, is desirable to increase the hydrogen production rate. Operating at such high current densities may lead to accelerated component degradation and performance decline due to extensive gas bubble formation. In particular, the electrochemical oxidation of ionomers and the dissolution of PGM-free catalysts at high anode potentials are major concerns.

## 6.3. Redox flow batteries

AEMs are being explored in a variety of flow batteries, such as zinc-bromine,[608] zinc/cerium,[609] various types of aqueous organic,[478,610–614] and non-aqueous organic RFB,[615,616] but

the all-vanadium RFB is the most extensively investigated type. Although Hwang and Ohya explored a vanadium RFB using an AEM as early as 1997,[617] it was not until a decade later other researchers began to follow suit. Still, fewer than 20 articles per year are reporting new AEMs for use in RFBs (Fig. 28a). It is noteworthy that AEMs have been shown to be more efficient than PEMs at blocking vanadium cations. Among the commercial membranes in the vanadium RFB field, Fumatech's Fumasep FAP-450, an AEM, is recognized as one of the standard options, alongside Nafion$^{™}$.

A primary motivation for using AEMs in vanadium RFBs is to enhance the CE, which is significantly influenced by the membrane's permeability to vanadium ions. Nafion membranes, commonly used in vanadium RFBs, are cation exchange membranes that readily transport vanadium ions, resulting in lower CE (Fig. 28b). The positively charged cation headgroups in AEMs effectively hinder the transport of vanadium cations. This is supported by general trends; the average CE of cells with Nafion$^{™}$ membrane is 93.1 ± 4.3% compared to 97.5 ± 2.2% of cells with AEMs. However, vanadium electrolyte solutions typically contain 2–3 M sulphuric acid and about 1.5 M vanadium sulphate. The high ionic strength of these electrolytes reduces the effectiveness of Donnan exclusion.[618,619] Membranes with an open morphology with large hydrophilic domains, as in Nafion$^{™}$ or other highly swollen membranes, tend to facilitate the transfer of co-ions. In this context, the typically lower degree of phase separation in AEMs is beneficial. Additionally, reduced access of highly oxidative VO$_2$$^+$ ions to the polymer chains in AEMs enhances their chemical resistance and, consequently, the lifetime of the polymers in vanadium RFBs.[620]

Although most AEMs exhibit lower conductivity compared to a commercial CEM like Nafion$^{™}$, it suggests that AEMs have higher resistance, which could potentially lead to a lower VE. However, optimized AEMs are better at blocking the crossover of vanadium ions than Nafion$^{™}$, which allows for the use of thinner membranes to retain VE. Consequently, because EE is the product of CE and VE, the average EE of the cells, as compared in Fig. 28, is 81.0 ± 5.6% for those using AEMs and 78.8 ± 4.6% for cells using Nafion$^{™}$.

In vanadium RFBs, the capacity loss due to the crossover of vanadium ions can be recovered by mixing the discharged electrolytes, making EE a crucial parameter. Among the over 70 membranes shown in Fig. 28a, the highest EE was achieved with PBI-based membranes. Du et al. developed a PBI-based AEM by reacting a PBI with glycidyl trimethylammonium chloride.[627] An even slightly higher EE was obtained by cells featuring a thin (1–2 μm) PBI layer to block vanadium crossover, supported by a porous or highly swollen gel-type PBI layer.[639,640] The superior performance of PBI-based cells can be attributed to the acid-doped PBI carrying charges directly on the polymer backbone, which inhibits phase separation. The narrow spacing between the PBI chains limits the transport of vanadium ions through size exclusion, in addition to electrostatic repulsion. The inclusion of quaternary ammonium side chains, as demonstrated by Du et al., results in a more open
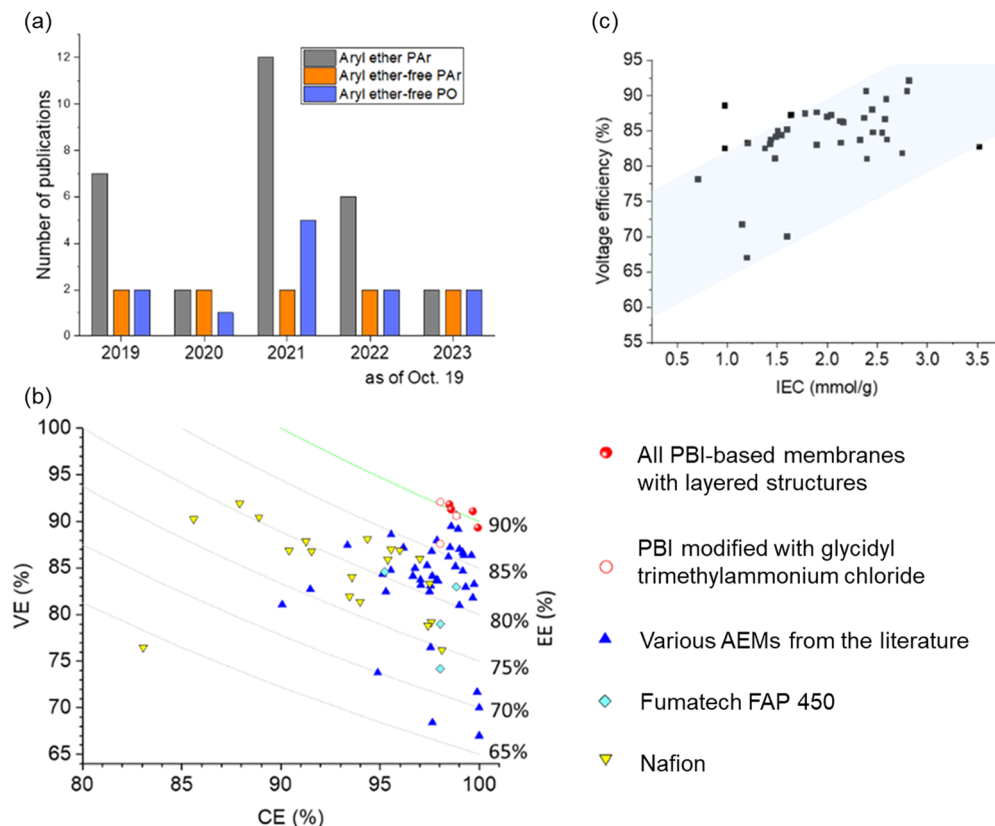
This journal is © The Royal Society of Chemistry 2024

Chem. Soc. Rev., 2024, 53, 5704–5780 | 5755

**Fig. 28** (a) Number of publications on new AEMs for RFB over the last 5 years; (b) vanadium RFB performances of cells operating at 80 mA cm$^{-2}$. 50 cells using AEMs[95,102,621–638] including commercial AEM Fumasep FAP-450[624,628,630,636] are compared with 7 cells using Nafion 115,[622,630–632,634,636,637] 3 cells using Nafion 117,[95,621,638] 10 cells using Nafion 212[102,623–629,633,635] and 4 cells using layered PBI membranes.[639,640] CE, VE, and EE are coulombic, voltage, and energy efficiency, respectively; (c) voltage efficiency *vs.* IEC. Please see Table S10 in ESI,† for detailed data.

membrane morphology, leading to an increase in VE and a decrease in CE.

Comparing published membrane conductivities can be misleading. For instance, the AEM with the highest EE in Fig. 28 has a conductivity of only 9.7 mS cm$^{-1}$,[627] yet achieved a VE of 92%. In contrast, a poly(ether ether ketone) (PEEK)-based AEM developed by Yang *et al.* had a higher conductivity of 65 mS cm$^{-1}$, but a lower VE of 86%, and an EE of 85%.[635] Since membrane thickness is optimized to balance VE and CE, the vanadium RFB community often focuses more on area-specific resistance (ASR, $\Omega$ cm$^2$) as a key parameter. Other complicating factors include variation in sulphuric acid electrolyte concentration across studies and a significant increase in ASR when transitioning membranes from sulphuric acid solution to vanadium-containing electrolyte. In some cases, membrane A may exhibit a lower ASR in sulphuric acid than membrane B, but the reverse order is observed in vanadium electrolytes.[641] Comparing VE values achieved with different membranes could be a potential solution, but VE is also heavily influenced by cell resistance and electrode activity. This is evident when comparing performances obtained with the Fumasep FAP-450 membrane, where VE ranges from 74.2% to 84.6%. A plot of VE values against IEC yields scattered results, suggesting a potential positive correlation between VE and IEC. Considering

the variation in VE values for Fumasep FAP-450, the scattering is within a reasonable range.

Similar to the alkaline degradation of AEM backbones, it has been suggested that aromatic ether bonds are also susceptible to reaction with VO$_2^+$ ions, leading to chain scission and membrane failure due to embrittlement. Therefore, AEMs based on newer chemistries that avoid aromatic ether bonds, such as polyphenylene-based AEMs,[478,628,631,637,642] and polybenzimidazolium-based AEMs, show promise.[643,644]

### 6.4. High-temperature PEMFCs

AEMs when paired with PA, play a crucial role in ion-pair HT-PEMFCs. To facilitate proton conduction under high temperature and anhydrous conditions, AEMs are doped with PA through the conventional imbibing process, resulting in the formation of PA-doped ion-pair membranes. There are distinct differences between ion-pair systems and conventional HT-PEMFCs based on PA-doped PBI. In PA-doped PBI systems, a proton of PA is transferred to benzimidazole, producing protonated benzimidazole, known as benzimidazolium. Conversely, ion-pair systems involve the abstraction of a proton from PA through interaction with a hydroxide anion, forming a quaternary ammonium-biphosphate anion interaction. The interaction, with a strength of approximately 110 kcal mol$^{-1}$,

**5756** | *Chem. Soc. Rev.*, 2024, **53**, 5704–5780

This journal is © The Royal Society of Chemistry 2024

significantly exceeds that between benzimidazole and PA, which is around 15 kcal mol$^{-1}$.[7] Due to this robust ion-pair interaction, ion-pair systems can achieve a greater doping level of acid at a given number of base sites. Initially developed methylated benzimidazole membranes were mechanically unstable and could only be utilized effectively through blending with a PBI membrane.[645] The first ion-pair system without blending was demonstrated with BTMA-functionalized DAPP AEM in 2016.[7] Other approaches to form ion-pair structure include using quaternary ammonium-modified polymers with intrinsic microporosity (PIM)[646,647] and incorporating ionic liquid moieties.[648–655] The ion-pair approaches prove beneficial for the stable operation of HT-PEMFCs, as they considerably reduce the risk of leaching out PA.[7]

The number of publications for ion-pair HT-PEMFCs has increased since 2016 (Fig. 29a). Table S11 (ESI†) summarizes the performance and durability of MEAs in ion-pair HT-PEMFCs. The most prevalent polymer backbones for ion-pair membranes are aryl ether-free PAr and PBI, each constituting 45% of the total, while aryl ether PAr AEMs make up the remaining 10% (Fig. 29b). No polyolefinic AEMs have been reported yet, likely due to their lower thermal stability. Various cationic headgroups including alkyl-A, BTMA, imidazolium, piperidinium, and pyrrolidinium were used. Unlike in AEMWE and AEMFC applications, the alkaline stability of the cations is not a primary requirement as HT-PEMFCs operate under low pH conditions. Fig. 29c shows the PPDs of ion-pair HT-PEMFCs as a function of operating temperatures. Most PPDs were reported at 120, 160, and 200 °C under H$_2$/O$_2$ and H$_2$/air conditions. The range of PPDs at a given operating temperature is relatively broad (0.5 to 1 W cm$^{-2}$), as performance depends

on several factors, including electrodes and other operating conditions such as reactant flow rate and back-pressure.

Fig. 29d summarizes the performance and durability of ion-pair HT-PEMFCs. In 2016, Kim and co-workers introduced the term 'ion-pair HT-PEMFCs'. They utilized a BTMA functionalized DAPP membrane and achieved the PPD of 0.75 W cm$^{-2}$ at 160 °C under H$_2$/O$_2$ conditions.[7] They demonstrated that ion-pair HT-PEMFCs can operate stably under dynamic operating temperature conditions with a water vapour pressure ($P_{H_2O}$) of 9.7 kPa and showcased 500 hours long-term durability at 120 °C and 0.4 V, with minimal current degradation rate (0.33 mA cm$^2$ h$^{-1}$). In 2020, Li *et al.* reported a slightly improved performance of ion-pair HT-PEMFCs over PBI-HT-PEMFCs.[108] However, rapid degradation occurred within 30 hours at 160 °C and 0.2 A cm$^{-2}$, indicating the instability of aryl ether-containing polysulfone in HT-PEMFC applications. In the same year, Wang and co-workers introduced a polybenzimidazolium membrane for ion-pair MEAs.[656] The fuel cell displayed moderate (PPD$_{160°C}$ = 0.64 W cm$^{-2}$ under H$_2$/O$_2$ conditions) and showed no degradation during 390 hours of operation at 160 °C. In 2021, a study using a similar polybenzimidazolium membrane demonstrated high PA retention of the membrane at 80 °C and 40% RH, with negligible degradation over 200 hours under anhydrous conditions at 160 °C.[649] Kim and colleagues reported improved ion-pair MEA performance (PPD$_{160°C}$ = 1.2 W cm$^{-2}$ under H$_2$/O$_2$ conditions) in the same year, achieved with a PA-functionalized ionomer instead of a PTFE binder.[658] The performance reached 240 °C where PPD reached 1.75 W cm$^{-2}$, and the cell operated stably at a constant current density of 0.6 A cm$^{-2}$ over 500 hours at 160 °C with a voltage degradation rate of 0.35 mV h$^{-1}$. The same group also
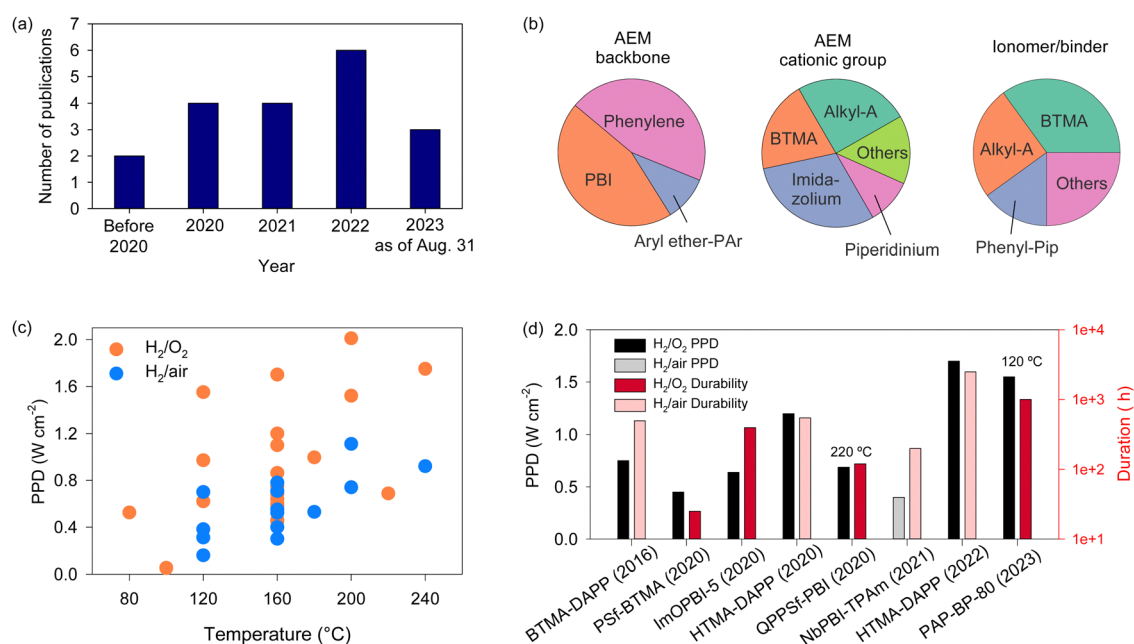


Fig. 29 Summary of performance and durability of ion-pair HT-PEMFC MEAs: (a) the number of recent publications on ion-pair HT-PEMFC. (b) The AEMs and AEIs used in ion-pair HT-PEMFCs. (c) PPD of ion-pair HT-PEMFC MEAs under H$_2$/O$_2$ and H$_2$/air conditions. (d) The performance and durability comparison of the reported ion-pair HT-PEMFCs at 160 °C.[7,9,108,186,649,656–661]

This journal is © The Royal Society of Chemistry 2024

Chem. Soc. Rev., 2024, 53, 5704–5780 | 5757

reported the highest cell performance of the HTMA-DAPP-biphosphate ion-pair PEM and protonated PA-functionalized ionomer ($PPD_{160°C}$ = 1.7 and 0.78 W cm$^{-2}$ under $H_2/O_2$ and $H_2$/air conditions, respectively) with stable operation at 160 °C and 0.6 A cm$^{-2}$ for 2500 hours.[9] In 2020, Arges et al. demonstrated stable ion-pair MEA performance in the presence of 25% CO at 220 °C.[657] This study was significant for illustrating practical high-temperature operation, which aids in increasing the operating temperatures of electrochemical hydrogen pumps that have high CO concentrations.[662] In 2023, Sun and co-workers demonstrated stable fuel cell performance using phenyl-piperidinium-based AEM at 120 °C for 1000 hours. They obtained high fuel cell performance at 120 °C ($PPD_{120°C}$ = 1.5 W cm$^{-2}$, 80 kPa), suggesting that phenyl-piperidinium AEM are promising for highly performing ion-pair HT-PEMFCs.[186]

## 6.5. $CO_2$ and CO electrolysers

AEPs are extensively used in $CO_2$ and CO electrolysers. The primary challenge in $CO_2$ electrolysis lies in achieving efficiency and selectivity of the $CO_2$ reduction reaction ($CO_2$RR). Consequently, the bulk of research has centred on the $CO_2$RR activity of various electrocatalysts under different system conditions, leading to the identification of some highly active electrocatalysts for $CO_2$ electrolysers in flow cells or MEA designs. Prior to 2017, the literature on $CO_2$ electrolysers using AEMs was sparse (Fig. 30a). However, post-2019, the literature on $CO_2$ and CO electrolyser performance has increased, with at least ten articles per year, and the trend is upward. A significant advantage of AEM-based $CO_2$ electrolysers is their high $CO_2$RR activity under near-neutral conditions. By contrast, in CEM-based $CO_2$ electrolysers, $CO_2$ quickly transforms into (bi)carbonate, leading to carbonate salt build-up in the cathode flow field and within gas diffusion electrodes. This hampers $CO_2$ access to the

catalyst, leading to increased hydrogen faradaic efficiencies.[663] To counteract this issue in AEM-based $CO_2$ electrolysers, the approach using BPMs was demonstrated; BPM-based $CO_2$ electrolysers can reconvert any formed (bi)carbonates back to $CO_2$ by supporting protons to the cathode chamber. The reversed-bias BPM technique has been employed in various studies to enhance $CO_2$ utilization in $CO_2$ electrolysis systems.[664–667] About 62% of the articles on $CO_2$ and CO electrolysers involve AEMs, while 13% and 25% utilize BPMs and CEMs, respectively (Fig. 30b). It is noteworthy that most AEMs used for $CO_2$ electrolysers are commercially available, indicating that $CO_2$ electrolyser research is more on the $CO_2$RR and device performance than on specific AEMs tailored for these devices (Table S12, ESI†).

Several studies have examined the role of AEMs and AEIs in $CO_2$ electrolysers' performance. Masel and co-workers observed that $CO_2$ electrolysers utilizing four acidic membranes-Nafion™, CMI-7001, SPEEK, and PA-doped PBI exhibited relatively low CO production rates compared to hydrogen evolution. Among AEM-based $CO_2$ electrolysers, those with imidazolium functionalized polymers demonstrated the highest CO selectivity.[668] Schmidt et al. used various polymeric membranes and ionomer combinations, concluding that balancing $CO_2$RR and HER demands an alkaline environment at the cathode to achieve high $CO_2$RR selectivity. However, fully alkaline cells showed increased $CO_2$ migration from the cathode to the anode. They suggested that a BPM system with an acidic membrane and an AEI-bonded cathode catalyst could address this issue effectively.[669] Rabinowitz and Kanan noted that the formation of carbonates not only impacts the energy balance by consuming hydroxide ions but also reduces the efficiency of oxygen evolution by lowering pH at the anode.[670] To address this issue, forward bias BPMs can be employed to
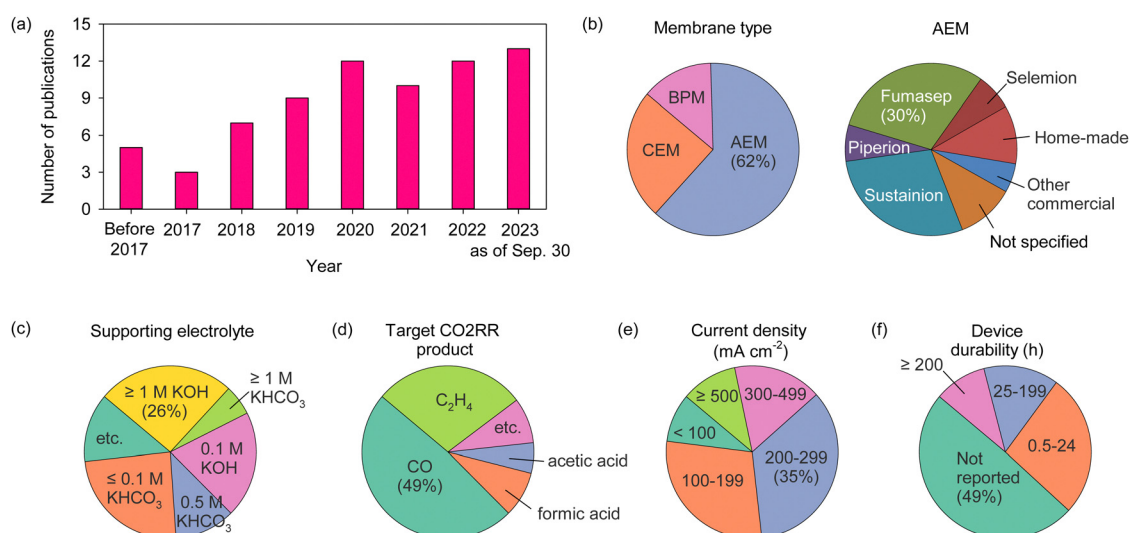


Fig. 30 Summary of performance and durability of $CO_2$ and CO electrolysers. (a) The number of publications of $CO_2$ and CO electrolysers over the last seven years, (b) membrane types that was used for the $CO_2$ and CO electrolysers, (c) AEMs used for $CO_2$ and CO electrolysers, (d) supporting electrolyte that was used for the AEM–based $CO_2$ and CO electrolysers, (e) the current density of $CO_2$ and CO electrolysers, and (f) durability of $CO_2$ and CO electrolysers.

5758 | Chem. Soc. Rev., 2024, 53, 5704–5780

This journal is © The Royal Society of Chemistry 2024

consume carbonate anions at the BPM interface. However, it is important to note that using BPMs introduces an additional overpotential for water dissociation. Janáky and co-workers underscored the importance of thin membranes in enhancing CO-forming capability by comparing the performance of cells with a thin membrane (PiperION, 15 μm thick) *versus* thicker ones (*e.g.*, Sustainion®, 50–70 μm thick). The PiperION membrane, with its low resistance (0.36 Ω cm²), facilitated a high CO formation current density of 630 mA cm⁻² in their zero-gap electrolyser.[671] Jiao and co-workers explored the impact of AEMs' alcohol permeation rate on the carboxylate production rates in CO electrolysers. They reported that membranes with higher diffusion rates for the products increased the molar production ratio towards carboxylates and the target product concentration.[672] Ju *et al.* investigated the influence of different ionomers on the cathode performance of $CO_2$ electrolysers, concluding that a balance of anionic conductivity and hydrophobicity is crucial for high CO faradaic efficiency.[673] Broekmann and co-workers compared the ionomer performance between Nafion™ (cationic) and Femion (anionic), emphasizing that electrolyte management – particularly preventing $K_2CO_3$/$KHCO_3$ precipitate formation – is more critical than ionomer hydrophobicity.[674] Seger *et al.* investigated the effect of cationic groups on CO selectivity.[371] They found that AEMs, while not directly affecting catalytic activity, create a local environment around the cathode catalyst layers through water management. The benzyl-*N*-methylpiperidinium-head group of RG-AEMs yielded the highest CO selectivity (>80%) compared to TMA or benzyl-*N*-methylpyrrolidinium head groups, thanks to improved water and ionic transport. The same research groups also demonstrated that minor variations in synthetic conditions of RG-AEMs can result in spectroscopically identical AEMs with markedly different hydration properties and CO₂RR performance.[413]

In AEM-based $CO_2$ and CO electrolysers, supporting electrolytes are commonly used alongside ionomers to suppress HER and enhance the CO₂RR at the cathode and OER at the anode. The most frequently used supporting electrolytes include KOH and $KHCO_3$ (Fig. 30c), with $CsHCO_3$ also being a popular choice due to its effectiveness in mitigating salt deposition caused by salt crossover to the cathode.[675,676] The supporting electrolytes significantly influenced the faradaic selectivity of CO₂RR products. For instance, Hori *et al.* demonstrated that the formation of $CH_4$ *via* CO₂RR electrocatalysts is favoured in environments with high concentrations of bicarbonate, a phenomenon attributed to variations in the buffer capacity of different electrolytes.[677] In contrast, C2 products are more prevalent in dilute $KHCO_3$ solutions. While achieving high faradaic CO₂RR efficiency alongside low OER overpotentials remains a challenge, several studies have reported $CO_2$ electrolyser systems that operate without supporting electrolytes.[678–681] The primary rationale behind these ionomer-only electrolyte systems is to avoid the inevitable formation of salts associated with supporting electrolytes, which can diminish the stability and efficiency of the overall system.[682] The choice of electrocatalysts plays a critical role in determining the CO₂RR products. For example,

Au and Ag catalysts exhibit high faradaic efficiency for CO production, accounting for nearly 50% of the AEM-based $CO_2$ electrolysers' output (Fig. 30d). In contrast, catalysts based on Pb, Sn, and Pd favour the production of formic acid, while Cu-based catalysts are known for generating $CH_4$, $C_2H_4$, and various alcohols.[683]

The reported performance of AEM-based $CO_2$ and CO electrolysers typically involves lower current density compared to water electrolysers (Fig. 30e). The most frequently observed current density is 200–299 mA cm⁻², accounting for 35% of reports, closely followed by 100–199 mA cm⁻², which represents 29% of cases. Notably, only 10% of the reports indicate current density exceeding 500 mA cm⁻². In 2018, Jiao and co-workers demonstrated a Cu-catalysed and Fumatech AEM-incorporated CO electrolyser, achieving $C_{2+}$ faradaic efficiency of 91% with $C_{2+}$ partial current density over 630 mA cm⁻² by optimizing the triple-phase boundary at the electrode–electrolyte interface. In 2019, Strasser *et al.* showcased a Ni–N–C catalysed $CO_2$ electrolyser capable of operating up to 700 mA cm⁻².[684] However, it was observed that the maximum faradaic efficiency (90%) of the Selemion AEM incorporated electrolyser was achieved in the 100 and 200 mA cm⁻² range. Beyond this, an increase in current density led to a gradual decrease in CO efficiency. Later, The same research group reported $CO_2$ electrolysers capable of operating at up to 700 mA cm⁻², achieving a remarkable $C_{2+}$ energy efficiency of 100% using a coupled tandem electrolyser approach.[685] Additionally, piperidinium-based AEM-based $CO_2$ electrolysers have demonstrated the capability to operate efficiently at high current density, such as 500 mA cm⁻².[671,686]

A significant challenge in $CO_2$ electrolysers is their limited durability. Notably, nearly half of the relevant studies did not report on the longevity of the electrolysers. Merely 7% of the publications document a lifespan exceeding 200 hours (Fig. 30f). The primary reason for the low stability is the salt accumulation and consequent clogging of flow channels. Additionally, the high operating cell voltage of $CO_2$ electrolysers, around 3.0 V, can potentially lead to the electrochemical oxidation of AEMs. In 2017, Masel and co-workers reported exceptional durability in $CO_2$ electrolysers, ranging from 550 to 4380 hours.[668,678] These highly durable cells were operated under deionized water or 0.01 M $KHCO_3$, conditions that are near neutral. The environment allowed the methylimidazolium-based polymers to operate for extended periods without degradation from hydroxide attack. Another noteworthy instance of durability in a $CO_2$ electrolyser was achieved using a toluene-functionalized Cu catalyst. Zheng *et al.* observed that while a pristine Cu catalyst failed to maintain a stable voltage beyond 50 hours of electrolysis, a toluene-modified Cu catalyst exhibited remarkable stability for over 400 hours. This stability was coupled with an ethylene faradaic efficiency of 50% by supplying 0.1 M $KHCO_3$.[687]

## 6.6. Other applications

DAC or $CO_2$ separation from coal-fired power plants, is pivotal in decarbonizing the economy. Current DAC methods primarily utilize amine solution-based or solid adsorbents. However,

This journal is © The Royal Society of Chemistry 2024

*Chem. Soc. Rev.*, 2024, **53**, 5704–5780 | **5759**

materials based on quaternary ammonium offer distinct advantages over these amine-based techniques. Employing a moisture-swing process driven by water evaporation energy, quaternary ammonium materials can efficiently capture atmospheric $CO_2$. This process involves sorption in low-humidity conditions and desorption when humidity increases, operating without external heat input. The DAC efficiency with these materials can reach 100% in dry conditions, exceeding amine-based counterparts.[688,689] Yan et al. demonstrated an electrochemically driven $CO_2$ separator utilizing a hydrogen-powered cell with an anion-conducting membrane.[690] In their configuration, the cathode facilitates the ORR, generating hydroxide ions that remove $CO_2$ from air by forming carbonates. Meanwhile, at the anode, the HOR generates protons, establishing a low pH environment. The formed carbonates at the cathode migrate to the anode via the membrane, where they convert into bicarbonates and eventually $CO_2$ due to the pH gradient. The shorted membrane was prepared by blending a phenyl piperidinium AEP with electronically conductive carbon additives, enabling electron transport through the membrane and facilitating a compact and high-performance module. Through optimization, the shorted membrane cell demonstrated >99% $CO_2$ removal from 2000 sccm air over a continuous operation period of 450 hours. Simari and co-workers utilized a quaternary ammonium-functionalized polyepichlorohydrin membrane for $CO_2$ sorption, demonstrating superior capture efficiency under simulated flue gas conditions and effective regeneration with minimal energy consumption in mild $N_2$ environments.[691] Singh and co-workers developed an integrated system, combining electrochemical $CO_2$ capture from flue gas and its reduction to value-added products and fuels, using an AEM.[692] Their approach involved capturing $CO_2$ in an organic liquid (KOH-saturated ethylene glycol, and choline hydroxide) and transporting $HCO_3^-$ across an AEM. A successful and continuous integration of migration-assisted moisture gradient $CO_2$ capture and electrochemical $CO_2$ reduction was demonstrated. In a recent study, Freeman et al. investigated DAC using the Fumasep FAA-3 membrane, and a reactive transport model suggested that carbon support rates in AEMs are primarily limited by moisture-swing reaction kinetics.[693] They concluded that polymer design optimization could enhance the moisture-swing effect, or coupling moisture gradient with electrochemical force could lead to more energy-efficient and rapid $CO_2$ separation.

Aryl ether-free AEMs are increasingly utilized in diffusion dialysis for acid recovery. These AEMs reject most cations through electrostatic repulsion and offer significant advantages over aryl ether-containing polymers[694,695] and polyolefinic AEMs.[696,697] Such benefits include lower swelling, higher selectivity, and higher chemical stability.[185,698–700] The superior membrane properties of aryl ether-free polyaromatics allow for higher IEC, ranging from 2.0–2.8 mequiv. $g^{-1}$, compared to those of other types of AEMs (0.8–2.0 mequiv. $g^{-1}$), resulting in better performance in acid recovery applications.

In research focusing on the selective removal of heavy metal ions[701–704] or minerals,[705–711] AEPs are employed in processes like MCDI or adsorption. In the MCDI process, the membrane traps co-ions into intraparticle pores, enhancing the accumulation of counterions in macropores. The application of an inverted voltage upon discharging, facilitated by ion-exchange membranes, prevents the re-adsorption of desorbed ions on the counter electrode, thereby increasing electrode regeneration efficiency. While commercial polyolefinic AEPs are commonly used in this context, less focus has been placed on AEP materials due to the strong dependence of cell performance on cell configuration and adsorbing materials.[712,713] Nonetheless, the importance of AEP properties such as IEC has been increasingly recognized as key parameters for the device performance.[714]

# 7. Perspective and outlook

This review presents a comprehensive overview of the chemical stability of AEPs and the various synthetic approaches to polyaromatic and vinyl-derived AEPs, charting the evolution of these chemistries to improve performance, chemical stability, and durability. The merits and weaknesses of each method to prepare aryl ether-free polymer electrolytes are summarized in Table 4. Additionally, this review explores the scale-up of AEPs and AEMs for prospective applications in the market. The final section discusses the performance of these devices in mainstream applications, including fuel cells, electrolysers, and flow batteries.

The last fifteen years have witnessed a resurgent interest in AEPs for a variety of applications beyond the core AEMFC application, which still accounts for the largest share of research papers. Over the last five years, research on AEMWE and $CO_2$ electrolysis has proportionately increased compared to other applications like ED, RED, and RFB, in part due to new opportunities and directed funding in these areas. The intended applications for AEPs span a broad range of environmental conditions under which they must operate stably. The structures of AEPs, in general, need to be specifically tailored to meet the requirements in which they operate. Fig. 3 summarizes the environmental regimes under which AEP applications operate.

In most applications, AEPs are in the form of AEMs, whose function is to maintain separation between reactants while allowing trans-membrane selective ion transport. Consequently, mechanical properties must be robust enough to maintain this separation boundary over a long period under specific environmental operating conditions. AEMs operating in entirely liquid environments include RO, RFB, ED, and MCDI. Since AEMs carry various amounts of fixed ionic charge, they are prone to liquid uptake, enhancing ion conductivity but becoming detrimental in excess. This often correlates with dimensional swelling, which weakens the mechanical strength and leads to AEM rupture, wrinkling, and defects at contact points. However, liquid uptake and dimensional swelling effects can be decoupled to some extent by various strategies, such as non-swelling mechanical supports, dipolar chain

5760 | Chem. Soc. Rev., 2024, 53, 5704–5780

This journal is © The Royal Society of Chemistry 2024

Table 4 Summary of the synthetic methods to prepare aryl ether-free polymer electrolytes

| AEP synthesis method | Merits | Weaknesses |
|---|---|---|
| **Chemistry of polyaromatics** | | |
| Acid-catalysed polyhydroxyalkylation | One-pot, low to room temperature, metal-free polymerization | Limited choice of reactors for a large-scale reaction due to the high acidity of the catalyst |
| | High tolerance of the acid catalyst towards functional monomers | Limited choice of monomers for high molecular weight growth |
| Metal-promoted coupling reaction | Various choices of monomers for polymerization | Requirement of a stoichiometric amount of the Ni catalyst or the use of an expensive Pd catalyst |
| Ionenes including poly-benzimidazoliums and polyimidazoliums | Incorporation of highly alkaline stable groups in the backbone | High water uptake and even water solubility |
| | | Difficulty in forming free-standing film and requirement of post-modification strategies |
| Diels–Alder polymerization | All phenylene backbone with high processability | Require high molecular weight to achieve good mechanical properties |
| | High gas permeability due to the bulky backbone structure | |
| **Chemistry of vinyl polymers** | | |
| Addition polymerization | Various polymer structures including random and block copolymers | Limited choice of monomers |
| | Fully saturated backbones at the polymerization stage | Questionable radical stability |
| Ring opening metathesis polymerization | High functional group tolerance including cations | The requirement of an expensive Ru catalyst |
| | | The requirement of a two-step process to achieve a fully saturated backbone |
| Radiation grafting method | AEM with complex nano-morphology | Limited choice of monomers for radical grafting |
| | Synthesis of high-performing particulate AEI | The requirement of access to high-energy radiation facilities |
| | | Difficult to control IEC precisely |
| Anionic polymerization | Well-defined block composition and narrow molecular weight distribution | Requirement of strict inert atmosphere and purity of monomers and solvents |
| | | Limited choice of monomers for polymerization |
| | | Requirement of post-functionalization |

interactions, hydrogen bonding, and branched or crosslinked polymer chain architecture.

In addition to the AEM applications, aryl-ether free AEPs have potential uses in creating high-performance and durable BPMs suitable for a range of electrochemical processes. These processes include nitrate reduction, $CO_2$ reduction, water electrolysers, and ionic separations like MCDI and ED.

AEP processability is crucial since the majority of AEMs are fabricated through solution casting followed by solvent evaporation. Crosslinking is necessarily done after the casting step, either in the presence of the casting solvent or in the dry state. AEPs containing a high proportion of rigid structural units, polar groups, or hydrogen bonding sites may require higher-boiling solvents for viable casting solutions, posing challenges for complete solvent removal during membrane formation. In the case of branched chain architecture, introducing free volume and increased chain entanglement is limited to low degrees of branching before gel formation occurs.

AEMs operating in more complex mixed-phase gas–liquid environments include AEMFC, AEMWE, and $CO_2$ electrolysers, where electrocatalytic reactions occur on the membrane surface. This leads to potentially more reactive species, such as free radicals and nascent hydrogen and oxygen, imposing a more demanding chemical degradative stress on the AEPs. AEIs are used in these applications where catalysts are employed, serving multiple functions critical to the performance and

durability of AEMFCs and other electrochemical devices. Firstly, they act as polymeric binders surrounding catalyst particles, requiring material compatibility with the AEM to avoid the delamination issue encountered in earlier work on PEMFC counterparts. Fortunately, much research and some commercially available AEIs have better compatibility with AEMs, being non-fluorinated. Secondly, unlike AEMs where low gas permeability is desired to prevent hydrogen crossover, AEIs should have high gas permeability. This is crucial, especially in AEMFCs during the hydrogen oxidation reaction at the cathode, where hydrogen permeation is limited by cationic group adsorption. Thirdly, AEIs function as a boundary phase, where gas, water, electron, and ion transport occur simultaneously. IEC values between AEM and AEI can be substantially different, and AEIs are typically dispersed in low-boiling solvents and mixed with catalysts to form inks. Some interesting characteristics, such as high gas permeability and low voltage degradation rates, have been observed for AEI particulates suspended in a solvent, providing new research opportunities for exploring high free-volume particulates as AEIs.

The chemical stability of AEPs under various application operating conditions is a critical requirement to ensure durability for commercial viability. Fig. 3 illustrates the typical pH and potential ranges of various electrochemical devices utilizing AEPs. AEM applications that do not employ catalysts, such as RO, ED, RED, and MCDI, operate in environments composed

This journal is © The Royal Society of Chemistry 2024

*Chem. Soc. Rev.*, 2024, **53**, 5704–5780 | 5761

of multivalent metal cations, requiring chemical stability typically within a pH range of 4–13. On the other hand, various fuel cell and electrolyser AEM applications employing catalysts, namely AEMFC, AEMWE, and $CO_2$ capture/electrolyser, have more stringent operating environments with pH levels exceeding 13, demanding high AEP chemical stability. Furthermore, high electrochemical stability at $> 2$ V is required for AEMWE and $CO_2$ electrolysers. Further research regarding the electrochemical stability of the fragments of AEPs under various electrode potentials and operating conditions needs to be explored.[129] In addition to strongly basic environments, AEMs are also used in strongly acidic environments. HT-PEMFC applications operate in a pH range of 1–3 at elevated temperatures of 100–200 °C, while RFB applications operate at a pH below 1.

Many of the earlier AEPs were based on the chloromethylation–quaternization structural modification of readily available hydrocarbon polymers, such as polystyrene, polysulfone, or PPO, due to their accessibility through a relatively simple process. While these AEPs may be appropriate for use in applications in less aggressive environments (e.g., ED), they are less suited to more stringent fuel cell and electrolyser application conditions where high pH and electrocatalytic oxygen radicals occur. Aryl ether-containing AEPs are known to undergo degradation in high-pH environments.

Beyond the polymer backbone, the stability of the cation headgroup must be considered, along with its relationship and proximity to the backbone, and its accessibility to hydroxide ion nucleophilic attack, as degradation relations do not necessarily occur in isolation between backbone and headgroup. In terms of oxidative stability, AEPs with high electron density are more susceptible to radical-induced oxidation, while those with electron-withdrawing groups have high electrophilic character and remain more stable toward oxygen radical attack.

In the last decade, aryl ether-free AEPs have become well-established, representing major progress in the wider field. Notable classes of these AEPs are based on hindered poly(benzimidazolium), polyphenylene, polynorbornene, and terphenyl piperidinium, which have considerably higher oxidative stability than aryl ether-containing polymers and are thus better suited for fuel cell and electrolyser applications. Higher oxidative stability is particularly required for electrolysers due to the higher electrode potentials in the devices, as degradation pathways are dependent upon operating conditions.

As noted earlier, the nature of degradation by hydroxide ion (alkaline, nucleophilic) and hydroxyl radical (oxidative, electrophilic) is different, highlighting the need to design AEPs with balanced chemical stability for each specific electrochemical device and operating condition. Contemporary research is primarily focused on these four classes of AEMs for fuel cell and electrolyser applications, with the outlook anticipating further tuning of specific properties tailored to individual application operating environments. Properties such as ion conductivity and mechanical strength are influenced by IEC, water uptake and dimensional swelling, polymer chain architecture, crosslinking, chain interactions, type of cation headgroup, and chemical composition of the AEMs.

The kinetics of water uptake and dimensional swelling of AEMs may vary depending on the temperature and time for measurement. It is important to note that polymer chain structures, their strength of intra-and intermolecular interactions, how dry the membranes are to begin with, and the solvents used to cast the membrane may also play crucial roles in water uptake and dimensional swelling.

The IEC of AEMs for AEMWEs may be somewhat lower than for AEMFCs when liquid electrolyte is supplied, while the AEM may be thicker to reduce gas crossover and withstand desirable differential pressure operations. There are likely more opportunities for improving alkaline stability by exploring new cation headgroups, such as metallocenes, or decreasing the susceptibility of cation headgroups to nucleophilic hydroxide attack, as seen in the hindered access approach used in poly(benzimidazolium) AEMs. Increasing oxidative stability can also be addressed by specific chemical structures of AEPs that avoid susceptible units and the possibility of using anti-oxidative additives. Other AEM work highlights opportunities for aligned through-membrane conduction channels,[575] although more scalable processes are essential for commercialization.

The main body of AEP (AEM and AEI) structural design for the past decade has been applied to AEMFC. However, similar structural design principles are usually applicable to AEMWE and $CO_2$ electrolysers, but with some structural and membrane fine-tuning according to the specific environment of the application. In particular, AEPs for AEMFC, AEMWE, and $CO_2$ capture/electrolyser applications all need chemical stability under higher pH conditions (pH $> 13$), which are highlighted in this review. As mentioned above, thicker AEMs are preferable for AEMWE to reduce gas crossover and mechanical stress from differential pressure. Since these AEMs are immersed in liquid, dimensional swelling must be controlled, either by AEM mechanical support, or mitigated by crosslinking or branching, and by a lower IEC. In many cases, commercially available AEMs are employed. Also, since the AEMs are thicker and require more material, there is more price sensitivity and a requirement for cheaper materials. In the case of $CO_2$ electrolysers, most investigations have focused on the $CO_2RR$ and device performance, using commercially available AEMs, rather than on specific AEMs tailored for these purposes (Table S12, ESI†).

The exploration of AEIs within catalyst layers has been comparatively limited compared to AEMs, yet their significance in enhancing device performance is increasingly recognized. Beyond the essential attributes required of AEMs – such as ion conductivity, mechanical resilience, dimensional integrity, and alkaline endurance – three specific criteria stand out for AEIs. Firstly, AEIs can regulate pH conducive to electrochemical reactions. This adjustment is facilitated by factors like cationic and non-cationic functional groups, IEC, and the ratio of ionomer to catalyst within the catalyst layers. Generally, a higher pH is favoured for AEMWEs as opposed to AEMFCs.

5762 | Chem. Soc. Rev., 2024, 53, 5704–5780

This journal is © The Royal Society of Chemistry 2024

However, a significantly lower pH proves advantageous for $CO_2RR$ in the $CO_2$ electrolysers.[715–720] Secondly, AEIs should exhibit minimal interactions with catalysts. Interactions between ionomers and catalysts not only influence catalytic efficiency but also impact device durability. Notably, the adsorption of cationic AEI groups at the anode of electrochemical devices is prominent, leading to electrochemical oxidative degradation at high electrode potentials. Opportunities exist for designing AEIs with lower adsorption energy on the surface of catalysts, exemplified by fluorene-based AEIs having fused ring structures.[134] This class of AEIs boasts high oxidative stability, which is particularly beneficial for electrolyser operating at high electrode potentials. Thirdly, AEIs with high gas permeability are desirable for a swift reactant or product transport. Conventional methods involve partial fluorination to enhance gas solubility.[173,556,721] Modern advancements include the development of ionomers with particulate structures[406,437,722,723] and increased free volume.[165,509,724]

The industrial implementation of AEMs and AEIs for fuel cells and electrolysers requires AEPs with the desired performance and functional characteristics, along with high stability, to ensure device durability. The principles of successful commercial adoption dictate that processes for making AEMs and AEIs should be cost-effective, simple, scalable, and sustainable.

## Glossary of acronyms

| | |
|---|---|
| ADMET | Acyclic diene metathesis polymerization |
| AEM | Anion exchange membrane |
| AEMFC | Anion exchange membrane fuel cell |
| AEMWE | Anion exchange membrane water electrolyser |
| AEI | Anion exchange ionomer |
| AEP | Anion exchange polymers |
| AFM | Atomic force microscopy |
| AMS | α-Methylstyrene (AMS) |
| ASR | Area specific resistance |
| Bpin | Pinacol boronate |
| BPM | Bipolar membrane |
| BTC | Bistetracyclone |
| BTMA | Benzyltrimethyl ammonium |
| CE | Coulombic efficiency |
| CEM | Cation exchange membrane |
| DABCO | Diazabicyclo[2.2.2] octane |
| DAC | Direct air capture |
| DAPP | Diels–Alder poly(phenylene) |
| DEB | Diethynylbenzene |
| DFT | Density functional theory |
| DIPEA | N,N-Diisopropylethylamine |
| DMAc | Dimethylacetamide |
| DMF | Dimethylformamide |
| DMI | 1,2-Dimethylimidazole |
| DMSO | Dimethyl sulfoxide |
| DMP | Dimethyl piperidinium |
| DMPZ | 1,4-Dimethylpiperazine |
| DOE | Department of Energy |

| | |
|---|---|
| ECSA | Electrochemical surface area |
| ED | Electrodialysis |
| EE | Energy efficiency |
| ETFE | Ethylene tetrafluoroethylene |
| FTIR | Fourier transform infrared |
| GPC | Gel permeation chromatography |
| HER | Hydrogen evolution reaction |
| HFTO | The hydrogen and fuel cell technologies office |
| HMT | Hexamethyl-p-terphenylene |
| HT-PEMFC | High temperature-proton exchange membrane fuel cell |
| IEC | Ion exchange capacity |
| LDPE | Low-density polyethylene |
| LT-PEMFC | Low temperature-proton exchange membrane fuel cell |
| MAN | Methylacrylonitrile |
| MCDI | Membrane capacitive deionization |
| MD | Molecular dynamics |
| MEA | Membrane electrode assembly |
| MIG | Mutual-(simultaneous)-grafting method |
| MMPH | N-Methylmorpholine |
| MPIP | N-Methylpiperidine |
| NMP | N-Methyl-2-pyrrolidone |
| MPY | N-Methylpyrrolidine |
| NMR | Nuclear magnetic resonance |
| OER | Oxygen evolution reaction |
| PBI | Polybenzimidazole |
| PDI | Polydispersity index |
| PE | Polyethylene |
| PEEK | Poly(ether ether ketone) |
| PEM | Proton exchange membrane |
| PES | Poly(ether sulfone) |
| PFSA | Perfluorosulfonic acid |
| PGM | Platinum group metal |
| PIG | Pre-irradiation grafting |
| PIP | Piperidinium |
| PPD | Peak power density |
| PPO | Poly(p-phenylene oxide) |
| PTFE | Polytetrafluoroethylene |
| PVDF | Polyvinylidene fluoride |
| PYR | Pyridine |
| QUN | Quinuclidine |
| RED | Reverse electrodialysis |
| RFB | Redox flow battery |
| RG | Radiation-grafted |
| RH | Relative humidity |
| RO | Reverse osmosis |
| ROD | Radical/oxidative degradation |
| ROMP | Ring opening metathesis polymerization |
| SAXS | Small angle X-ray scattering |
| SBS | Poly(styrene-b-butadiene-b-styrene) |
| SEBS | Poly(styrene-b-(ethylene-co-butylene)-b-styrene) |
| TFA | Trifluoroacetic acid |
| TFSA | Trifluoromethanesulfonic acid |
| TMBG | 2-Butyl-1,1,3,3-tetramethyl-butylguanidine |
| TMBTC | Tetramethylbis(cyclopentadienone) |

This journal is © The Royal Society of Chemistry 2024

Chem. Soc. Rev., 2024, 53, 5704–5780 | 5763

| TMI | 1,2,4,5-Tetramethylimidazole |
| UV | Ultraviolet |
| VBC | Vinylbenzyl chloride |
| VE | Voltage efficiency |

## Conflicts of interest

CB is a founder of Orion Polymer. SH is a scientific advisor to Ionomr Innovations Inc.
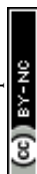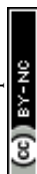
## Acknowledgements

## References

1 S. Al-Amshawee, M. Y. B. Yunus, A. A. M. Azoddein, D. G. Hassell, I. H. Dakhil and H. Abu Hasan, *Chem. Eng. J.*, 2020, **380**, 122231.

2 J. G. Hong, B. P. Zhang, S. Glabman, N. Uzal, X. M. Dou, H. G. Zhang, X. Z. Wei and Y. S. Chen, *J. Membr. Sci.*, 2015, **486**, 71–88.

3 J.-B. Lee, K.-K. Park, H.-M. Eum and C.-W. Lee, *Desalination*, 2006, **196**, 125–134.

4 B. Shrimant, T. Kulkarni, M. Hasan, C. Arnold, N. Khan, A. N. Mondal and C. G. Arges, *ACS Appl. Mater. Interfaces*, 2024, **16**, 11206–11216.

5 S. Gottesfeld, D. R. Dekel, M. Page, C. Bae, Y. S. Yan, P. Zelenay and Y. S. Kim, *J. Power Sources*, 2018, **375**, 170–184.

6 N. Seselj, D. Aili, S. Celenk, L. N. Cleemann, H. A. Hjuler, J. O. Jensen, K. Azizi and Q. F. Li, *Chem. Soc. Rev.*, 2023, **52**, 4046–4070.

7 K. S. Lee, J. S. Spendelow, Y. K. Choe, C. Fujimoto and Y. S. Kim, *Nat. Energy*, 2016, **1**, 16120.

8 K. H. Lim, I. Matanovic, S. Maurya, Y. Kim, E. S. De Castro, J. H. Jang, H. Park and Y. S. Kim, *ACS Energy Lett.*, 2023, **8**, 529–536.

9 K. H. Lim, A. S. Lee, V. Atanasov, J. Kerres, E. J. Park, S. Adhikari, S. Maurya, L. D. Manriquez, J. Jung, C. Fujimoto, I. Matanovic, J. Jankovic, Z. D. Hu, H. F. Jia and Y. S. Kim, *Nat. Energy*, 2022, **7**, 248–259.

10 K. Ayers, N. Danilovic, R. Ouimet, M. Carmo, B. Pivovar and M. Bornstein, *Ann. Rev. Chem. Biomol. Eng.*, 2019, **10**, 219–239.

11 J. Liu, Z. Kang, D. Li, M. Pak, S. M. Alia, C. Fujimoto, G. Bender, Y. S. Kim and A. Z. Weber, *J. Electrochem. Soc.*, 2021, **168**, 054522.

12 L. Zeng, T. S. Zhao, L. Wei, H. R. Jiang and M. C. Wu, *Appl. Energy*, 2019, **233**, 622–643.

13 Q. D. Shu, M. Haug, M. Tedesco, P. Kuntke and H. V. M. Hamelers, *Environ. Sci. Technol.*, 2022, **56**, 11559–11566.

14 P. Zhu, Z.-Y. Wu, A. Elgazzar, C. Dong, T.-U. Wi, F.-Y. Chen, Y. Xia, Y. Feng, M. Shakouri, J. Y. Kim, Z. Fang, T. A. Hatton and H. Wang, *Nature*, 2023, **618**, 959.

15 D. A. Salvatore, C. M. Gabardo, A. Reyes, C. P. O'Brien, S. Holdcroft, P. Pintauro, B. Bahar, M. Hickner, C. Bae, D. Sinton, E. H. Sargent and C. P. Berlinguette, *Nat. Energy*, 2021, **6**, 339–348.

16 S. Z. Oener, L. P. Twight, G. A. Lindquist and S. W. Boettcher, *ACS Energy Lett.*, 2021, **6**, 1–8.

17 L. Chen, Q. Xu, S. Z. Oener, K. Fabrizio and S. W. Boettcher, *Nat. Commun.*, 2022, **13**, 3846.

18 T. Kulkarni, A. M. I. Al Dhamen, D. Bhattacharya and C. G. Arges, *ACS ES&T Eng.*, 2023, **3**, 2171–2182.

19 K. S. Barros, M. C. Martí-Calatayud, V. Pérez-Herranz and D. C. R. Espinosa, *Desalination*, 2020, **492**, 114628.

20 K. Matsui, E. Tobita, K. Sugimoto, K. Kondo, T. Seita and A. Akimoto, *J. Appl. Polym. Sci.*, 1986, **32**, 4137–4143.

21 D. S. Kim, C. H. Fujimoto, M. R. Hibbs, A. Labouriau, Y. K. Choe and Y. S. Kim, *Macromolecules*, 2013, **46**, 7826–7833.

22 A. M. Park, Z. R. Owczarczyk, L. E. Garner, A. C. Yang-Neyerlin, H. Long, C. M. Antunes, M. R. Sturgeon, M. J. Lindell, S. J. Hamrock, M. A. Yandrasits and B. S. Pivovar, *Polym. Electrolyte Fuel Cells 17 (PEFC 17)*, 2017, **80**, 957–966.

23 M. S. J. Jung, C. G. Arges and V. Ramani, *J. Mater. Chem.*, 2011, **21**, 6158–6160.

5764 | *Chem. Soc. Rev.*, 2024, **53**, 5704–5780
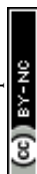
This journal is © The Royal Society of Chemistry 2024

24 M. A. Vandiver, J. L. Horan, Y. Yang, E. T. Tansey, S. Seifert, M. W. Liberatore and A. M. Herring, *J. Polym. Sci., Part B: Polym. Phys.*, 2013, **51**, 1761–1769.

25 D. M. Hillman, S. H. Stephens, S. D. Poynton, S. Murphy, A. L. Ong and J. R. Varcoe, *J. Mater. Chem. A*, 2013, **1**, 1018–1021.

26 A. Bosnjakovic, M. Danilczuk, S. Schlick, P. N. Xiong, G. M. Haugen and S. J. Hamrock, *J. Membr. Sci.*, 2014, **467**, 136–141.

27 M. F. Rabuni, N. M. N. Sulaiman, M. K. Aroua and N. A. Hashim, *Ind. Eng. Chem. Res.*, 2013, **52**, 15874–15882.

28 N. A. Hashim, Y. T. Liu and K. Li, *Chem. Eng. Sci.*, 2011, **66**, 1565–1575.

29 A. G. Divekar, M. R. Gerhardt, C. M. Antunes, L. Osmieri, A. C. Yang-Neyerlin, A. Z. Weber, B. S. Pivovar, G. Bender and A. M. Herring, *Electrochim. Acta*, 2022, **406**, 139812.

30 P. Zschocke and D. Quellmalz, *J. Membr. Sci.*, 1985, **22**, 325–332.

31 E. Avram, M. A. Brebu, A. Warshawasky and C. Vasile, *Polym. Degrad. Stab.*, 2000, **69**, 175–181.

32 J. L. Yan and M. A. Hickner, *Macromolecules*, 2010, **43**, 2349–2356.

33 Z. Zhao, J. H. Wang, S. H. Li and S. B. Zhang, *J. Power Sources*, 2011, **196**, 4445–4450.

34 N. W. Li, T. Z. Yan, Z. Li, T. Thurn-Albrecht and W. H. Binder, *Energy Environ. Sci.*, 2012, **5**, 7888–7892.

35 C. G. Arges, L. H. Wang, M. S. Jung and V. Ramani, *J. Electrochem. Soc.*, 2015, **162**, F686–F693.

36 J. L. Yan, L. Zhu, B. L. Chaloux and M. A. Hickner, *Polym. Chem.*, 2017, **8**, 2442–2449.

37 J.-S. Park, S.-H. Park, S.-D. Yim, Y.-G. Yoon, W.-Y. Lee and C.-S. Kim, *J. Power Sources*, 2008, **178**, 620–626.

38 M. Tanaka, K. Fukasawa, E. Nishino, S. Yamaguchi, K. Yamada, H. Tanaka, B. Bae, K. Miyatake and M. Watanabe, *J. Am. Chem. Soc.*, 2011, **133**, 10646–10654.

39 G. Wang, Y. Weng, D. Chu, R. Chen and D. Xie, *J. Membr. Sci.*, 2009, **332**, 63–68.

40 J. Wang, S. Li and S. Zhang, *Macromolecules*, 2010, **43**, 3890–3896.

41 J. Zhou, M. Unlu, J. A. Vega and P. A. Kohl, *J. Power Sources*, 2009, **190**, 285–292.

42 C. X. Lin, Y. Z. Zhuo, A. N. Lai, Q. G. Zhang, A. M. Zhu, M. L. Ye and Q. L. Liu, *J. Membr. Sci.*, 2016, **513**, 206–216.

43 X. Lin, L. Wu, Y. Liu, A. L. Ong, S. D. Poynton, J. R. Varcoe and T. Xu, *J. Power Sources*, 2012, **217**, 373–380.

44 T. W. Xu and W. H. Yang, *J. Membr. Sci.*, 2001, **190**, 159–166.

45 L. Zhu, J. Pan, C. M. Christensen, B. Lin and M. A. Hickner, *Macromolecules*, 2016, **49**, 3300–3309.

46 N. Li, Q. Zhang, C. Y. Wang, Y. M. Lee and M. D. Guiver, *Macromolecules*, 2012, **45**, 2411–2419.

47 B. Bauer, H. Strathmann and F. Effenberger, *Desalination*, 1990, **79**, 125–144.

48 J. Xue, J. Zhang, X. Liu, T. Huang, H. Jiang, Y. Yin, Y. Qin and M. D. Guiver, *Electrochem. Energy Rev.*, 2022, **5**, 348–400.

49 S. Chempath, B. R. Einsla, L. R. Pratt, C. S. Macomber, J. M. Boncella, J. A. Rau and B. S. Pivovar, *J. Phys. Chem. C*, 2008, **112**, 3179–3182.

50 Y. Ye and Y. A. Elabd, *Macromolecules*, 2011, **44**, 8494–8503.

51 B. Lin, H. Dong, Y. Li, Z. Si, F. Gu and F. Yan, *Chem. Mater.*, 2013, **25**, 1858–1867.

52 A. A. Zagorodni, D. L. Kotova and V. F. Selemenev, *React. Funct. Polym.*, 2002, **53**, 157–171.

53 J. Hnat, M. Paidar, J. Schauer, J. Zitka and K. Bouzek, *J. Appl. Electrochem.*, 2011, **41**, 1043–1052.

54 G. Cerichelli, G. Illuminati and C. Lillocci, *J. Org. Chem.*, 1980, **45**, 3952–3957.

55 G. Cospito, G. Illuminati, C. Lillocci and H. Petride, *J. Org. Chem.*, 1981, **46**, 2944–2947.

56 G. Illuminati and C. Lillocci, *J. Org. Chem.*, 1977, **42**, 2201–2203.

57 M. G. Marino and K. D. Kreuer, *ChemSusChem*, 2015, **8**, 513–523.

58 A. D. Mohanty and C. Bae, *J. Mater. Chem. A*, 2014, **2**, 17314–17320.

59 W. You, K. M. Hugar, R. C. Selhorst, M. Treichel, C. R. Peltier, K. J. T. Noonan and G. W. Coates, *J. Org. Chem.*, 2021, **86**, 254–263.

60 K. Y. Zhang, W. S. Yu, X. L. Ge, L. Wu and T. W. Xu, *J. Membr. Sci.*, 2023, **678**, 121672.

61 O. I. Deavin, S. Murphy, A. L. Ong, S. D. Poynton, R. Zeng, H. Herman and J. R. Varcoe, *Energy Environ. Sci.*, 2012, **5**, 8584–8597.

62 S. A. Nunez and M. A. Hickner, *ACS Macro Lett.*, 2013, **2**, 49–52.

63 M. R. Sturgeon, C. S. Macomber, C. Engtrakul, H. Long and B. S. Pivovar, *J. Electrochem. Soc.*, 2015, **162**, F366–F372.

64 K. J. T. Noonan, K. M. Hugar, H. A. Kostalik, E. B. Lobkovsky, H. D. Abruña and G. W. Coates, *J. Am. Chem. Soc.*, 2012, **134**, 18161–18164.

65 B. R. Einsla, S. Chempath, L. R. Pratt, J. M. Boncella, J. A. Rau, C. S. Macomber and B. Pivovar, *ECS Trans.*, 2007, **11**, 1173–1180.

66 J. S. Olsson, T. H. Pham and P. Jannasch, *Adv. Funct. Mater.*, 2018, **28**, 1702758.

67 H.-S. Dang and P. Jannasch, *ACS Appl. Energy Mater.*, 2018, **1**, 2222–2231.

68 A. Allushi, P. Thanh Huong, J. S. Olsson and P. Jannasch, *J. Mater. Chem. A*, 2019, **7**, 27164–27174.

69 A. Allushi, T. H. Pham and P. Jannasch, *J. Membr. Sci.*, 2021, **632**, 119376.

70 D. Pan, P. Thanh Huong and P. Jannasch, *ACS Appl. Energy Mater.*, 2021, **4**, 11652–11665.

71 D. Pan, P. M. Bakvand, T. H. Pham and P. Jannasch, *J. Mater. Chem. A*, 2022, **10**, 16478–16489.

72 Y. Yang, C. R. Peltier, R. Zeng, R. Schimmenti, Q. Li, X. Huang, Z. Yan, G. Potsi, R. Selhorst, X. Lu, W. Xu, M. Tader, A. V. Soudackov, H. Zhang, M. Krumov, E. Murray, P. Xu, J. Hitt, L. Xu, H.-Y. Ko, B. G. Ernst, C. Bundschu, A. Luo, D. Markovich, M. Hu, C. He, H. Wang, J. Fang, R. A. DiStasio, Jr., L. F. Kourkoutis,

This journal is © The Royal Society of Chemistry 2024

*Chem. Soc. Rev.*, 2024, **53**, 5704–5780 | **5765**

A. Singer, K. J. T. Noonan, L. Xiao, L. Zhuang, B. S. Pivovar, P. Zelenay, E. Herrero, J. M. Feliu, J. Suntivich, E. P. Giannelis, S. Hammes-Schiffer, T. Arias, M. Mavrikakis, T. E. Mallouk, J. D. Brock, D. A. Muller, F. J. DiSalvo, G. W. Coates and H. D. Abruña, *Chem. Rev.*, 2022, **122**, 6117–6321.

73 B. Soresi, E. Quartarone, P. Mustarelli, A. Magistris and G. Chiodelli, *Solid State Ionics*, 2004, **166**, 383–389.

74 H. Su, S. Pasupathi, B. Bladergroen, V. Linkov and B. G. Pollet, *Int. J. Hydrogen Energy*, 2013, **38**, 11370–11378.

75 G. J. Ross, J. F. Watts, M. P. Hill and P. Morrissey, *Polymer*, 2000, **41**, 1685–1696.

76 J. Sharma, C. Totee, V. Kulshrestha and B. Ameduri, *Eur. Polym. J.*, 2023, **201**, 112580.

77 G. Merle, M. Wessling and K. Nijmeijer, *J. Membr. Sci.*, 2011, **377**, 1–35.

78 B. C. Lin, L. H. Qiu, J. M. Lu and F. Yan, *Chem. Mater.*, 2010, **22**, 6718–6725.

79 M. L. Guo, J. Fang, H. K. Xu, W. Li, X. H. Lu, C. H. Lan and K. Y. Li, *J. Membr. Sci.*, 2010, **362**, 97–104.

80 F. X. Zhang, H. M. Zhang and C. Qu, *J. Mater. Chem.*, 2011, **21**, 12744–12752.

81 J. R. Varcoe, R. C. T. Slade and E. Lam How Yee, *Chem. Commun.*, 2006, 1428–1429.

82 K. Fukuta, presented in part at the 2011 AMFC Workshop, 2011.

83 Y. S. Li and T. S. Zhao, *Int. J. Hydrogen Energy*, 2012, **37**, 4413–4421.

84 Y. Zhao, H. M. Yu, D. L. Yang, J. Li, Z. G. Shao and B. L. Yi, *J. Power Sources*, 2013, **221**, 247–251.

85 C. Fujimoto, D. S. Kim, M. Hibbs, D. Wrobleski and Y. S. Kim, *J. Membr. Sci.*, 2012, **423**, 438–449.

86 C. G. Arges and V. Ramani, *Proc. Natl. Acad. Sci. U. S. A.*, 2013, **110**, 2490–2495.

87 Y. K. Choe, C. Fujimoto, K. S. Lee, L. T. Dalton, K. Ayers, N. J. Henson and Y. S. Kim, *Chem. Mater.*, 2014, **26**, 5675–5682.

88 A. D. Mohanty, S. E. Tignor, J. A. Krause, Y. K. Choe and C. Bae, *Macromolecules*, 2016, **49**, 3361–3372.

89 A. Amel, L. Zhu, M. Hickner and Y. Ein-Eli, *J. Electrochem. Soc.*, 2014, **161**, F615–F621.

90 A. Marinkas, I. Struzynska-Piron, Y. Lee, A. Lim, H. S. Park, J. H. Jang, H. J. Kim, J. Kim, A. Maljusch, O. Conradi and D. Henkensmeier, *Polymer*, 2018, **145**, 242–251.

91 J. J. Han, W. F. Song, X. Q. Cheng, Q. Cheng, Y. Y. Zhang, C. F. Liu, X. R. Zhou, Z. D. Ren, M. X. Hu, T. S. Ning, L. Xiao and L. Zhuang, *ChemSusChem*, 2021, **14**, 5021–5031.

92 C. G. Arges, L. Wang, J. Parrondo and V. Ramani, *J. Electrochem. Soc.*, 2013, **160**, F1258.

93 R. A. Becerra-Arciniegas, R. Narducci, G. Ercolani, S. Antonaroli, E. Sgreccia, L. Pasquini, P. Knauth and M. L. Di Vona, *Polymer*, 2019, **185**, 121931.

94 T. Mohammadi and M. Skyllas-Kazacos, *J. Appl. Electrochem.*, 1997, **27**, 153–160.

95 Y. Ahn and D. Kim, *J. Ind. Eng. Chem.*, 2019, **71**, 361–368.

96 G. Shukla and V. K. Shahi, *J. Membr. Sci.*, 2019, **575**, 109–117.

97 Z. Wang, S. Zhang, Q. Liu, Y. Chen, Z. Weng and X. Jian, *J. Membr. Sci.*, 2021, **633**, 119416.

98 E. J. Park, S. Maurya, U. Martinez, Y. S. Kim and R. Mukundan, *J. Membr. Sci.*, 2021, **617**, 118565.

99 X. Hao, Z. Zhou, Y. Chen, L. Xiong and D. Chen, *Mater. Chem. Phys.*, 2022, **277**, 125490.

100 Z. Wang, S. Zhang, Q. Liu, L. Zhuo, Z. Liu, P. Xu, D. Wang, Z. Weng and X. Jian, *J. Membr. Sci.*, 2022, **656**, 120646.

101 B. Zhang, X. Zhang, Q. Liu, M. Zhao, Z. Yang, Y. Fu, E. Zhang, K. Wang, G. Wang, Z. Zhang and S. Zhang, *J. Power Sources*, 2022, **548**, 232095.

102 Y. Chen, Y. Li, J. Xu, S. Chen and D. Chen, *ACS Appl. Mater. Interfaces*, 2021, **13**, 18923–18933.

103 J. Qian, S. Cai, J. Hu, C. Wang and G. Li, *Ind. Eng. Chem. Res.*, 2023, **62**, 2719–2728.

104 Y. Xing, L. Liu, C. Y. Wang and N. W. Li, *J. Mater. Chem. A*, 2018, **6**, 22778–22789.

105 X. Hao, N. Chen, Y. Chen and D. Chen, *Polym. Degrad. Stab.*, 2022, **197**, 109864.

106 D. Y. Chen and M. A. Hickner, *Phys. Chem. Chem. Phys.*, 2013, **15**, 11299–11305.

107 S. Olivella, A. Sole and J. M. Bofill, *J. Chem. Theory Comput.*, 2009, **5**, 1607–1623.

108 H. Tang, K. Geng, J. Hao, X. Zhang, Z. Shao and N. Li, *J. Power Sources*, 2020, **475**, 228521.

109 A. Laconti, H. Liu, C. Mittelsteadt and R. McDonald, *ECS Trans.*, 2006, **1**, 199.

110 S. Wierzbicki, J. C. Douglin, A. Kostuch, D. R. Dekel and K. Kruczala, *J. Phys. Chem. Lett.*, 2020, **11**, 7630–7636.

111 J. Parrondo, Z. Wang, M.-S. J. Jung and V. Ramani, *Phys. Chem. Chem. Phys.*, 2016, **18**, 19705–19712.

112 Y. Z. Zhang, J. Parrondo, S. Sankarasubramanian and V. Ramani, *ChemSusChem*, 2017, **10**, 3056–3062.

113 T. Nemeth, T. Nauser and L. Gubler, *ChemSusChem*, 2022, **15**, e20221571.

114 R. Espiritu, B. T. Golding, K. Scott and M. Mamlouk, *J. Mater. Chem. A*, 2017, **5**, 1248–1267.

115 R. Espiritu, B. T. Golding, K. Scott and M. Mamlouk, *J. Power Sources*, 2018, **375**, 373–386.

116 T. Holmes, T. J. G. Skalski, M. Adamski and S. Holdcroft, *Chem. Mater.*, 2019, **31**, 1441–1449.

117 F. De Vleeschouwer, V. Van Speybroeck, M. Waroquier, P. Geerlings and F. De Proft, *Org. Lett.*, 2007, **9**, 2721–2724.

118 L. Balducci, D. Bianchi, R. Bortolo, R. D'Aloisio, M. Ricci, R. Tassinari and R. Ungarelli, *Angew. Chem., Int. Ed.*, 2003, **42**, 4937–4940.

119 J. H. Yang, G. Sun, Y. J. Gao, H. B. Zhao, P. Tang, J. Tan, A. H. Lu and D. Ma, *Energy Environ. Sci.*, 2013, **6**, 793–798.

120 G. Ding, W. Wang, T. Jiang, B. Han, H. Fan and G. Yang, *ChemCatChem*, 2013, **5**, 192–200.

121 D. H. Deng, X. Q. Chen, L. Yu, X. Wu, Q. F. Liu, Y. Liu, H. X. Yang, H. F. Tian, Y. F. Hu, P. P. Du, R. Si, J. H. Wang, X. J. Cui, H. B. Li, J. P. Xiao, T. Xu, J. Deng, F. Yang,
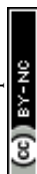
5766 | *Chem. Soc. Rev.*, 2024, **53**, 5704–5780

This journal is © The Royal Society of Chemistry 2024

P. N. Duchesne, P. Zhang, J. G. Zhou, L. T. Sun, J. Q. Li, X. L. Pan and X. H. Bao, *Sci. Adv.*, 2015, **1**, e150046.

122 D. G. Li, I. Matanovic, A. S. Lee, E. J. Park, C. Fujimoto, H. T. Chung and Y. S. Kim, *ACS Appl. Mater. Interfaces*, 2019, **11**, 9696–9701.

123 S. Maurya, A. S. Lee, D. G. Li, E. J. Park, D. P. Leonard, S. Noh, C. Bae and Y. S. Kim, *J. Power Sources*, 2019, **436**, 226866.

124 C. Chen, F. Chen, L. Zhang, S. Pan, C. Bian, X. Zheng, X. Meng and F.-S. Xiao, *Chem. Commun.*, 2015, **51**, 5936–5938.

125 R. Peng, S. Li, X. Sun, Q. Ren, L. Chen, M. Fu, J. Wu and D. Ye, *Appl. Catal., B*, 2018, **220**, 462–470.

126 C.-S. Chen, T.-C. Chen, H.-C. Wu, P.-H. Huang and H.-M. Kao, *J. Catal.*, 2021, **402**, 275–288.

127 R. A. Krivina, G. A. Lindquist, M. C. Yang, A. K. Cook, C. H. Hendon, A. R. Motz, C. Capuano, K. E. Ayers, J. E. Hutchison and S. W. Boettcher, *ACS Appl. Mater. Interfaces*, 2022, **14**, 18261–18274.

128 J. Parrondo and V. Ramani, *J. Electrochem. Soc.*, 2014, **161**, F1015–F1020.

129 J. Nikl, K. Hofman, S. Mossazghi, I. C. Möller, D. Mondeshki, F. Weinelt, F.-E. Baumann and S. R. Waldvogel, *Nat. Commun.*, 2023, **14**, 4565.

130 I. G. Irtegova, V. F. Starichenko, I. A. Kirilyuk and I. A. Grigor″ev, *Russ. Chem. Bull.*, 2002, **51**, 2065–2069.

131 Y. Kawamata, M. Yan, Z. Liu, D.-H. Bao, J. Chen, J. T. Starr and P. S. Baran, *J. Am. Chem. Soc.*, 2017, **139**, 7448–7451.

132 L. Xue, W. Hu, C. Feng, N. Chen, H. Chen and Z. Hu, *Desalination Water Treatment*, 2020, **188**, 212–222.

133 S. Maurya, C. H. Fujimoto, M. R. Hibbs, C. N. Villarrubia and Y. S. Kim, *Chem. Mater.*, 2018, **30**, 2188–2192.

134 I. Matanovic, S. Maurya, E. J. Park, J. Y. Jeon, C. Bae and Y. S. Kim, *Chem. Mater.*, 2019, **31**, 4195–4204.

135 I. Matanovic, H. T. Chung and Y. S. Kim, *J. Phys. Chem. Lett.*, 2017, **8**, 4918–4924.

136 Y. Y. Zhao, E. Tsuchida, Y. K. Choe, J. Wang, T. Ikeshoji and A. Ohira, *J. Membr. Sci.*, 2015, **487**, 229–239.

137 S. Maurya, E. Baca, K. K. Bejagam, H. Pratt, T. Anderson, R. Mukundan and C. Fujimoto, *J. Power Sources*, 2022, **520**, 230805.

138 Y. S. Kim, *Adv. Sci.*, 2023, **10**, 2303914.

139 H. T. Chung, U. Martinez, I. Matanovic and Y. S. Kim, *J. Phys. Chem. Lett.*, 2016, **7**, 4464–4469.

140 G. A. Lindquist, J. C. Gaitor, W. L. Thompson, V. Brogden, K. J. T. Noonan and S. W. Boettcher, *Energy Environ. Sci.*, 2023, **16**, 4373–4387.

141 T. Luo, O. David, Y. Gendel and M. Wessling, *J. Power Sources*, 2016, **312**, 45–54.

142 R. Ye, D. Henkensmeier, S. J. Yoon, Z. Huang, D. K. Kim, Z. Chang, S. Kim and R. Chen, *J. Electrochem. Energy Conversion Storage*, 2018, **15**, 010801.

143 X. L. Zhou, T. S. Zhao, L. An, L. Wei and C. Zhang, *Electrochim. Acta*, 2015, **153**, 492–498.

144 S. Maurya, S. D. Abad, E. J. Park, K. Ramaiyan, Y. S. Kim, B. L. Davis and R. Mukundan, *J. Membr. Sci.*, 2023, **668**, 121233.

145 S. H. Eberhardt, T. Lochner, F. N. Buechi and T. J. Schmidt, *J. Electrochem. Soc.*, 2015, **162**, F1367–F1372.

146 A. T. Pingitore, F. Huang, G. Qian and B. C. Benicewicz, *ACS Appl. Energy Mater.*, 2019, **2**, 1720–1726.

147 D. Aili, D. Henkensmeier, S. Martin, B. Singh, Y. Hu, J. O. Jensen, L. N. Cleemann and Q. Li, *Electrochem. Energy Rev.*, 2020, **3**, 793–845.

148 K. Likit-anurak, I. Karki, B. I. Howard, L. Murdock, N. Mukhin, J. Brannon, A. Hepstall, B. Young, S. Shimpalee, B. Benicewicz and B. Meekins, *ACS Appl. Energy Mater.*, 2023, **6**, 5429–5434.

149 B. Hu, Y. Huang, L. Liu, X. Hu, K. Geng, Q. Ju, M. Liu, J. Bi, S. Luo and N. Li, *J. Membr. Sci.*, 2022, **643**, 120042.

150 M. R. Kraglund, M. Carmo, G. Schiller, S. A. Ansar, D. Aili, E. Christensen and J. O. Jensen, *Energy Environ. Sci.*, 2019, **12**, 3313–3318.

151 M. L. A. Trisno, A. Dayan, S. J. Lee, F. Egert, M. Gerle, M. R. Kraglund, J. O. Jensen, D. Aili, A. Roznowska, A. Michalak, H. S. Park, F. Razmjooei, S.-A. Ansar and D. Henkensmeier, *Energy Environ. Sci.*, 2022, **15**, 4362–4375.

152 E. J. Park and Y. S. Kim, *J. Mater. Chem. A*, 2018, **6**, 15456–15477.

153 G. A. Olah, *Angew. Chem., Int. Ed. Engl.*, 1993, **32**, 767–788.

154 G. A. Olah, G. Rasul, C. York and G. K. S. Prakash, *J. Am. Chem. Soc.*, 1995, **117**, 11211–11214.

155 O. Hernández-Cruz, M. G. Zolotukhin, S. Fomine, L. Alexandrova, C. Aguilar-Lugo, F. A. Ruiz-Treviño, G. Ramos-Ortíz, J. L. Maldonado and G. Cadenas-Pliego, *Macromolecules*, 2015, **48**, 1026–1037.

156 M. Zolotukhin, S. Fomine, R. Salcedo and L. Khalilov, *Chem. Commun.*, 2004, 1030–1031.

157 M. T. Guzmán-Gutiérrez, M. H. Rios-Dominguez, F. A. Ruiz-Treviño, M. G. Zolotukhin, J. Balmaseda, D. Fritsch and E. Prokhorov, *J. Membr. Sci.*, 2011, **385–386**, 277–284.

158 A. R. Cruz, M. C. G. Hernandez, M. T. Guzmán-Gutiérrez, M. G. Zolotukhin, S. Fomine, S. L. Morales, H. Kricheldorf, E. S. Wilks, J. Cárdenas and M. Salmón, *Macromolecules*, 2012, **45**, 6774–6780.

159 L. I. Olvera, M. T. Guzmán-Gutiérrez, M. G. Zolotukhin, S. Fomine, J. Cárdenas, F. A. Ruiz-Trevino, D. Villers, T. A. Ezquerra and E. Prokhorov, *Macromolecules*, 2013, **46**, 7245–7256.

160 M. T. Guzmán-Gutiérrez, D. R. Nieto, S. Fomine, S. L. Morales, M. G. Zolotukhin, M. C. G. Hernandez, H. Kricheldorf and E. S. Wilks, *Macromolecules*, 2011, **44**, 194–202.

161 W.-H. Lee, Y. S. Kim and C. Bae, *ACS Macro Lett.*, 2015, **4**, 814–818.

162 W.-H. Lee, A. D. Mohanty and C. Bae, *ACS Macro Lett.*, 2015, **4**, 453–457.

163 W.-H. Lee, E. J. Park, J. Han, D. W. Shin, Y. S. Kim and C. Bae, *ACS Macro Lett.*, 2017, **6**, 566–570.

This journal is © The Royal Society of Chemistry 2024
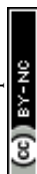
*Chem. Soc. Rev.*, 2024, **53**, 5704–5780 | **5767**

164 S. Maurya, S. Noh, I. Matanovic, E. J. Park, C. Narvaez Villarrubia, U. Martinez, J. Han, C. Bae and Y. S. Kim, *Energy Environ. Sci.*, 2018, **11**, 3283–3291.

165 E. J. Park, S. Maurya, A. S. Lee, D. P. Leonard, D. Li, J. Y. Jeon, C. Bae and Y. S. Kim, *J. Mater. Chem. A*, 2019, **7**, 25040–25046.

166 J. Wang, Y. Zhao, B. P. Setzler, S. Rojas-Carbonell, C. Ben Yehuda, A. Amel, M. Page, L. Wang, K. Hu, L. Shi, S. Gottesfeld, B. Xu and Y. Yan, *Nat. Energy*, 2019, **4**, 392–398.

167 R. Ren, S. Zhang, H. A. Miller, F. Vizza, J. R. Varcoe and Q. He, *J. Membr. Sci.*, 2019, **591**, 117320.

168 M. S. Cha, J. E. Park, S. Kim, S.-H. Han, S.-H. Shin, S. H. Yang, T.-H. Kim, D. M. Yu, S. So, Y. T. Hong, S. J. Yoon, S.-G. Oh, S. Y. Kang, O.-H. Kim, H. S. Park, B. Bae, Y.-E. Sung, Y.-H. Cho and J. Y. Lee, *Energy Environ. Sci.*, 2020, **13**, 3633–3645.

169 T. H. Pham, A. Allushi, J. S. Olsson and P. Jannasch, *Polym. Chem.*, 2020, **11**, 6953–6963.

170 N. Chen, H. H. Wang, S. P. Kim, H. M. Kim, W. H. Lee, C. Hu, J. Y. Bae, E. S. Sim, Y.-C. Chung, J.-H. Jang, S. J. Yoo, Y. Zhuang and Y. M. Lee, *Nat. Commun.*, 2021, **12**, 2367.

171 N. Chen, C. Hu, H. H. Wang, S. P. Kim, H. M. Kim, W. H. Lee, J. Y. Bae, J. H. Park and Y. M. Lee, *Angew. Chem., Int. Ed.*, 2021, **60**, 7710–7718.

172 B. Xue, W. Cui, S. Zhou, Q. Zhang, J. Zheng, S. Li and S. Zhang, *Macromolecules*, 2021, **54**, 2202–2212.

173 S. Adhikari, D. P. Leonard, K. H. Lim, E. J. Park, C. Fujimoto, O. Morales-Collazo, J. F. Brennecke, Z. Hu, H. Jia and Y. S. Kim, *ACS Appl. Energy Mater.*, 2022, **5**, 2663–2668.

174 D. Pan, J. S. Olsson and P. Jannasch, *ACS Appl. Energy Mater.*, 2022, **5**, 981–991.

175 A. Mohamed Ahmed Mahmoud and K. Miyatake, *ACS Appl. Polym. Mater.*, 2023, **5**, 2243–2253.

176 S. Adhikari, I. Matanovic, D. Leonard, J. M. Klein, T. Agarwal and Y. S. Kim, *ACS Macro Lett.*, 2023, **13**, 28–33.

177 M. G. Zolotukhin, S. Fomine, L. M. Lazo, R. Salcedo, L. E. Sansores, G. G. Cedillo, H. M. Colquhoun, J. M. Fernandez-G and A. F. Khalizov, *Macromolecules*, 2005, **38**, 6005–6014.

178 E. J. Park, C. B. Capuano, K. E. Ayers and C. Bae, *J. Power Sources*, 2018, **375**, 367–372.

179 D. P. Leonard, S. Maurya, E. J. Park, L. Delfin Manriquez, S. Noh, X. Wang, C. Bae, E. D. Baca, C. Fujimoto and Y. S. Kim, *J. Mater. Chem. A*, 2020, **8**, 14135–14144.

180 T. Wang, J. Dong, N. Yu, W. Tang, Y. Jin, Y. Xu and J. Yang, *Eur. Polym. J.*, 2022, **173**, 111271.

181 L. I. Olvera, M. G. Zolotukhin, O. Hernández-Cruz, S. Fomine, J. Cárdenas, R. L. Gaviño-Ramírez and F. A. Ruiz-Trevino, *ACS Macro Lett.*, 2015, **4**, 492–494.

182 D. Pan, S. Chen and P. Jannasch, *ACS Macro Lett.*, 2023, **12**, 20–25.

183 Q. Wang, L. Huang, Z. Wang, J. Zheng, Q. Zhang, G. Qin, S. Li and S. Zhang, *Macromolecules*, 2022, **55**, 10713–10722.

184 X. Wu, N. Chen, H.-A. Klok, Y. M. Lee and X. Hu, *Angew. Chem., Int. Ed.*, 2022, **61**, e202114892.

185 B. Liu, T. Li, Q. Li, S. Zhu, Y. Duan, J. Li, H. Zhang and C. Zhao, *J. Membr. Sci.*, 2022, **660**, 120816.

186 W. Yuan, L. Zeng, T. Zhang, Y. Zhou, J. Wang, S. Jiang, L. Li, Q. Liao and Z. Wei, *Adv. Funct. Mater.*, 2023, **33**, 2307041.

187 M. Jayakannan and S. Ramakrishnan, *Macromol. Rapid Commun.*, 2001, **22**, 1463–1473.

188 H. Ono, J. Miyake, S. Shimada, M. Uchida and K. Miyatake, *J. Mater. Chem. A*, 2015, **3**, 21779–21788.

189 A. G. Wright, T. Weissbach and S. Holdcroft, *Angew. Chem., Int. Ed.*, 2016, **55**, 4818–4821.

190 A. M. A. Mahmoud, A. M. M. Elsaghier, K. Otsuji and K. Miyatake, *Macromolecules*, 2017, **50**, 4256–4266.

191 M. Ozawa, T. Kimura, R. Akiyama, J. Miyake, J. Inukai and K. Miyatake, *Bull. Chem. Soc. Jpn.*, 2017, **90**, 1088–1094.

192 H. Ono, T. Kimura, A. Takano, K. Asazawa, J. Miyake, J. Inukai and K. Miyatake, *J. Mater. Chem. A*, 2017, **5**, 24804–24812.

193 A. M. Ahmed Mahmoud and K. Miyatake, *J. Mater. Chem. A*, 2018, **6**, 14400–14409.

194 M. Ozawa, T. Kimura, K. Otsuji, R. Akiyama, J. Miyake, M. Uchida, J. Inukai and K. Miyatake, *ACS Omega*, 2018, **3**, 16143–16149.

195 D. Koronka, A. M. A. Mahmoud and K. Miyatake, *J. Polym. Sci., Part A: Polym. Chem.*, 2019, **57**, 1059–1069.

196 D. Koronka, A. Matsumoto, K. Otsuji and K. Miyatake, *RSC Adv.*, 2019, **9**, 37391–37402.

197 T. Kimura, A. Matsumoto, J. Inukai and K. Miyatake, *ACS Appl. Energy Mater.*, 2020, **3**, 469–477.

198 D. Koronka and K. Miyatake, *RSC Adv.*, 2021, **11**, 1030–1038.

199 A. M. Ahmed Mahmoud and K. Miyatake, *J. Membr. Sci.*, 2022, **643**, 120072.

200 Y. Shirase, A. Matsumoto, K. L. Lim, D. A. Tryk, K. Miyatake and J. Inukai, *ACS Omega*, 2022, **7**, 13577–13587.

201 Y. Ozawa, Y. Shirase, K. Otsuji and K. Miyatake, *Mole. Syst. Des. Eng.*, 2022, **7**, 798–808.

202 A. M. Ahmed Mahmoud and K. Miyatake, *ACS Appl. Energy Mater.*, 2022, **5**, 15211–15221.

203 Y. Ozawa and K. Miyatake, *Bull. Chem. Soc. Jpn.*, 2023, **96**, 16–23.

204 T. Yamamoto, S. Wakabayashi and K. Osakada, *J. Organomet. Chem.*, 1992, **428**, 223–237.

205 A. F. Nugraha, S. Kim, F. Wijaya, B. Bae and D. Shin, *Polymers*, 2020, **12**, 1614.

206 A. Jasti, S. Prakash and V. K. Shahi, *J. Membr. Sci.*, 2013, **428**, 470–479.

207 I. Hosaka, M. Kusakabe and K. Miyatake, *Chem. Lett.*, 2018, **47**, 257–259.

208 F. Xu, Y. Chen, B. Lin, J. Li, K. Qiu and J. Ding, *ACS Macro Lett.*, 2021, **10**, 1180–1185.

209 H. Lim, I. Jeong, J. Choi, G. Shin, J. Kim, T.-H. Kim and T. Park, *Appl. Surf. Sci.*, 2023, **610**, 155601.

5768 | *Chem. Soc. Rev.*, 2024, **53**, 5704–5780

This journal is © The Royal Society of Chemistry 2024

210 C. Gibbs, E. Littmann and C. Marvel, *J. Am. Chem. Soc.*, 1933, **55**, 753–757.

211 A. Rembaum, W. Baumgartner and A. Eisenberg, *J. Polym. Sci., Part B: Polym. Lett.*, 1968, **6**, 159–171.

212 J. C. Salamone and B. Snider, *J. Polym. Sci., Part A-1: Polym. Chem.*, 1970, **8**, 3495–3501.

213 S. R. Williams and T. E. Long, *Prog. Polym. Sci.*, 2009, **34**, 762–782.

214 J. E. Bara and K. E. O'Harra, *Macromol. Chem. Phys.*, 2019, **220**, 1900078.

215 W. You, K. J. T. Noonan and G. W. Coates, *Prog. Polym. Sci.*, 2020, **100**, 101177.

216 K. E. O'Harra and J. E. Bara, *Polym. Int.*, 2021, **70**, 944–950.

217 J. S. Lee, A. Hocken and M. D. Green, *Mol. Syst. Des. Eng.*, 2021, **6**, 334–354.

218 T. H. Pham, J. S. Olsson and P. Jannasch, *J. Am. Chem. Soc.*, 2017, **139**, 2888–2891.

219 X. Qiao, X. Wang, S. Liu, Y. Shen and N. Li, *J. Membr. Sci.*, 2021, **630**, 119325.

220 A. Das, B. Sana, R. Bhattacharyya, P. Chandra Ghosh and T. Jana, *ACS Appl. Polym. Mater.*, 2022, **4**, 1523–1534.

221 J. Dong, N. Yu, X. Che, R. Liu, D. Aili and J. Yang, *Polym. Chem.*, 2020, **11**, 6037–6046.

222 N. Yu, J. Dong, T. Wang, Y. Jin, W. Tang and J. Yang, *Polymer*, 2022, **240**, 124491.

223 I. Strużyńska-Piron, M. Jung, A. Maljusch, O. Conradi, S. Kim, J. H. Jang, H.-J. Kim, Y. Kwon, S. W. Nam and D. Henkensmeier, *Eur. Polym. J.*, 2017, **96**, 383–392.

224 K. M. Lee, R. Wycisk, M. Litt and P. N. Pintauro, *J. Membr. Sci.*, 2011, **383**, 254–261.

225 F. H. Liu, Q. Yang, X. L. Gao, H. Y. Wu, Q. G. Zhang, A. M. Zhu and Q. L. Liu, *J. Membr. Sci.*, 2020, **595**, 117560.

226 S. T. Hemp, M. Zhang, M. Tamami and T. E. Long, *Polym. Chem.*, 2013, **4**, 3582–3590.

227 N. Chen, Y. Jin, H. Liu, C. Hu, B. Wu, S. Xu, H. Li, J. Fan and Y. M. Lee, *Angew. Chem., Int. Ed.*, 2021, **60**, 19272–19280.

228 K. Müllen, J. Lex, R. C. Schulz and F. Walter, *Polym. Bull.*, 1990, **24**, 263–269.

229 G. Zhang, R. Li, X. Wang, X. Chen, Y. Shen and Y. Fu, *Sep. Purif. Technol.*, 2022, **291**, 120950.

230 X. Chen, R. Li, G. Zhang, Y. Sun, Q. Hao, T. Guo, Y. Shen, Y. Fu and S. Dai, *Ind. Eng. Chem. Res.*, 2023, **62**, 8793–8803.

231 J. P. Hallett and T. Welton, *Chem. Rev.*, 2011, **111**, 3508–3576.

232 T. K. Carlisle, J. E. Bara, A. L. Lafrate, D. L. Gin and R. D. Noble, *J. Membr. Sci.*, 2010, **359**, 37–43.

233 O. D. Thomas, K. J. W. Y. Soo, T. J. Peckham, M. P. Kulkarni and S. Holdcroft, *J. Am. Chem. Soc.*, 2012, **134**, 10753–10756.

234 K. M. Hugar, H. A. I. V. Kostalik and G. W. Coates, *J. Am. Chem. Soc.*, 2015, **137**, 8730–8737.

235 K. Brinker and I. Robinson, US2895948A, 1959.

236 H. Vogel and C. S. Marvel, *J. Polym. Sci.*, 1961, **50**, 511–539.

237 T.-S. Chung, *J. Macromol. Sci., Part C*, 1997, **37**, 277–301.

238 J. S. Wainright, J. T. Wang, D. Weng, R. F. Savinell and M. Litt, *J. Electrochem. Soc.*, 1995, **142**, L121.

239 D. J. Jones and J. Rozière, *J. Membr. Sci.*, 2001, **185**, 41–58.

240 Y. Iwakura, K. Uno and Y. Imai, *J. Polym. Sci., Part A: Gen. Pap.*, 1964, **2**, 2605–2615.

241 M. J. Sansone, *US Pat.*, 4898917, 1990.

242 C. S. Marvel and H. A. Vogel, *US Pat.*, 3174947, 1965.

243 M. Hu, E. M. Pearce and T. K. Kwei, *J. Polym. Sci., Part A: Polym. Chem.*, 1993, **31**, 553–561.

244 D. Henkensmeier, H.-J. Kim, H.-J. Lee, D. H. Lee, I.-H. Oh, S.-A. Hong, S.-W. Nam and T.-H. Lim, *Macromol. Mater. Eng.*, 2011, **296**, 899–908.

245 O. D. Thomas, K. J. W. Y. Soo, T. J. Peckham, M. P. Kulkarni and S. Holdcroft, *Polym. Chem.*, 2011, **2**, 1641–1643.

246 A. G. Wright and S. Holdcroft, *ACS Macro Lett.*, 2014, **3**, 444–447.

247 A. G. Wright, J. Fan, B. Britton, T. Weissbach, H.-F. Lee, E. A. Kitching, T. J. Peckham and S. Holdcroft, *Energy Environ. Sci.*, 2016, **9**, 2130–2142.

248 X. Cao, D. Novitski and S. Holdcroft, *ACS Mater. Lett.*, 2019, **1**, 362–366.

249 E. M. Schibli, A. G. Wright, S. Holdcroft and B. J. Frisken, *J. Phys. Chem. B*, 2018, **122**, 1730–1737.

250 H. Ma, H. Zhu and Z. Wang, *J. Polym. Sci. Polm. Chem.*, 2019, **67**, 1087–1096.

251 H. Long and B. Pivovar, *J. Phys. Chem. C*, 2014, **118**, 9880–9888.

252 J. Fan, A. G. Wright, B. Britton, T. Weissbach, T. J. G. Skalski, J. Ward, T. J. Peckham and S. Holdcroft, *ACS Macro Lett.*, 2017, **6**, 1089–1093.

253 J. Fan, S. Willdorf-Cohen, E. M. Schibli, Z. Paula, W. Li, T. J. G. Skalski, A. T. Sergeenko, A. Hohenadel, B. J. Frisken, E. Magliocca, W. E. Mustain, C. E. Diesendruck, D. R. Dekel and S. Holdcroft, *Nat. Commun.*, 2019, **10**, 2306.

254 T. Luo, S. Abdu and M. Wessling, *J. Membr. Sci.*, 2018, **555**, 429–454.

255 T. J. Omasta, L. Wang, X. Peng, C. A. Lewis, J. R. Varcoe and W. E. Mustain, *J. Power Sources*, 2018, **375**, 205–213.

256 C. E. Diesendruck and D. R. Dekel, *Curr. Opin. Electrochem.*, 2018, **9**, 173–178.

257 P. Overton, W. Li, X. Cao and S. Holdcroft, *Macromolecules*, 2020, **53**, 10548–10560.

258 H. Vogel and C. S. Marvel, *J. Polym. Sci., Part A: Gen. Pap.*, 1963, **1**, 1531–1541.

259 K. Y. Wang, M. Weber and T.-S. Chung, *J. Mater. Chem. A*, 2022, **10**, 8687–8718.

260 O. Olabisi and K. Adewale, *Handbook of thermoplastics*, CRC Press, 2016.

261 L. Xiao, H. Zhang, E. Scanlon, L. S. Ramanathan, E.-W. Choe, D. Rogers, T. Apple and B. C. Benicewicz, *Chem. Mater.*, 2005, **17**, 5328–5333.

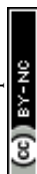262 E. Chauveau, C. Marestin and R. Mercier, *Polymer*, 2014, **55**, 6435–6438.

This journal is © The Royal Society of Chemistry 2024

*Chem. Soc. Rev.*, 2024, **53**, 5704–5780 | 5769

263 E. Chauveau, C. Marestin, V. Martin and R. Mercier, *Polymer*, 2008, **49**, 5209–5214.

264 S. Saxer, C. Marestin, R. Mercier and J. Dupuy, *Polym. Chem.*, 2018, **9**, 1927–1933.

265 P. Overton, A. Konovalova, K. Fraser and S. Holdcroft, *Macromolecules*, 2023, **56**, 2801–2808.

266 J. Kim, H. Y. Jung and M. J. Park, *Macromolecules*, 2020, **53**, 746–763.

267 W. Ried and D. Freitag, *Naturwissenschaften*, 1966, **53**, 306.

268 W. Ried and K. H. Bönnighausen, *Chem. Ber.*, 1960, **93**, 1769–1773.

269 H. Mukamal, F. W. Harris and J. K. Stille, *J. Polym. Sci., Part A-1: Polym. Chem.*, 1967, **5**, 2721–2729.

270 G. K. Noren and J. K. Stille, *J. Polym. Sci.: Macromol. Rev.*, 1971, **5**, 385–430.

271 J. K. Stille and G. K. Noren, *Macromolecules*, 1972, **5**, 49–55.

272 H. F. VanKerckhoven, Y. K. Gilliams and J. K. Stille, *Macromolecules*, 1972, **5**, 541–546.

273 J. M. Tour, *Adv. Mater.*, 1994, **6**, 190–198.

274 C. Fujimoto, E. Sorte, N. Bell, C. Poirier, E. J. Park, S. Maurya, K.-S. Lee and Y. S. Kim, *Polymer*, 2018, **158**, 190–197.

275 T. J. G. Skalski, B. Britton, T. J. Peckham and S. Holdcroft, *J. Am. Chem. Soc.*, 2015, **137**, 12223–12226.

276 C. H. Fujimoto, M. A. Hickner, C. J. Cornelius and D. A. Loy, *Macromolecules*, 2005, **38**, 5010–5016.

277 A. A. Zagorodni, D. L. Kotova and V. F. Selemenev, *React. Funct. Polym.*, 2002, **53**, 157–171.

278 B. Bauer, H. Strathmann and F. Effenberger, *Desalination*, 1990, **79**, 125–144.

279 V. Neagu, I. Bunia and I. Plesca, *Polym. Degrad. Stab.*, 2000, **70**, 463–468.

280 M. R. Hibbs, C. H. Fujimoto and C. J. Cornelius, *Macromolecules*, 2009, **42**, 8316–8321.

281 D. S. Kim, A. Labouriau, M. D. Guiver and Y. S. Kim, *Chem. Mater.*, 2011, **23**, 3795–3797.

282 B. Qiu, B. Lin, L. Qiu and F. Yan, *J. Mater. Chem.*, 2012, **22**, 1040–1045.

283 S. Gu, R. Cai, T. Luo, Z. Chen, M. Sun, Y. Liu, G. He and Y. Yan, *Angew. Chem., Int. Ed.*, 2009, **48**, 6499–6502.

284 M. Tomoi, K. Yamaguchi, R. Ando, Y. Kantake, Y. Aosaki and H. Kubota, *J. Appl. Polym. Sci.*, 1997, **64**, 1161–1167.

285 M. R. Hibbs, *J. Polym. Sci., Part B: Polym. Phys.*, 2013, **51**, 1736–1742.

286 E. J. Park, S. Maurya, M. R. Hibbs, C. H. Fujimoto, K.-D. Kreuer and Y. S. Kim, *Macromolecules*, 2019, **52**, 5419–5428.

287 A. R. Lavoie and R. M. Waymouth, *Tetrahedron*, 2004, **60**, 7147–7155.

288 C. Janiak and P. G. Lassahn, *J. Mol. Catal. A: Chem.*, 2001, **166**, 193–209.

289 F. Blank and C. Janiak, *Coord. Chem. Rev.*, 2009, **253**, 827–861.

290 M. V. Bermeshev and P. P. Chapala, *Prog. Polym. Sci.*, 2018, **84**, 1–46.

291 M. V. Bermeshev, B. A. Bulgakov, A. M. Genaev, J. V. Kostina, G. N. Bondarenko and E. S. Finkelshtein, *Macromolecules*, 2014, **47**, 5470–5483.

292 R. G. Schultz, *J. Polym. Sci., Part B: Polym. Lett.*, 1966, **4**, 541–546.

293 T. Hasan, K. Nishii, T. Shiono and T. Ikeda, *Macromolecules*, 2002, **35**, 8933–8935.

294 T. Hasan, T. Ikeda and T. Shiono, *Macromolecules*, 2004, **37**, 7432–7436.

295 F. Blank, J. K. Vieth, J. Ruiz, V. Rodríguez and C. Janiak, *J. Organomet. Chem.*, 2011, **696**, 473–487.

296 W. S. R. Lago, C. Aymes-Chodur, A. P. Ahoussou and N. Yagoubi, *J. Mater. Sci.*, 2017, **52**, 6879–6904.

297 D. A. Barnes, G. M. Benedikt, B. L. Goodall, S. S. Huang, H. A. Kalamarides, S. Lenhard, L. H. McIntosh, K. T. Selvy, R. A. Shick and L. F. Rhodes, *Macromolecules*, 2003, **36**, 2623–2632.

298 P. Huo, W. Liu, X. He, Z. Wei and Y. Chen, *Polym. Chem.*, 2014, **5**, 1210–1218.

299 S. Martínez-Arranz, A. C. Albéniz and P. Espinet, *Macromolecules*, 2010, **43**, 7482–7487.

300 X. He, J. Liu, H. Zhu, Y. Zheng and D. Chen, *RSC Adv.*, 2015, **5**, 63215–63225.

301 M. Mandal, G. Huang and P. A. Kohl, *J. Membr. Sci.*, 2019, **570–571**, 394–402.

302 R. Selhorst, J. Gaitor, M. Lee, D. Markovich, Y. Yu, M. Treichel, C. Olavarria Gallegos, T. Kowalewski, L. F. Kourkoutis, R. C. Hayward and K. J. T. Noonan, *ACS Appl. Energy Mater.*, 2021, **4**, 10273–10279.

303 M. Lehmann, D. Leonard, J. Zheng, L. He, X. Tang, X. C. Chen, K. H. Lim, S. Maurya, Y. S. Kim and T. Saito, *ACS Appl. Energy Mater.*, 2023, **6**, 1822–1833.

304 J. H. Hsu, C. R. Peltier, M. Treichel, J. C. Gaitor, Q. Li, R. Girbau, A. J. Macbeth, H. D. Abruña, K. J. T. Noonan, G. W. Coates and B. P. Fors, *Angew. Chem., Int. Ed.*, 2023, **62**, e202304778.

305 M. Mandal, G. Huang, N. U. Hassan, W. E. Mustain and P. A. Kohl, *J. Mater. Chem. A*, 2020, **8**, 17568–17578.

306 K. R. Gmernicki, E. Hong, C. R. Maroon, S. M. Mahurin, A. P. Sokolov, T. Saito and B. K. Long, *ACS Macro Lett.*, 2016, **5**, 879–883.

307 M. Mandal, G. Huang, N. Ul Hassan, X. Peng, T. L. Gu, A. H. Brooks-Starks, B. Bahar, W. E. Mustain and P. A. Kohl, *J. Electrochem. Soc.*, 2019, **167**, 054501.

308 M. Mandal, G. Huang and P. A. Kohl, *ACS Appl. Energy Mater.*, 2019, **2**, 2447–2457.

309 G. Huang, M. Mandal, X. Peng, A. C. Yang-Neyerlin, B. S. Pivovar, W. E. Mustain and P. A. Kohl, *J. Electrochem. Soc.*, 2019, **166**, F637.

310 M. Chen, M. Mandal, K. Groenhout, G. McCool, H. M. Tee, B. Zulevi and P. A. Kohl, *J. Power Sources*, 2022, **536**, 231495.

311 T. Wang, Y. Wang and W. You, *J. Membr. Sci.*, 2023, **685**, 121916.

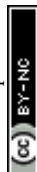312 X. He, X. Jiang, Z. Wang, Y. Deng, Z. Han, Y. Yang and D. Chen, *Polym. Eng. Sci.*, 2018, **58**, 13–21.

5770 | *Chem. Soc. Rev.*, 2024, **53**, 5704–5780

This journal is © The Royal Society of Chemistry 2024

313 Q. Li, X. He, L. Huang, Y. Lu, S. Zou, J. Ye, L. Huang, N. Yu, Z. Fu, X. Zang and D. Chen, *J. Appl. Polym. Sci.*, 2023, **140**, 1–17.

314 X. He, J. Zou, Y. Wen, B. Wu, X. Zang, J. Deng, Z. Qin, G. Yang, J. Xu and D. Chen, *Int. J. Hydrogen Energy*, 2022, **47**, 69–80.

315 L. Delaude and A. F. Noels, *Kirk-Othmer Encyclopedia of Chemical Technology*, 2005.

316 P. Jean-Louis Hérisson and Y. Chauvin, *Die Makromoleku-lare Chemie*, 1971, **141**, 161–176.

317 C. W. Bielawski and R. H. Grubbs, *Prog. Polym. Sci.*, 2007, **32**, 1–29.

318 P. Atallah, K. B. Wagener and M. D. Schulz, *Macromole-cules*, 2013, **46**, 4735–4741.

319 P. Schwab, M. B. France, J. W. Ziller and R. H. Grubbs, *Angew. Chem., Int. Ed. Engl.*, 1995, **34**, 2039–2041.

320 C. W. Bielawski and R. H. Grubbs, *Angew. Chem., Int. Ed.*, 2000, **39**, 2903–2906.

321 T.-L. Choi and R. H. Grubbs, *Angew. Chem., Int. Ed.*, 2003, **42**, 1743–1746.

322 R. Walker, R. M. Conrad and R. H. Grubbs, *Macromole-cules*, 2009, **42**, 599–605.

323 W. T. Chen, M. Mandal, G. Huang, X. M. Wu, G. H. He and P. A. Kohl, *ACS Appl. Energy Mater.*, 2019, **2**, 2458–2468.

324 M. Treichel, C. Tyler Womble, R. Selhorst, J. Gaitor, T. M. S. K. Pathiranage, T. Kowalewski and K. J. T. Noonan, *Macromolecules*, 2020, **53**, 8509–8518.

325 W. L. Truett, D. R. Johnson, I. M. Robinson and B. A. Montague, *J. Am. Chem. Soc.*, 1960, **82**, 2337–2340.

326 G. Natta, G. Dall'Asta and G. Mazzanti, *Angew. Chem., Int. Ed. Engl.*, 1964, **3**, 723–729.

327 S. Hayano, H. Kurakata, Y. Tsunogae, Y. Nakayama, Y. Sato and H. Yasuda, *Macromolecules*, 2003, **36**, 7422–7431.

328 S. Hayano, T. Sugawara and Y. Tsunogae, *J. Polym. Sci., Part A: Polym. Chem.*, 2006, **44**, 3153–3158.

329 S. Hayano, Y. Takeyama, Y. Tsunogae and I. Igarashi, *Macromolecules*, 2006, **39**, 4663–4670.

330 S. Hayano and Y. Tsunogae, *Macromolecules*, 2006, **39**, 30–38.

331 B. Autenrieth, H. Jeong, W. P. Forrest, J. C. Axtell, A. Ota, T. Lehr, M. R. Buchmeiser and R. R. Schrock, *Macromole-cules*, 2015, **48**, 2480–2492.

332 B. Autenrieth and R. R. Schrock, *Macromolecules*, 2015, **48**, 2493–2503.

333 B. Ai-Samak, V. Amir-Ebrahimi, A. G. Carvill, J. G. Hamilton and J. J. Rooney, *Polym. Int.*, 1996, **41**, 85–92.

334 Y. Nakama, S. Hayano and K. Tashiro, *Macromolecules*, 2021, **54**, 8122–8134.

335 Z. Wu and R. H. Grubbs, *Macromolecules*, 1994, **27**, 6700–6703.

336 H. A. Kostalik, T. J. Clark, N. J. Robertson, P. F. Mutolo, J. M. Longo, H. D. Abruña and G. W. Coates, *Macromole-cules*, 2010, **43**, 7147–7150.

337 L.-B. W. Lee and R. A. Register, *Macromolecules*, 2005, **38**, 1216–1222.

338 T. J. Clark, N. J. Robertson, H. A. Kostalik Iv, E. B. Lobkovsky, P. F. Mutolo, H. D. Abruña and G. W. Coates, *J. Am. Chem. Soc.*, 2009, **131**, 12888–12889.

339 N. J. Robertson, H. A. Kostalik, T. J. Clark, P. F. Mutolo, H. D. Abruña and G. W. Coates, *J. Am. Chem. Soc.*, 2010, **132**, 3400–3404.

340 C. R. Peltier, W. You, D. F. Volcanjk, Q. H. Li, A. J. Macbeth, H. D. Abruna and G. W. Coates, *ACS Energy Lett.*, 2023, **8**, 2365–2372.

341 W. You, J. M. Ganley, B. G. Ernst, C. R. Peltier, H. Y. Ko, R. A. DiStasio, R. R. Knowles and G. W. Coates, *Chem. Sci.*, 2021, **12**, 3898–3910.

342 S. C. Price, X. Ren, A. M. Savage and F. L. Beyer, *Polym. Chem.*, 2017, **8**, 5708–5717.

343 Y. Zhao, L. Feng, J. Gao, Y. Zhao, S. Wang, V. Ramani, Z. Zhang and X. Xie, *Int. J. Hydrogen Energy*, 2016, **41**, 16264–16274.

344 C. Wang, B. Mo, Z. He, Q. Shao, D. Pan, E. Wujick, J. Guo, X. Xie, X. Xie and Z. Guo, *J. Membr. Sci.*, 2018, **556**, 118–125.

345 W. You, K. M. Hugar and G. W. Coates, *Macromolecules*, 2018, **51**, 3212–3218.

346 W. You, E. Padgett, S. N. MacMillan, D. A. Muller and G. W. Coates, *Proc. Natl. Acad. Sci. U. S. A.*, 2019, **116**, 9729–9734.

347 C. Cheng, X. He, S. Huang, F. Zhang, Y. Guo, Y. Wen, B. Wu and D. Chen, *Int. J. Hydrogen Energy*, 2020, **45**, 19676–19690.

348 F. Zhang, X. He, C. Cheng, S. Huang, Y. Duan, C. Zhu, Y. Guo, K. Wang and D. Chen, *Int. J. Hydrogen Energy*, 2020, **45**, 13090–13100.

349 R. Schwesinger, R. Link, P. Wenzl, S. Kossek and M. Keller, *Chem. – Eur. J.*, 2006, **12**, 429–437.

350 J. C. Gaitor, M. Treichel, T. Kowalewski and K. J. T. Noonan, *ACS Appl. Polym. Mater.*, 2022, **4**, 8032–8042.

351 T. Zhu, S. Xu, A. Rahman, E. Dogdibegovic, P. Yang, P. Pageni, M. P. Kabir, X.-D. Zhou and C. Tang, *Angew. Chem., Int. Ed.*, 2018, **57**, 2388–2392.

352 T. Zhu and C. Tang, *Polym. Chem.*, 2020, **11**, 4542–4546.

353 T. Zhu, Y. Sha, H. A. Firouzjaie, X. Peng, Y. Cha, D. M. M. M. Dissanayake, M. D. Smith, A. K. Vannucci, W. E. Mustain and C. Tang, *J. Am. Chem. Soc.*, 2020, **142**, 1083–1089.

354 H. Yuan, Y. Liu, T.-H. Tsai, X. Liu, S. B. Kim, R. Gupta, W. Zhang, S. P. Ertem, S. Seifert, A. M. Herring and E. B. Coughlin, *Polyhedron*, 2020, **181**, 114462.

355 S. Gu, J. Wang, R. B. Kaspar, Q. Fang, B. Zhang, E. Bryan Coughlin and Y. Yan, *Sci. Rep.*, 2015, **5**, 11668.

356 K. M. Hugar, W. You and G. W. Coates, *ACS Energy Lett.*, 2019, **4**, 1681–1686.

357 Y. Zha, M. L. Disabb-Miller, Z. D. Johnson, M. A. Hickner and G. N. Tew, *J. Am. Chem. Soc.*, 2012, **134**, 4493–4496.

358 M. L. Disabb-Miller, Y. Zha, A. J. DeCarlo, M. Pawar, G. N. Tew and M. A. Hickner, *Macromolecules*, 2013, **46**, 9279–9287.
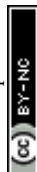
This journal is © The Royal Society of Chemistry 2024

*Chem. Soc. Rev.*, 2024, **53**, 5704–5780 | 5771

359 M. T. Kwasny and G. N. Tew, *J. Mater. Chem. A*, 2017, **5**, 1400–1405.

360 M. T. Kwasny, L. Zhu, M. A. Hickner and G. N. Tew, *J. Polym. Sci., Part A: Polym. Chem.*, 2018, **56**, 328–339.

361 H. Zhang, X. Wang, Y. Wang, Y. Zhang, W. Zhang and W. You, *Angew. Chem., Int. Ed.*, 2023, **62**, e202217742.

362 J.-M. Lehn and F. Montavon, *Helv. Chim. Acta*, 1978, **61**, 67–82.

363 A. Bozzi and A. Chapiro, *Int. J. Radiat. Appl. Instrumentation, Part C. Radiat. Phys. Chem.*, 1988, **32**, 193–196.

364 S. D. Poynton, R. C. T. Slade, T. J. Omasta, W. E. Mustain, R. Escudero-Cid, P. Ocón and J. R. Varcoe, *J. Mater. Chem. A*, 2014, **2**, 5124–5130.

365 A. Abbasi, M. M. Nasef, S. Kheawhom, R. Faridi-Majidi, M. Takeshi, E. Abouzari-Lotf and T. Choong, *Radiat. Phys. Chem.*, 2019, **156**, 58–66.

366 N. Rajabalizadeh Mojarrad, S. Sadeghi, B. Yarar Kaplan, E. Güler and S. Alkan Gürsel, *ACS Appl. Energy Mater.*, 2020, **3**, 532–540.

367 M. M. Nasef, S. A. Gürsel, D. Karabelli and O. Güven, *Prog. Polym. Sci.*, 2016, **63**, 1–41.

368 T. Zhou, R. Shao, S. Chen, X. He, J. Qiao and J. Zhang, *J. Power Sources*, 2015, **293**, 946–975.

369 M. M. Nasef, *Chem. Rev.*, 2014, **114**, 12278–12329.

370 L. Gubler, *Adv. Energy Mater.*, 2014, **4**, 1300827.

371 C. A. Giron Rodriguez, B. Ó. Joensen, A. B. Moss, G. O. Larrazábal, D. K. Whelligan, B. Seger, J. R. Varcoe and T. R. Willson, *ACS Sustainable Chem. Eng.*, 2023, **11**, 1508–1517.

372 A. Chakraborty, I. Salam, M. Choolaei, J. Lee, C. Crean, D. K. Whelligan, R. Bance-Soualhi and J. R. Varcoe, *Mater. Adv.*, 2023, **4**, 2099–2105.

373 R. Bance-Soualhi, M. Choolaei, S. A. Franklin, T. R. Willson, J. Lee, D. K. Whelligan, C. Crean and J. R. Varcoe, *J. Mater. Chem. A*, 2021, **9**, 22025–22038.

374 D. V. Golubenko, B. Van der Bruggen and A. B. Yaroslavtsev, *J. Power Sources*, 2021, **511**, 230460.

375 M. Abdiani, E. Abouzari-Lotf, T. M. Ting, P. Moozarm Nia, S. S. Sha'rani, A. Shockravi and A. Ahmad, *J. Power Sources*, 2019, **424**, 245–253.

376 O. Nibel, T. Rojek, T. J. Schmidt and L. Gubler, *ChemSusChem*, 2017, **10**, 2767–2777.

377 J. H. Park, M. J. Han, D. S. Song and J. Y. Jho, *ACS Appl. Mater. Interfaces*, 2014, **6**, 22847–22854.

378 Y. Ding, X. Shen, J. Zeng, X. Wang, L. Peng, P. Zhang and J. Zhao, *Solid State Ionics*, 2018, **323**, 16–24.

379 L. Chen, Z. Hou, X. Lu, P. Chen, Z. Liu, L. Shen, X. Bian and Q. Qin, *J. Appl. Polym. Sci.*, 2013, **128**, 3949–3956.

380 J. Ao, H. Zhang, X. Xu, F. Yao, L. Ma, L. Zhang, B. Ye, Q. Li, L. Xu and H. Ma, *RSC Adv.*, 2019, **9**, 28588–28597.

381 E. M. Kornacka, G. Przybytniak, L. Fuks, M. Walo and K. Łyczko, *Radiat. Phys. Chem.*, 2014, **94**, 115–118.

382 M. Grasselli and E. E. Smolko, *Radiat. Phys. Chem.*, 2022, **194**, 110055.

383 A. Elizalde-Cárdenas, M. González-Torres, G. Leyva-Gómez, H. Cortés, O. González-Mendoza, M. A. Pérez-Díaz, C. Pineda and R. M. Ribas-Aparicio, *Mater. Lett.*, 2022, **324**, 132783.

384 L. Dong, X. Liu, Z. Xiong, D. Sheng, C. Lin, Y. Zhou and Y. Yang, *Appl. Surf. Sci.*, 2018, **444**, 497–504.

385 V. Sproll, T. J. Schmidt and L. Gubler, *Polym. Int.*, 2016, **65**, 174–180.

386 K. Czaja and M. Sudoł, *Radiat. Phys. Chem.*, 2011, **80**, 514–521.

387 R. Bryant, *Radiat. Phys. Chem.*, 2020, **174**, 108895.

388 A. S. Barbosa, A. L. G. Biancolli, A. J. C. Lanfredi, O. Rodrigues, F. C. Fonseca and E. I. Santiago, *J. Membr. Sci.*, 2022, **659**, 120804.

389 A. L. G. Biancolli, S. Bsoul-Haj, J. C. Douglin, A. S. Barbosa, R. R. de Sousa, O. Rodrigues, A. J. C. Lanfredi, D. R. Dekel and E. I. Santiago, *J. Membr. Sci.*, 2022, **641**, 119879.

390 P. Posadas, J. L. Valentín, R. Benavente, E. Blázquez-Blázquez, A. Urtiaga, J. A. Álvarez and M. L. Cerrada, *Radiat. Phys. Chem.*, 2023, **204**, 110694.

391 A. L. G. Biancolli, A. S. Barbosa, Y. Kodama, R. R. de Sousa, A. J. C. Lanfredi, F. C. Fonseca, J. F. Q. Rey and E. I. Santiago, *J. Power Sources*, 2021, **512**, 230484.

392 L. Wang, J. J. Brink, Y. Liu, A. M. Herring, J. Ponce-González, D. K. Whelligan and J. R. Varcoe, *Energy Environ. Sci.*, 2017, **10**, 2154–2167.

393 L. Wang, X. Peng, W. E. Mustain and J. R. Varcoe, *Energy Environ. Sci.*, 2019, **12**, 1575–1579.

394 W. H. Lee, C. Crean, J. R. Varcoe and R. Bance-Soualhi, *RSC Adv.*, 2017, **7**, 47726–47737.

395 T. N. Danks, R. C. T. Slade and J. R. Varcoe, *J. Mater. Chem.*, 2003, **13**, 712–721.

396 A. J. Samaniego, A. K. Arabelo, M. Sarker, F. Mojica, J. Madrid, P.-Y. A. Chuang, J. Ocon and R. Espiritu, *J. Appl. Polym. Sci.*, 2021, **138**, 49947.

397 E. Abouzari-lotf, H. Ghassemi, M. M. Nasef, A. Ahmad, M. Zakeri, T. M. Ting, A. Abbasi and S. Mehdipour-Ataei, *J. Mater. Chem. A*, 2017, **5**, 15326–15341.

398 Y. Zhao, K. Yoshimura, S. Sawada, T. Motegi, A. Hiroki, A. Radulescu and Y. Maekawa, *Macromolecules*, 2022, **55**, 7100–7109.

399 Y. Zhao, K. Yoshimura, H. Takamatsu, A. Hiroki, Y. Kishiyama, H. Shishitani, S. Yamaguchi, H. Tanaka, S. Koizumi, A. Radulescu, M.-S. Appavou and Y. Maekawa, *J. Electrochem. Soc.*, 2019, **166**, F472.

400 K. Yoshimura, Y. Zhao, A. Hiroki, Y. Kishiyama, H. Shishitani, S. Yamaguchi, H. Tanaka, S. Koizumi, J. E. Houston, A. Radulescu, M.-S. Appavou, D. Richter and Y. Maekawa, *Soft Matter*, 2018, **14**, 9118–9131.

401 Y. Zhao, K. Yoshimura, H. Shishitani, S. Yamaguchi, H. Tanaka, S. Koizumi, N. Szekely, A. Radulescu, D. Richter and Y. Maekawa, *Soft Matter*, 2016, **12**, 1567–1578.

402 T. P. Pandey, A. M. Maes, H. N. Sarode, B. D. Peters, S. Lavina, K. Vezzù, Y. Yang, S. D. Poynton, J. R. Varcoe, S. Seifert, M. W. Liberatore, V. Di Noto and A. M. Herring, *Phys. Chem. Chem. Phys.*, 2015, **17**, 4367–4378.

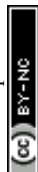403 B.-S. Ko, K. Yoshimura, A. Hiroki and Y. Maekawa, *J. Polym. Sci.*, 2021, **59**, 108–116.

**5772** | *Chem. Soc. Rev.*, 2024, **53**, 5704–5780

This journal is © The Royal Society of Chemistry 2024

404 V. Sproll, G. Nagy, U. Gasser, J. P. Embs, M. Obiols-Rabasa, T. J. Schmidt, L. Gubler and S. Balog, *Macromolecules*, 2016, **49**, 4253–4264.

405 A. L. Gonçalves Biancolli, D. Herranz, L. Wang, G. Stehlíková, R. Bance-Soualhi, J. Ponce-González, P. Ocón, E. A. Ticianelli, D. K. Whelligan, J. R. Varcoe and E. I. Santiago, *J. Mater. Chem. A*, 2018, **6**, 24330–24341.

406 L. Wang, E. Magliocca, E. L. Cunningham, W. E. Mustain, S. D. Poynton, R. Escudero-Cid, M. M. Nasef, J. Ponce-González, R. Bance-Souahli, R. C. T. Slade, D. K. Whelligan and J. R. Varcoe, *Green Chem.*, 2017, **19**, 831–843.

407 B.-S. Ko, K. Yoshimura, S. Warapon, H. Shishitani, S. Yamaguchi, H. Tanaka and Y. Maekawa, *J. Polym. Sci., Part A: Polym. Chem.*, 2019, **57**, 503–510.

408 H. Koshikawa, K. Yoshimura, W. Sinnananchi, T. Yamaki, M. Asano, K. Yamamoto, S. Yamaguchi, H. Tanaka and Y. Maekawa, *Macromol. Chem. Phys.*, 2013, **214**, 1756–1762.

409 T. A. Sherazi, J. Yong Sohn, Y. Moo Lee and M. D. Guiver, *J. Membr. Sci.*, 2013, **441**, 148–157.

410 M. Mamlouk, J. A. Horsfall, C. Williams and K. Scott, *Int. J. Hydrogen Energy*, 2012, **37**, 11912–11920.

411 A. Zhegur-Khais, F. Kubannek, U. Krewer and D. R. Dekel, *J. Membr. Sci.*, 2020, **612**, 118461.

412 Y. Zheng, U. Ash, R. P. Pandey, A. G. Ozioko, J. Ponce-González, M. Handl, T. Weissbach, J. R. Varcoe, S. Holdcroft, M. W. Liberatore, R. Hiesgen and D. R. Dekel, *Macromolecules*, 2018, **51**, 3264–3278.

413 T. R. Willson, C. A. Giron Rodriguez, Q. Xu, J. Frow, F. Foglia, K. Smith, R. Ravikumar, M. Vinothkannan, N. Mahmoudi, I. Salam, A. P. Periasamy, D. K. Whelligan, M. Mamlouk, H. Lin, B. Seger and J. R. Varcoe, *J. Mater. Chem. A*, 2023, **11**, 20724–20740.

414 M. Najibah, J. Kong, H. Khalid, J. Hnát, H. S. Park, K. Bouzek and D. Henkensmeier, *J. Membr. Sci.*, 2023, **670**, 121344.

415 J. Ponce-González, D. K. Whelligan, L. Wang, R. Bance-Soualhi, Y. Wang, Y. Peng, H. Peng, D. C. Apperley, H. N. Sarode, T. P. Pandey, A. G. Divekar, S. Seifert, A. M. Herring, L. Zhuang and J. R. Varcoe, *Energy Environ. Sci.*, 2016, **9**, 3724–3735.

416 E. Abouzari-Lotf, M. V. Jacob, H. Ghassemi, M. Zakeri, M. M. Nasef, Y. Abdolahi, A. Abbasi and A. Ahmad, *Sci. Rep.*, 2021, **11**, 3764.

417 T. A. Sherazi, S. Zahoor, R. Raza, A. J. Shaikh, S. A. R. Naqvi, G. Abbas, Y. Khan and S. Li, *Int. J. Hydrogen Energy*, 2015, **40**, 786–796.

418 B.-S. Ko, J.-Y. Sohn and J. Shin, *Polymer*, 2012, **53**, 4652–4661.

419 J. Fang, Y. Yang, X. Lu, M. Ye, W. Li and Y. Zhang, *Int. J. Hydrogen Energy*, 2012, **37**, 594–602.

420 K. Aggarwal, N. Gjineci, A. Kaushansky, S. Bsoul, J. C. Douglin, S. Li, I. Salam, S. Aharonovich, J. R. Varcoe, D. R. Dekel and C. E. Diesendruck, *ACS Mater. Au*, 2022, **2**, 367–373.

421 L. Wang and M. A. Hickner, *Polym. Chem.*, 2014, **5**, 2928–2935.

422 K. M. Meek, C. M. Reed, B. Pivovar, K.-D. Kreuer, J. R. Varcoe and R. Bance-Soualhi, *RSC Adv.*, 2020, **10**, 36467–36477.

423 J. Müller, A. Zhegur, U. Krewer, J. R. Varcoe and D. R. Dekel, *ACS Mater. Lett.*, 2020, **2**, 168–173.

424 J. C. Douglin, J. R. Varcoe and D. R. Dekel, *J. Power Sources Adv.*, 2020, **5**, 100023.

425 J. Ponce-González, J. R. Varcoe and D. K. Whelligan, *ACS Appl. Energy Mater.*, 2018, **1**, 1883–1887.

426 J. Ponce-González, I. Ouachan, J. R. Varcoe and D. K. Whelligan, *J. Mater. Chem. A*, 2018, **6**, 823–827.

427 O. M. M. Page, S. D. Poynton, S. Murphy, A. Lien Ong, D. M. Hillman, C. A. Hancock, M. G. Hale, D. C. Apperley and J. R. Varcoe, *RSC Adv.*, 2013, **3**, 579–587.

428 X. Li, Y. Yu, Q. Liu and Y. Meng, *Int. J. Hydrogen Energy*, 2013, **38**, 11067–11073.

429 S. Willdorf-Cohen, A. Zhegur-Khais, J. Ponce-González, S. Bsoul-Haj, J. R. Varcoe, C. E. Diesendruck and D. R. Dekel, *ACS Appl. Energy Mater.*, 2023, **6**, 1085–1092.

430 D. Li, E. J. Park, W. Zhu, Q. Shi, Y. Zhou, H. Tian, Y. Lin, A. Serov, B. Zulevi, E. D. Baca, C. Fujimoto, H. T. Chung and Y. S. Kim, *Nat. Energy*, 2020, **5**, 378–385.

431 K. Jetsrisuparb, H. Ben youcef, A. Wokaun and L. Gubler, *J. Membr. Sci.*, 2014, **450**, 28–37.

432 S. Wierzbicki, J. C. Douglin, R. K. Singh, D. R. Dekel and K. Kruczała, *ACS Catal.*, 2023, **13**, 2744–2750.

433 R. Espiritu, M. Mamlouk and K. Scott, *Int. J. Hydrogen Energy*, 2016, **41**, 1120–1133.

434 T. Hamada, K. Yoshimura, K. Takeuchi, S. Watanabe, Y. Zhao, A. Hiroki, T. Hagiwara, H. Shishitani, S. Yamaguchi, H. Tanaka, A. Radulescu, K. Ohwada and Y. Maekawa, *Macromol. Chem. Phys.*, 2021, **222**, 2100028.

435 A. M. A. Mahmoud, K. Yoshimura and Y. Maekawa, *J. Membr. Sci.*, 2021, **620**, 118844.

436 T. Hamada, K. Yoshimura, A. Hiroki and Y. Maekawa, *J. Appl. Polym. Sci.*, 2018, **135**, 46886.

437 H. Adabi, A. Shakouri, N. Ul Hassan, J. R. Varcoe, B. Zulevi, A. Serov, J. R. Regalbuto and W. E. Mustain, *Nat. Energy*, 2021, **6**, 834–843.

438 N. Zion, J. C. Douglin, D. A. Cullen, P. Zelenay, D. R. Dekel and L. Elbaz, *Adv. Funct. Mater.*, 2021, **31**, 2100963.

439 R. Ren, X. Wang, H. Chen, H. A. Miller, I. Salam, J. R. Varcoe, L. Wu, Y. Chen, H.-G. Liao, E. Liu, F. Bartoli, F. Vizza, Q. Jia and Q. He, *Angew. Chem., Int. Ed.*, 2021, **60**, 4049–4054.

440 J. C. Douglin, R. K. Singh, S. Haj-Bsoul, S. Li, J. Biemolt, N. Yan, J. R. Varcoe, G. Rothenberg and D. R. Dekel, *Chem. Eng. J. Adv.*, 2021, **8**, 100153.

441 X. Peng, T. J. Omasta, E. Magliocca, L. Wang, J. R. Varcoe and W. E. Mustain, *Angew. Chem., Int. Ed.*, 2019, **58**, 1046–1051.

442 T. de Wild, T. Nemeth, P. Becker, D. Günther, T. Nauser, T. J. Schmidt and L. Gubler, *J. Power Sources*, 2023, **560**, 232525.

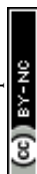443 A. Shirole, P. M. Bakvand and P. Jannasch, *ACS Appl. Energy Mater.*, 2023, **6**, 7240–7249.

This journal is © The Royal Society of Chemistry 2024

*Chem. Soc. Rev.*, 2024, **53**, 5704–5780 | 5773

444 J. Zhou, P. Chen, Q. Weng, J. Fang, X. Chen and Z. An, *Int. J. Hydrogen Energy*, 2016, **41**, 5765–5775.

445 Y. Buchmüller, Z. Zhang, A. Wokaun and L. Gubler, *RSC Adv.*, 2014, **4**, 51911–51915.

446 D. Henkensmeier, H. Ben youcef, F. Wallasch and L. Gubler, *J. Membr. Sci.*, 2013, **447**, 228–235.

447 T. Hamada, Y. Zhao, K. Yoshimura, A. Radulescu, K. Ohwada and Y. Maekawa, *ChemistrySelect*, 2021, **6**, 8879–8888.

448 F. S. Bates and G. H. Fredrickson, *Phys. Today*, 1999, **52**, 32–38.

449 K. I. Winey, D. A. Gobran, Z. Xu, L. J. Fetters and E. L. Thomas, *Macromolecules*, 1994, **27**, 2392–2397.

450 G. Kim and M. Libera, *Macromolecules*, 1998, **31**, 2569–2577.

451 A. Hirao, R. Goseki and T. Ishizone, *Macromolecules*, 2014, **47**, 1883–1905.

452 S. Elamathi, G. Nithyakalyani, D. Sangeetha and S. Ravichandran, *Ionics*, 2008, **14**, 377–385.

453 J. Won, S. W. Choi, Y. S. Kang, H. Y. Ha, I.-H. Oh, H. S. Kim, K. T. Kim and W. H. Jo, *J. Membr. Sci.*, 2003, **214**, 245–257.

454 P. Dai, Z.-H. Mo, R.-W. Xu, S. Zhang and Y.-X. Wu, *ACS Appl. Mater. Interfaces*, 2016, **8**, 20329–20341.

455 Q. H. Zeng, Q. L. Liu, I. Broadwell, A. M. Zhu, Y. Xiong and X. P. Tu, *J. Membr. Sci.*, 2010, **349**, 237–243.

456 L. Sun, J. Guo, J. Zhou, Q. Xu, D. Chu and R. Chen, *J. Power Sources*, 2012, **202**, 70–77.

457 A. D. Mohanty, C. Y. Ryu, Y. S. Kim and C. Bae, *Macromolecules*, 2015, **48**, 7085–7095.

458 A. D. Mohanty, S. E. Tignor, M. R. Sturgeon, H. Long, B. S. Pivovar and C. Bae, *J. Electrochem. Soc.*, 2017, **164**, F1279–F1285.

459 C. Xiao Lin, X. Qin Wang, E. Ning Hu, Q. Yang, Q. Gen Zhang, A. Mei Zhu and Q. Lin Liu, *J. Membr. Sci.*, 2017, **541**, 358–366.

460 J. Y. Jeon, S. Park, J. Han, S. Maurya, A. D. Mohanty, D. Tian, N. Saikia, M. A. Hickner, C. Y. Ryu, M. E. Tuckerman, S. J. Paddison, Y. S. Kim and C. Bae, *Macromolecules*, 2019, **52**, 2139–2147.

461 Y. Li, Y. Liu, A. M. Savage, F. L. Beyer, S. Seifert, A. M. Herring and D. M. Knauss, *Macromolecules*, 2015, **48**, 6523–6533.

462 S. P. Ertem, B. R. Caire, T.-H. Tsai, D. Zeng, M. A. Vandiver, A. Kusoglu, S. Seifert, R. C. Hayward, A. Z. Weber, A. M. Herring, E. B. Coughlin and M. W. Liberatore, *J. Polym. Sci., Part B: Polym. Phys.*, 2017, **55**, 612–622.

463 C. Trant, S. Hwang, C. Bae and S. Lee, *Macromolecules*, 2020, **53**, 8548–8561.

464 H. Strathmann, *AIChE J.*, 2001, **47**, 1077–1087.

465 W. Grot, *Fluorinated ionomers*, William Andrew, 2011.

466 A. Loh, X. Li, S. Sluijter, P. Shirvanian, Q. Lai and Y. Liang, *Hydrogen*, 2023, **4**, 257–271.

467 D. Henkensmeier, M. Najibah, C. Harms, J. Žitka, J. Hnát and K. Bouzek, *J. Electrochem. Energy Conversion Storage*, 2020, **18**, 024001.

468 W. Jiang, A. Y. Faid, B. F. Gomes, I. Galkina, L. Xia, C. M. S. Lobo, M. Desmau, P. Borowski, H. Hartmann, A. Maljusch, A. Besmehn, C. Roth, S. Sunde, W. Lehnert and M. Shviro, *Adv. Funct. Mater.*, 2022, **32**, 2203520.

469 H. Khalid, M. Najibah, H. S. Park, C. Bae and D. Henkensmeier, *Membranes*, 2022, **12**, 989.

470 J. Park, L. Wang, S. G. Advani and A. K. Prasad, *J. Electrochem. Soc.*, 2012, **159**, F864.

471 J. J. Kaczur, H. Yang, Z. Liu, S. A. Sajjad and R. I. Masel, *Front. Chem.*, 2018, **6**, 263.

472 Z. Liu, S. D. Sajjad, Y. Gao, H. Yang, J. J. Kaczur and R. I. Masel, *Int. J. Hydrogen Energy*, 2017, **42**, 29661–29665.

473 M. Moreno-Gonzalez, P. Mardle, S. Zhu, B. Gholamkhass, S. Jones, N. Chen, B. Britton and S. Holdcroft, *J. Power Sources Adv.*, 2023, **19**, 100109.

474 Ionomr, 2023, https://ionomr.com/wp-content/uploads/2023/2005/FM-6063-B-Properties-of-2023rd-Gen-Aemion-Water-Electrolysis-Membranes-2023rd-Gen-2023-2001-2011.pdf.

475 J. Hnát, M. Plevová, J. Žitka, M. Paidar and K. Bouzek, *Electrochim. Acta*, 2017, **248**, 547–555.

476 TailorMem, 2023, tailormem.com/#products.

477 X. Luo, S. Rojas-Carbonell, Y. Yan and A. Kusoglu, *J. Membr. Sci.*, 2020, **598**, 117680.

478 W. J. Song, K. Peng, W. Xu, X. Liu, H. Q. Zhang, X. Liang, B. J. Ye, H. J. Zhang, Z. J. Yang, L. Wu, X. L. Ge and T. W. Xu, *Nat. Commun.*, 2023, **14**, 2732.

479 J. W. Gooch, *Encyclopedic dictionary of polymers*, Springer Science & Business Media, 2010.

480 M. Chatenet, B. G. Pollet, D. R. Dekel, F. Dionigi, J. Deseure, P. Millet, R. D. Braatz, M. Z. Bazant, M. Eikerling, I. Staffell, P. Balcombe, Y. Shao-Horn and H. Schäfer, *Chem. Soc. Rev.*, 2022, **51**, 4583–4762.

481 H.-P. Brack and G. G. Scherer, *Macromol. Symp.*, 1998, **126**, 25–49.

482 D. E. Curtin, R. D. Lousenberg, T. J. Henry, P. C. Tangeman and M. E. Tisack, *J. Power Sources*, 2004, **131**, 41–48.

483 T. Steenberg, H. A. Hjuler, C. Terkelsen, M. T. R. Sánchez, L. N. Cleemann and F. C. Krebs, *Energy Environ. Sci.*, 2012, **5**, 6076–6080.

484 D. Igali, A. Perveen, D. Zhang and D. Wei, *Processes*, 2020, **8**, 1524.

485 N. N. Krishnan, D. Henkensmeier, J. H. Jang and H.-J. Kim, *Macromol. Mater. Eng.*, 2014, **299**, 1031–1041.

486 D. Aili, J. Yang, K. Jankova, D. Henkensmeier and Q. Li, *J. Mater. Chem. A*, 2020, **8**, 12854–12886.

487 É. Ujaczki, V. Stark-Rogel, M. Olbrich, M. Fuetsch and J. Backmann, *Environ. Sci. Eur.*, 2022, **34**, 101.

488 Risk Evaluation for *N*-Methylpyrrolidone (NMP) https://(www.epa.gov/assessing-and-managing-chemicals-under-tsca/risk-evaluation-n-methylpyrrolidone-nmp-0).

489 R. Moore Iii and C. Martin, *Macromolecules*, 1988, **21**, 1334–1339.

490 Y. S. Kim, C. F. Welch, R. P. Hjelm, N. H. Mack, A. Labouriau and E. B. Orler, *Macromolecules*, 2015, **48**, 2161–2172.

5774 | *Chem. Soc. Rev.*, 2024, **53**, 5704–5780

This journal is © The Royal Society of Chemistry 2024

491 T. D. Myles, K. N. Grew, A. A. Peracchio and W. K. S. Chiu, *J. Power Sources*, 2015, **296**, 225–236.

492 Y. S. Kim and K.-S. Lee, *Polym. Rev.*, 2015, **55**, 330–370.

493 F. Wang, M. Hickner, Y. S. Kim, T. A. Zawodzinski and J. E. McGrath, *J. Membr. Sci.*, 2002, **197**, 231–242.

494 Z. Xie, C. Song, B. Andreaus, T. Navessin, Z. Shi, J. Zhang and S. Holdcroft, *J. Electrochem. Soc.*, 2006, **153**, E173.

495 Y. Sone, P. Ekdunge and D. Simonsson, *J. Electrochem. Soc.*, 1996, **143**, 1254.

496 A. Amel, N. Gavish, L. Zhu, D. R. Dekel, M. A. Hickner and Y. Ein-Eli, *J. Membr. Sci.*, 2016, **514**, 125–134.

497 M. Irfan, E. Bakangura, N. U. Afsar, M. M. Hossain, J. Ran and T. Xu, *J. Power Sources*, 2017, **355**, 171–180.

498 K. Zhang, M. B. McDonald, I. E. A. Genina and P. T. Hammond, *Chem. Mater.*, 2018, **30**, 6420–6430.

499 A. M. Kiss, T. D. Myles, K. N. Grew, A. A. Peracchio, G. J. Nelson and W. K. S. Chiu, *J. Electrochem. Soc.*, 2013, **160**, F994.

500 N. Ziv and D. R. Dekel, *Electrochem. Commun.*, 2018, **88**, 109–113.

501 F. N. Büchi, A. Marek and G. G. Scherer, *J. Electrochem. Soc.*, 1995, **142**, 1895.

502 T. E. Springer, T. A. Zawodzinski, M. S. Wilson and S. Gottesfeld, *J. Electrochem. Soc.*, 1996, **143**, 587.

503 K. R. Cooper and M. Smith, *J. Power Sources*, 2006, **160**, 1088–1095.

504 B. S. Pivovar and Y. S. Kim, *J. Electrochem. Soc.*, 2007, **154**, B739.

505 N. Yaghini, L. Nordstierna and A. Martinelli, *Phys. Chem. Chem. Phys.*, 2014, **16**, 9266–9275.

506 D. R. P. Morris, S. P. Liu, D. Villegas Gonzalez and J. T. Gostick, *ACS Appl. Mater. Interfaces*, 2014, **6**, 18609–18618.

507 F. Wang, D. Wang and Y. Nagao, *ChemSusChem*, 2021, **14**, 2694–2697.

508 U. N. Shrivastava, A. Zhegur-Khais, M. Bass, S. Willdorf-Cohen, V. Freger, D. R. Dekel and K. Karan, *J. Phys. Chem. C*, 2020, **124**, 23469–23478.

509 X. Luo, D. I. Kushner, J. Li, E. J. Park, Y. S. Kim and A. Kusoglu, *Adv. Funct. Mater.*, 2021, **31**, 2008778.

510 E. J. Park, S. Komini Babu and Y. S. Kim, *Front. Energy Res.*, 2022, **10**, 945654.

511 M. Bernt, J. Schröter, M. Möckl and H. A. Gasteiger, *J. Electrochem. Soc.*, 2020, **167**, 124502.

512 P. D. Beattie, V. I. Basura and S. Holdcroft, *J. Electroanal. Chem.*, 1999, **468**, 180–192.

513 S. S. Kocha, J. Deliang Yang and J. S. Yi, *AIChE J.*, 2006, **52**, 1916–1925.

514 T. Sakai, H. Takenaka, N. Wakabayashi, Y. Kawami and E. Torikai, *J. Electrochem. Soc.*, 1985, **132**, 1328.

515 D. Li, A. R. Motz, C. Bae, C. Fujimoto, G. Yang, F.-Y. Zhang, K. E. Ayers and Y. S. Kim, *Energy Environ. Sci.*, 2021, **14**, 3393–3419.

516 L. Wang, S. Rojas-Carbonell, K. Hu, B. P. Setzler, A. R. Motz, M. E. Ueckermann and Y. Yan, *Front. Energy Res.*, 2022, **10**, 887893.

517 C. G. Arges, J. Parrondo, G. Johnson, A. Nadhan and V. Ramani, *J. Mater. Chem.*, 2012, **22**, 3733–3744.

518 M. R. Hibbs, M. A. Hickner, T. M. Alam, S. K. McIntyre, C. H. Fujimoto and C. J. Cornelius, *Chem. Mater.*, 2008, **20**, 2566–2573.

519 F. Karas, J. Hnát, M. Paidar, J. Schauer and K. Bouzek, *Int. J. Hydrogen Energy*, 2014, **39**, 5054–5062.

520 T. Weissbach, A. G. Wright, T. J. Peckham, A. Sadeghi Alavijeh, V. Pan, E. Kjeang and S. Holdcroft, *Chem. Mater.*, 2016, **28**, 8060–8070.

521 Y. Mei, Z. Yao, L. Ji, P. H. Toy and C. Y. Tang, *J. Membr. Sci.*, 2018, **549**, 295–305.

522 A. D. Mohanty, Y.-B. Lee, L. Zhu, M. A. Hickner and C. Bae, *Macromolecules*, 2014, **47**, 1973–1980.

523 X. Ge, Y. He, K. Zhang, X. Liang, C. Wei, M. A. Shehzad, W. Song, Z. Ge, G. Li, W. Yu, L. Wu and T. Xu, *Research*, 2021, **2021**, 9762709.

524 C. G. Arges, V. Ramani, Z. Wang and R. J. Ouimet, *Front. Energy Res.*, 2022, **10**, 871851.

525 K.-D. Kreuer and P. Jannasch, *J. Power Sources*, 2018, **375**, 361–366.

526 S. Willdorf-Cohen, A. N. Mondal, D. R. Dekel and C. E. Diesendruck, *J. Mater. Chem. A*, 2018, **6**, 22234–22239.

527 H. T. Chung, Y.-K. Choe, U. Martinez, J. H. Dumont, A. Mohanty, C. Bae, I. Matanovic and Y. S. Kim, *J. Electrochem. Soc.*, 2016, **163**, F1503.

528 X. Chen, I. T. McCrum, K. A. Schwarz, M. J. Janik and M. T. M. Koper, *Angew. Chem., Int. Ed.*, 2017, **56**, 15025–15029.

529 D. Li, H. T. Chung, S. Maurya, I. Matanovic and Y. S. Kim, *Curr. Opin. Electrochem.*, 2018, **12**, 189–195.

530 I. Matanovic and Y. S. Kim, *Curr. Opin. Electrochem.*, 2023, **38**, 101218.

531 K. Fraser, K. Dosaev, E. Savinova, S. Holdcroft and T. Asset, *ChemCatChem*, 2024, **16**, e202301304.

532 J. H. Dumont, A. J. Spears, R. P. Hjelm, M. Hawley, S. Maurya, D. Li, G. Yuan, E. B. Watkins and Y. S. Kim, *ACS Appl. Mater. Interfaces*, 2020, **12**, 1825–1831.

533 A. Y. Faid, A. O. Barnett, F. Seland and S. Sunde, *Int. J. Hydrogen Energy*, 2022, **47**, 23483–23497.

534 R. A. Krivina, G. A. Lindquist, S. R. Beaudoin, T. N. Stovall, W. L. Thompson, L. P. Twight, D. Marsh, J. Grzyb, K. Fabrizio, J. E. Hutchison and S. W. Boettcher, *Adv. Mater.*, 2022, **34**, 2203033.

535 B. Pivovar, *Alkaline Membrane Fuel Cell Workshop*, 2012.

536 B. Pivovar and Y. S. Kim, *Anion Exchange Membrane Workshop*, 2019.

537 B. Pivovar and Y. S. Kim, *Alkaline Membrane Fuel Cell Workshop*, 2016.

538 S. T. Thompson, D. Peterson, D. Ho and D. Papageorgopoulos, *J. Electrochem. Soc.*, 2020, **167**, 084514.

539 DOE, DE-FOA-0002922 Bipartisan Infrastructure Law: Clean Hydrogen Electrolysis, Manufacturing, and Recycling, 2023.

540 D. R. Dekel, *J. Power Sources*, 2018, **375**, 158–169.

This journal is © The Royal Society of Chemistry 2024

*Chem. Soc. Rev.*, 2024, **53**, 5704–5780 | **5775**

541 W. E. Mustain, M. Chatenet, M. Page and Y. S. Kim, *Energy Environ. Sci.*, 2020, **13**, 2805–2838.

542 Y. Wang, G. Wang, G. Li, B. Huang, J. Pan, Q. Liu, J. Han, L. Xiao, J. Lu and L. Zhuang, *Energy Environ. Sci.*, 2015, **8**, 177–181.

543 J. Xue, J. C. Douglin, K. Yassin, T. Huang, H. Jiang, J. Zhang, Y. Yin, D. R. Dekel and M. D. Guiver, *Joule*, 2024, **8**, 1–21.

544 T. Wang, Y. Zhao, S. Wang, S. Cheng, S. Yang, H. Wei and Y. Ding, *J. Power Sources*, 2023, **557**, 232590.

545 S. C. Xu, Y. Gu, T. Y. Ma, X. Su, J. Y. Chen and R. H. He, *ACS Sustainable Chem. Eng.*, 2023, **11**, 10402–10412.

546 R. X. Ma, Y. F. Kang, T. Wang, T. Jiang, H. Y. Yin, C. Liu, H. B. Wei and Y. S. Ding, *J. Membr. Sci.*, 2023, **678**, 121667.

547 D. P. Leonard, M. Lehmann, J. M. Klein, I. Matanovic, C. Fujimoto, T. Saito and Y. S. Kim, *Adv. Energy Mater.*, 2023, **13**, 2203488.

548 X. F. Wan, X. T. Wei, J. M. Ge, L. F. Lu, Z. Q. Liu and Y. Q. Zhu, *J. Membr. Sci.*, 2023, **680**, 121760.

549 J. Y. Chen, S. C. Xu, X. Su, W. Wei, Y. J. Li, R. L. Du and R. H. He, *ACS Appl. Polym. Mater.*, 2023, **5**, 6222–6231.

550 N. Xie, T. Wang, S. H. Du, Q. Weng, K. Zheng, T. Zhang, X. M. Ning, P. Chen, X. B. Chen and Z. W. An, *J. Power Sources*, 2023, **574**, 233121.

551 J. M. Li, Q. Liu, L. Tian, W. L. Ma, F. H. Wang, Z. Q. Wang and H. Zhu, *Int. J. Hydrogen Energy*, 2022, **47**, 32262–32272.

552 X. F. Li, K. Yang, Z. M. Wang, Y. H. Chen, Y. G. Li, J. Guo, J. F. Zheng, S. H. Li and S. B. Zhang, *Macromolecules*, 2022, **55**, 10607–10617.

553 L. L. Ma, L. Li, M. H. Yuan, L. Bai, A. R. Zhang, X. M. Yan, G. H. He and F. X. Zhang, *ACS Sustainable Chem. Eng.*, 2022, **10**, 5748–5757.

554 X. Z. Wang, W. T. Chen, T. T. Li, X. M. Yan, Y. Zhang, F. Zhang, X. M. Wu, B. Pang, J. N. Li and G. H. He, *J. Mater. Chem. A*, 2021, **9**, 7522–7530.

555 X. Y. Wu, N. J. Chen, C. Hu, H. A. Klok, Y. M. Lee and X. L. Hu, *Adv. Mater.*, 2023, **35**, 2210432.

556 C. Hu, J. H. Park, N. Y. Kang, X. Zhang, Y. J. Lee, S. W. Jeong and Y. M. Lee, *J. Mater. Chem. A*, 2023, **11**, 2031–2041.

557 Z. Yu, W. T. Gao, Y. J. Liu, Q. G. Zhang, A. M. Zhu and Q. L. Liu, *J. Colloid Interface Sci.*, 2023, **651**, 404–414.

558 X. Li, B. Zhang, J. Guo, Y. Chen, L. Dai, J. Zheng, S. Li and S. Zhang, *J. Mater. Chem. A*, 2023, **11**, 10738–10747.

559 G. D. Xu, J. Pan, X. Y. Zou, Z. Y. Jin, J. L. Zhang, P. D. Fang, Q. H. Zhang, Z. Sun and F. Yan, *Adv. Funct. Mater.*, 2023, **33**, 2302364.

560 J. J. Wang, W. T. Gao, Y. S. L. Choo, Z. H. Cai, Q. G. Zhang, A. M. Zhu and Q. L. Liu, *J. Colloid Interface Sci.*, 2023, **629**, 377–387.

561 W. T. Gao, X. L. Gao, W. W. Gou, J. J. Wang, Z. H. Cai, Q. G. Zhang, A. M. Zhu and Q. L. Liu, *J. Membr. Sci.*, 2022, **655**, 120578.

562 Q. L. Wei, X. Z. Cao, P. Veh, A. Konovalova, P. Mardle, P. Overton, S. Cassegrain, S. Vierrath, M. Breitwieser and S. Holdcroft, *Sustainable Energy Fuels*, 2022, **6**, 3551–3564.

563 M. L. Guo, T. Ban, Y. J. Wang, Y. N. Wang, Y. Y. Zhang, J. S. Zhang and X. L. Zhu, *J. Membr. Sci.*, 2022, **647**, 120299.

564 J. J. Chen, C. H. Shen and S. J. Gao, *Desalination*, 2023, **557**, 116600.

565 J. J. Zhang, K. Y. Zhang, X. Liang, W. S. Yu, X. L. Ge, M. A. Shehzad, Z. J. Ge, Z. J. Yang, L. Wu and T. W. Xu, *J. Mater. Chem. A*, 2021, **9**, 327–337.

566 S. Favero, I. E. L. Stephens and M.-M. Titirci, *Adv. Mater.*, 2023, 2308238.

567 A. C. Yang-Neyerlin, S. Medina, K. M. Meek, D. J. Strasser, C. He, D. M. Knauss, W. E. Mustain, S. Pylypenko and B. S. Pivovar, *J. Electrochem. Soc.*, 2021, **168**, 044525.

568 Y. S. Kim, *ACS Appl. Polym. Mater.*, 2021, **3**, 1250–1270.

569 X. J. Zhang, Y. J. Cao, M. Zhang, Y. G. Wang, H. Y. Tang and N. W. Li, *J. Membr. Sci.*, 2020, **598**, 117793.

570 X. M. Chu, Y. Shi, L. Liu, Y. D. Huang and N. W. Li, *J. Mater. Chem. A*, 2019, **7**, 7717–7727.

571 L. Liu, X. M. Chu, J. Y. Liao, Y. D. Huang, Y. Li, Z. Y. Ge, M. A. Hickner and N. W. Li, *Energy Environ. Sci.*, 2018, **11**, 435–446.

572 K. Yang, X. M. Chu, X. J. Zhang, X. F. Li, J. F. Zheng, S. H. Li, N. W. Li, T. A. Sherazi and S. B. Zhang, *J. Membr. Sci.*, 2020, **603**, 118025.

573 N. J. Chen, J. H. Park, C. Hu, H. H. Wang, H. M. Kim, N. Y. Kang and Y. M. Lee, *J. Mater. Chem. A*, 2022, **10**, 3678–3687.

574 N. Ul Hassan, M. J. Zachman, M. Mandal, H. A. Firouzjaie, P. A. Kohl, D. A. Cullen and W. E. Mustain, *ACS Catal.*, 2022, **12**, 8116–8126.

575 X. Liu, N. Xie, J. Xue, M. Li, C. Zheng, J. Zhang, Y. Qin, Y. Yin, D. R. Dekel and M. D. Guiver, *Nat. Energy*, 2022, **7**, 329–339.

576 H. S. Shiau, I. V. Zenyuk and A. Z. Weber, *J. Electrochem. Soc.*, 2017, **164**, E3583–E3591.

577 H. Ito, N. Kawaguchi, S. Someya, T. Munakata, N. Miyazaki, M. Ishida and A. Nakano, *Int. J. Hydrogen Energy*, 2018, **43**, 17030–17039.

578 A. Kiessling, J. C. Fornaciari, G. Anderson, X. Peng, A. Gerstmayr, M. R. Gerhardt, S. McKinney, A. Serov, Y. S. Kim, B. Zulevi, A. Z. Weber and N. Danilovic, *J. Electrochem. Soc.*, 2021, **168**, 084512.

579 B. Mayerhöfer, F. D. Speck, M. Hegelheimer, M. Bierling, D. Abbas, D. McLaughlin, S. Cherevko, S. Thiele and R. Peach, *Int. J. Hydrogen Energy*, 2022, **47**, 4304–4314.

580 I. Gatto, A. Caprì, C. Lo Vecchio, S. Zignani, A. Patti and V. Baglio, *Int. J. Hydrogen Energy*, 2023, **48**, 11914–11921.

581 Y. Leng, G. Chen, A. J. Mendoza, T. B. Tighe, M. A. Hickner and C.-Y. Wang, *J. Am. Chem. Soc.*, 2012, **134**, 9054–9057.

582 M. Faraj, M. Boccia, H. Miller, F. Martini, S. Borsacchi, M. Geppi and A. Pucci, *Int. J. Hydrogen Energy*, 2012, **37**, 14992–15002.

583 Z. Feng, P. O. Esteban, G. Gupta, D. A. Fulton and M. Mamlouk, *Int. J. Hydrogen Energy*, 2021, **46**, 37137–37151.

584 G. Gupta, K. Selvakumar, N. Lakshminarasimhan, S. M. Senthil Kumar and M. Mamlouk, *J. Power Sources*, 2020, **461**, 228131.

5776 | *Chem. Soc. Rev.*, 2024, **53**, 5704–5780

This journal is © The Royal Society of Chemistry 2024

585 G. Gupta, K. Scott and M. Mamlouk, *J. Power Sources*, 2018, **375**, 387–396.

586 X. Wu and K. Scott, *Int. J. Hydrogen Energy*, 2013, **38**, 3123–3129.

587 M. Liu, X. Hu, B. Hu, L. Liu and N. W. Li, *J. Membr. Sci.*, 2022, **642**, 119966.

588 C. Lei, K. C. Yang, G. Z. Wang, G. W. Wang, J. T. Lu, L. Xiao and L. Zhuang, *ACS Sustainable Chem. Eng.*, 2022, **10**, 16725–16733.

589 M. Makrygianni, S. Aivali, Y. Xia, M. R. Kraglund, D. Aili and V. Deimede, *J. Membr. Sci.*, 2023, **669**, 121331.

590 X. Hu, B. Hu, C. Niu, J. Yao, M. Liu, H. Tao, Y. Huang, S. Kang, K. Geng and N. Li, *Nat. Energy*, 2024, DOI: **10.1038/s41560-023-01447-w**.

591 G. A. Lindquist, S. Z. Oener, R. Krivina, A. R. Motz, A. Keane, C. Capuano, K. E. Ayers and S. W. Boettcher, *ACS Appl. Mater. Interfaces*, 2021, **13**, 51917–51924.

592 F. Razmjooei, T. Morawietz, E. Taghizadeh, E. Hadjixeno-phontos, L. Mues, M. Gerle, B. D. Wood, C. Harms, A. S. Gago, S. A. Ansar and K. A. Friedrich, *Joule*, 2021, **5**, 1776–1799.

593 N. Ul Hassan, Y. W. Zheng, P. A. Kohl and W. E. Mustain, *J. Electrochem. Soc.*, 2022, **169**, 044526.

594 A. R. Motz, D. G. Li, A. Keane, L. D. Manriquez, E. J. Park, S. Maurya, H. Chung, C. Fujimoto, J. Jeon, M. K. Pagels, C. Bae, K. E. Ayers and Y. S. Kim, *J. Mater. Chem. A*, 2021, **9**, 22670–22683.

595 L. Wan, J. Liu, Z. Xu, Q. Xu, M. B. Pang, P. C. Wang and B. G. Wang, *Small*, 2022, **18**, 2200380.

596 P. Thangavel, H. Lee, T.-H. Kong, S. Kwon, A. Tayyebi, J.-H. Lee, S. M. Choi and Y. Kwon, *Adv. Energy Mater.*, 2023, **13**, 2203401.

597 C. C. Pavel, F. Cecconi, C. Emiliani, S. Santiccioli, A. Scaffidi, S. Catanorchi and M. Comotti, *Angew. Chem., Int. Ed.*, 2014, **53**, 1378–1381.

598 Z. Xu, V. Wilke, J. J. Chmielarz, M. Tobias, V. Atanasov, A. S. Gago and K. A. Friedrich, *J. Membr. Sci.*, 2023, **670**, 121302.

599 M. J. Jang, S. H. Yang, M. G. Park, J. Jeong, M. S. Cha, S. H. Shin, K. H. Lee, Z. Y. Bai, Z. W. Chen, J. Y. Lee and S. M. Choi, *ACS Energy Lett.*, 2022, **7**, 2576–2583.

600 L. Wang, T. Weissbach, R. Reissner, A. Ansar, A. S. Gago, S. Holdcroft and K. A. Friedrich, *ACS Appl. Energy Mater.*, 2019, **2**, 7903–7912.

601 N. Chen, S. Y. Paek, J. Y. Lee, J. H. Park, S. Y. Lee and Y. M. Lee, *Energy Environ. Sci.*, 2021, **14**, 6338–6348.

602 B. Motealleh, Z. Liu, R. I. Masel, J. P. Sculley, Z. R. Ni and L. Meroueh, *Int. J. Hydrogen Energy*, 2021, **46**, 3379–3386.

603 S. C. Zignani, M. Lo Faro, A. Carbone, C. Italiano, S. Trocino, G. Monforte and A. S. Arico, *Electrochim. Acta*, 2022, **413**, 140078.

604 Z. Jiang, G. Yi, X. Yao, Y. Ma, X. Su, Q. Liu and Q. Zhang, *Chem. Eng. J.*, 2023, **467**, 143442.

605 A. W. Tricker, T. Y. Ertugrul, J. K. Lee, J. R. Shin, W. Choi, D. I. Kushner, G. Wang, J. Lang, I. V. Zenyuk, A. Z. Weber and X. Peng, *Adv. Energy Mater.*, 2024, **14**, 2303629.

606 C. Hu, N. Y. Kang, H. W. Kang, J. Y. Lee, X. Zhang, Y. J. Lee, S. W. Jung, J. H. Park, M.-G. Kim, S. J. Yoo, S. Y. Lee, C. H. Park and Y. M. Lee, *Angew. Chem., Int. Ed.*, 2024, **63**, e202316697.

607 Z. P. Wang, K. Chi, S. X. Yang, J. W. Xiao, F. Xiao, X. X. Zhao and S. Wang, *Small*, 2023, **19**, 2301403.

608 M. Q. Li, H. Su, Q. G. Qiu, G. Zhao, Y. Sun and W. J. Song, *J. Chem.*, 2014, **2014**, 321629.

609 K. Amini and M. D. Pritzker, *Electrochim. Acta*, 2020, **356**, 134785.

610 B. Hu, C. DeBruler, Z. Rhodes and T. L. Liu, *J. Am. Chem. Soc.*, 2017, **139**, 1207–1214.

611 Y. Xiao, L. Hu, L. Gao, M. T. Di, X. J. Sun, J. Liu, X. M. Yan and G. H. He, *Chem. Eng. J.*, 2022, **432**, 134268.

612 M. T. Tsehaye, X. Yang, T. Janoschka, M. D. Hager, U. S. Schubert, F. Alloin and C. Iojoiu, *Membranes*, 2021, **11**, 367.

613 T. Hagemann, J. Winsberg, M. Grube, I. Nischang, T. Janoschka, N. Martin, M. D. Hager and U. S. Schubert, *J. Power Sources*, 2018, **378**, 546–554.

614 X. L. Lv, P. Sullivan, H. C. Fu, X. X. Hu, H. H. Liu, S. Jin, W. J. Li and D. W. Feng, *ACS Energy Lett.*, 2022, **7**, 2428–2434.

615 F. Alkhayri and C. A. Dyker, *J. Electrochem. Soc.*, 2021, **168**, 070501.

616 G. D. Charlton, S. M. Barbon, J. B. Gilroy and C. A. Dyker, *J. Energy Chem.*, 2019, **34**, 52–56.

617 G. J. Hwang and H. Ohya, *J. Membr. Sci.*, 1997, **132**, 55–61.

618 D. Y. Chen, M. A. Hickner, E. Agar and E. C. Kumbur, *ACS Appl. Mater. Interfaces*, 2013, **5**, 7559–7566.

619 S. J. Seo, B. C. Kim, K. W. Sung, J. Shim, J. D. Jeon, K. H. Shin, S. H. Shin, S. H. Yun, J. Y. Lee and S. H. Moon, *J. Membr. Sci.*, 2013, **428**, 17–23.

620 Z. Mai, H. Zhang, H. Zhang, W. Xu, W. Wei, H. Na and X. Li, *ChemSusChem*, 2013, **6**, 328–335.

621 M. Abdiani, E. Abouzari-Lotf, T. M. Ting, P. M. Nia, S. S. Sha'rani, A. Shockravi and A. Ahmad, *J. Power Sources*, 2019, **424**, 245–253.

622 M. S. Cha, S. W. Jo, S. H. Han, S. H. Hong, S. So, T. H. Kim, S. G. Oh, Y. T. Hong and J. Y. Lee, *J. Power Sources*, 2019, **413**, 158–166.

623 Y. Chen, Z. C. Liu, M. J. Lin, Q. L. Lin, B. H. Tong and D. Y. Chen, *Science China-Chemistry*, 2019, **62**, 479–490.

624 H. Cho, H. M. Krieg and J. A. Kerres, *Membranes*, 2019, **9**, 31.

625 S. H. Roh, M. H. Lim, T. Sadhasivam and H. Y. Jung, *Electrochim. Acta*, 2019, **325**, 134944.

626 H. Cho, V. Atanasov, H. M. Krieg and J. A. Kerres, *Polymers*, 2020, **12**, 915.

627 Y. Du, L. Gao, L. Hu, M. T. Di, X. M. Yan, B. G. An and G. H. He, *J. Membr. Sci.*, 2020, **603**, 118011.

628 T. S. Wang, J. Y. Jeon, J. Han, J. H. Kim, C. Bae and S. Kim, *J. Membr. Sci.*, 2020, **598**, 117665.

629 B. G. Zhang, F. F. Wang, S. S. Guan, M. H. Zhao, E. L. Zhang, G. S. Wang, Z. G. Zhang, X. Q. Liu and S. H. Zhang, *J. Power Sources*, 2020, **477**, 229011.

This journal is © The Royal Society of Chemistry 2024

*Chem. Soc. Rev.*, 2024, **53**, 5704–5780 | **5777**

630 M. Charyton, C. Iojoiu, P. Fischer, G. Henrion, M. Etienne and M. L. Donten, *Membranes*, 2021, **11**, 436.

631 W. Q. Tang, T. Mu, X. F. Che, J. H. Dong and J. S. Yang, *ACS Sustainable Chem. Eng.*, 2021, **9**, 14297–14306.

632 W. Q. Tang, Y. F. Yang, X. L. Liu, J. H. Dong, H. H. Li and J. S. Yang, *Electrochim. Acta*, 2021, **391**, 138919.

633 Z. W. Tao, C. Y. Wang, S. J. Cai, J. F. Qian and J. Li, *ACS Appl. Energy Mater.*, 2021, **4**, 14488–14496.

634 Z. Q. Wang, S. H. Zhang, Q. Liu, Y. I. Chen, Z. H. Weng and X. G. Jian, *J. Membr. Sci.*, 2021, **633**, 119416.

635 S. Yang, X. F. Chu, B. Xue, T. Lv, B. C. Lin and Z. H. Zhang, *ACS Appl. Energy Mater.*, 2021, **4**, 6787–6796.

636 Y. Ahn and D. Kim, *J. Ind. Eng. Chem.*, 2022, **110**, 395–404.

637 X. F. Che, W. Q. Tang, J. H. Dong, D. Aili and J. S. Yang, *Sci. China: Mater.*, 2022, **65**, 683–694.

638 A. K. Singh, P. Sharma, K. Singh and V. K. Shahi, *J. Power Sources*, 2022, **520**, 230856.

639 X. H. Do, S. Abbas, M. M. Ikhsan, S. Y. Choi, H. Y. Ha, K. Azizi, H. A. Hjuler and D. Henkensmeier, *Small*, 2022, **18**, e2206284.

640 T. T. Bui, M. Shin, M. Rahimi, A. Bentien, Y. Kwon and D. Henkensmeier, *Carbon Energy*, 2024, e473.

641 M. Mara Ikhsan, S. Abbas, X. H. Do, S.-Y. Choi, K. Azizi, H. A. Hjuler, J. H. Jang, H. Y. Ha and D. Henkensmeier, *Chem. Eng. J.*, 2022, **435**, 134902.

642 A. Khataee, D. Pan, J. S. Olsson, P. Jannasch and R. W. Lindstrom, *J. Power Sources*, 2021, **483**, 229202.

643 B. Shanahan, T. Bohm, B. Britton, S. Holdcroft, R. Zengerle, S. Vierrath, S. Thiele and M. Breitwieser, *Electrochem. Commun.*, 2019, **102**, 37–40.

644 E. Lallo, A. Khataee and R. W. Lindstroem, *Processes*, 2022, **10**, 270.

645 H. Cho, E. Hur, D. Henkensmeier, G. Jeong, E. Cho, H. J. Kim, J. H. Jang, K. Y. Lee, H. A. Hjuler, Q. Li, J. O. Jensen and L. N. Cleemann, *Eur. Polym. J.*, 2014, **58**, 135–143.

646 T. Huang, X. Qiu, J. Zhang, X. Li, Y. Pei, H. Jiang, R. Yue, Y. Yin, Z. Jiang, X. Zhang and M. D. Guiver, *J. Power Sources*, 2022, **527**, 231143.

647 H. Tang, K. Geng, L. Wu, J. Liu, Z. Chen, W. You, F. Yan, M. D. Guiver and N. Li, *Nat. Energy*, 2022, **7**, 153–162.

648 M. D. Guiver, M. Yahia, M. M. Dal-Cin, G. P. Robertson, S. Saeedi Garakani, N. Du and N. Tavajohi, *Macromolecules*, 2020, **53**, 8951–8959.

649 F. Liu, S. Wang, D. Wang, G. Liu, Y. Cui, D. Liang, X. Wang, Z. Yong and Z. Wang, *J. Power Sources*, 2021, **494**, 229732.

650 G. Skorikova, D. Rauber, D. Aili, S. Martin, Q. Li, D. Henkensmeier and R. Hempelmann, *J. Membr. Sci.*, 2020, **608**, 118188.

651 F. Liu, S. Wang, H. Chen, J. Li, X. Wang, T. Mao and Z. Wang, *Renewable Energy*, 2021, **163**, 1692–1700.

652 Y. Xiao, X. Shen, R. Sun, S. Wang, J. Xiang, L. Zhang, P. Cheng, X. Du, Z. Yin and N. Tang, *J. Power Sources*, 2022, **543**, 231802.

653 P. Wang, J. Lin, Y. Wu and L. Wang, *J. Power Sources*, 2023, **560**, 232665.

654 Y. Jin, X. Che, Y. Xu, J. Dong, C. Pan, D. Aili, Q. Li and J. Yang, *J. Electrochem. Soc.*, 2022, **169**, 024504.

655 Y. Xiao, H. Chen, R. Sun, L. Zhang, J. Xiang, P. Cheng, H. Han, S. Wang and N. Tang, *Polymers*, 2023, **15**, 3197.

656 C. Gao, M. Hu, L. Wang and L. Wang, *Polymers*, 2020, **12**, 515.

657 G. Venugopalan, K. Chang, J. Nijoka, S. Livingston, G. M. Geise and C. G. Arges, *ACS Appl. Energy Mater.*, 2020, **3**, 573–585.

658 V. Atanasov, A. S. Lee, E. J. Park, S. Maurya, E. D. Baca, C. Fujimoto, M. Hibbs, I. Matanovic, J. Kerres and Y. S. Kim, *Nat. Mater.*, 2021, **20**, 370–377.

659 F. Arslan, K. Chuluunbandi, A. T. S. Freiberg, A. Kormanyos, F. Sit, S. Cherevko, J. Kerres, S. Thiele and T. Boehm, *ACS Appl. Mater. Interfaces*, 2021, **13**, 56594–56606.

660 J. Jiang, Z. Li, M. Xiao, S. Wang, K. Miyatake and Y. Meng, *J. Membr. Sci.*, 2022, **660**, 120878.

661 Q. Ju, H. Tang, G. Chao, T. Guo, K. Geng and N. Li, *J. Mater. Chem. A*, 2022, **10**, 25295–25306.

662 G. Venugopalan, D. Bhattacharya, E. Andrews, L. Briceno-Mena, J. Romagnoli, J. Flake and C. G. Arges, *ACS Energy Lett.*, 2022, **7**, 1322–1329.

663 M. Sassenburg, M. Kelly, S. Subramanian, W. A. Smith and T. Burdyny, *ACS Energy Lett.*, 2023, **8**, 321–331.

664 D. A. Salvatore, D. M. Weekes, J. F. He, K. E. Dettelbach, Y. G. C. Li, T. E. Mallouk and C. P. Berlinguette, *ACS Energy Lett.*, 2018, **3**, 149–154.

665 K. L. Yang, M. R. Li, S. Subramanian, M. A. Blommaert, W. A. Smith and T. Burdyny, *ACS Energy Lett.*, 2021, **6**, 4291–4298.

666 K. Xie, R. K. Miao, A. Ozden, S. J. Liu, Z. Chen, C. T. Dinh, J. E. Huang, Q. C. Xu, C. M. Gabardo, G. Lee, J. P. Edwards, C. P. O'Brien, S. W. Boettcher, D. Sinton and E. H. Sargent, *Nat. Commun.*, 2022, **13**, 3609.

667 B. Eriksson, T. Asset, F. Spanu, F. Lecoeur, M. Dupont, F. A. Garcés-Pineda, J. R. Galán-Mascarós, S. Cavaliere, J. Rozière and F. Jaouen, *J. Electrochem. Soc.*, 2022, **169**, 034508.

668 R. B. Kutz, Q. Chen, H. Yang, S. D. Sajjad, Z. Liu and I. R. Masel, *Energy Technol.*, 2017, **5**, 929–936.

669 A. Pǎtru, T. Binninger, B. Pribyl and T. J. Schmidt, *J. Electrochem. Soc.*, 2019, **166**, F34.

670 J. A. Rabinowitz and M. W. Kanan, *Nat. Commun.*, 2020, **11**, 5231.

671 B. Endrődi, E. Kecsenovity, A. Samu, T. Halmágyi, S. Rojas-Carbonell, L. Wang, Y. Yan and C. Janáky, *Energy Environ. Sci.*, 2020, **13**, 4098–4105.

672 S. Overa, B. S. Crandall, B. Shrimant, D. Tian, B. H. Ko, H. Shin, C. Bae and F. Jiao, *Nat. Catal.*, 2022, **5**, 738–745.

673 J. Wang, T. R. Willson, S. Brückner, D. K. Whelligan, C. Sun, L. Liang, X. Wang, P. Strasser, J. Varcoe and W. Ju, *Electrochim. Acta*, 2023, **461**, 142613.

674 M. Liu, H. Hu, Y. Kong, I. Z. Montiel, V. Kolivoška, A. V. Rudnev, Y. Hou, R. Erni, S. Vesztergom and P. Broekmann, *Appl. Catal., B*, 2023, **335**, 122885.

5778 | *Chem. Soc. Rev.*, 2024, **53**, 5704–5780

This journal is © The Royal Society of Chemistry 2024

675 S. Garg, Q. Xu, A. B. Moss, M. Mirolo, W. Deng, I. Chorkendorff, J. Drnec and B. Seger, *Energy Environ. Sci.*, 2023, **16**, 1631–1643.

676 A. G. Fink, E. W. Lees, Z. Zhang, S. Ren, R. S. Delima and C. P. Berlinguette, *ChemElectroChem*, 2021, **8**, 2094–2100.

677 Y. Hori, R. Takahashi, Y. Yoshinami and A. Murata, *J. Phys. Chem. B*, 1997, **101**, 7075–7081.

678 H. Yang, J. J. Kaczur, S. D. Sajjad and R. I. Masel, *J. CO2 Utiliz.*, 2017, **20**, 208–217.

679 W. Li, Z. Yin, Z. Gao, G. Wang, Z. Li, F. Wei, X. Wei, H. Peng, X. Hu, L. Xiao, J. Lu and L. Zhuang, *Nat. Energy*, 2022, **7**, 835–843.

680 Z. Yin, H. Peng, X. Wei, H. Zhou, J. Gong, M. Huai, L. Xiao, G. Wang, J. Lu and L. Zhuang, *Energy Environ. Sci.*, 2019, **12**, 2455–2462.

681 B. Endrődi, A. Samu, E. Kecsenovity, T. Halmágyi, D. Sebők and C. Janáky, *Nat. Energy*, 2021, **6**, 439–448.

682 Y. Xu, J. P. Edwards, S. Liu, R. K. Miao, J. E. Huang, C. M. Gabardo, C. P. O'Brien, J. Li, E. H. Sargent and D. Sinton, *ACS Energy Lett.*, 2021, **6**, 809–815.

683 Y. Y. Birdja, E. Pérez-Gallent, M. C. Figueiredo, A. J. Göttle, F. Calle-Vallejo and M. T. M. Koper, *Nat. Energy*, 2019, **4**, 732–745.

684 T. Möller, W. Ju, A. Bagger, X. Wang, F. Luo, T. Ngo Thanh, A. S. Varela, J. Rossmeisl and P. Strasser, *Energy Environ. Sci.*, 2019, **12**, 640–647.

685 T. Möller, M. Filippi, S. Brückner, W. Ju and P. Strasser, *Nat. Commun.*, 2023, **14**, 5680.

686 K. Ye, G. Zhang, X.-Y. Ma, C. Deng, X. Huang, C. Yuan, G. Meng, W.-B. Cai and K. Jiang, *Energy Environ. Sci.*, 2022, **15**, 749–759.

687 Z. Liu, X. Lv, S. Kong, M. Liu, K. Liu, J. Zhang, B. Wu, Q. Zhang, Y. Tang, L. Qian, L. Zhang and G. Zheng, *Angew. Chem., Int. Ed.*, 2023, **62**, e202309319.

688 E. S. Sanz-Pérez, C. R. Murdock, S. A. Didas and C. W. Jones, *Chem. Rev.*, 2016, **116**, 11840–11876.

689 Y. Kaneko and K. S. Lackner, *Phys. Chem. Chem. Phys.*, 2022, **24**, 14763–14771.

690 L. Shi, Y. Zhao, S. Matz, S. Gottesfeld, B. P. Setzler and Y. Yan, *Nat. Energy*, 2022, **7**, 238–247.

691 I. Nicotera, A. Policicchio, G. Conte, R. G. Agostino, M. H. U. Rehman, E. Lufrano and C. Simari, *J. CO2 Utiliz.*, 2022, **63**, 102135.

692 A. Prajapati, R. Sartape, M. T. Galante, J. Xie, S. L. Leung, I. Bessa, M. H. S. Andrade, R. T. Somich, M. V. Rebouças, G. T. Hutras, N. Diniz and M. R. Singh, *Energy Environ. Sci.*, 2022, **15**, 5105–5117.

693 J. L. Wade, H. Lopez Marques, W. Wang, J. Flory and B. Freeman, *J. Membr. Sci.*, 2023, **685**, 121954.

694 J. Liao, H. Ruan, X. Gao, Q. Chen and J. Shen, *J. Membr. Sci.*, 2021, **621**, 118999.

695 W. Xia, Y. Yang, X. Shang, X. Yang, S. Wang, F. Gong, L. Wang, X. Wang and X. Chen, *Desalination*, 2022, **529**, 115646.

696 C. Cheng, Z. Yang, Y. He, A. N. Mondal, E. Bakangura and T. Xu, *J. Membr. Sci.*, 2015, **493**, 645–653.

697 M. Irfan, N. U. Afsar, E. Bakangura, A. N. Mondal, M. I. Khan, K. Emmanuel, Z. Yang, L. Wu and T. Xu, *Sep. Purif. Technol.*, 2017, **178**, 269–278.

698 X. Du, Z. Wang, H. Zhang, Y. Yuan, H. Wang and Z. Zhang, *J. Membr. Sci.*, 2021, **619**, 118805.

699 B. Liu, Y. Duan, T. Li, J. Li, H. Zhang and C. Zhao, *Sep. Purif. Technol.*, 2022, **282**, 120032.

700 L. Xu, H. Wang, L. Min, W. Xu and W. Zhang, *Sep. Purif. Technol.*, 2023, **312**, 123396.

701 Q. Dong, X. Guo, X. Huang, L. Liu, R. Tallon, B. Taylor and J. Chen, *Chem. Eng. J.*, 2019, **361**, 1535–1542.

702 C. Wang, T. Li, G. Yu and S. Deng, *Chemosphere*, 2021, **284**, 131341.

703 C. Wang, L.-F. Ren, D. Ying, J. Jia and J. Shao, *ACS ES&T Water*, 2023, **3**, 185–194.

704 A. Saravanan, P. R. Yaashikaa, P. Senthil Kumar, S. Karishma, P. Thamarai, V. C. Deivayanai, G. Rangasamy, R. Selvasembian and T. M. Aminabhavi, *Sep. Purif. Technol.*, 2023, **317**, 123897.

705 P. Nativ, O. Lahav and Y. Gendel, *Desalination*, 2018, **425**, 123–129.

706 R. McNair, L. Cseri, G. Szekely and R. Dryfe, *ACS Appl. Polym. Mater.*, 2020, **2**, 2946–2956.

707 Q. Wu, D. Liang, S. Lu, J. Zhang, H. Wang, Y. Xiang and D. Aurbach, *ACS Appl. Mater. Interfaces*, 2021, **13**, 46537–46548.

708 K. Singh, S. Sahin, J. G. Gamaethiralalage, R. L. Zornitta and L. C. P. M. de Smet, *Chem. Eng. J.*, 2022, **432**, 128329.

709 A. Siekierka and M. Bryjak, *Membranes*, 2022, **12**, 103.

710 C. Carey, J. C. Díaz, D. Kitto, C. Espinoza, E. Ahn and J. Kamcev, *J. Membr. Sci.*, 2023, **669**, 121301.

711 Y. Zhang, X. Bu, X. Dong, Y. Wang and Z. Chen, *Desalination*, 2023, **556**, 116571.

712 X. Zhao, H. Wei, H. Zhao, Y. Wang and N. Tang, *J. Electroanal. Chem.*, 2020, **873**, 114416.

713 S. Kumar, N. M. Aldaqqa, E. Alhseinat and D. Shetty, *Angew. Chem., Int. Ed.*, 2023, **62**, e202302180.

714 J. Xi, H. Ming, S. Liu, X. Shen, C. Geng, W. Gao, J. Meng, Y. Gao, Z. Zhao, J. Lv, Y. Guan and J. Liang, *Environ. Technol.*, 2023, **44**, 3585–3591.

715 J. Herranz, A. Pătru, E. Fabbri and T. J. Schmidt, *Curr. Opin. Electrochem.*, 2020, **23**, 89–95.

716 M. Mandal, *ChemElectroChem*, 2021, **8**, 1448–1450.

717 B. Mayerhöfer, K. Ehelebe, F. D. Speck, M. Bierling, J. Bender, J. A. Kerres, K. J. J. Mayrhofer, S. Cherevko, R. Peach and S. Thiele, *J. Mater. Chem. A*, 2021, **9**, 14285–14295.

718 M. A. Blommaert, D. Aili, R. A. Tufa, Q. Li, W. A. Smith and D. A. Vermaas, *ACS Energy Lett.*, 2021, **6**, 2539–2548.

719 M. A. Blommaert, S. Subramanian, K. Yang, W. A. Smith and D. A. Vermaas, *ACS Appl. Mater. Interfaces*, 2022, **14**, 557–563.

720 X. She, L. Zhai, Y. Wang, P. Xiong, M. M.-J. Li, T.-S. Wu, M. C. Wong, X. Guo, Z. Xu, H. Li, H. Xu, Y. Zhu, S. C. E. Tsang and S. P. Lau, *Nat. Energy*, 2024, **9**, 81–91.

This journal is © The Royal Society of Chemistry 2024

*Chem. Soc. Rev.*, 2024, **53**, 5704–5780 | 5779

721 M. Hu, Q. Li, H. Peng, H. Ma, L. Xiao, G. Wang, J. Lu and L. Zhuang, *J. Power Sources*, 2020, **472**, 228471.

722 T. J. Omasta, A. M. Park, J. M. LaManna, Y. Zhang, X. Peng, L. Wang, D. L. Jacobson, J. R. Varcoe, D. S. Hussey, B. S. Pivovar and W. E. Mustain, *Energy Environ. Sci.*, 2018, **11**, 551–558.

723 G. Huang, M. Mandal, N. U. Hassan, K. Groenhout, A. Dobbs, W. E. Mustain and P. A. Kohl, *J. Electrochem. Soc.*, 2020, **167**, 164514.

724 B. Wang, J. Pan, X. Zou, J. Zhao, G. Xu, Z. Jin, Z. Sun and F. Yan, *J. Mater. Chem. A*, 2022, **10**, 13355–13367.

5780 | *Chem. Soc. Rev.*, 2024, **53**, 5704–5780

This journal is © The Royal Society of Chemistry 2024